Aromatic peptide amphiphiles: Design rules for hydrogelation and co-assembly

A thesis submitted to the University of Strathclyde for the degree of
Doctor of Philosophy
in the Department of Pure and Applied Chemistry

2014

Scott Fleming

Declaration

This thesis is the result of the author's original research. It has been composed by the author and has not been previously submitted for examination which has led to the award of a degree.

Signed: Date:

Acknowledgements

Firstly, I would like to thank my supervisor Rein Ulijn, for affording me opportunity to undertake this research project, and for his help and guidance throughout.

Within the Ulijn group, I would like to thank my supervising postdoc Sisir Debnath for his helpful discussions. I also thank current or former postdocs: Mischa Zelzer, Louise Birchall, Sangita Roy, Nadeem Javid, and Vineetha Jayawarna, for assistance and/or training with respective instrumentation. In addition, my thanks to Pim Frederix, for recording and/or assisting in the interpretation of several FTIR spectra. I would also like to thank all other Ulijn group members, past and present, for their time and assistance over the course of my project, and for contributing to a pleasant working environment in the lab and office.

In terms of external collaborators, I would like to thank Neil Hunt for his helpful discussions regarding FTIR. I am also grateful to Keith Mathieson and Robert Scharf for their assistance and respective contributions to the ongoing MEA hydrogel coating and impedance work – this would not have been possible without them.

Finally, I would like to thank my parents for their support and patience throughout my studies.

The author

Publications

S. Fleming, S. Debnath, P. W. J. M. Frederix, N. T. Hunt, and R. V. Ulijn, Insights into the co-assembly of hydrogelators and surfactants based on aromatic peptide amphiphiles. *Biomacromolecules*, 2014, **15**, 1171-1184.

G. Scott, S. Roy, Y. M. Abul-Haija, **S. Fleming**, S. Bai, and R. V. Ulijn, Pickering Stabilized Peptide Gel Particles as Tunable Microenvironments for Biocatalysis. *Langmuir*, 2013, **29**, 14321-14327.

S. Fleming, S. Debnath, P. W. J. M. Frederix, T. Tuttle, R. V. Ulijn, Aromatic peptide amphiphiles: Significance of the Fmoc moiety. *Chem. Commun.*, 2013, **49**, 10587-10589.

S. Fleming, P. W. J. M. Frederix, I. Ramos-Sasselli, N. Hunt, R. V. Ulijn, T. Tuttle, Assessing the Utility of Infrared Spectroscopy as a Structural Diagnostic Tool for β-sheets in Self-assembling Aromatic Peptide Amphiphiles. *Langmuir*, 2013, **29**, 9510–9515.

S. Fleming, A. Mills, and T. Tuttle, Predicting the UV–vis Spectra of Oxazine Dyes. *Beilstein J. Org. Chem.*, 2011, **7**, 432–441.

Presentations

ACS Indianapolis 2013 conference (Talk) and WestCHEM 2013 research day (Talk) – "Hydrogels: Co-assembly and neural interfaces"

Nanopeptide 2012 Manchester conference (Poster) – "Electro-conductive peptide amphiphile hydrogels: exploiting aromatic stacking interactions"

Abbreviations

1D	One dimensional
2D	Two dimensional
3D	Three dimensional
A	Alanine
AFM	Atomic force microscopy
Bhcmoc	6-bromo-7-hydroxycoumarin-4-ylmethoxycarbonyl
Boc	Tert-butoxycarbonyl
BPmoc	Para-borono-phenylmethoxycarbonyl
C	Cysteine
CAC	Critical aggregation concentration
Cbz	Carboxybenzyl
CD	Circular dichroism
C log P	Calculated partition coefficient
D	Aspartic acid
DAPI	4',6-diamidino-2-phenylindole
DCL	Dynamic combinatorial library
DCM	Dichloromethane
ddH_2O	Doubly distilled water
D_2O	Deuterium oxide
DIPEA	Diisopropylethylamine
DMF	Dimethylformamide
DMSO	Dimethyl sulfoxide
DNA	Deoxyribonucleic acid
E	Glutamic acid
ESI	Electrospray ionization
EtOAc	Ethyl acetate
F	Phenylalanine
Fmc	9-Fluorenylmethylcarbonyl
Fmoc	9-Fluorenylmethoxycarbonyl
FTIR	Fourier transform infrared
G	Glycine
GdL	Glucono delta lactone
H	Histidine

H-bonding	Hydrogen bonding
HBTU	*O*-Benzotriazole-*N*,*N*,*N'*,*N'*-tetramethyluroniumhexafluorophosphate
HPLC	High performance liquid chromatography
HT	High tension
I	Isoleucine
ITO	Indium tin oxide
K	Lysine
L	Leucine
LC	Liquid chromatography
LCR	Inductance, Capacitance, and Resistance
LMW	Low molecular weight
M	Methionine
MEA	Micro electrode array
MeCN	Acetonitrile
MeOH	Methanol
MS	Mass spectrometry
N	Asparagine
NDI	Naphthalene diimide
NHS	*N*-Hydroxysuccinimide
NMR	Nuclear magnetic resonance
NPmoc	Para-nitro-phenylmethoxycarbonyl
OEG	Oligoethylenegycol
P	Proline
PCB	Printed circuit board
PDI	Perylene diimide
PEG	Polyethylene glycol
PTFE	Polytetrafluoroethylene
Pyr	Pyrene
Q	Glutamine
R	Arginine
S	Serine
SEM	Scanning electron microscopy
SPPS	Solid phase peptide synthesis
T	Threonine
T3P	Propylphosphonic anhydride

TEM	Transmission electron microscopy
TFA	Trifluoroacetic acid
THF	Tetrahydrofuran
UV	Ultraviolet
V	Valine
W	Tryptophan
WAXS	Wide angle X-ray scattering
XRD	X-ray diffraction
Y	Tyrosine

Abstract

The overall objective of this thesis was to elucidate molecular design rules for the preparation of self-assembled aromatic peptide amphiphile based hydrogels. Aromatic peptide amphiphiles can be considered as having three distinct parts: the N-terminal aromatic group, peptide sequence, and the linker between the two. A systematic variation of these three molecular components has in the first instance revealed that contrary to popular belief, the antiparallel or parallel H-bonding supramolecular conformations associated with aromatic peptide amphiphiles cannot be distinguished by FTIR experiments alone. Instead, the 1685 cm^{-1} peak commonly assigned to an antiparallel arrangement, relates to the methoxycarbonyl linker if present in these systems. The choice of linker is also seen to have implications for assembly in both the aromatic and peptidic domains – as seen by fluorescence emission and FTIR respectively. In addition, the linker influences the supramolecular chirality of the fibrous nanostructures by CD. The optimal linker for effective self-assembly and gelation is observed to depend primarily on the corresponding aromatic moiety, with fluorenyl and pyrenyl systems exhibiting differential preferences for relatively rigid and relatively flexible linkers, respectively. Besides covalent alterations, aromatic peptide amphiphile materials can also be modified through co-assembly. Here, the co-assembly structure is found to vary depending upon the aromatic and peptide segments associated with co-assembly constituents. Orthogonal co-assembly is observed in systems with different aromatic and peptide parts, as inferred by a preservation of characteristic spectroscopy and material properties associated with the assembly of individual constituents. In contrast, nanoscale phase separation is found to be disfavoured in systems that share either a common aromatic or peptide segment between co-assembly constituents. Consequently, for cooperative and disruptive systems, spectroscopy reveals substantial interactions between constituents, whilst material properties are also found to be affected through co-assembly. Finally, preliminary work demonstrates the functionalisation of bulk electrodes and MEA devices with electrochemically deposited hydrogel coatings possessing an electronic core furnished with a biocompatible coating as derived from the aforementioned co-assembly design rules. Coated electrodes are found to exhibit similar impedances to those of uncoated nodes, but prove inferior to platinised equivalents. Future work will focus on optimising said electrode impedances for potential neuron-device interface applications.

Contents

– Chapter 1 –

Introduction

1.1 The gel state

A gel can be defined as a colloidal state of matter,[1,2] possessing both solid and liquid like properties. Notably, gels are viscoelastic materials where the elastic (solid) component should be greater than the viscous (liquid) component – e.g. gels are self-supporting upon vial inversion.

Ultimately, gels consist of nanoscale fibres dispersed throughout a solvent. In this respect gels can be classified according to their liquid phase; for example hydrogels[3–5] or organogels[6–8] are respectively formed in aqueous or organic media. Moreover, gels can be further subdivided according to their dispersed phase which mainly falls into one of two categories; polymeric[9] or supramolecular[10] networks. Polymer gels consist of monomers, which are covalently bonded together. These polymeric materials can form a gel network either *via* extensive covalent crosslinkage (chemical gel), or alternatively *via* intermolecular interactions and entanglement of the polymer chains (physical gel). In contrast, supramolecular gels are composed from small molecules, which rely solely on intermolecular forces to form the resultant gel network (physical gel).

While covalently crosslinked hydrogels based on hydrophilic synthetic or natural polymers are widely known and applied, such as poly(ethylene oxide), poly(acryl amide), poly(vinyl alcohol), agarose or methylcellulose,[11–19] the use of supramolecular materials based on small molecules is potentially more versatile and gives rise to a distinct class of hydrogel materials. Supramolecular materials contrast those prepared using traditional covalent polymers, in that assembly is dynamic and reversible, with readily tuneable characteristics.[20–25,10,26,27] The dynamic properties of these systems and the fact that these features can be kinetically trapped in the gel phase, has advantages for the preparation and tailoring of these materials.

An important class of LMW hydrogels are those composed of aromatic peptide amphiphiles: short chain (e.g. di-) peptides, which have been capped at the N-terminus with an aromatic moiety.[28–31] For these materials, supramolecular assembly is governed by aromatic stacking interactions, with the resulting architecture also influenced by peptidic H-bonding interactions that form a β-sheet type arrangement.[32–37] These bio-inspired materials provide a design approach focused on mimicry of the interactions which govern peptide/protein assembly[38] combined with synthetic aromatics to give rise to materials that are robust, simple and versatile.

Owing to their high water content (e.g. 99 %), tuneable mechanical properties,[39–42] and their dynamic nature,[43] LMW hydrogel systems have the potential to be utilised in a variety of applications,[44] such as catalyst encapsulation,[45] nanofabrication,[46–49] sensors,[50–52,5] antimicrobial materials,[53] controlled drug delivery devices,[54–59] and tissue engineering.[60,61,37,62–64] In addition, the supramolecular aromatic stacking interactions that are specific to the self-assembly of aromatic peptide amphiphiles, may lead to the development of soft optoelectronic devices which possess some degree of electro-conductivity.[65–69]

1.2 Project aims

The ultimate aim of this project was to develop aromatic peptide amphiphile based hydrogels suitable for the culture and/or characterisation of nerve or nerve-like cells.

For this intended application, electro-conductivity was desirable. Previous work has shown that the stacking of the N-terminal aromatic moieties can give rise to some degree of electro-coductivity.[65] Hence, the intial aim of this project was to investigate the gelation and self-assembly of aromatic peptide amphiphiles with a variety of aromatic functionalities. Inadvertently, this work led to an investigation of the corresponding linker moieties and the origin of characteristic FTIR modes associated with aromatic peptide amphiphiles.

In addition, chemical functionality introduced *via* co-assembly has been previously shown to be important to achieve efficacious materials for cell culture.[60] Hence, an assessment of aromatic peptide amphiphile co-assembly motifs was also an important aim of this project.

1.3 Thesis overview

In Chapter 2, the self-assembly and hydrogelation of aromatic peptide amphiphiles will be comprehensively assessed. Here, the N-terminal aromatic moiety, linker segment, peptide sequence, and C-termini will be examined in detail, in terms of literature prominence and their respective roles in the self-assembly process. Various possible supramolecular stacking conformations such a parallel, antiparallel, and interlocked antiparallel will also be considered. In addition, the higher order aggregation mechanisms, which generally favour the formation of 1D fibrous structures as opposed to 2D nanostructures, will be rationalised and explained in terms of a dependence on molecular structure. Furthermore, the influence of environmental factors towards the supramolecular organisation of aromatic peptide amphiphiles will be assessed. Thermodynamic and kinetic aspects associated with the preparation of self-assembled hydrogels will also be considered, with gelator concentration and temperature determining whether a continuous hydrogel network is formed, whilst the rate of assembly can influence fibre growth, the number of fibre nucleation sites, and the

corresponding properties of the resultant gels. Finally in this section, co-assembly will be examined as an effective means of tailoring hydrogel properties in a modular fashion.

Chapter 3 details the synthesis and characterisation of the aromatic peptide amphiphiles utilised in this study. In addition, the hydrogelation protocols, and corresponding characterisation methodologies are provided.

In Chapter 4, an aspect that is fundamental to the supramolecular structure of aromatic peptide amphiphiles will be considered: the utility of FTIR in elucidating either a parallel or antiparallel H-bonding arrangement. Here, experiments will focus on determining the true origin of the 1685 cm^{-1} absorption commonly assigned to an antiparallel arrangement in aromatic peptide amphiphile materials.

Chapter 5 moves on to consider the pivotal role of the linker segment in determining whether or not hydrogelation is favourable. Here, for an extensive series of aromatic peptide amphiphiles, the aromatic, peptide, and linker will be varied. Hydrogels then will be assessed in terms of their fibrous morphologies, rheological properties, and gelation pH values. In addition, a detailed spectroscopic analysis encompassing FTIR, fluorescence emission, and CD will attempt to reveal how the corresponding aromatic stacking and H-bonding self-assembly aspects are indirectly affected by the choice of linker.

In Chapter 6, we will attempt to elucidate design rules governing the co-assembly of aromatic peptide amphiphiles. Here, Pyr-YL, Fmoc-YL, Pyr-S, and Fmoc-S, will be co-assembled in all possible two-component systems. Hence, this should allow the extent of aromatic stacking and peptidic interactions between the co-assembly constituents to be inferred throughout spectroscopic means. The important question being, whether co-assembly constituents undergo nanoscale phase separation or whether a mixed elementary stacking arrangement is instead formed. Within this context, a simple means of being able to modify the surface chemistry of existing gelator systems is sought; without the additional complication of changes to the underlying fibrous assembly process and corresponding hydrogel material properties.

Chapter 7 looks at a potential applications for surface functionalised co-assembly materials such as Pyr-YL/Fmoc-S. Here, a fibrous core with extensive aromatic stacking interactions, coupled with biocompatible hydrophilic functionality at the fibre-aqueous interface is hypothesized to be an ideal candidate system for neuron-device interfaces. Preliminary work will consider the efficacy of an electrochemical deposition process for the hydrogel functionalisation of MEA. Coated electrodes will be assessed in terms of surface coverage and impedance, relative to established MEA preparation protocols such as platinisation. This work is at a preliminary stage, but further down the line could lead to a novel setup for

characterising neural networks.

1.4 References

1. T. Graham, *J. Chem. Soc.*, 1862, **15**, 216–270.
2. T. Graham, *J. Chem. Soc.*, 1864, **17**, 318–327.
3. A. M. Mathur, S. K. Moorjani, and A. B. Scranton, *J. Macromol. Sci. Part C Polym. Rev.*, 1996, **36**, 405–430.
4. A. C. Jen, M. C. Wake, and A. G. Mikos, *Biotechnol. Bioeng.*, 1996, **50**, 357–364.
5. A. Richter, G. Paschew, S. Klatt, J. Lienig, K.-F. Arndt, and H.-J. P. Adler, *Sensors*, 2008, **8**, 561–581.
6. A. Vintiloiu and J.-C. Leroux, *J. Controlled Release*, 2008, **125**, 179–192.
7. A. Ajayaghosh, V. K. Praveen, and C. Vijayakumar, *Chem. Soc. Rev.*, 2007, **37**, 109–122.
8. D. J. Abdallah and R. G. Weiss, *Adv. Mater.*, 2000, **12**, 1237–1247.
9. W. A. Laftah, S. Hashim, and A. N. Ibrahim, *Polym.-Plast. Technol. Eng.*, 2011, **50**, 1475–1486.
10. C. Y. Xu and J. Kopecek, *Polym Bull*, 2007, **58**, 53–63.
11. S. J. Kim, S. J. Park, I. Y. Kim, M. S. Shin, and S. I. Kim, *J Appl Polym Sci*, 2002, **86**, 2285–2289.
12. Y. Q. Xia, T. Y. Guo, M. D. Song, B. H. Zhang, and B. L. Zhang, *Biomacromolecules*, 2005, **6**, 2601–2606.
13. T. Dai, X. Qing, Y. Lu, and Y. Xia, *Polymer*, 2009, **50**, 5236–5241.
14. D. Myung, N. Farooqui, L. L. Zheng, W. Koh, S. Gupta, A. Bakri, J. Noolandi, J. R. Cochran, C. W. Frank, and C. N. Ta, *J Biomed Mater Res Part A*, 2009, **90A**, 70–81.
15. P. Schexnailder and G. Schmidt, *Colloid Polym Sci*, 2009, **287**, 1–11.
16. T. Y. Dai, X. T. Qing, C. Shen, J. Wang, and Y. Lu, *Adv. Mater. Res.*, 2010, **123-125**, 117–120.
17. T. Dai, Z. Shi, C. Shen, J. Wang, and Y. Lu, *Synth. Met.*, 2010, **160**, 1101–1106.
18. L. Q. Xu, F. Yao, G. D. Fu, and E. T. Kang, *Biomacromolecules*, 2010, **11**, 1810–1817.
19. D. Mawad, E. Stewart, D. L. Officer, T. Romeo, P. Wagner, K. Wagner, and G. G. Wallace, *Adv. Funct. Mater.*, 2012, **22**, 2692–2699.
20. D. J. Adams, *Macromol. Biosci.*, 2011, **11**, 160–173.
21. D. M. Ryan and B. L. Nilsson, *Polym. Chem.*, 2012, **3**, 18–33.
22. T. Aida, E. W. Meijer, and S. I. Stupp, *Science*, 2012, **335**, 813–817.
23. L. A. Estroff and A. D. Hamilton, *Chem. Rev.*, 2004, **104**, 1201–1218.
24. L. Yu and J. Ding, *Chem Soc Rev*, 2008, **37**, 1473–1481.
25. M. C. Branco and J. P. Schneider, *Acta Biomater.*, 2009, **5**, 817–831.
26. B. O. Okesola and D. K. Smith, *Chem. Commun.*, 2013, **49**, 11164–11166.
27. D. K. Smith, *Nat. Chem.*, 2010, **2**, 162–163.
28. D. J. Adams and P. D. Topham, *Soft Matter*, 2010, **6**, 3707–3721.
29. R. V. Ulijn and A. M. Smith, *Chem. Soc. Rev.*, 2008, **37**, 664–675.
30. A. L. Boyle and D. N. Woolfson, *Chem Soc Rev*, 2011, **40**, 4295–4306.
31. M. Zelzer and R. V. Ulijn, *Chem Soc Rev*, 2010, **39**, 3351–3357.
32. H. Shao and J. R. Parquette, *Chem Commun*, 2010, **46**, 4285–4287.
33. L. Chen, K. Morris, A. Laybourn, D. Elias, M. R. Hicks, A. Rodger, L. Serpell, and D. J. Adams, *Langmuir*, 2010, **26**, 5232–5242.
34. R. Orbach, I. Mironi-Harpaz, L. Adler-Abramovich, E. Mossou, E. P. Mitchell, V. T. Forsyth, E. Gazit, and D. Seliktar, *Langmuir*, 2012, **28**, 2015–2022.
35. A. R. Hirst, S. Roy, M. Arora, A. K. Das, N. Hodson, P. Murray, S. Marshall, N. Javid, J. Sefcik, J. Boekhoven, J. H. van Esch, S. Santabarbara, N. T. Hunt, and R. V. Ulijn, *Nat. Chem.*, 2010, **2**, 1089–1094.

36. A. M. Smith, R. F. Collins, R. V. Ulijn, and E. Blanch, *J. Raman Spectrosc.*, 2009, **40**, 1093–1095.
37. M. Zhou, A. M. Smith, A. K. Das, N. W. Hodson, R. F. Collins, R. V. Ulijn, and J. E. Gough, *Biomaterials*, 2009, **30**, 2523–2530.
38. M. Biancalana, K. Makabe, A. Koide, and S. Koide, *J Mol Biol*, 2008, **383**, 205–213.
39. D. E. Discher, D. J. Mooney, and P. W. Zandstra, *Science*, 2009, **324**, 1673–1677.
40. J. H. Collier, *Soft Matter*, 2008, **4**, 2310–2315.
41. M. A. Greenfield, J. R. Hoffman, M. O. de la Cruz, and S. I. Stupp, *Langmuir*, 2010, **26**, 3641–3647.
42. L. Chen, J. Raeburn, S. Sutton, D. G. Spiller, J. Williams, J. S. Sharp, P. C. Griffiths, R. K. Heenan, S. M. King, A. Paul, S. Furzeland, D. Atkins, and D. J. Adams, *Soft Matter*, 2011, **7**, 9721–9727.
43. P.-F. Caponi, X.-P. Qiu, F. Vilela, F. M. Winnik, and R. V. Ulijn, *Polym. Chem.*, 2011, **2**, 306–308.
44. N. M. Sangeetha and U. Maitra, *Chem Soc Rev*, 2005, **34**, 821–836.
45. P. W. J. M. Frederix, R. Kania, J. A. Wright, D. A. Lamprou, R. Ulijn, C. J. Pickett, and N. T. Hunt, *Dalton Trans.*, 2012, **41**, 13112–13119.
46. X. Yan, P. Zhu, and J. Li, *Chem. Soc. Rev.*, 2010, **39**, 1877–1890.
47. M. Reches and E. Gazit, *Science*, 2003, **300**, 625–627.
48. B. Adhikari and A. Banerjee, *Chem. – Eur. J.*, 2010, **16**, 13698–13705.
49. S. Roy and A. Banerjee, *Soft Matter*, 2011, **7**, 5300–5308.
50. L. S. Birchall, R. V. Ulijn, and S. J. Webb, *Chem. Commun.*, 2008, 2861–2863.
51. Z. Yang and B. Xu, *Chem. Commun.*, 2004, 2424–2425.
52. Z. Yang, P.-L. Ho, G. Liang, K. H. Chow, Q. Wang, Y. Cao, Z. Guo, and B. Xu, *J Am Chem Soc*, 2007, **129**, 266–267.
53. S. Debnath, A. Shome, D. Das, and P. K. Das, *J. Phys. Chem. B*, 2010, **114**, 4407–4415.
54. Y. Gao, Y. Kuang, Z.-F. Guo, Z. Guo, I. J. Krauss, and B. Xu, *J. Am. Chem. Soc.*, 2009, **131**, 13576–13577.
55. G. Liang, Z. Yang, R. Zhang, L. Li, Y. Fan, Y. Kuang, Y. Gao, T. Wang, W. W. Lu, and B. Xu, *Langmuir*, 2009, **25**, 8419–8422.
56. Y. Zhang, H. Gu, Z. Yang, and B. Xu, *J. Am. Chem. Soc.*, 2003, **125**, 13680–13681.
57. A. Mahler, M. Reches, M. Rechter, S. Cohen, and E. Gazit, *Adv Mater*, 2006, **18**, 1365–1366.
58. J. Nanda and A. Banerjee, *Soft Matter*, 2012, **8**, 3380–3386.
59. J. K. Oh, R. Drumright, D. J. Siegwart, and K. Matyjaszewski, *Prog Polym Sci*, 2008, **33**, 448–477.
60. V. Jayawarna, S. M. Richardson, A. R. Hirst, N. W. Hodson, A. Saiani, J. E. Gough, and R. V. Ulijn, *Acta Biomater.*, 2009, **5**, 934–943.
61. O. Z. Fisher, A. Khademhosseini, R. Langer, and N. A. Peppas, *Acc Chem Res*, 2010, **43**, 419–428.
62. Z. Yang, G. Liang, M. Ma, Y. Gao, and B. Xu, *Small*, 2007, **3**, 558–562.
63. Z. Yang, G. Liang, L. Wang, and B. Xu, *J Am Chem Soc*, 2006, **128**, 3038–3043.
64. G. Cheng, V. Castelletto, R. R. Jones, C. J. Connon, and I. W. Hamley, *Soft Matter*, 2011, **7**, 1326–1333.
65. H. X. Xu, A. K. Das, M. Horie, M. S. Shaik, A. M. Smith, Y. Luo, X. F. Lu, R. Collins, S. Y. Liem, A. M. Song, P. L. A. Popelier, M. L. Turner, P. Xiao, I. A. Kinloch, and R. V. Ulijn, *Nanoscale*, 2010, **2**, 960–966.
66. L. Zang, Y. K. Che, and J. S. Moore, *Acc Chem Res*, 2008, **41**, 1596–1608.
67. S. R. Diegelmann, J. M. Gorham, and J. D. Tovar, *J Am Chem Soc*, 2008, **130**, 13840–13841.
68. W.-W. Tsai, I. D. Tevis, A. S. Tayi, H. Cui, and S. I. Stupp, *J Phys Chem B*, 2010, **114**, 14778–14786.
69. Y. Yamauchi, M. Yoshizawa, and M. Fujita, *J Am Chem Soc*, 2008, **130**, 5832–5833.

– Chapter 2 –

Literature review: Aromatic peptide amphiphile based nanostructures

2.1 Abstract

This chapter examines the factors which govern the self-assembly of aromatic peptide amphiphiles used in the "bottom-up" preparation of nanomaterials, mainly hydrogels. These aromatic peptide amphiphile molecules are composed of four segments, and hence the influence of the N-terminal aromatic component, linker segment, (di)peptide sequence, and C-termini upon the self-assembly process and resultant supramolecular architectures is examined in detail. Parallel, antiparallel, and interlocked antiparallel stacking conformations have all been proposed depending primarily upon the aromatics (both peptidic and N-terminal) associated with the gelator in question. Furthermore, both "coiling tape" and "helical lamellar" 1D growth mechanisms are proposed to account for the fibrous morphologies generally observed for these materials. The impact of environmental conditions is also assessed; with high pH values and divalent ions found to favour the formation of crosslinked worm-like micelles as opposed to the aforementioned fibres. In thermodynamic terms, gelator concentration and temperature effects indicate the metastable nature of the nanoscale phase separated gel state; with the precise enthalpic and entropic contributions towards hydrogel formation likely to vary depending upon the hydrophobicity of a given gelator. Finally, the self-assembly initiation method is considered in terms of affecting the final properties of the kinetically trapped hydrogel product – with both pH-switch and enzymatic methods commonly used to tailor the number of nucleation sites and hence the overall fibrous network morphology. Overall, this chapter elucidates many of the trends and design rules that underpin the field of aromatic peptide amphiphile assembly.

2.2 Introduction

Supramolecular self-assembly provides a means of achieving the nanoscale "bottom-up" design and fabrication of materials, whereby supramolecular complexity and functionality can arise from the assembly of relatively simple molecular building blocks.[1–5] Various self-assembly processes can be exploited in the laboratory setting; such as the well defined base-pairing seen in DNA constructs.[6,7] It is also possible to combine naturally disparate self-assembly processes, such as DNA base pairing and peptide assembly,[8] or glycoside[9] and

peptide interactions,[10–12] within a single construct.[13] Hence, self-assembly motifs that are natively found within their respective biopolymers, can also be utilised within the context of small molecule assembly.

Peptides are highly attractive building blocks for the construction of supramolecular materials - as evidenced by the fact that the apparatus of life itself is largely devoted to the expression of approximately 20 gene-encoded amino acids. Note that throughout this chapter, for brevity, peptide sequences will often be referred to using their one letter amino acid codes (Fig. 2.9, Section 2.4.3.1 lists the 20 gene encoded amino acids). The diverse range of structures and functions that can be obtained based on these materials is extensive. In contrast to their synthetic polymeric counterparts, peptide-based materials offer a rich variety of sides chains which, unlike what is currently possible with synthetic polymers, are organised in a precise sequence that may encompass a range of chemical functionalities and non-covalent bonds.[5,14–21] For example, a range of charged (e.g. D, E, H, R, K), hydrophilic (e.g. S, T, Q, N), hydrophobic (e.g. A, V, L, I, M), aromatic (e.g. F, Y, W) and other (e.g. P, C, G) residues can all contribute towards the molecular assembly of peptides and proteins, which in turn affects the higher ordered structuring of these molecules.[22–24]

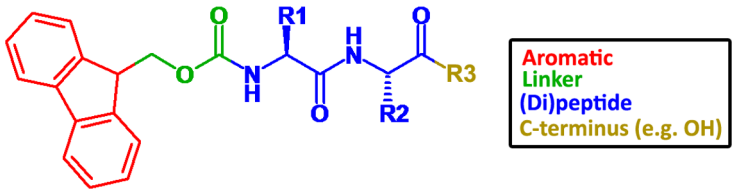

Figure 2.1 Generic structure of an aromatic peptide amphiphile.

Using insights gleaned from protein structure, synthetic peptides can be designed which contain sequences predisposed to form various supramolecular structures such as alpha helices, coiled coils, and β-sheets.[15,25–28] It can also be advantageous to utilise shorter peptide sequences; where the resultant supramolecular structures are easier to modify on account of the relative simplicity of their molecular structures,[29,19] allowing a relatively facile chemical synthesis and ultimately easier translation towards real world applications, due to lower costs and regulatory barriers in the case of biomedical materials. In addition to numerous literature examples of small molecule (peptide or otherwise) self-assembly motifs,[30–36] structures based upon relatively short (e.g. di-, tri-, etc) peptide sequences often require a synthetic hydrophobic group in order to facilitate self-assembly or gelation.[37–39] To this end, peptide amphiphiles are commonly functionalised with hydrophobic groups such as aliphatic chains.[40,38,41–49,37,50–52] An alternative approach is to utilise synthetic aromatic functionalities - where in this case self-assembly will also be influenced by the directionality associated with the resultant aromatic stacking interactions. Hence, this chapter will focus on providing an

overview of the literature relating specifically to the self-assembly and hydrogelation of aromatic peptide amphiphiles (Fig. 2.1) as a separate class of self-assembling peptide systems.

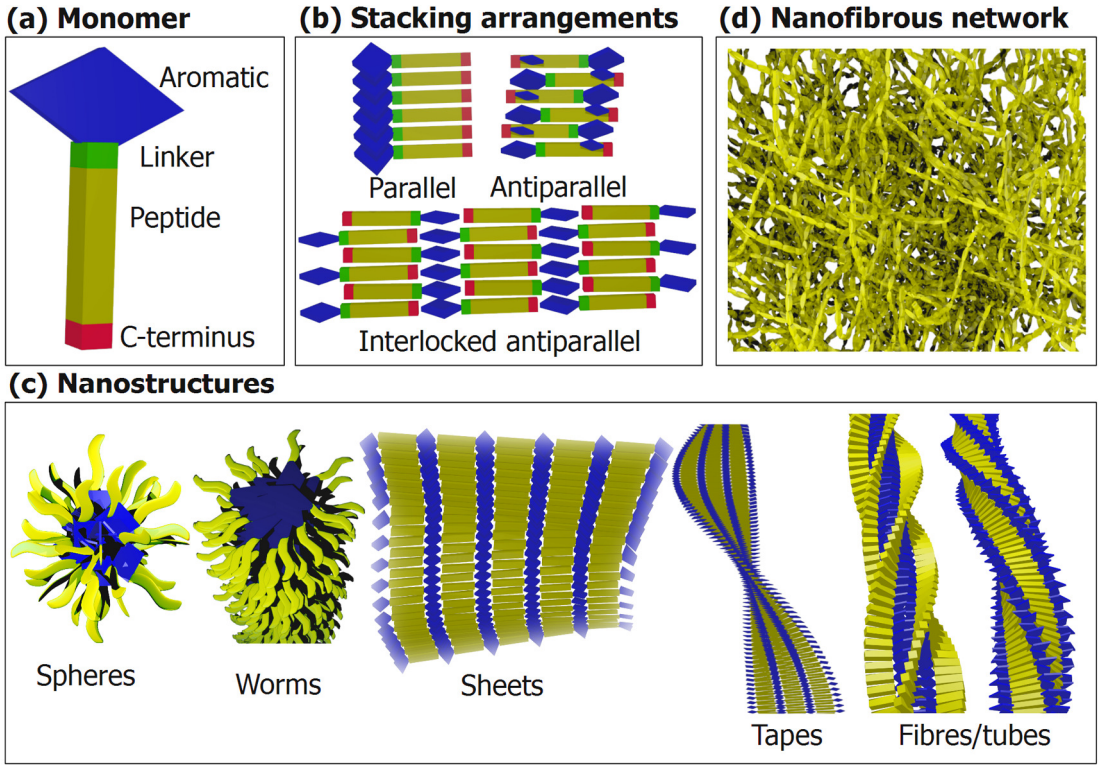

Figure 2.2 An overview of aromatic peptide amphiphile self-assembly and gelation showing; (a) a simplified aromatic peptide amphiphile; (b) some possible elementary stacking arrangements; (c) supramolecular nanostructures; and (d) a depiction of the overall fibrous network morphology of a typical hydrogel.

For aromatic peptide amphiphile systems, the peptide component is composed of a relatively short sequence - such as a dipeptide - and is capped at the N-terminus with a synthetic aromatic moiety.[17,53–55] The linker segment between N-terminal aromatic and peptide sequence is also a potentially important structural parameter,[56] that has consequences for the relative orientation of the other structural segments. In addition, the C-terminus may also be functionalised,[57–59] or is otherwise important for achieving a balance between protonated and ionised forms. Hence, these materials are distinct from but share some similarities in terms of the interactions which govern peptide/protein assembly;[26] adhering to a minimalist design strategy that is facilitated by the inclusion of a synthetic aromatic moiety. For these systems, supramolecular assembly is thought to be governed by a combination of aromatic stacking interactions, and the propensity of the peptide to form a β-sheet-type H-bonding arrangement.[60–66] This mode of assembly is different from that of aliphatic peptide amphiphiles; whose linear hydrophilic head/hydrophobic tail structure usually predicates the formation of spherical and cylindrical micelles or lamellar

structures.[67–73,38,74] In contrast, the self-assembly of aromatic peptide amphiphiles is also influenced by the planarity of aromatic moieties and the geometric restrictions associated with their preferred stacking arrangements.[19,75]

Much work has been carried out in an attempt to rationalise and control, both the self-assembly behaviour and resultant properties of aromatic peptide amphiphiles and similar small molecule gelators, *via* the modification of peptide or aromatic components.[76–84] We will consider the impact of molecular structure upon the self-assembly and properties of aromatic peptide amphiphile based materials, with separate sections to focus on the roles of the N-terminal aromatic, linker, peptide sequence, and C-terminus (Fig. 2.1). In addition, various supramolecular architectures that have been proposed in the literature will be examined: including the elementary stacking arrangements; chiral nanofibrous architectures (Fig. 2.2); and the formation of worm-like micelles. Finally, the impact of the gelation protocol itself will be considered; addressing the importance of the kinetic pathway towards the final properties of these materials.[85]

Various views on the most likely self-assembly mode have been proposed in the literature by our own group and others, and in this respect we have attempted to provide an impartial, systematic account of the relevant literature, which we hope will provide a useful reference regarding aromatic peptide amphiphile self-assembly. There is no question that aromatic peptide amphiphiles are increasingly studied and are rapidly becoming an important subset within the growing field of small molecule self-assembly.

2.3 Aromatic peptide amphiphiles: A historic perspective

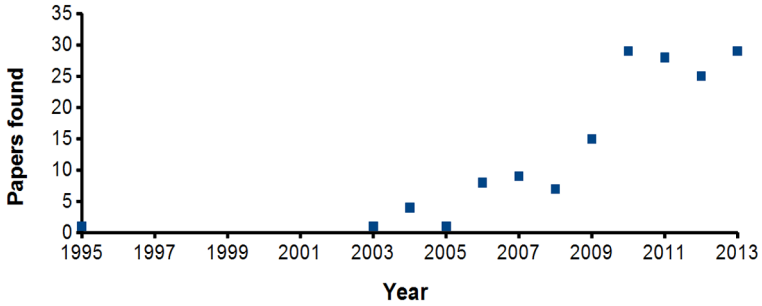

Figure 2.3 Timeline showing the prominence of aromatic peptide amphiphiles in the literature. This is unlikely to be exhaustive since field has lacked specific terminology, but it does illustrate the lag period and growth following initial work byVegners.[86]

The first known example of an aromatic peptide amphiphile hydrogelator was reported in 1995 by Vegners, where Fmoc-LD was found to form a thermoreversible gel after a heat-cool cycle.[86] This initial gel which was prepared from an aromatic peptide amphiphile was used as a carrier (or *adjuvant*) for the delivery of antigen presentation, with the loaded

material successfully eliciting an antibody response when injected into rabbits. However, it was not until 2003 onwards that a variety of Fmoc dipeptide hydrogels were serendipitously rediscovered by Xu,[87,88] en-route to a subsequently reported pyrenyl analogue.[89] In addition, Xu reported the first enzyme triggered self-assembly of an Fmoc amino acid, whereby hydrogelation was initiated via cleavage of a pendant phosphate group to form the gelator Fmoc-Y *in situ*.[90,91] Concurrently, Gazit's group demonstrated the role of aromatic amino acids in formation of amyloid structures, and through a reductionist approach identified diphenylalanine as a minimal sequence to form peptide nanostructures.[92–100] Diphenylalanine is in itself able to form peptide nanotubes on account of the directionality offered by a combination of H-bonding and repeated phenyl stacking interactions.[101–104] It was then by the addition of various N and C-terminal capping groups to investigate the possible role of electrostatic interactions in the FF assembly process, which resulted in the discovery of the now ubiquitous Fmoc-FF.[105] This initial work on diphenylalanine based nanostructures led to the approximately simultaneous, but independent, discovery of physiologically stable hydrogels based on Fmoc-FF by our group[106] and Gazit[107] for use in cell culture, thus opening up potential applications within a biological and biomedical context. In 2006 a variety of other aromatic peptide amphiphile hydrogelator studies were published,[108–112] and since then the field has continued to grow (Fig. 2.3); 2007,[113–115,80,116] 2008,[117–121,17,122] 2009,[123–132,83,64,3,65] 2010,[133–150,63,57,78,61,81,53,82,60,4] 2011,[151–165,77,76,166,39,84,59,58,167,168] 2012,[169–182,79,62,183] and 2013.[184–200,66,85,201–204] With a diverse range of studies, such as; structure-relationships, the effects of ions and other additives, protocols to control gelation kinetics, supramolecular structure elucidation, and biomedical and nanotechnological applications.

2.4 Aromatic peptide amphiphiles: The four segments

2.4.1 The N-terminal aromatic moiety

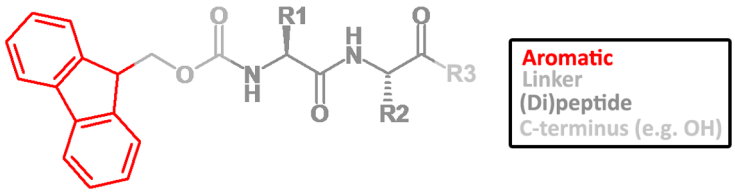

Figure 2.4 Generic structure of an aromatic peptide amphiphile with the aromatic moiety highlighted.

Self-assembling peptide hydrogels featuring the Fmoc moiety are commonplace; due to its use as a protecting group in peptide synthesis. Fmoc has been found to assist the self-assembly process and facilitate gelation for a number of systems.[203] For example, various phenylalanine and tyrosine derivatives have demonstrated that (unlike Fmoc) an N-terminal Cbz group is not found to be conducive to hydrogelation.[142] This suggests that for these

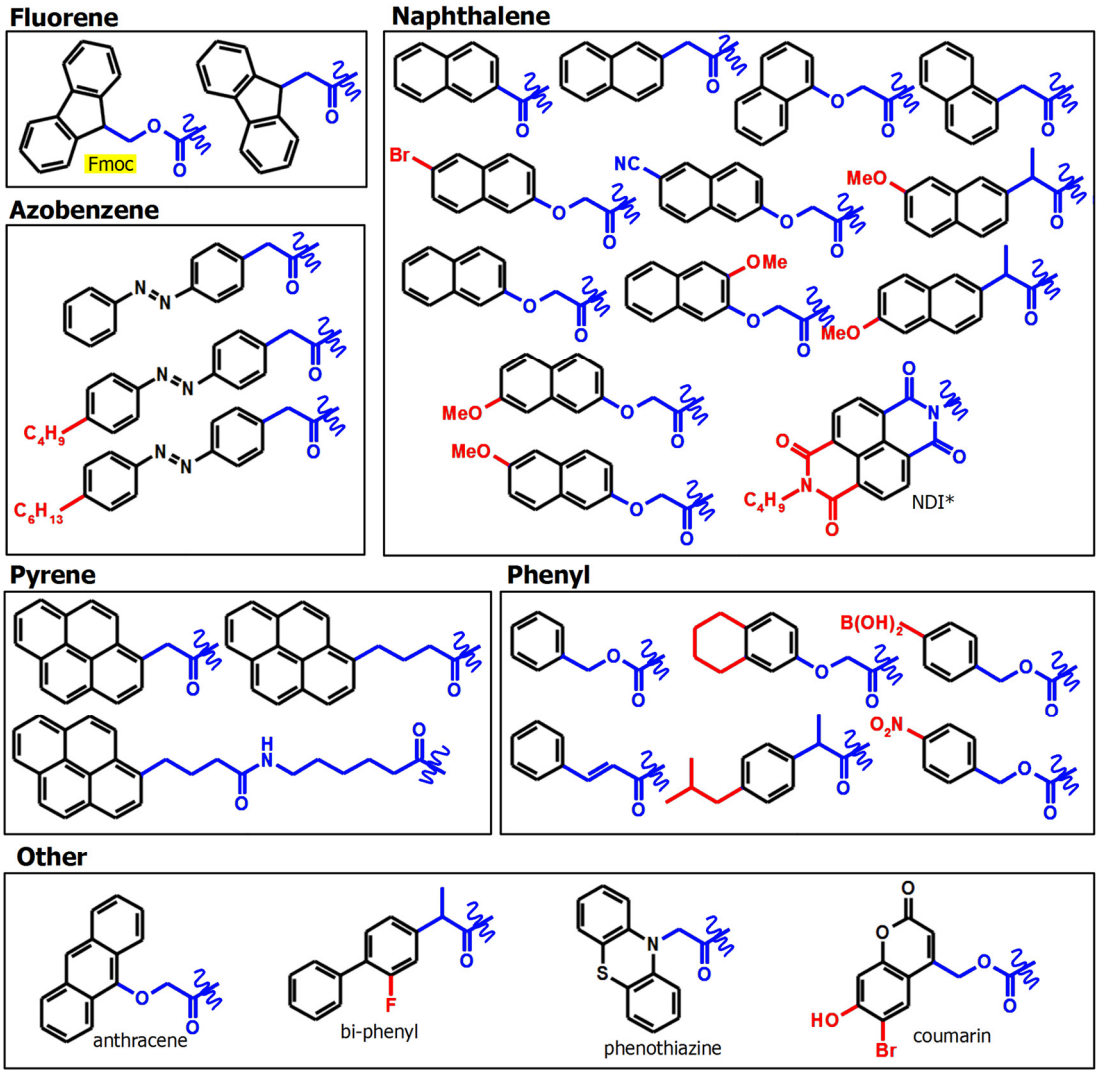

Figure 2.5 A selection of aromatic moieties reported in the literature classified according to structure. Red indicates a substituent not part of the core aromatic functionality, whilst blue indicates the linker that connects to the N-terminus of a peptide sequence. *Attached to lysine side chain, not N-terminus.

systems, the Cbz moiety provides insufficient aromatic stacking interactions and/or hydrophobicity to allow a robust intermolecular arrangement. In addition, the antioxidant carnosine, otherwise known as βAH, can undergo successful gelation only after modification with the Fmoc moiety.[39] The importance of aromatic stacking interactions has also been illustrated for a series of dipeptide and amino acid based derivatives, where the aromatic Fmoc group at the N-terminus has also been found to be a more consistent facilitator of gelation when compared to a simple hydrophobic group such as Boc.[57] The weaker Boc based hydrogels indicate that although hydrophobicity does contribute to the self-assembly of these materials, planarity and specific aromatic stacking interactions are likely important to achieve ordered intermolecular stacking.

Given that the N-terminal aromatic moiety is the key design aspect that differentiates aromatic peptide amphiphiles from other self-assembling peptide systems, it is unsurprising

that a variety of synthetic aromatic moieties - besides Fmoc - have been utilised to augment the hydrogelation of these systems. To this end, various aromatic moieties have been utilised at the N-terminus such as phenyl, naphthalene, azobenzene and pyrene derivatives. However, the various linkers, substitutions and peptide sequences associated with alternative aromatic functionalities make a systematic comparison impractical (Fig. 2.5), nevertheless some general trends are apparent.

For instance, pyrene based peptide amphiphile hydrogelators have been studied, however as might be anticipated these systems often utilise less hydrophobic sequences such as dialanine (as opposed to diphenylalanine).[89] Furthermore, the VYGGG pentapeptide sequence is found to be too hydrophobic for achieving hydrogelation (or indeed dissolution) when used in conjunction with an N-terminal pyrene moiety, whereas similar Fmoc and naphthalene compounds do form hydrogels.[141] However, in the same study other pentapeptide (GAGAS, GVGVP, VTEEI, YGFGG) based pyrene peptide amphiphiles do prove amenable to hydrogelation. Hence, these observations can only be partly explained by the pyrene based gelators requiring a more appropriate balance of hydrophilic or charged substituents. Since GVGVP and YGFGG are both more hydrophobic than VYGGG, the precipitation of the pyrenyl VYGGG compound is likely caused in part by the flexible GGG peptide segment, which may disrupt the self-assembly process. Hence, although some general conclusions may be drawn on the basis of the relative hydrophobicities, there is no obvious means of predicting the appropriate peptide sequence for a given N-terminal aromatic functionality.

Some studies have shown naphthalene to be preferential to Fmoc, e.g. as defined by the respective minimum gelation concentrations of analogous compounds.[76] Furthermore, the self-assembly properties of naphthalene based systems have been augmented *via* nitrile or bromo substitutions on the aromatic system.[78] These types of modifications provide another means of altering the hydrophobicity of the molecule – with important consequences for the correlation between the C log P and the apparent pK_a/maximum gelation pH associated with a given gelator (see section 2.4.4.1). In addition, the electron-withdrawing nature of the bromo and nitro groups will also reduce the electron density of the π-system, which consequently is likely to have an impact on the aromatic stacking interactions and the overall self-assembly structure. Hence, ring substitutions are another potential variable to consider – particularly for introducing complementary aromatic stacking interactions (e.g. within the context of co-assembly as discussed in section 2.8.1).

Furthermore, the aromatic group may in itself have a functional role, in addition to being a structural motif incorporated for the purposes of self-assembly. Indeed there are examples of

dynamic gels whose responsiveness originates not from the peptide, but from the aromatic N-terminal group. For example, azobenzene has been exploited due to the cis/trans conformational switches that are mediated under UV irradiation.[164] Using this mechanism it is possible to induce reversible photo-responsive gel-solution transitions.[84] In addition a change in the azobezene conformation has been observed to initiate a morphological change in the fibres associated with a diglycine derivative.[160] In this example, nanoribbons can be converted to short fibres upon UV irradiation; a result that is symptomatic of an alteration in the precise stacking arrangement of these molecules. Other stimuli responsive systems have also been demonstrated using a range of cleavable aromatic moieties. For example, gel to solution transitions can be initiated using oxidative, reductive or photolytic cleavages of respective BPmoc, NPmoc or Bhcmoc functionalities.[157] These responsive gels are potentially useful for the triggered release of an encapsulated material.

2.4.2 The linker segment

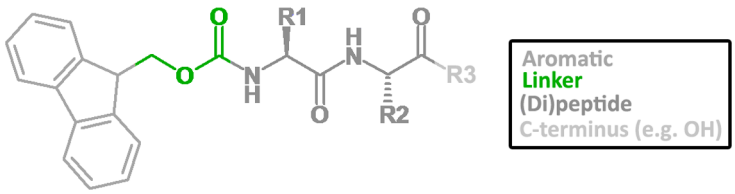

Figure 2.6 Generic structure of an aromatic peptide amphiphile with the linker segment highlighted.

The choice of linker (see Fig. 2.5 for examples) between the aromatic and peptide component is also vital to achieving hydrogelation of these materials. For example, while the naphthoxy group promotes gelation, equivalent naphthalene based amphiphiles with alternative linkers fail to form hydrogels.[80] These observations have been rationalised to some extent by molecular modelling of the angles between the various linkers (Fig. 2.7), with increased curvature of the energy minimised state associated with the molecules found to be detrimental to effective assembly. Here, gelators seem to require relatively linear geometries in order to allow effective intermolecular interactions in both the aromatic and peptide self-assembly domains. In addition, the fact that the methoxy linker is a potential H-bond acceptor may also have implications for self-assembly.

Another recent study has also shown the utility of the methoxy linker associated with the Fmoc moiety in comparison to analogous alkyl fluorenyl linkers.[56] Here, both the linker length and flexibility are proposed to be important; with the carbamate moiety of Fmoc providing a relatively rigid fluorenyl conformation for robust aromatic stacking interactions. In addition, the number of methylene units was found to alter the handedness of the observed supramolecular chirality by CD. These results mirror similar findings for aromatic-steroidal

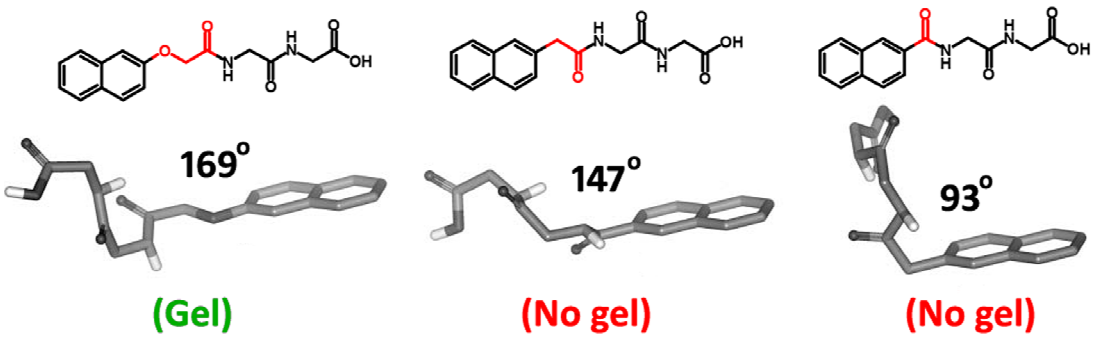

Figure 2.7 The effect of the linker on the overall molecular geometry; with a relatively linear conformation being optimal for gelation. Adapted from.[80]

based organogelator systems, where an odd or even number of methylene units in an analogous linker segment influenced the gelation properties.[36,205] Although not directly related to aromatic peptide amphiphiles, this work also highlights the impact this region of the gelator can have on self-assembly and consequent material properties. Hence, the linker clearly influences the conformations available to the gelator molecules, and as such the optimal linker is likely to depend upon the aromatic group and peptide sequence in question. Unfortunately, although aromatic peptide amphiphiles have generally utilised a variety of linkers, side-by-side comparisons in the literature are rare - we propose this should be a more active area of research in the field of aromatic peptide amphiphile assembly.

2.4.3 The peptide sequence

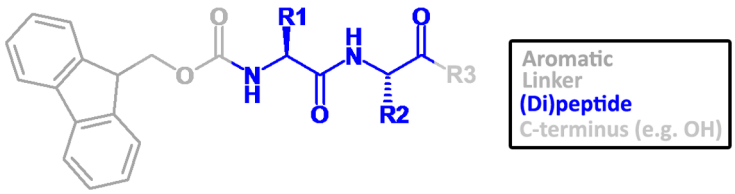

Figure 2.8 Generic structure of an aromatic peptide amphiphile with the peptide sequence highlighted.

2.4.3.1 Amino acid summary

There are twenty gene encoded amino acids across all living systems (Fig. 2.9), with a further set formed by post translational modification. An increasing number of non-natural amino acids are also available. Amino acids can be broadly classified in terms of their relative affinity for water, based on whether they possess hydrophobic or hydrophilic side chains.[206,207] For instance, aromatic residues like Y and aliphatic residues like L are classed as hydrophobic. Whereas residues with side chains capable of hydrogen bonding with water, such as S are hydrophilic – though clearly this rule is not universal, since the hydrophobic Y residue also possesses a phenol moiety capable of forming H-bonds. In addition, there are five amino acids that are charged at physiological pH, which possess either an acidic (e.g. D)

or basic (e.g. K) side chain - similarly these are also hydrophilic. Furthermore, there are three special amino acids: glycine the most flexible and the only non-chiral amino acid; proline whose rigidity in conjunction with glycine's flexibility is important in forming beta turns (within a protein context);[208] and cysteine which can be readily oxidised to form disulfide bonds.[209,146]

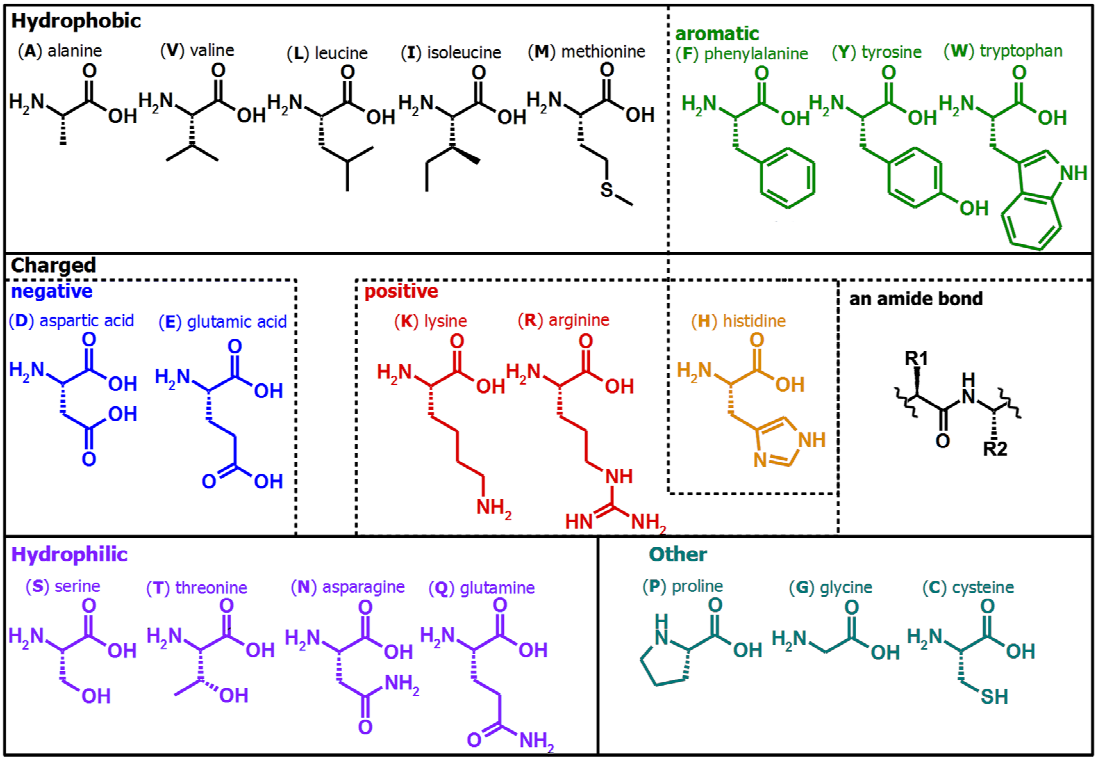

Figure 2.9 Twenty "natural" (which are gene encoded from their corresponding triplet codons) amino acids.

2.4.3.2 The assembly of peptide fragments

Self-assembly processes are driven by maximising complimentary intramolecular and intermolecular interactions, whilst also minimising unfavourable configurations. In addition, a certain amount of freedom is also required to be viable in terms of entropy. Various intermolecular interactions (Fig. 2.10) are possible depending upon the amino acid sequence, such as electrostatics,[210] hydrogen bonding, aromatic stacking, and van der Waals forces. The relative importance of these contributions varies, but within the context of aqueous self-assembly hydrophobic interactions dominate - since the influence of any permanent dipoles or charges associated with the gelator will be diminished through H-bonding with water and electrostatic interactions with any dissolved ions.

The importance of hydrophobic interactions in the assembly of short peptides has also been elucidated through extensive work on the amyloid formation of peptide fragments (e.g. FF) in an effort to deduce some of the possible mechanisms in protein misfolding diseases

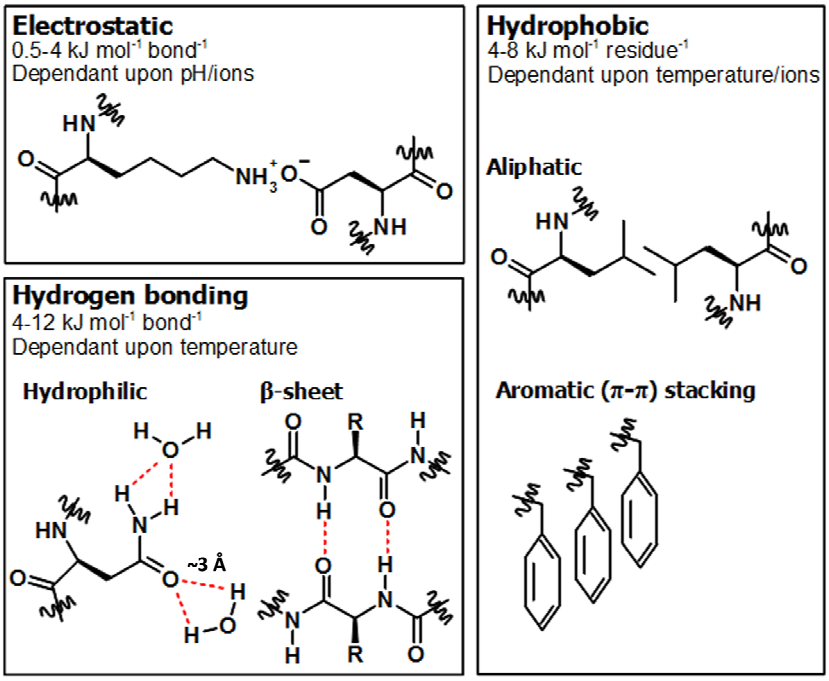

Figure 2.10 Summary of non-covalent interactions associated with peptidic interactions.

such as Alzheimer's.[92,93] This work revealed that aromatic interactions are the dominant contributor towards amyloid formation, with H-bonding interactions also a major factor. The importance of peptidic aromatic stacking interactions can be illustrated by using the intercalation of polyphenols to disrupt the normal amyloid assembly process.[211] Furthermore, the propensity of hydrophobic - and in particular aromatic - residues to effect the self-assembly of short peptides, has also been previously revealed in a computational study of all 400 natural dipeptide combinations.[212] The aim of this work was to identify potential candidate sequences, predisposed to aggregation, in a logical and systematic fashion, as opposed to employing laborious experimental trial and error. Although these amyloid and computational dipeptide systems are evidently not aromatic peptide amphiphiles, this comprehensive assessment of the self assembly of all possible dipeptide motifs provides useful insights, which are also relevant to aromatic peptide amphiphile assembly. Hence, the apparent predominance of aromatic residues (Fig. 2.11) in literature examples[121] of aromatic peptide amphiphiles should come as no surprise.

2.4.3.3 General sequence space trends

The choice of peptide sequence is of course paramount to the self-assembly and gelation ability of aromatic peptide amphiphiles. Ultimately, for effective gelation a hydrophobic/hydrophilic balance must be reached where aggregation is favoured, but precipitation does not take place. However, whilst these general principles are understood, designing novel gelators, and rationalising their behaviour, remains a challenge.[213] A

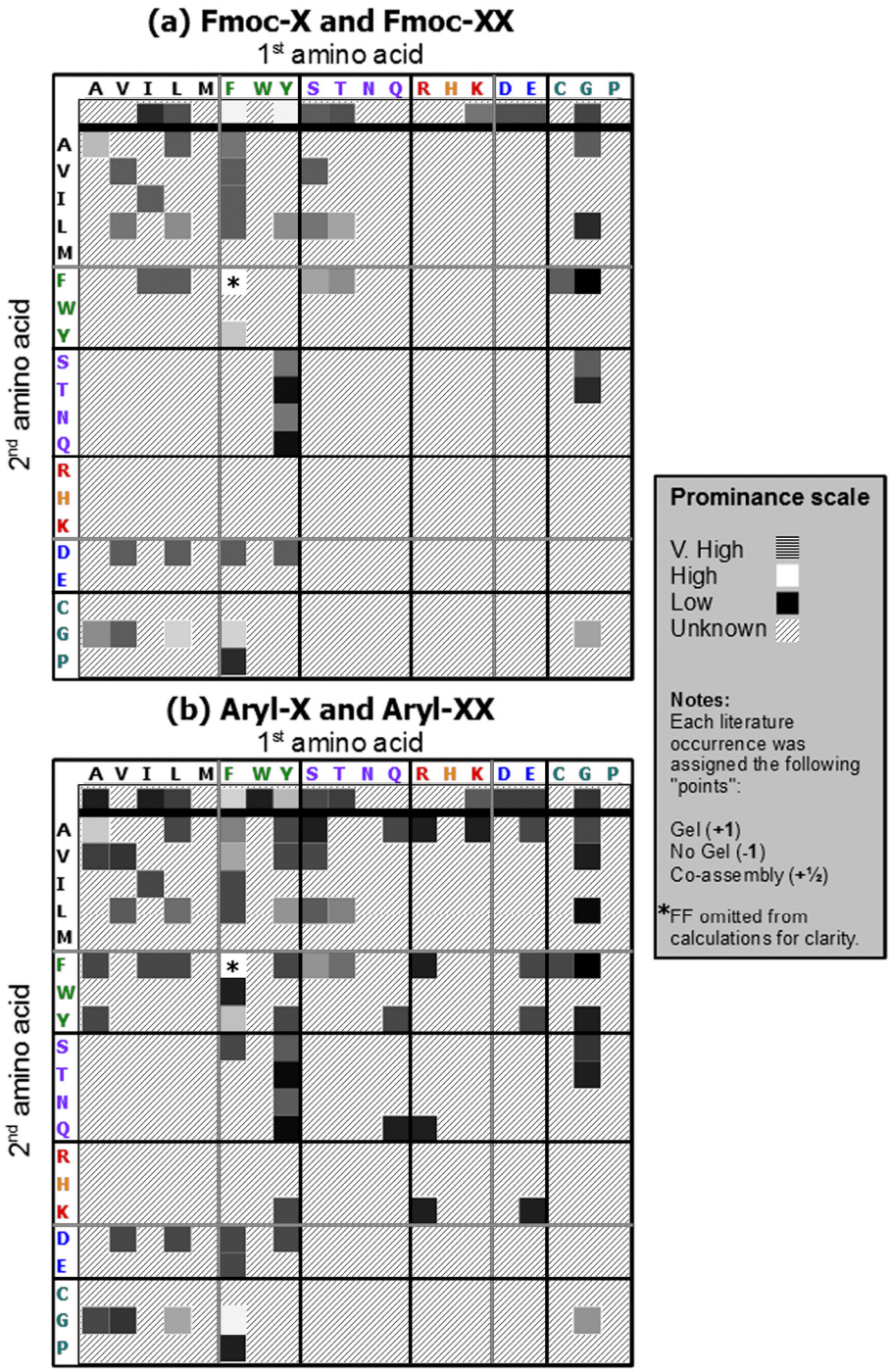

Figure 2.11 Literature/self-assembly prominence summary for all natural amino acid and dipeptides (respectively separated by thick black horizontal lines) as pertaining to (a) Fmoc and (b) N-terminal aromatics in general. Thin black lines define hydrophobic, hydrophilic, charged, and other side chain classifications. Thin grey lines define subcategories (as far as reasonably possible) – i.e. aliphatic/aromatic and positive/negative. See appendices section A.1.4 for calculation details.

systematic comparison of the experimentally observed gelation ability of aromatic peptide amphiphiles based upon their amino acid or dipeptide sequence is difficult. This is in part because the gel state often represents a kinetic trapped, non-equilibrium state so many different metastable structures may be formed from any particular gelator molecule,

depending on the route of gelation. Indeed, different authors almost invariably follow different gelation protocols.[85,177,214] In addition, a variety of N-terminal functionalities are utilised that influence the balance between the aromatic and peptidic parts of the self-assembling molecule. However, despite these difficulties in making direct comparisons, a literature analysis of Fmoc (Fig. 2.11 (a)) and more generally aromatic (Fig. 2.11 (b)) peptide amphiphiles, highlights the importance of hydrophobic and in particular aromatic residues in terms of self-assembly and gelation capability (note that for the purposes of Fig. 2.11, only gene-encoded α amino acids were considered). However, it should be acknowledged from the outset that other factors (besides self-assembly utility), such as synthetic considerations and existing literature bias, may also have contributed to this trend.

As touched upon already, the diphenylalanine sequence is present in by far the greatest number of successful gelators including Fmoc-FF,[117,62,63,65,77,81,83,127,107,135,121,106,156,215,131,177] various naphthalene derivatives,[78,128,153,176] azobenzene,[84] and others.[157] In addition, some diphenylalanine gelators feature C-termini modifications (see section 2.4.4.3) such as pyridine deriatives,[57] or OEG based functionality.[159] Hence, the prominence of the diphenylalanine sequence shows the importance of hydrophobic aromatic residues in the self-assembly of peptide amphiphiles. However, there is also clearly a historic bias from Gazit's pioneering work, and the role of diphenylalanine in amyloid formation as described above, making it a natural first choice for many novel hydrogelators,[10,92,49,149,103,216,98] Nonetheless, this indicates that the presence of aromatic amino acids can facilitate the gelation process either through hydrophobic or specific aromatic stacking interactions,[150] which may act to reinforce the H-bonded β-sheet type arrangement.[121] Beyond Fmoc-FF, prevalent successful gelators are mainly: hydrophobic dipeptides such as FY,[63,145,84,184] FV,[78,81] FA,[81,84,159] and AA;[78,81,87,106,153,176,120,174,89] or those which contain at least one hydrophobic amino acid such as FG.[62,77,78,81,83,106] In addition, single amino acid based gelators are almost exclusively aromatic, based upon either phenylalanine or tyrosine.[108,90,130,164,150,132,142,163] Furthermore, it has been found that for a wide variety of naphthalene and Fmoc dipeptides, there is a correlation between the C log P values, and the minimum gelation concentration and/or highest gelation pH.[78,81] Similarly increasing aromatic residues in the peptide backbone is found to increase the rate of hydrogelation and the stiffness/elasticity of the network formed.[62,83] Although general trends can be observed with respect to the hydrophobicity/aromaticity associated with the peptide sequence and the corresponding physical properties of the resultant systems; it is not possible to reliably predict whether a given molecule will form a hydrogel solely on the basis of C log P values alone.

In this respect, some notable outliers do exist; unsurprisingly the minimalistic diglycine (GG) sequence has been the subject of several studies.[77,80,81,87,160] There are also examples of successful aromatic peptide amphiphile gelator systems, which also feature hydrophilic and/or charged residues such as S, T, Q, N, and E.[171,152] Although the ability of relatively hydrophilic sequences, to undergo hydrogelation is often dependant upon the corresponding N- and C-termini – for instance, the gelator Fmoc-TF-OMe is obviously more hydrophobic than the corresponding free acid would be.[79] Despite this, even non- or weakly- gelating hydrophilic sequences can be used to tailor the properties of existing gelators through co-assembly (see section 2.8.2),[127,77] or alternatively some charged examples can exhibit co-dependence via electrostatic interactions between components.[152] Furthermore, beyond amino acids and dipeptide sequences, the tripeptide RGD cell binding sequence has been utilised in a variety of self-assembly and hydrogel materials intended for cell culture applications.[83,217] Although, the primary role of the RGD sequence is to encourage cell integrin binding and adhesion to the supramolecular matrix, the alternating base-acid sequence of Fmoc-RGD and the scrambled Fmoc-GRD, are also capable of undergoing self-assembly and hydrogelation.[155] Hence, despite the fact that large areas of the dipeptide space remains apparently unexplored, there is clearly significant scope for covering the entire range of amino acids and dipeptides.

2.4.3.4 Short sequences, large impact

Relatively small changes to the molecular structure can also have a large impact upon the self-assembly, gelation, and properties of these materials. Fmoc-Y and Fmoc-F hydrogels differ only by an –OH group, yet substantial rheological differences are observed.[132] Whilst the elastic and viscous moduli of Fmoc-Y are observed to be largely independent of the applied frequency, Fmoc-F exhibits moduli that are heavily influenced by the frequency. In addition, encapsulated dyes are released more easily from the Fmoc-F hydrogel. This suggests that Fmoc-F forms a more flexible network, which adapts to applied mechanical stresses. Whereas Fmoc-Y is a significantly stronger gelator; presumably the additional H-bonding donor has an impact upon the H-bonding arrangement and the precise supramolecular orientation adopted. Similarly, small structural alterations to hydrophilic amino acids utilised in position two of a range of Fmoc free acid molecules appears to strongly impact the gelation process.[171] Here, Fmoc-YT and Fmoc-YQ are solutions, whereas in comparison Fmoc-YS and Fmoc-YN form hydrogels. In this example, the steric bulk associated with an additional methyl or methylene unit has a profound impact upon the self-assembly and material properties of these systems. Furthermore, by utilising alternative peptidic interactions, atypical responsiveness can be built into aromatic peptide amphiphile

hydrogels. For example, with the rich peptide chemistry available, it is possible to augment supramolecular materials with covalent disulfide linkages. Here, the self-assembled Fmoc-CF-OMe hydrogel can be formed in a reducing environment, with subsequent heating resulting in the collapse of the network *via* oxidation of the cysteine residues.[146] Hence, with short peptide sequences it is possible to cover the full range of assembly processes available to natural peptides and proteins. However, on this scale small changes to the peptide sequence can have a relatively large impact upon self-assembly structures and material properties. Compared to a high molecular weight protein or oligopeptide, a single amino acid can have a comparatively large impact upon aromatic peptide amphiphile assembly.

2.4.3.5 Non-natural amino acid derivatives

It is also possible to alter the peptide component by modifying or replacing naturally occurring amino acids with non-natural derivatives. The most straight forward methodology involves modifying an amenable side chain functionality. For example, in Fmoc-KK(NDI), a lysine residue is exploited as a pseudo N-terminus in order to introduce aromatic n-type semiconductor functionality.[60] Similarly, in order to achieve an appropriate hydrophobic balance for effective self-assembly and gelation, protecting groups such as Boc may simply be left uncleaved.[138] In addition, given the prominence of aromatic amino acid residues in the literature it is unsurprising that non-natural amino acids such as naphthylalanine have been utilised in formation of amyloid based nanostructures,[100] and indeed hydrogels.[83] For example, Fmoc-2-naphthylalanine has been found to exhibit relatively high thermal stability and fast hydrogelation on account of the aromaticity/hydrophobicity of its amino acid derivative.[62] This suggests that increased aromaticity/hydrophobicity can facilitate fibre nucleation – contributing to a robust, interconnected, network morphology.

In addition, as seen previously with the N-terminal aromatic moieties, the electronic properties of natural aromatic amino acid residues have been modified *via* various ring substitutions. For example, Fmoc-F has been halogenated with F, Cl, and Br, at ortho, meta, and para positions.[82] In this work, electron deficient side chains are found to enhance the self-assembly rate, illustrating that these single atom modifications have a significant impact on self-assembly and consequent hydrogelation behaviour, with F proving to have the most dramatic effect. Both electronic and steric effects are thought to alter the monomer conformations and the resultant helicity of the fibres, thus resulting in changes to the precise aromatic stacking interactions present within the supramolecular assembly. In addition to mono-halogenated Fmoc-F derivatives, the penta-fluorinated Fmoc-F analogue has also been studied.[58,142] It was found to undergo hydrogelation, and exhibited a minimum gelation concentration of 0.1%wt (compared to 0.2%wt for Fmoc-Y, whilst Fmoc-F failed to undergo

hydrogelation under similar conditions).[142] Electronic, steric, and hydrophobic effects are all believed to be potential contributors to the relative stability of this system. Hence, alteration of the electronics of the aromatic side chains is clearly a useful technique for the tailoring of the structural and physical properties of aromatic peptide amphiphile based materials by enhancing π-stacking interactions between aromatic substituents.

Furthermore, one common strategy to enhance the lifetime of peptide based materials intended for use in biological applications, for example *in vivo*, is the replacement of α with β amino acids. β peptides - such as Nap-βFβF - are less likely to be metabolised due to their increased resistance to proteolytic enzymes.[111] For example, analogous Nap-FFY α and β peptide gelators have demonstrated enhanced biostability associated with the β sequence analogue.[116] In addition, for dipeptide sequences enhanced proteolytic stability can also be imparted by a single β-alanine residue; for instance Fmoc-βAV and Fmoc-βAF are biostable hydrogels for potential *in vivo* drug release devices.[218] Here, the single β-alanine is sufficient to ensure the stability of the amide bond with the natural valine or phenylalanine residue. Alternatively, gelators can utilise the dextro (D-) enantiomers of the natural levo (L-) amino acids.[89,219] This reversal of handedness can also result in enhanced biostability, as illustrated in a comprehensive study of various Nap-FF derivatives.[128] In this example, α, β, D-, and para fluorinated diphenylalanine Nap-FF gelators were considered for potential drug delivery applications. Only the β and D- variants were found to exhibit resistance to proteinase K digestion – thus highlighting the utility of these modifications for potential *in vivo* applications necessitating biostability.

2.4.4 The C-terminus

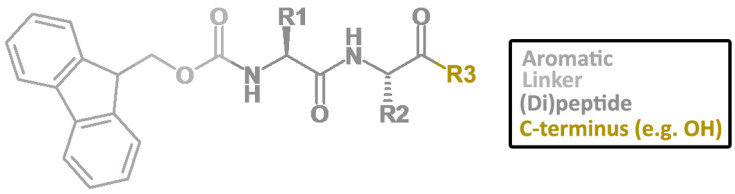

Figure 2.12 Generic structure of an aromatic peptide amphiphile with the C-terminus highlighted.

For aromatic peptide amphiphiles, which are composed of short (e.g. di- and tri-) peptide sequences, the normally free, acidic, C-termini, constitutes a significant part of the molecule, and is often vital for achieving a ratio of ionised to neutral gelator molecules conducive to gelation.[131] Hence in this section the profound influence of COOH molecular segment shall be examined in detail, in terms of the effects of pH and ions upon the self-assembly process and physical properties.

2.4.4.1 pH: controlling the ratio of COOH to COO^-

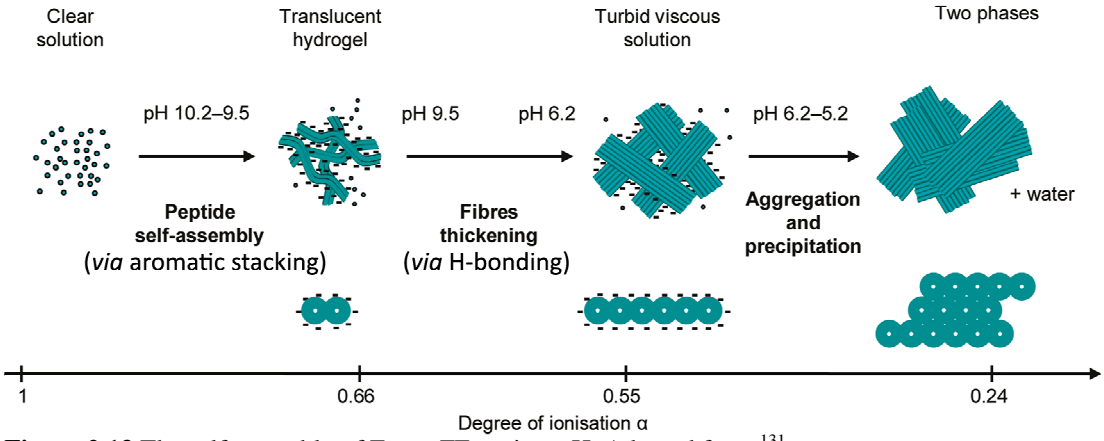

Figure 2.13 The self-assembly of Fmoc-FF against pH. Adapted from.[131]

As previously alluded to, the gelation, properties, and supramolecular structure of a given aromatic peptide amphiphile is usually found to be highly dependant upon the pH of the medium concerned.[177] Aromatic peptide amphiphiles, almost invariably, have an associated negative charge from the normally unprotected peptide C-terminus. Hence, altering the pH changes the ratio of acid to conjugate base, which in turn affects the aqueous solubility of the system. Ultimately it is the solubility and charge associated with the aromatic peptide amphiphiles that determines whether or not aggregation and gelation is favourable. Therefore it is unsurprising that pH is the primary means of controlling and initiating the gelation of these systems.

Since the assembly of aromatic peptide amphiphiles possessing a terminal carboxylic acid is largely dependant upon the neutralisation of negative charge, one might expect that gelation would only occur at a relatively low pH, below the pK_a of the molecular constituent. However, this is clearly not the case, with many examples of gelation at physiological pH - whilst the typical pK_a for a C-terminal carboxylic acid is approximately 3.5. For example, when pH titration experiments are performed on Fmoc-FF two distinct pK_a shifts are observed.[131] It should be noted that an alternative study reports only a single pK_a associated with Fmoc-FF,[177] this may be due to differences in the precise titration protocol adopted - as the initial Fmoc-FF/pH study used heat-cool cycles between titrations in order to help ensure a thermodynamic minimum was attained at each pH value. Further studies have shown that Fmoc-FF is apparently unique among closely related systems (FG, GF, GG, LL, LG, GF), which each only exhibit a single apparent pK_a shift under identical experimental conditions.[220,77] In any event, the initial Fmoc-FF/pH study[131] reports shifted pK_a values at about pH 9.5 and pH 6.2; which corresponds with the formation of a cloudy gel and the gradual precipitation of Fmoc-FF, respectively. Substantial differences were also observed by FTIR; with decreasing pH initially resulting in the appearance of amide I bands typical of

a β-sheet type H-bonding arrangement. At low pH, below the second pK_a, additional FTIR modes also become apparent, presumably corresponding with the formation of precipitate. Overall this points to a multistep aggregation mechanism with respect to pH (Fig. 2.13). At high pH, Fmoc-FF is in an ionised and disordered state; below the first shifted pK_a, fibre formation and hydrogelation occurs; fibres continue to aggregate further with decreasing pH and neutralisation of charge; until eventually below the second shifted pK_a precipitation occurs – corresponding with complete phase separation of water and peptide amphiphile. Hence, this illustrates that hydrogelation requires the presence of some remaining ionised material in order to prevent precipitation – the precise ratio required largely depends upon the relative hydrophobicity of the gelator - in line with C log P correlations.[78,81,77,220] In addition, the observed apparent pK_a shifts show that the self-assembly and gelation process itself acts as a proton sink, which buffers against pH changes while supramolecular reorganisation is proceeding. Although, fibres are often observed at high pH values, the network integrity only increases *via* H-bonding interactions as protonation allows.[61,220,123] Hence, there is likely a distinct supramolecular arrangement associated with aromatic peptide amphiphiles high pH conditions as discussed in section 2.5.4 below.

2.4.4.2 Ions and buffers

Following on from pH based assembly, the presence of various ions and the composition of buffer can also help to facilitate the gelation process. For example, an azobenzene-GG derivative is found to require a sufficient concentration of NaCl in order to exhibit nanoribbon formation by TEM, chirality by CD, and undergo hydrogelation.[160] In this instance NaCl screens the negative charge associated with the carboxylate anions, which would otherwise preclude self-assembly. Hence, the underlying mechanism behind ion induced gelation is similar to the pH based methods, where protonation of the carboxylate group is the driving force of self-assembly.

However, the vast array of ions available means that this is another means of potentially augmenting the properties of aromatic peptide amphiphile based materials. For instance, the use of various buffers can alter the mechanical properties of Fmoc-FF hydrogels prepared *via* the dilution of a Fmoc-FF DMSO solution in the aqueous phase.[177] Although the main determinant is the final pH of the system, the choice of buffer also has a non-trivial impact on the elastic modulus obtained. Elsewhere, the carbonate buffer has been used in the gelation of various Fmoc based systems.[150] Here, the carbonate anion is believed to be an integral part of the H-bonding arrangement associated with various individual and co-assembly systems.[90,88] In this instance, increasing the number of carbonate equivalents results in subtle spectroscopic shifts associated with CD – indicating that the carbonate can

influence the predominance of a specific supramolecular arrangement. Phosphate buffers have also been extensively reported throughout the literature. Due to its utility in pH regulation, phosphate buffer is often utilised in enzymatic hydrogelation processes – since enzymes generally have an optimal pH range.[59] Phosphate buffer is also useful to define a narrow pH range for gelation.[162,177] In addition, enzymatically cleavable phosphate in conjunction with calcium ions allows for mineralisation on the fibrous surface of Fmoc-Y based hydrogels.[108]

Some attempts have been made to rationalise the role of anions in augmenting the gelation of aromatic peptide amphiphiles.[179,178] Here, anions can be classified according to the Hofmeister series,[221] which assesses their relative tendency to be kosmotropes (encourages H-bonding with water) or chaotropes (breaks H-bonding with water). Elastic moduli and T_{gel} temperatures are also found to follow the same trend. Generally more resilient gels are obtained from kosmotropes such as citrate or phosphate. Furthermore, by fluorescence, the ratio of excimer to monomer is found to follow the Hofmeister series, with kosmotropes displaying a more prominent excimer – suggestive of a greater degree of extended aromatic stacking interactions. In addition, the extent of chiral organisation by CD is also found to follow the Hofmeister series, with kosmotropes enhancing the magnitude of the negative 303 nm peak. However, the Hofmeister relationship with respect to CD is complex, with the absolute magnitude and direction of the CD signals strongly influenced enzymatically, where a chiral inversion takes place relative to gels prepared chemically – in this instance, kosmotropes are similarly found to further enhance the magnitude of the now positive 303 nm peak.

Divalent cations have been observed to alter the fibre morphology of various systems based on intermolecular ionic bonding interactions.[152] Here, with divalent Ca or Mg cations, straight as opposed to helical fibres are observed by AFM. This difference is believed to be mediated by charge screening of the usual electrostatic interactions which underpin the co-assembly of for example K and Fmoc-E. The morphological differences are also accompanied by an apparent loss of supramolecular chirality by CD. Similarly for an Fmoc-βAH system, chelation with Zn induces hydrogelation and is also shown to cause a transition from twisted fibrils towards wide nanotapes.[39] Furthermore, because cell culture medium contains a variety of ions, including divalent cations, existing aromatic peptide amphiphile hydrogels can be utilised in conjunction with cell culture medium,[155] or alternatively gelation can be effected by the addition of cell culture medium itself.[127,177] Here, divalent cations can facilitate the gelation process *via* crosslinking interactions between the fibres, which allow for aromatic peptide amphiphiles to undergo hydrogelation over a wider pH range, and can

potentially alter the morphology of the fibrous network.

Overall, pH and ions clearly have a strong influence upon the structure and properties of aromatic peptide amphiphile based systems. Here, the choice of a particular salt is a thermodynamic consideration, which can alter the morphology of the fibrous network. Hence, this is clearly a useful means of increasing the utility of existing gelator systems.

2.4.4.3 C-terminus modifications

As discussed above, the main advantage of using the free acid C-terminus, is that the self-assembly of the gelator can be easily triggered by pH adjustments. Hence, a range of peptidic functionality can potentially be accommodated, since pH adjustments will alter the balance between deprotonated and protonated forms. As such the vast majority of aromatic peptide amphiphiles utilise the free acid.

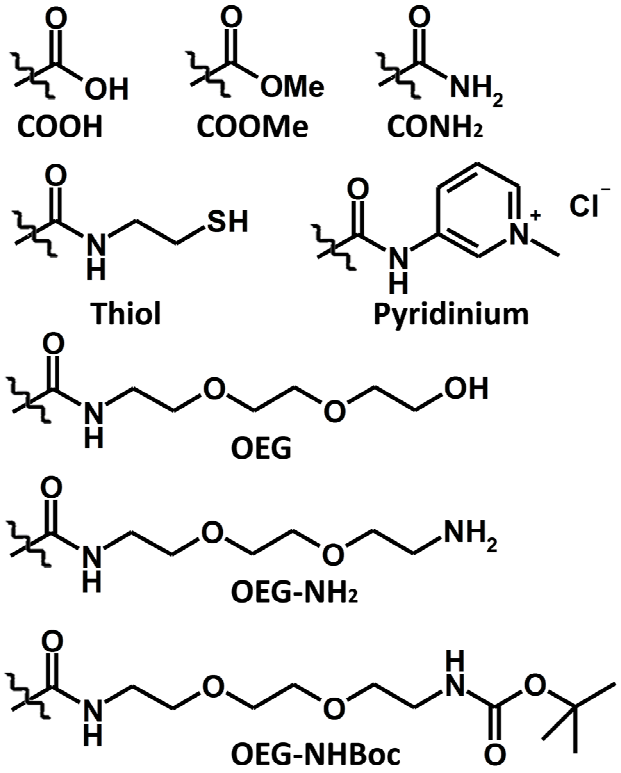

Figure 2.14 A selection of C-termini reported in the literature. COOH is overwhelmingly the most common of these.

However, when the C-terminus is functionalised (Fig. 2.14) with a methyl ester, solubility in water can be problematic. Hence, methyl ester functionalised peptide sequences normally possess at least one hydrophilic residue to aid solubility and dispersion in water.[59,79,124] In addition, self-assembly and gelation of these systems is often initiated enzymatically using a condensation reaction of freely soluble amino acid building blocks (often catalysed by the protease thermolysin as discussed in section 2.7.3.3). Hence, kinetic aspects which can otherwise hinder the gelation of poorly soluble methyl ester derivatives, can be overcome

with an *in situ* enzymatic condensation methodology.

A systematic variation of the C-terminus of various side chain halogenated Fmoc-phenylalanine derivatives has broadly revealed that COOH promotes gelation, COOMe promotes precipitation, and $CONH_2$ generally results in solutions for these systems.[58] Of course, although these C-termini solubility trends generally hold ($CONH_2$ > COOH > COOMe), depending upon the hydrophobicity of the corresponding N-terminal aromatic and peptide sequence, COOMe[79] and $CONH_2$[187] C-termini can both prove perfectly amenable to undergo gelation. Hence, simple modifications to the C-terminus can have a significant impact on the solubility and consequently the self-assembly characteristics of these materials.

Other C-termini modifications used for aromatic peptide amphiphile based hydrogelators include a thiol,[115] several pyridinium derivatives,[57] and variations of a OEG chain.[159,143] The pyridinium derivatives are of note, since for these systems the C-termini charge has been reversed from negative to positive. In addition, pyridinium is also of interest due to its antibacterial activity. Unsurprising, the pyridinium gelator with the lowest minimum gelation concentration was based on the familiar Fmoc-FF motif. In addition, one of the OEG based hydrogelator systems,[159] also possesses a cationic C-terminus, Boc protection of which allows for the preparation of organogelators. Hence, there is clearly a lot of scope for augmenting or altering the self-assembly properties of aromatic peptide amphiphile materials *via* modification of the C-terminus. Ultimately the hydrophobicity of the corresponding aromatic and peptide components must be suited to a given C-terminus for hydrogelation to take place.

2.5 Supramolecular organisation

2.5.1 Possible stacking conformations

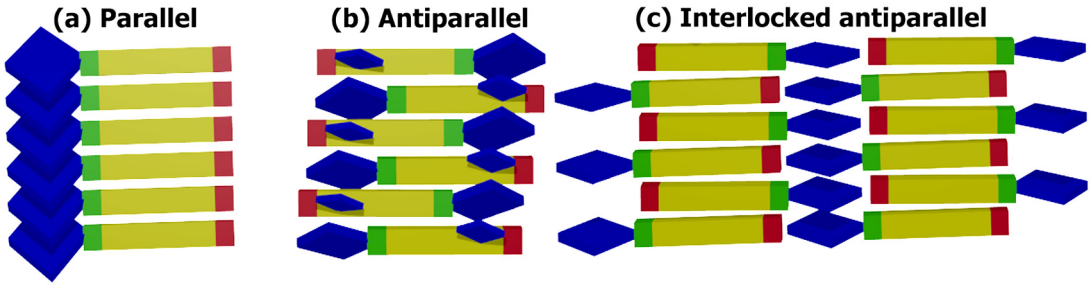

Figure 2.15 Depiction of possible aromatic stacking interactions present in aromatic peptide amphiphile nanostructures: blue diamonds represents the N-terminal aromatic moiety; cuboids represent the dipeptide sequence, and the small blue squares in (b) correspond to aromatic side chains.

The self-assembly of aromatic peptide amphiphiles is based upon the alignment of relatively hydrophobic and relatively hydrophilic regions of the molecules.[115] For aromatic peptide

amphiphiles, hydrophobic contributions are dominated by the influence of the aromatic functionality at the N-terminus, whereas the peptidic H-bonding arrangement assumes the role of the relatively hydrophilic motif. One of the key questions associated with this supramolecular stacking arrangement is whether a parallel or an antiparallel stacking conformation is adopted, with evidence for both modes of assembly presented in the literature.

2.5.1.1 Parallel versus antiparallel

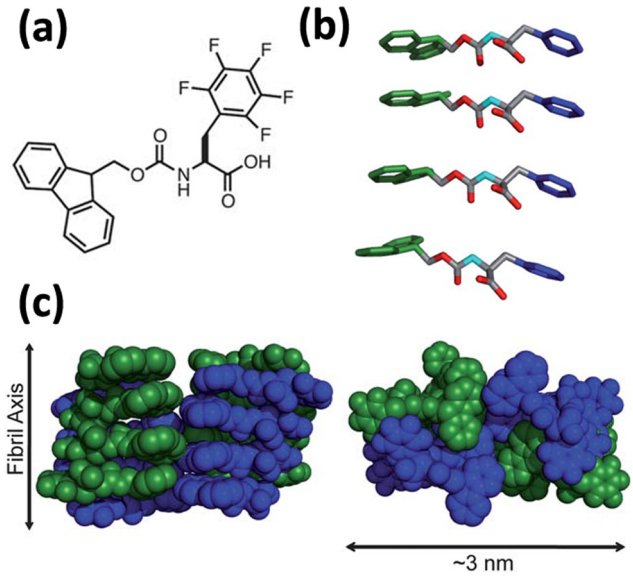

Figure 2.16 (a) Penta fluorinated Fmoc-F (a representative example of a Fmoc-F/Y derivative); (b) Parallel stacking arrangement; (c) Further aggregation of the elementary stacks. Adapted from.[183]

Parallel stacking (Fig. 2.15(a)) arrangements have been proposed for a variety of side chain halogenated Fmoc-F and Fmoc-Y derivatives (Fig. 2.16). This assignment is partly based upon CD signals at 270-310 nm and 200-230 nm, which are attributed to chiral Fmoc-Fmoc and phenyl-phenyl stacking interactions respectively,[82] but this does not preclude the alternative antiparallel structures. Furthermore, XRD spacings of 14 and 30 Å are proposed to be consistent with the length of a single Fmoc-(penta-fluorinated)-phenylalanine molecule and the association of multiple parallel fibrils, respectively; such that the relatively hydrophobic Fmoc moiety remains buried in the core, whilst the carboxylates interact with the aqueous medium.[142] This proposed structure, based upon buried hydrophobics and parallel H-bonded stacking (4 Å XRD spacing) interactions, is analogous to the fibrous aggregation arrangements seen for longer, predominately aliphatic, peptide amphiphile systems.[222–227] However, similar spacings (WAXS) are also observed in (for example) the Fmoc-FF system,[121] which is proposed to form an interlocked antiparallel supramolecular arrangement (see section 2.5.1.2) – hence the elucidation of stacking arrangements from

characteristic spacings can be somewhat subjective.

The pH dependence of the self-assembly process is also cited as an argument for the parallel stacking arrangements of these Fmoc-F and Fmoc-Y based systems,[58] since at high pH adjacent carboxylates would presumably repel one another and preclude self-assembly and gelation. However, substantial apparent pK_a shifts are often observed for aromatic peptide amphiphile hydrogels in general (irrespective of the proposed stacking arrangement); with self-assembly occurring at a higher pH than would intuitively be expected,[131,177] suggesting that carboxylic acids are in a hydrophobic environment. In addition, an antiparallel arrangement (e.g. similar to Fig. 2.15 (b)) could be energetically advantageous given the potentially complementary aromatic stacking interactions between Fmoc and, for example, the electron deficient penta-fluorinated phenylalanine ring system.[142] It could also be argued that single amino acid gelators such as these, are not necessarily representative of other aromatic (e.g. di- and tri-) peptide amphiphiles, since the single carbamate group precludes the formation of any β-sheet type H-bonding arrangement.

In any case, aromatic peptide amphiphiles that possess aromatic side chains at least have the option of adopting an antiparallel conformation (Fig. 2.15(b)). For instance, a naphthalene-FFGEY derivative is believed to adopt an antiparallel structure, with a β-sheet type H-bonding arrangement indicated by positive (near 196 nm) and negative (near 215 nm) CD bands.[110] The lack of significant excimer formation at 450 nm, and the presence of a shoulder above 400 nm adjacent to a monomeric naphthalene peak at ~340 nm by fluorescence, indicates naphthalene-phenyl stacking interactions as opposed to extensive naphthalene-naphthalene stacking. These antiparallel stacks are then proposed to undergo further aggregation into nanotubes, *via* interactions between the pendant EY sequences (presumably by an interlocking mechanism different from both analogous to Fig. 2.15(c)).

Aromatic residues are also shown to be a prerequisite for the antiparallel conformation in a study where distinct stacking arrangements have been proposed for aromatic peptide amphiphile with different dipeptide sequences.[111] With naphthoxy-GβA exhibiting stronger naphthalene stacking interactions than naphthoxy-βFβF on account of an increased fluorescence emission redshift. This is rationalised on the basis of naphthoxy-GβA adopting a parallel aromatic stacking arrangement, featuring H-bonding interactions with at least two other monomers, with layers almost perpendicularly orientated with respect to one another (Fig. 2.17(a)). In comparison, naphthoxy-βFβF is proposed to assemble through H-bonding between the amide group adjacent to the naphthalene and the terminal carboxylic acid, thus giving rise to a helical structure (Fig. 2.17(b)) that assembles into fibres through the further aggregation of these helices. Hence, it can be surmised that if there is aromaticity associated

with the peptidic part of the gelator, then this can potentially compete with the nominal stacking of the N-terminal aromatic groups. These radically different models, from closely related gelators, illustrate that a single supramolecular structure, which is representative of all aromatic peptide amphiphile systems is unlikely.

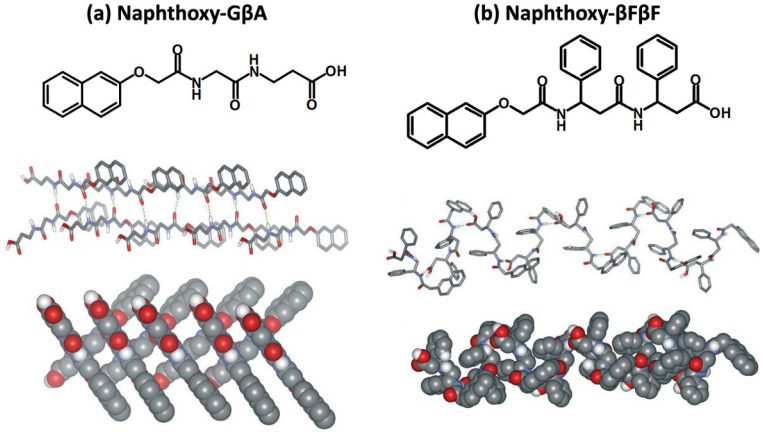

Figure 2.17 Aromatic side chains lead to an apparent disruption of parallel stacking arrangement. Adapted from.[111]

2.5.1.2 Interlocked antiparallel

As alluded to, a distinct antiparallel arrangement can be envisaged whereby stacks of H-bonded peptides are interlocked via antiparallel stacking between adjacent N-terminal groups (Fig. 2.15(c)).[168] This interlocking mechanism is an attractive proposal, which manages to address the disparity in aromatic stacking distances that would otherwise arise from this conformation.[121] Henceforth, this will be referred to as the interlocked antiparallel stacking arrangement (Fig. 2.15(c)), to avoid confusion with the aforementioned antiparallel structure (Fig. 2.15(b)), which is obviously side chain dependant.

For example, the stacking conformation of the popular Fmoc moiety has been hypothesized to adopt a number of possible aromatic stacking conformations, with the interlocked antiparallel arrangement one of the most prolific. These structural assignments have been made partly on account of the various fluorescence emission bands normally observed for these materials,[228,90] with gelation often accompanied by a redshift in the emission spectrum. For instance, Fmoc-LG is proposed to exhibit an interlocked antiparallel stacking arrangement on the basis of a fluorescence emission redshift from 320 to 330 nm.[123] With self-assembly and gelation also accompanied by an increasing CD signal. Similar results are also observed in a study that included Fmoc-LL and Fmoc-LG hydrogels, with an emission redshift from 313 to 317-330 nm attributed to an interlocked antiparallel fluorenyl stacking arrangement.[220,120] Furthermore, a fluorescence shift from 309 to 323 associated with the co-assembly of Fmoc-L and Fmoc-K, is also thought to coincide with a predominately interlocked antiparallel arrangement in the gel state.[88] However, the existence

of a shoulder at 380 nm is believed to be indicative of a small portion of parallel Fmoc-Fmoc interactions – this is in agreement with the excimer emission observed for an intramolecular parallel fluorenyl interaction.[228] Others have attributed a similar shoulder at 370-380 nm to parallel interactions within micellar aggregates.[184,220] Furthermore, parallel, antiparallel, and interlocked antiparallel dimers are suggested to be present for a Fmoc-Y system on the basis of 400, 350, and 380 nm peaks, respectively.[90] In addition, there is also often an excimer emission peak at approximately 450 nm from the extended aggregation of these aromatic moieties. Hence, there appears to be some inconsistency in the interpretation of these characteristic fluorescence bands – but generally speaking, a more pronounced redshift corresponds with more extensive interlocked antiparallel structure. However, the variety of stacking conformations proposed also indicates that various stacking arrangements can potentially co-exist, depending upon any aromaticity associated with the peptide component, and the degree of disorder associated with a particular system.

2.5.1.3 H-bonding within the supramolecular stacking conformation

In addition to the aforementioned aromatic interactions, H-bonding between peptides is also likely to contribute to any proposed stacking conformation. Hence, FTIR absorptions at ~1685 and ~1625 cm^{-1} have been extensively utilised as experimental evidence of an antiparallel β-sheet type arrangement associated with aromatic peptide amphiphile based hydrogels.[218] However, these characteristic assignments originate from the elucidation of secondary protein structures, where the higher wavenumber peak at ~1685 cm^{-1} is associated with an antiparallel structure.[229] Whereas, for aromatic peptide amphiphiles, the 1685 cm^{-1} band actually originates from the carbamate of the Fmoc functionality.[66,175] Nevertheless, FTIR amide I peaks can still indicate the formation of an extended β-sheet type H-bonding structure, which in conjunction with other techniques may be interpreted as antiparallel. For instance, Fmoc-βAH is proposed to adopt an antiparallel, aromatic stacked, β-sheet type structure on the basis of characteristic amide I bands at 1636 and 1684 cm^{-1} by FTIR, and XRD spacings of 3.2 Å, 4.6 Å, and 12.4 Å providing evidence for aromatic stacking, β-sheet type H-bonding, and inter-sheet stacking distances, respectively.[39] Furthermore, the antiparallel arrangement is suggested for a variety of other aromatic peptide amphiphiles from FTIR, fluorescence, and XRD results.[57] Here, as discussed above, the fluorescence redshift is cited as evidence of an interlocked antiparallel fluorenyl conformation. In addition, the XRD spacings of 3.5 Å, 4.6 Å, and 9.4 Å are indicative of Fmoc-Fmoc stacking, inter-strand β-sheet type H-bonding, and inter-sheet stacking distances, respectively. This suggests an overall supramolecular conformation composed of antiparallel H-bonded stacks, which are then interlocked with aromatic stacking interactions (Fig.

2.15(c)).[121,147]

Hence, besides the overall hydrophobicity of a peptide amphiphile, H-bonding interactions and by extension the peptide sequence also have important implications for the structural and physical properties.[106] For instance, when various glycine residue substitutions are applied to the popular Fmoc-FF and Fmoc-LL hydrogel systems, several trends become apparent (Table. 2.1).[77,220] Although all sequences form supramolecular structures primarily through hydrophobic interactions. The Fmoc-GF and Fmoc-GL systems precipitated, whereas Fmoc-GG formed a meta-stable gel that precipitated over time. Only in the Fmoc-FG and Fmoc-LG examples (also see[123]) where the phenylalanine or leucine residue is adjacent to the N-terminal Fmoc moiety does stable gelation take place. Here, the position of the flexible glycine residue – that is not predisposed to form β-sheets – clearly influences whether or not the supramolecular stacking arrangement is conducive to gelation; with overly flexible examples exhibiting less propensity for forming a β-sheet type H-bonding arrangement as assessed by FTIR (~1685 and ~1625 cm^{-1}) and WAXS (~4.6 Å inter-strand spacing). Similarly other hydrogel systems appear sensitive to the sequence order, since upon the inversion of an Fmoc-VLK(Boc) sequence, Fmoc-K(Boc)LV exhibits relatively unoriented assemblies, branched fibres and a larger elastic modulus.[138] Hence, the order of the peptide sequence is again seen to have consequences for backbone flexibility and H-bonding conformations available to the molecule. Overall, as a rule of thumb for Fmoc dipeptides, a relatively flexible residue (e.g. glycine) in the first position increases the likelihood of precipitation as opposed to facilitating gelation – by disfavouring the formation of a β-sheet type H-bonding arrangement.

Table 2.1 Gelation, and relative inference of a β-sheet type H-bonding arrangement depending upon Fmoc-dipeptide sequence.[77,220]

Sequence	FF	FG	GF	GG	LL	LG	GL
Gelation	Yes	Yes	No	Yes[a]	Yes	Yes	No
FTIR[b]	Yes	Disordered	No	No	Yes	Disordered	No
WAXS[c]	Yes	No	No	No	No	No	No

[a]metastable with gel precipitating over time. [b]Yes if amide I peak observed at ~1625 cm^{-1}, Disordered if amide I peak observed at ~1640^{-1}. [c]Waxs β-sheet type spacing ~4.6 Å

2.5.2 1D and 2D growth mechanisms

Despite all of the discussed stacking conformations (Fig. 2.15), evidently, further aggregation mechanisms are responsible for the 1D fibrous morphologies normally observed in these hydrogel materials – two main mechanisms are proposed herein. In either case, curvature associated with the (interlocked) H-bonded stacking structure is ultimately responsible for the observed supramolecular chirality,[64] this is important, because in general self-assembly terms, chirality has been cited as a key factor or requirement for self-assembly

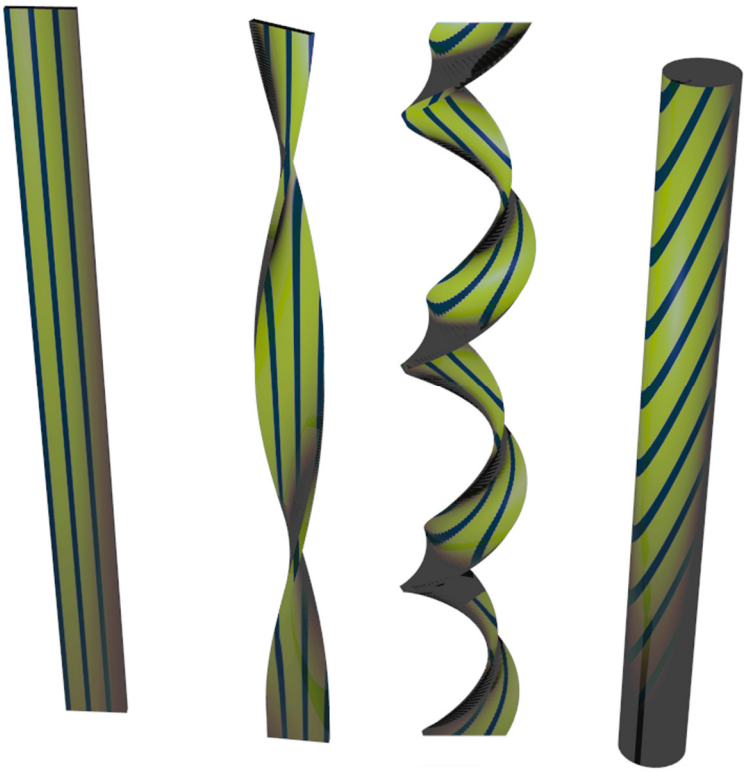

Figure 2.18 Depicts coiling tape mechanism (as applied to aromatic peptide amphiphiles featuring interlocked antiparallel stacking conformation – with aromatic and peptide stacking shown in blue and yellow respectively).

into fibres/nanotubes.[230–232] Here, for what shall be referred to as the coiling tape mechanism (Fig. 2.18), elementary tapes, which would otherwise form 2D structures via lateral growth, develop into twisted and then coiled tapes over the course of the self-assembly process.[71] This closing mechanism is found to proceed *via* a combination of two possible routes; growing width and closing pitch (increasing helicity) of the elementary tape. Finally when the coiled tapes close over, the resultant fibre or nanotube morphology is obtained. For aromatic peptide amphiphiles, the outside and/or core of this structure could potentially be stabilised *via* hydrophilic and/or hydrophobic amino acid side chains respectively, depending of course on the precise peptide sequence in question.

A similar fibrous aggregation mechanism is also proposed on the basis of helicity.[233] Here, with increasing concentration, helical tapes undergo plane-to-plane bilayer and then lamellar type stacking interactions to form ribbons, fibrils, and finally fibres. Hence, the lateral growth of the elementary tapes is inherently limited by their helicity, explaining why 2D structures are not generally observed. In addition, an infinite lamellar stack composed of these tapes is also generally disfavoured on the basis of helicity. Hence, this shall be referred to herein as the helical lamellar growth mechanism (Fig. 2.19), where for the specific case of aromatic peptide amphiphiles, lamellar type stacking would be stabilised via complementary peptide side chain interactions.

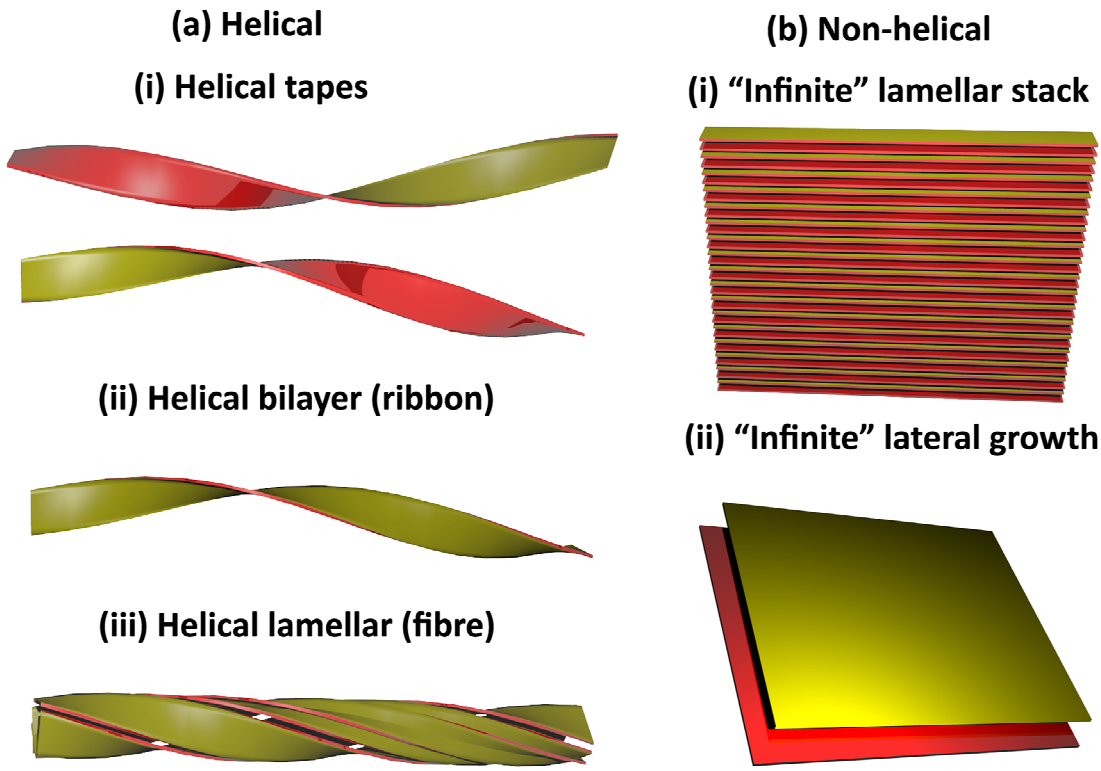

Figure 2.19 Depicts (a) helical lamellar growth mechanism, where red and yellow faces refer to generic self-complementary interactions; (b) for comparison, non-helical tapes could hypothetically yield "infinite" (i) lamellar stacks or (ii) lateral growth.

For example, the ubiquitous Fmoc-FF system (Fig. 2.20) has been proposed to give an interlocked antiparallel stacking conformation, followed by a higher ordered aggregation mechanism that in part appears to be akin to the coiling tape growth mechanism (Fig. 2.18).[121] Similar to previous examples the intermolecular stacking arrangement is supported by ordered H-bonding interactions by FTIR, and a 218 nm peak by CD that is also attributed to this β-sheet type arrangement. In addition, the interlocking of these β-sheet stacks is inferred from a fluorescence shift to 330 nm suggestive of an antiparallel orientation of the Fmoc groups.[88] Furthermore, this system exhibits a fluorescence excimer at 460 nm, indicating extensive J-aggregate formation. The interlocked β-sheet structure is also rationalised on the basis that the Fmoc moieties would otherwise be too far apart to allow effective overlap. Due to a twist present in the β-sheet which is a consequence of the presence of chiral centres,[233] the sheets are believed to rotate to allow full fluorenyl overlap. Overall this results in a cylindrical arrangement, with four interlocked sheets forming a the pseudo-tertiary structure 30 Å in width, with a 7 Å cavity in the centre. Further side by side aggregation of these cylindrical structures, yields the observed ribbons by TEM. These proposals are also supported by WAXS, which features several of the spacing that would be characteristic of this supramolecular assembly. Nanotubes are also observed for the Fmoc-

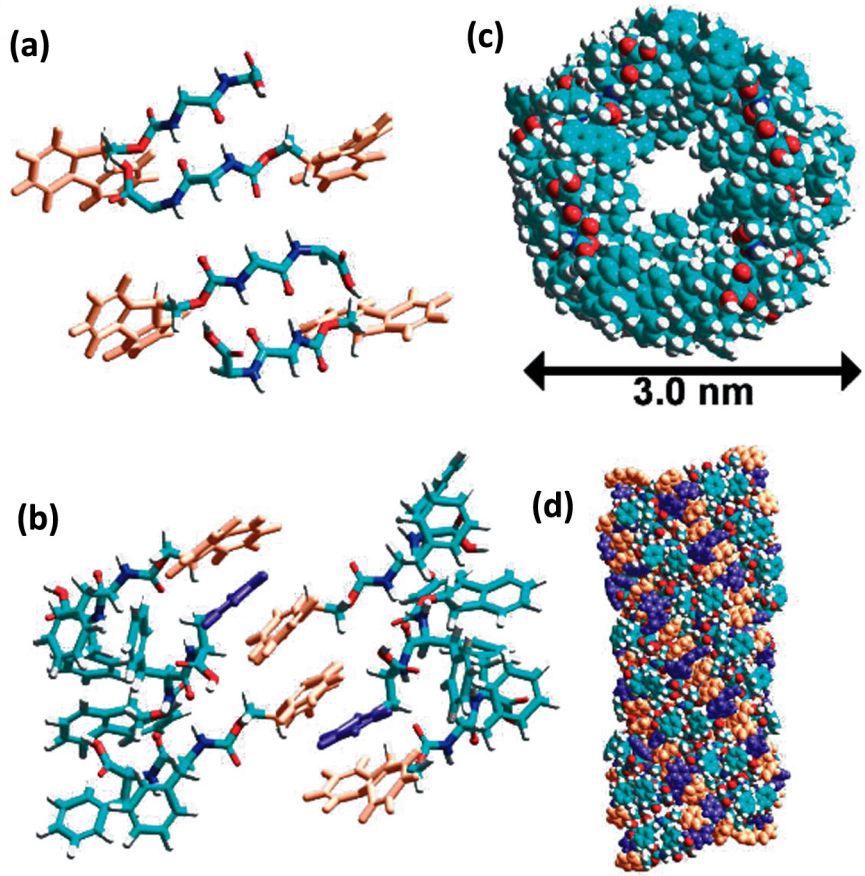

Figure 2.20 Supramolecular structure of Fmoc-FF; (a) interlocked antiparallel arrangement, (b) sheet helicity, (c, d) cylindrical structure, as depicted in.[121]

LLL system, with several β-sheets interlocked *via* aromatic stacking.[147] In this case multiple (e.g. three) β-sheet layers are believed to be associated with a given cylinder – as indicated by WAXS and molecular dynamics simulations. Overall, for both Fmoc-FF and Fmoc-LLL, the curvature associated with the interlocked sheets provides the basis of 1D fibrous/cylindrical assembly, *via* the coiling tape mechanism, as opposed to an infinite 2D sheet.

However, the higher order aggregation mechanism adopted is found to be sensitive to small changes in the peptide sequence, with the sterics associated with peptide side chains a major factor, as has been observed for a range of Fmoc dipeptide methyl ester systems.[79] Here, spectroscopic evidence suggests that the underlying aromatic stacking (e.g. by fluorescence redshift and excimer formation) and H-bonding (by FTIR) processes underpinning the interlocked antiparallel assembly process are similar across the systems; Fmoc-SF-OMe, Fmoc-TF-OMe, Fmoc-SL-OMe, and Fmoc-TL-OMe. In addition, similar characteristic spacings are observed by WAXS; 3.8 Å Fmoc stacking, 4.6 Å β-sheet type H-bonding, and a ~15 Å spacing from the length of the peptide backbone. Despite this, different supramolecular architectures are seen to be dependant upon minimal changes to the

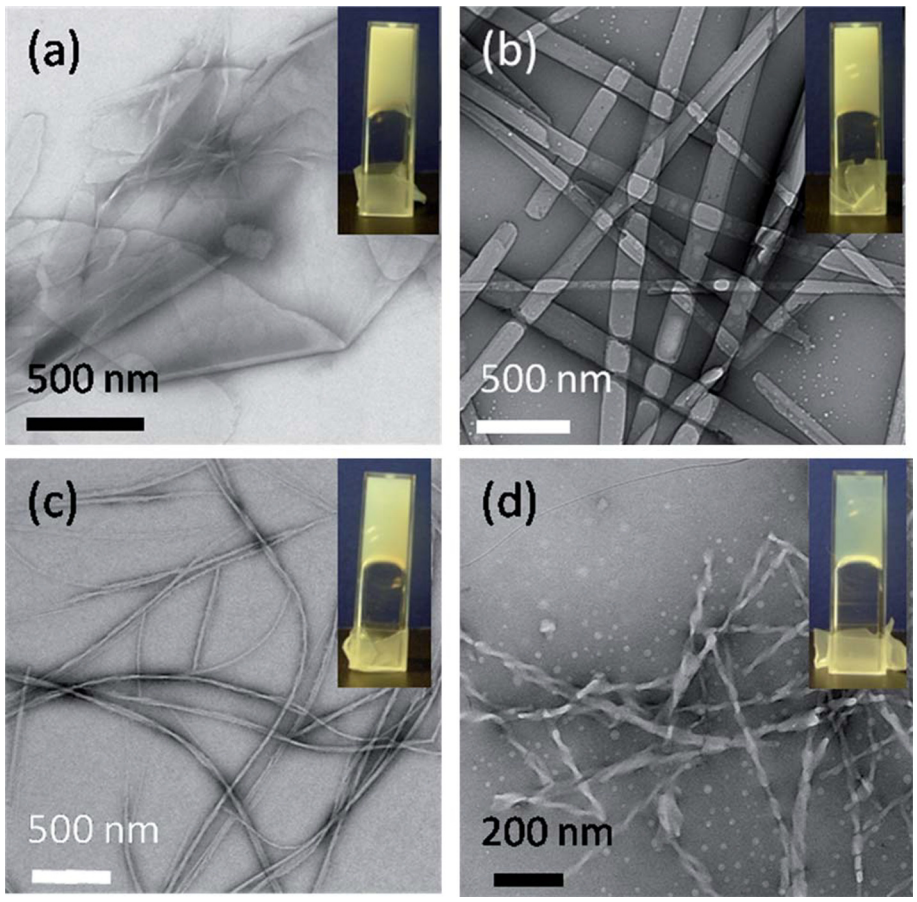

Figure 2.21 TEM images of (a) Fmoc-SF-OMe, (b) Fmoc-SL-OMe, (c) Fmoc-TF-OMe, and (d) Fmoc-TL-OMe based nanostructures. Adapted from.[79]

peptide sequence. For instance, a hydrophilic serine residue adjacent to the Fmoc moiety (Fig. 2.21) induces more planar structures, with Fmoc-SF-OMe being the most dramatic example - exhibiting 2D sheets.[59] In contrast, when serine is substituted for threonine, this promotes the formation of 1D fibres or twisted ribbons. These dramatic morphological differences can be explained on the basis of minimising water contact with the additional methyl group of threonine, thus inducing a twist in the supramolecular structure. Furthermore, the additional chiral centre associated with threonine may also be an important factor here. In any case, Fmoc-SF-OMe is believed to promote a planar structure *via* the formation of a bilayer exhibiting an extensive lateral growth mechanism (e.g. Fig. 2.19 (b)(ii)); with the hydrophobic phenylalanine residues buried within the structure, whilst the hydrophilic serine residues interact with the aqueous phase. These planar structures associated with SF and SL are also supported by a WAXS spacing of ~9.3 Å, which could coincide with the side chain spacings between interacting sheets. It is also possible that these bilayers could assemble further in a lamellar fashion as depicted in Fig. 2.19(b)(i). TEM results suggest a possible mechanism for sheet formation; initially twisted ribbons are observed to undergo branching, while later the nucleation of ribbons can be observed from

the edges of the nanosheets. These apparent intermediary structures indicates that there is a fine balance between the 2D nanostructures observed for this system, and the 1D fibres normally obtained. This is partly ascribed to the reversed hydrolysis enzymatic assembly mechanism used in this instance – a reversible process driven by the attainment of the most thermodynamically favourable nanostructure – hence, it is difficult to directly compare these systems.

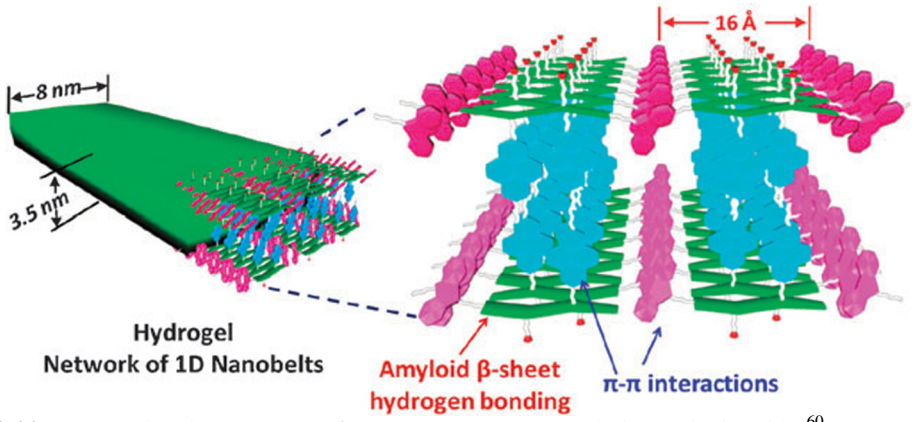

Figure 2.22 Supramolecular structure of Fmoc-KK(NDI) "nanobelt" as depicted in.[60]

In an example that is similar to the hydrophilic/-phobic sequence of Fmoc-SF-OMe, the aggregation of aromatic interlocked antiparallel β-sheets type structures, may also be subject to the lamellar growth mechanism. For instance, the Fmoc-KK(NDI) system is proposed to form "nanobelts" (i.e. bilayer tape structures with limited lateral growth), where the Fmoc interlocked sheets assemble in a face to face manner that utilises the aromatic stacking of the n-type NDI groups, whilst the unfunctionalised lysine residues point outwards into the aqueous medium (Fig. 2.22).[60] Here, stacked K(NDI) side chains and separately stacked N-terminal Fmoc groups stabilise the H-bonded antiparallel dilysine supramolecular arrangement. This material exhibits substantial fluorescence quenching upon self-assembly, and is potentially well suited for 1D charge migration. The supramolecular arrangement is supported by characteristic XRD spacings, and fluorescence emission spectroscopy which suggests orthogonal Fmoc-Fmoc and NDI-NDI aromatic stacks. However the mechanism responsible for inhibiting the continued lateral assembly of the Fmoc interlocked structures is unclear. It is possibly the charge associated with the lysine residues that limits the aggregation mechanism, as if there is a helicity associated with the ribbons (e.g. Fig. 2.19 (a)(ii)) then lateral growth would bring these surface charges into close contact with one another. In addition, the fact that previously described sheets of Fmoc-SF-OMe were assembled under thermodynamic control,[59] suggests that elementary stacking imperfections may contribute to the inherent helicity of the interlocked β-sheet type structures. Elsewhere, an independent study of various Fmoc-peptide (e.g. FF, FRGD, RGDF) gelators has found

XRD spacings of about 4.7 Å and 10 Å, associated with the β-sheet interstrand stacking and lamellar stacking distances, respectively.[62] Here, it was observed that the latter stacking distance was variable depending upon the precise peptide sequence employed. Hence, while the precise mechanism and supramolecular structure may be dependant upon the peptide sequence or gelation protocol utilised, it is clear that supramolecular chirality is important for the formation of 1D nanostructures.

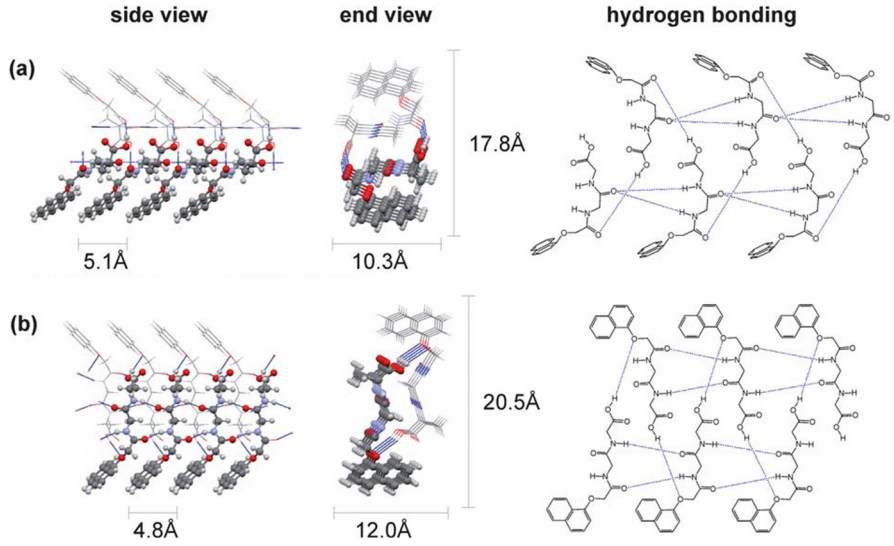

Figure 2.23 An example of a 1D compact stacking arrangement predicted for naphthoxy-GA. Adapted from.[133]

Hence, despite the predominance of 1D aromatic peptide amphiphile nanostructures, 2D structures can also be obtained depending upon the peptide sequence. In this respect, efforts have been made to rationalise similar behavioural differences between a naphthoxy-GA meta-stable hydrogel and a naphthoxy-AG crystalline material.[133] Computed packing arrangements and XRD experiments suggest that 1D H-bonded molecular aggregates are energetically more favourable for the successful gelator, whereas the crystalline material preferentially exhibits a 2D H-bonding network. Both systems demonstrate potential 1D stacking arrangements composed of open tapes, which possess a parallel conformation with aromatic stacking at the periphery, and carboxylic acids H-bonding with one another at the centre between two parallel molecular stacks. However, only the naphthoxy-GA hydrogelator exhibits a significant number of relatively low energy, compact, 1D H-bonding arrangements. These more compact stacking arrangements, similarly feature parallel H-bonding and aromatic stacking interactions, but often with the carboxylic acids H-bonding to an amide carbonyl or the naphthoxy oxygen (Fig. 2.23). In addition, the angle between the aromatic and peptide is also suggested as a reason for the differential self-assembly behaviour of these systems. This is a concept that was previously discussed in section 2.4.2, whereby naphthoxy linkers displayed the greatest potential for hydrogelation on the basis of

a relatively linear molecular conformation.[80] These findings reinforce the complexities associated with supramolecular self-assembly, and reiterate the multitude of proposed stacking arrangements. However, a similar theme re-emerges; the fine balance between 2D crystallisation/precipitation and 1D fibrous hydrogel assembly.

2.5.3 Disorder in the supramolecular assembly

In addition to the proposed supramolecular models that feature a β-sheet type arrangement with ordered aromatic stacking interactions, disorder is likely to be a significant aspect of the supramolecular structure. This is evidenced, by for example the "random coil" type contributions (~1650 cm^{-1}) visible within the FTIR spectra of many gels,[220,66,79,170] with the relative intensity of this band seen to vary, thus indicating a varying degree of disorder and heterogeneity associated with these materials.

For example, from computational stimulations and accompanying experimental data, a model based on a prominent "polyproline II" type conformation (i.e. a supramolecular structure lacking substantial internal H-bonding interactions) has been proposed for the Fmoc-AA system.[174] Computational simulations were initiated using starting structures based upon various parallel stacking conformations; with the aromatic groups concentrated at the core, whilst the peptides point out towards the aqueous interface.[142] Given the limited simulation sizes, edge effects are likely to disproportionately affect the results. In any event, these starting structures were found to be unstable, with a more disordered "polyproline II" type conformation observed after the simulations were completed. In agreement with previous studies,[90] a variety of aromatic stacking arrangements were exhibited by the Fmoc groups. Furthermore, instead of a β-sheet type structure, results showed prominent H-bonding interactions with water and between the carbamate and terminal alanines. Torsion angles[80,133] also inferred an apparent preference for "polyproline II" conformations; although some angles characteristic of antiparallel structures were also observed. Experimentally, WAXS demonstrates the presence of a 4.35 Å spacing, which on account their computational results is assigned to aromatic stacking as opposed to β-sheets. The authors also report some FTIR and CD absorptions typically attributed to β-sheet type structures. However, the authors note that the CD peak positions are shifted with respect to proteins, and the FTIR also shows a prominent absorption at 1644 cm^{-1}, which is assigned to random coil type structures. Similar FTIR results were also demonstrated in a recent study that featured Fmoc-AA.[66] In terms of a higher order assembly mechanism, the authors note that the supramolecular "polyproline II" type structure yields an amphiphilic surface, with some of the Fmoc moieties exposed to the bulk. These hydrophobic features on the surface of the

elementary fibres, may help to facilitate further aggregation mechanisms between fibres, resulting in extensive interconnectivity. Overall, this is an interesting study; however, it is unfortunate that the computational simulations did not consider some of the discussed antiparallel stacking arrangements, particularly since the torsion angle results indicated that this conformation might be favourable. Nevertheless the study highlights that disorder is likely to be a significant factor in the supramolecular assembly of aromatic peptide amphiphile materials, and that protein secondary structure analogies should be applied with a degree of caution.

2.5.4 Worm like micelles at high pH

As discussed previously in sections 2.4.4.1 and 2.4.4.2, the supramolecular assembly of aromatic peptide amphiphiles is also sensitive to environmental factors. For instance, one fairly intuitive proposal is the adoption of worm like micelle structures at high pH, with the charged carboxylates at the surface and the aromatic moiety buried in the core.[153] The presence of worm like micelles has been inferred by sample viscosity and *via* the observation of structures by TEM at high pH. Here, crosslinking of the surface carboxylates could also be facilitated using divalent cations to improve the network integrity. Supporting the cation crosslinking worm-like micelle model is the observation that the gelation of various naphthoxy-dipeptide derivatives at high pH is most easily facilitated by divalent cations such as Mg and Ca, as opposed to monovalent Li, Na, or K.[153] Furthermore, divalent species increase the elastic moduli of these systems by over an order of magnitude. There is also some dependence on the counter ion, but these rheological differences are far less dramatic. Hence, crosslinking interactions between worm like micelles allow for aromatic peptide amphiphiles to undergo hydrogelation over a wider pH range, altering the morphology and properties of the fibrous network in the process. The worm like micelle model also makes sense within the context of an amphiphilic species, whose bulky aromatic most likely precludes the formation of spherical aggregates. In addition, these high pH systems are inherently more disorganised, since these structures lack the ordered H-bonding arrangements normally associated with peptide amphiphiles.[220,77] This pH dependant, and ultimately distinct supramolecular structure associated with aromatic peptide amphiphiles, simply represents a different, more disordered, stage of the aggregation process before the pH is lowered, and before extended H-bonding begins to lock the network into place.[131] Since TEM fibrils and fluorescence emission peaks at ~375 nm corresponding to micellar aggregates have been reported for Fmoc systems at high pH,[220,77] and a preference for parallel stacking interactions between Fmoc moieties have been inferred by molecular

dynamics simulations at relatively low (virtual) subgelation concentrations,[204] we believe that micellar aggregation is a more general phenomena associated with aromatic peptide amphiphiles while in the relatively ionised state – the addition of divalent cations simply allows for gelation to take place under these conditions.

2.6 Hydrogelation: Concentration and temperature dependence

Besides pH and ions, other environmental factor such as temperature and the gelator concentration also have an impact on self-assembly, gelation, and the properties of aromatic peptide amphiphile materials. As discussed previously, self-assembly is governed to a large extent by the apparent pK_a of a given gelator. However, the apparent pKa is also sensitive to the concentration of the gelator - increasing in line with concentration before reaching a plateau.[220] In addition, gelation is also temperature dependant, as the strength of intermolecular interactions is heavily influenced by temperature; for example at elevated temperatures, aromatic stacking interactions begin to form before a H-bonding network is established.[63] So all of these thermodynamic factors are in fact interlinked, and have a profound effect on the gelation process.

Altering the final concentration of the gelator, has an intuitive impact upon the properties of the resultant hydrogels; with higher concentrations resulting in more rigid materials.[107] The generality of this rule stems from the fact that supramolecular hydrogelators typically have an associated minimum gelation concentration.[84,159,234] Of course, the minimum gelation concentration does not necessarily correspond with the critical aggregation concentration; fibres may simply be too diffuse to form a coherent network or fail to coalesce because of electrostatic repulsion. In any event, the concentration of the gelator is one of the primary factors that influences the properties of hydrogel materials, with the minimum concentration differing greatly, depending upon the molecular structure of gelator concerned, and prevailing conditions such as pH.

This relationship between hydrogel properties and gelator concentration is also reflected in an increasing gel-solution transition (T_{gel}) temperature as the concentration of the gelator is increased.[134,162,159] Firstly these results reiterate that, as would be anticipated, higher concentrations result in a more dense fibrous network, which in turn enhances the rigidity and stability of the supramolecular network. However, the interdependence between concentration and T_{gel} highlights the importance of temperature in the self-assembly process. Most hydrogels exhibit a T_{gel} temperature, above which the supramolecular network breaks down and a gel to solution transition takes place. Hence, by exploiting the T_{gel} parameter it is

possible to prepare hydrogels *via* a heat-cool cycle.[150] This process is easily reversible and can be repeated without a significant impact upon the properties of the final material.[111] In addition, hydrogels prepared using a heat-cool cycle often have properties which are distinct from those prepared using alternative methods (e.g. pH switch etc).[179] Temperature affects the entire sample, and the rate at which the sample is cooled can be precisely controlled. Hence, by using temperature the self-assembly process can be allowed to progress over a longer time period before the system becomes kinetically trapped in the gel state. In this way, arguably, a more thermodynamically favourable supramolecular network can be obtained.

$$\Delta G_{mix} = \Delta H_{mix} - T\Delta S_{mix}$$

Four possibilities:

			ΔG_{mix}	
	ΔH_{mix}	ΔS_{mix}	As $T \rightarrow 0$	As $T \rightarrow \infty$
(a)	+	+	Precipitate	Solution
(b)	-	-	Solution	Precipitate
(c)	+	-	Precipitate	Precipitate
(d)	-	+	Solution	Solution

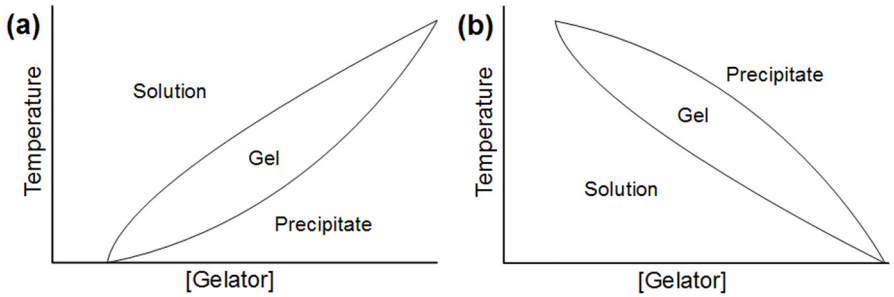

Figure 2.24 Simplified free energy description of gelation process. (a) and (b) can potentially allow gelation between precipitate and solution phases depending upon temperature/concentration, whereas in (c) and (d) gelation cannot occur as "compound" is too (in)soluble at all temperatures. Note that more than one of these mechanisms could apply to a given gelator depending on pH for example. In addition, above scheme makes the false assumption that intermolecular force strengths are independent of temperature.

For example, a heat-cool protocol is found to increase the rate of assembly associated with Fmoc-F based materials prepared using the DMSO dilution method.[143] Furthermore, heating has been found to help induce the gelation of Fmoc-GG and Fmoc-FG prepared *via* pH adjustment.[77] Here, heating followed by subsequent cooling is believed to facilitate the dispersion of kinetically trapped aggregates, resulting in more reproducible and continuous gel phase materials.[131] In the majority of instances increasing the temperature intuitively

increases the solubility of the gelator - *via* the disruption of H-bonding between water molecules, which negates the entropic penalty of mixing. However, some examples, such as Fmoc-AA have been observed to precipitate upon heating,[87] this lower critical solution temperature type behaviour seems to indicate an enthalpic contribution to the self-assembly process between gelator and surrounding water molecules for some systems, which becomes entropically disfavoured at higher temperatures. Ultimately, with respect to concentration and temperature, gelation can be thought as metastable kinetically trapped state, where the free energy of mixing (between water and gelator) is close to zero, such that nanoscale phase separation takes place as opposed to spontaneous bulk phase separation (Fig. 2.24). As discussed in the next section, the kinetically trapped nature of the gel state has important implications for the preparation of aromatic peptide amphiphile based hydrogels under kinetic control.

2.7 Kinetic considerations: the route of self-assembly

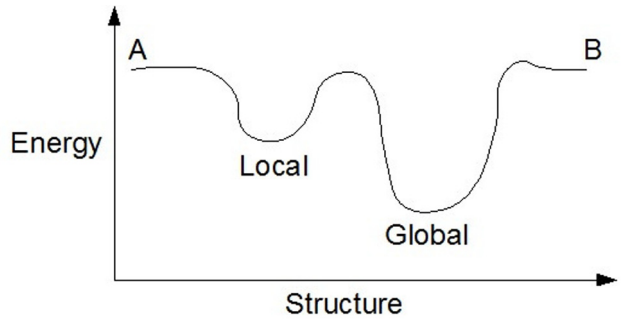

Figure 2.25 Simplified illustration of a slice through the supramolecular energy landscape – featuring a local and global minimum that are (in)accessible depending upon the generic self-assembly route (e.g. A or B).

As is clear from the above, self-assembly is an extremely versatile process, driven by various intermolecular interactions that are inherently dependant upon the molecular structure of the gelator in question, and prevailing environmental conditions such as pH, concentration, and temperature. However, another important aspect that can be considered is the means by which self-assembly is effected.[235,85] Ultimately, most hydrogels are thought to be kinetically-trapped, meta-stable materials (with the phase-separated, crystalline form ultimately representing the lowest free energy state). A single gelator can potentially access a variety of supramolecular structures, depending upon the self-assembly protocol (conditions, kinetics) utilised (Fig. 2.25). This allows the formation of highly diverse materials from identical building blocks. Seemingly simple parameters, such as the adjustment of pH is a complex balance between encouraging the thermodynamically favoured aggregation of the gelator below its pK_a, and kinetic/heterogeneity considerations.[123,156] In contrast, enzymatic

processes can utilise an inactive gelation precursor, which can be converted to the relevant self-assembling monomer in a controlled fashion.[63] More generally, by altering the route of self-assembly, the precise properties of the resultant materials can be changed, even if the underlying chemical compositions are identical. Hence, in this section we will consider some of the common gelation initiation methodologies, and the corresponding kinetic aspects that can influence aromatic peptide amphiphile based materials.

2.7.1 Dilution method

A relatively simple, but effective, hydrogel formation strategy involves adding a concentrated solution of the gelator to water. The concentrated solution of typically 25 to 100 mg cm^{-3} is made up in a solvent capable of dissolving the species such as DMSO,[82,83,143,151] methanol,[170] or hexafluoroisopropanol.[107] Upon dilution in water, the gelator undergoes self-assembly to minimise unfavourable interactions with the aqueous environment. This procedure has been utilised successfully for a variety of peptide amphiphile systems, including Fmoc-FF. Ultimately, this dilution method yields a kinetic product – assuming that the self-assembly and gelation begins on a faster timescale than sample mixing. Hence, this diffusion controlled methodology is unlikely to give the most thermodynamically stable structure. In addition, some systems, which are able to assemble *via* the dilution method, are unable to gel using different initiation methods, despite possessing similar final conditions. For instance, it is reported that *via* sonication of aqueous Fmoc-FF it is possible to obtain an aqueous solution, but no self-assembly occurs, whereas the DMSO dilution methodology facilitates gelation.[135] However, this result could equally be a consequence of the DMSO co-solvent affecting the self-assembly process,[177] with hydrogel properties found to differ considerably depending upon the volume fraction of DMSO utilised in their preparation.[154]

2.7.2 pH: as a kinetic trigger

2.7.2.1 Dropwise addition

Most commonly the pH is altered *via* the dropwise addition of acid (e.g. HCl) to an alkaline solution (e.g. NaOH) of the gelator. [64,155,121,164,111] As seen previously, pH based initiation can also be combined with other gelation parameters such as temperature, in order to help maintain sample homogeneity during the addition of acid.[77,84] As one of the major issues with the dropwise pH adjustment method, is achieving a consistent pH change throughout the sample. Unlike the aforementioned heat-cool method, dropwise addition does not occur simultaneously throughout the sample. Instead, after dropwise addition of acid, often a more

localised gelation is observed. Ultimately this leads to more heterogeneous materials, which can be difficult to reliably reproduce. Hence, the dropwise pH method leads to a kinetic product, which is highly dependant on the individual performing the experiment.

Due to the local nature of dropwise addition, the mechanics associated with the gelation process can be crucial in determining the properties of the resultant hydrogels.[156] Usually vortexing is applied to samples in between acid additions in order to try to minimise local pH variations. The precise nature of the agitation protocol utilised, has been found to result in gels that exhibit moduli differences of up to an order of magnitude, by rheology. In addition, differences in the material properties have also been found to be reflected in subtle morphological differences associated with the fibrous networks. These trends are difficult to rationalise, but ultimately highlight the susceptibility of the kinetic hydrogel product to small changes in the adopted dropwise pH protocol.

2.7.2.2 GdL decomposition

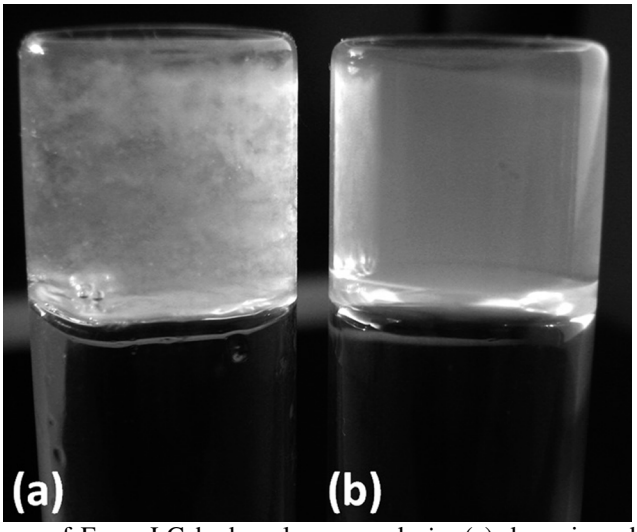

Figure 2.26 Appearance of Fmoc-LG hydrogels prepared *via*: (a) dropwise addition of acid; or (b) GdL decomposition. Adapted from.[123]

In order to address the reproducibility issues associated with the dropwise addition method, hydrogels are frequently prepared using compounds such as GdL,[133,132,137] which when added decompose to alter the pH gradually, allowing for more controlled gelation.

GdL hydrolysis occurs more rapidly at higher pH and temperature, and results in the slow release of gluconic acid over the course of several hours.[123] NMR results indicate that GdL is not incorporated into the gel fibres, instead remaining largely solvated in the aqueous phase. The corresponding pH drop is significantly slower than the rate of dissolution, such that the material properties of the final hydrogels do not depend upon, for example, mixing. This also has the advantage of allowing the gelation process to be monitored in real time using for example, TEM, fluorescence, rheology, and (despite the CD signature of GdL itself[236]) CD.[61]

The results indicate that at high pH, aggregation is primarily driven by the aromatic stacking of Fmoc groups – potentially in a worm-like micelle structure (see section 2.5.4). As the pH is lowered the fibrous network becomes more extensive and the supramolecular chirality is observed to increase over time; presumably corresponding with the development of a more extensive H-bonding arrangement, as the electrostatic repulsive forces between gelator molecules decrease. Overall, the resultant hydrogels appear more transparent and possess far more homogeneous structures and hence more reproducible properties (Fig. 2.26).

Not only are the properties of hydrogels prepared using GdL often more reproducible. Some hydrogels such as Fmoc-LG, are also found to exhibit a higher elastic modulus (e.g. 184 versus 5.9 kPa) when prepared using the GdL methodology, compared with equivalent gels prepared using dropwise pH.[81,123] This reiterates the importance of the kinetics of the initiation method towards the supramolecular properties. During the GdL mediated gelation process, the evolution of the sample pH is found to depend strongly upon the gelator in question – with different apparent pK_a values observed in each case. As discussed previously, the observed pK_a is thought to correspond with the commencement of the assembly process. As a consequence of the different apparent pK_a values and corresponding maximum gelation pH values associated with distinct hydrogelators, it is desirable to be able to control the final pH. With GdL a predetermined concentration can be added, which dictates the final pH of the resultant hydrogel.[61,78,177] Interestingly with the GdL method, when the apparent pK_a is reached, the pH begins to rise slightly for a period of time before beginning to decrease again.[81] This is an indication that GdL hydrolysis occurs on a slower timescale than the assembly process itself, and hence GdL is unable to release protons faster than the supramolecular construct absorbs them as assembly proceeds. Hence, the much slower and controlled kinetics associated with GdL hydrolysis mean that the gelator potentially has more time to assume an optimal supramolecular structure before being kinetically trapped in the gel state. In this way, despite the fact that the final pH conditions may be identical, the GdL method is likely to yield a more thermodynamically favourable hydrogel product than for example dropwise addition of HCl.

2.7.2.3 Localised gelation under pH control

Due to the influence of pH upon the assembly of aromatic peptide amphiphiles, potentially the self-assembly and gelation of these materials can be coupled to any chemical process that releases protons. For example, it has been demonstrated that the hydrogelation of various peptide amphiphiles can be triggered using UV irradiation.[176] This process is mediated *via* a photo acid generator, which is found to induce a local pH change upon exposure to radiation. Hence, using this methodology it is possible to induce local self-assembly and gelation by

utilising a UV mask. It can thus be envisaged that a similar technique could be used to prepare surfaces patterned with hydrogel, in a manner similar to the photolithographic preparation of polymeric devices.[237]

In addition, electrochemistry is extremely versatile, and has also been applied in the pH activation of self-assembling systems.[140] For example, self-assembly was achieved *via* an electrochemically induced change in the local pH, effecting gelation of Fmoc-LG below pH 4. The local pH changes were brought about *via* the anodic two-electron oxidation of hydroquinone to 1,4-benzoquinone, thus releasing two protons at the surface of the gold electrode. Although a pH drop could also be induced in the absence of hydroquinone, this inevitably requires a greater potential difference and results in degradation of the electrode surface. In any event, the electro-deposition process produces a layer of the desired hydrogel, which can only form within the low pH region. The membrane thickness (e.g. 0-100 nm, though ~1 mm layers are also reported) can be controlled to some extent by altering the time and magnitude of the applied current. The diffusion of protons into the bulk allows for the continued growth of the hydrogel once the current has been turned off. In addition, this procedure can be reversed with dissolution of the hydrogel membrane when a reversed bias is applied. This technique could potentially be applied in the preparation of multilayered materials.[238] Similar results have also been reported for the electro-deposition of Fmoc-F,[161] indicating the generality of this process. Overall, this procedure is most likely to find applications in the micro patterning of hydrogels onto a surface.

2.7.3 Enzyme responsive self-assembly

In nature, self-assembly processes are normally regulated as opposed to exhibiting unattenuated aggregation in the bulk; for example, in response to stimuli, actin and tubulin dynamically form microfilaments and microtubules, respectively.[239–242] Laboratory methodologies that utilise enzymes in the self-assembly process have recently attracted attention, and generally involve conversion of inactive precursor(s) to a self-assembling product.[4,243,244,114,109,245] For instance, β-lactamase has been applied to substrates containing β-lactam (cyclic amide) rings, resulting in ring opening and subsequent rearrangement to a suitable supramolecular building block.[115] In the majority of cases the conversion of substrate to product is thermodynamically favourable, and for all intents and purposes irreversible. For these examples, enzymes are a means of accessing a range of kinetic products; since nucleation and fibre growth is likely to take place within the immediate vicinity of the enzyme itself. Hence, by adjusting the enzyme concentration, the number of potential nucleation sites can be altered, which will have consequences for the properties of

the resultant supramolecular constructs as discussed below.

2.7.3.1 Subtilisin

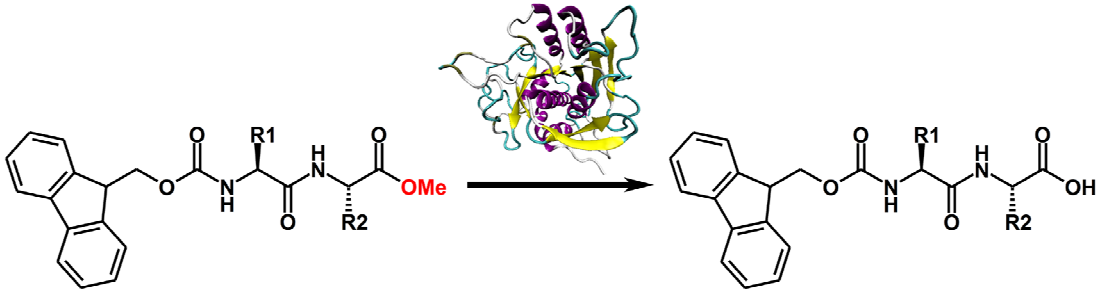

Figure 2.27 Subtilisin catalysed methyl ester cleavage of a generic aromatic peptide amphiphile.

A common enzymatic process in the field of aromatic peptide amphiphile self-assembly, is the subtilisin-catalysed hydrolysis of a methyl ester (Fig. 2.27). Although as discussed in section 2.4.4.3, there are examples of methyl esters that are able to undergo hydrogelation,[124] in the majority of cases they prove too insoluble and instead are used as precursors.[147,171] It has been shown that the hydrogel stability, as assessed by the T_{gel} temperature, increases with higher subtilisin concentrations.[63] This indicates that additional fibre nucleation sites are beneficial to the integrity of the supramolecular network. In addition, this was also reflected in an increased supramolecular ellipticity by CD, and increased fluorescence quenching with higher subtilisin concentrations. Furthermore, in terms of morphology the lower enzyme concentrations resulted in shorter fibres that exhibited less bundling. To further support the fact that these observations are due to the kinetic influence of differing enzyme concentrations, when the enzymatic hydrogels are subjected to a heat-cool cycle, the results are essentially identical – with each sample exhibiting a T_{gel} characteristic of a high enzyme concentration. The other striking aspect of the subtilisin based hydrogelation strategy, is the observation that the handedness associated with the supramolecular structure is often reversed relative to gels prepared under pH control.[179] The reason behind this is unclear, though it can be hypothesized that various supramolecular orientations are possible, and that the predominance of one over the other is sensitive to the kinetic aspects of the self-assembly process already discussed.

2.7.3.2 Alkaline phosphatase

Alkaline phosphatase has also been used extensively for hydrogel preparation *via* the cleavage of an attached phosphate group – usually a tyrosine residue (Fig. 2.28).[76,126,116,90,108] In contrast, to methyl esters, phosphorylated precursors are more soluble than the desired gelator products. However, it has been suggested that in certain instances some unreacted phosphorylated substrate incorporated into the fibres can be beneficial in terms of assembly;

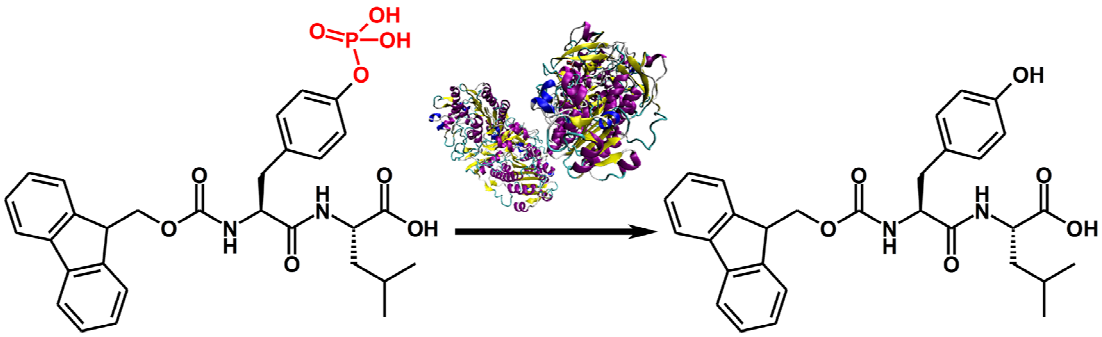

Figure 2.28 Alkaline phosphatase catalysed phosphate cleavage of an aromatic peptide amphiphile.

particularly if the product itself is normally too hydrophobic to undergo hydrogelation.[125] Enzymatically controlled gelation, has been exploited as a means of testing phosphatase inhibitors – providing a simple visible assay.[91] Similar to subtilisin mediated gelation, higher concentrations of phosphatase are found to increase the supramolecular order associated with the resultant gel network.[130] This was demonstrated by the increased elastic modulus of the dephosphorylated Fmoc-Y gels with higher phosphatase concentrations. In addition, enzymatic gels were stronger and exhibited a finer fibre morphology from those prepared under pH control. Again these differences are thought to be a consequence of the kinetics associated with the enzymatic process, whereby the number of fibre nucleation sites is more precisely controlled.

Alkaline phosphatase has also been observed to cause dramatic morphological changes, such as micelle to fibre transitions as inferred by the release of a pyrene probe.[145,184] In this way chemical energy is effectively being converted into mechanical energy, during the reconfiguration of the supramolecular structure. The cleavage of the phosphate group is also potentially a reversible process, and gel-sol-gel transitions have been demonstrated through the utilisation of a two component enzyme system – comprising of kinase and phosphatase.[110] Overall, phosphatase controlled gelation has potential utility for injectable hydrogels, that could potentially undergo self-assembly in response to phosphatase present *in vivo*. Furthermore, phosphatase mediated substrate conversion and consequent fibre formation has been observed inside of living cells.[246] In these respects phosphorylated precursors are preferable to methyl esters; whose insolubility, coupled with the higher temperature requirements of the subtilisin based conversion, renders them of less biological relevance.

2.7.3.3 Thermolysin

Subtilisin and phosphatase mediated initiation processes are based upon thermodynamically favourable reactions. However in other instances, reactions which are unfavourable can be driven *via* the self-assembly process itself. Such a situation is encountered with thermolysin,

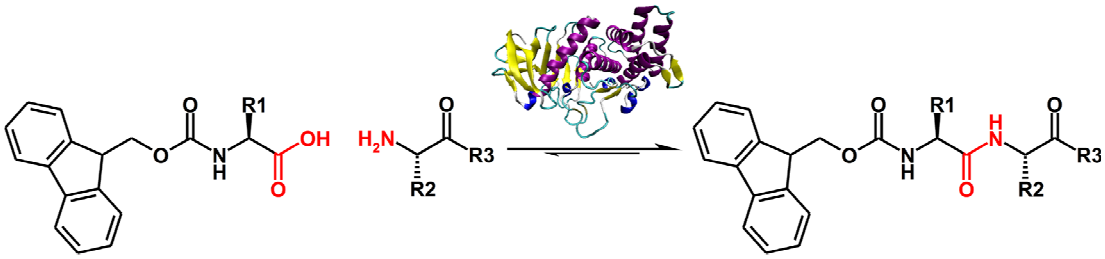

Figure 2.29 Thermolysin catalysed amide coupling yielding a generic aromatic peptide amphiphile. Note that this process is reversible, with the equilibrium driven to the right by the free energy associated with the self-assembly process.

which normally acts as a protease to hydrolyse substrates. Despite this, thermolysin can be utilised in such a way that amide bond formation becomes the predominant process (Fig. 2.29).[79,146,112] Here, the reversed hydrolysis reaction is driven by the formation of the thermodynamically stable supramolecular hydrogel structure.

In addition, because the thermolysin based amide coupling is inherently reversible, these systems are believed to preferentially yield the more thermodynamically favourable supramolecular structure. Promoting in certain cases, for example, the formation of two dimensional nanostructures over the more conventional one dimensional fibres.[59] Thus imperfections in the supramolecular structure can be corrected as the system strives towards the thermodynamic product, as opposed to a less stable kinetic product. The thermodynamic driving force can also lead to the evolution of the molecular composition over time.[3] This concept was demonstrated succinctly with a system composed of Fmoc-L and L_2, which initially gave rise to a supramolecular structure dominated with Fmoc-L_3. However, as time progressed Fmoc-L_5 formation was accompanied by a restructuring of the supramolecular network, to a more thermodynamically stable system. This ability of thermolysin to self select the optimal peptide sequence has been repeatedly exploited for DCL systems.[187] These DCLs allow thermolysin to cleave and form amide bonds from a variety of potential substrates as appropriate – the hypothesis being that the most favoured product, in terms of self-assembly, will eventually predominate. For instance, although kinetics may initially determine the product distribution - with thermolysin observed to have a preference for hydrophobic residues - over time an equilibrium is reached.[124] (Furthermore, thermolysin has also been utilised in conjunction with subtilisin to induce solution-gel-solution transitions.[120]) Hence, for the thermolysin mediated reversed hydrolysis of aromatic peptide amphiphiles, not only do we have the usual kinetic considerations in terms of enzyme concentration correlating with the number of fibre nucleation sites. There are also thermodynamic considerations with a reversible system capable of correcting supramolecular "defects". Ultimately enzymes grant access to a greater proportion of the supramolecular energy landscape, with a higher degree of precision than many of the other initiation

techniques already discussed.

2.7.3.4 Non-equilibrium self-assembly

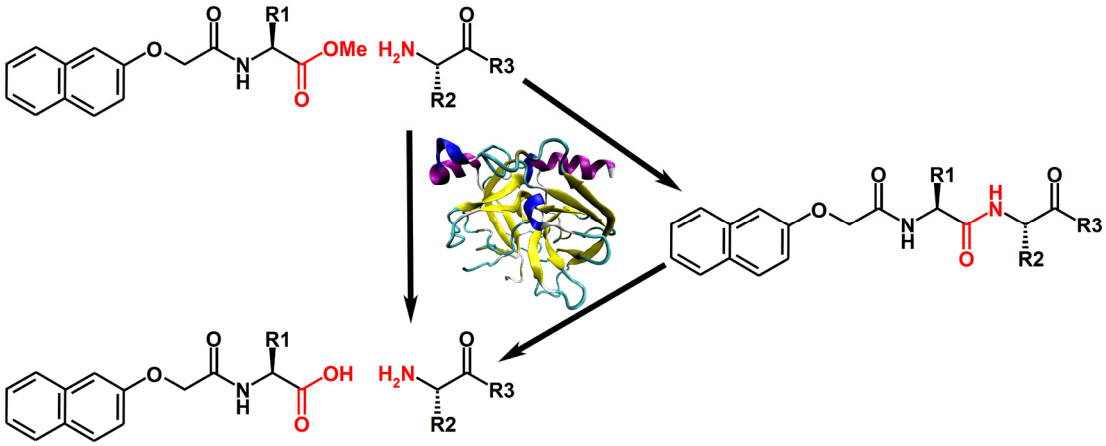

Figure 2.30 Chymotrypsin catalysed amide coupling and respective hydrolyses. Gelator (right) is a non-equilibrium product such that hydrogelation is temporary or fuel dependant.

For all the aforementioned enzymatic systems gelation is the equilibrium state, and unless interfered with the corresponding hydrogels are relatively stable. However, non-equilibrium self-assembly is also of interest, in part because this more closely resembles what is observed in natural systems – where energy input is required even for homeostasis.

Recently, non-equilibrium self-assembly has been demonstrated for aromatic peptide amphiphiles using the enzyme chymotrypsin (Fig. 2.30).[201] Here, the naphthoxy-YY-NH_2 gelator is formed *in situ* from the enzymatic amide coupling of the corresponding naphthoxy-Y-OMe and Y-NH_2 starting materials. However, the competing enzymatic hydrolyses of starting material and gelator "product" mean that the system tends towards a solution of naphthoxy-Y and Y-NH_2. However, the system is able exceed the critical gelation concentration of naphthoxy-YY-NH_2 for several hours before reverting to a solution once more. In addition, the refuelling of the system with additional naphthoxy-Y-OMe substrate has been demonstrated - unfortunately this can only be repeated a finite number of times before becoming saturated with naphthoxy-Y. Ultimately, this is an interesting non-equilibrium self-assembly example, but could be improved upon if a more elegant means of refuelling the methyl ester starting material was realised.

2.7.3.5 Other considerations

Aside from co-assembly with other gelators (see section 2.8), the hydrogelation process can be heavily influenced by the addition of other additives, this may have ramifications for the enzymatic methods described above.

For example, binding to vancomycin – an antibiotic – can induce the gel-to-sol transition of the Fmoc-(D-)A(D-)A system.[87] Interestingly, the stereoisomer, Fmoc-AA, is relatively

insensitive to the addition of vancomycin – indicating that the binding mechanism responsible is stereochemically selective. Furthermore, morphological studies of Fmoc-(D-)A(D-)A demonstrate the complete collapse of the fibrous supramolecular network upon vancomycin addition. In comparison, a related study shows that the addition of vancomycin to a pyrenyl-(D-)A(D-)A derivative actually causes an enhancement in the elasticity of the hydrogel.[89] Again a binding mechanism is proposed, but in this instance the precise orientation of the complex also facilitates self-association between adjacent vancomycin molecules in addition to the pyrenyl-(D-)A(D-)A supramolecular stacks. The impact of vancomycin (sometimes as low as 0.01 eq) binding upon the self-assembly properties of these systems is remarkable. However, these observations also have potential implications for enzymatically assembled peptide amphiphile systems – where it can be envisaged that similar recognition mechanisms are possible.

Furthermore, even weakly interacting additives can have an impact upon the assembly and hydrogelation of aromatic dipeptide amphiphiles. For example, dextran has been shown to increase the gelation time, and decrease the elastic moduli associated with a naphthoxy-AG derivative.[137] These effects are believed to be mediated *via* an increase in the viscosity of the aqueous medium, thus slowing diffusion and self-assembly rates in a linear fashion with respect to dextran concentration.

The binding specificity of aromatic peptide amphiphile based hydrogels with various proteins has been investigated.[247] Here, a hydrogel protein pull-down assay revealed that tubulin and various other intracellular proteins of HeLa cells were bound to the hydrophobic nanofibres. In addition, nanofibre-glycoprotein binding interactions have been inferred from the gelation of naphthalene-FFG upon the surface of platelets - this surface coating acts to inhibit platelet aggregation *via* electrostatic repulsion.[248] Elsewhere, the gelation of a relatively hydrophobic naphthalene-GFFY derivative is found to be dependant upon the presence of bovine serum albumin.[249] In the absence of bovine serum albumin, precipitate is formed, with the compound unable to form a stable dispersion in water. In contrast, bovine serum albumin is able to help stabilise the hydrophobic fibres and prevent the formation of insoluble aggregates. Hence, these examples show the generality of protein-nanofibre interactions, and illustrate their potential impact upon the self-assembly process.

In another study the co-assembly of bovine serum albumin or β-lactoglobulin with various Fmoc-dipeptides (YL, YN, YS, and VL) is found to have significant consequences for the supramolecular organisation and physical properties of the resultant hydrogels.[250] Here, even at concentrations of ≤ 0.2 %wt, the proteins are observed to form "fractual-like clusters", where the slower relaxation dynamics of these clusters are believed to affect the aromatic

peptide amphiphile gelation process by inhibiting solution mobility. In terms of material properties, self-assembly in conjunction with protein is found to increase the elastic moduli of the hydrophobic Fmoc-dipeptides (YL and VL), although at higher protein concentrations (0.2 versus 0.03 %wt) this enhancement is less evident – indicating an optimal protein:Fmoc-dipeptide ratio. In contrast, the elastic moduli of the relatively hydrophilic Fmoc-YN and Fmoc-YS systems is found to deteriorate with protein co-assembly. The influence of this co-assembly process can also be monitored spectroscopically, where for example the supramolecular chirality of Fmoc-YL is completely reversed, and the associated fluorescence emission somewhat quenched, upon assembly with β-lactoglobulin. Similar trends are also observed with Fmoc-YL and bovine serum albumin, however, in this case the effects are less pronounced – indicating that the increased hydrophobicity associated with β-lactoglobulin may responsible for this difference. In any event, the addition of protein is consistently found to favour the opposite chirality of that associated with the Fmoc-dipeptide alone – this is similar to the chiral inversion often observed for enzyme catalysed hydrogelation. The generality of this phenomenon suggests a templating effect is ultimately responsible, hence, secondary effects associated with any enzymatic additives is a potential aspect of the assembly process that should be taken into consideration.

2.8 Co-assembly of aromatic peptide amphiphiles

Finally, the co-assembly of different gelators can be a useful means of modifying the properties of the resultant hydrogel materials in a modular fashion.

2.8.1 Co-assembly: energy transfer

For instance, through the co-assembly of molecules bearing different aromatic moieties, it is possible to incorporate a variety of aromatic groups in a single system – a strategy that can help stabilise aromatic stacking interactions *via* complementary interactions. In this way intermolecular energy transfer mechanisms can be observed between the respective fluorophores.[251–254] For instance, a dansyl acceptor/naphthalene donor system has been demonstrated, whereby the naphthalene-diphenylalanine derivative forms fibres based partly on aromatic stacking interactions, with the dansyl component intercalating within this construct (Fig. 2.31).[136] In addition, this study also showed an energy transfer mechanism between co-gelating peptide amphiphiles, with naphthalene continuing to act as a donor to an anthracene based amphiphile acceptor. In both cases, energy transfer is shown by a redshift in the fluorescence emission and the corresponding quenching of the emission associated with the donor species. Similarly, functional co-assembly has recently been demonstrated

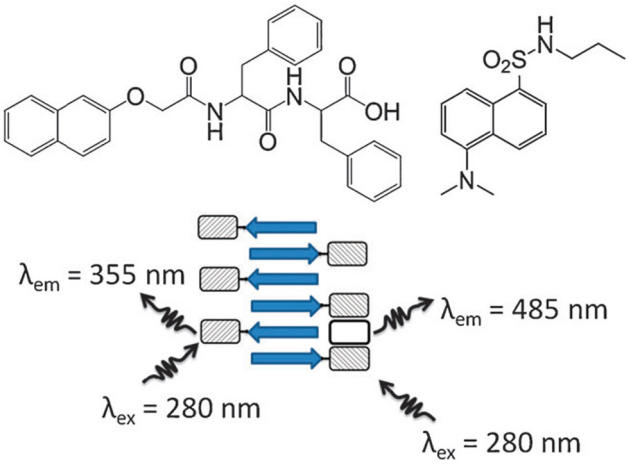

Figure 2.31 (left) Napthoxymethyl-FF; (right) dansyl derivative; (bottom) depiction of the energy transfer mechanism *via* the intercalation of dansyl within the supramolecular structure. Adapted from.[136]

using a DCL approach that incorporated a dansyl derivative acceptor, which intercalates with a naphthalene donor based peptide amphiphile.[187] In this case, the enzyme thermolysin mediated the selection of gelator candidates *via* a reversible peptide coupling process, in order to attain the most thermodynamically favourable hydrogel system, where free energy of the gelation process actually drives the equilibrium. Here, the enzymatic conversion to yield the YF sequence was seen to increase with the inclusion of the dansyl derivative. Hence, this example demonstrates that the inclusion of an acceptor molecule can potentially increase the aromatic stacking interactions within the nanostructure, improve the stability of an existing hydrogel system, and possibly attain materials with some degree of electroconductivity.[147]

2.8.2 Co-assembly: hydrophobicity, charge and chirality

Given that the self-assembly and gelation properties of aromatic peptide amphiphiles are strongly influenced by the overall hydrophobicity of the peptide sequence, it makes sense to further tune this attribute *via* co-assembly. This methodology assumes that co-assembly components yield a mixed supramolecular structure, featuring the usual aromatic stacking and H-bonding interactions between the constituents.[90,88] For example, a 1:1 ratio of Fmoc-FF and Fmoc-GG produces hydrogels with higher elastic moduli than Fmoc-FF alone.[156] This is despite Fmoc-GG failing to gel individually under similar conditions. In this instance, the optimal 1:1 molar ratio suggests that regular (possibly alternating) intercalation of Fmoc-GG into the Fmoc-FF fibres provides an effective balance for gelation. In comparison, Fmoc-FF/Fmoc-RGD hydrogels show the largest elastic moduli with a 1:4 molar ratio of Fmoc-RGD to Fmoc-FF content.[65] Similarly, this is indicative of Fmoc-RGD becoming an integral part of the Fmoc-FF fibrous structure. The co-assembly of Fmoc-FF, with Fmoc-K,

Fmoc-S, or Fmoc-D similarly resulted in significant changes to rheological properties and fibre morphology.[127] Though it should also be noted that the rheological properties of the Fmoc-FF system are generally very sensitive to the preparative conditions employed.[177] Nevertheless, these results indicate that tailoring the hydrophobicity of Fmoc-FF fibres is a useful strategy for augmenting the hydrogelation properties of the system.

In other co-assembly examples, gelators can be chosen that have complementary characteristics. For example, when penta-fluorinated or mono-halogenated Fmoc-F derivatives are co-assembled with unfunctionalised Fmoc-F, this process is assisted by complementary interactions between the phenyl side chains, which possess differing electronic properties.[163] Given that penta- and mono- substituted derivatives gave similar enhancements in rheological properties; this is not believed to be mediated by face-to-face stacking of the phenyl groups, instead electronic effects from the halogen substituent(s) are believed to result in more subtle offset π- π interactions. Similarly, electrostatics also has a role to play in the co-assembly of aromatic peptide amphiphiles, with oppositely charged Fmoc penta and hexa peptides co-assembling in this manner.[148] Individually, positively (KKRGDK) or negatively charged (VRGDV, GRGDG) peptides could assemble, but only in the co-assembly setup, where the charge is balanced, could gelation be effected at a neutral pH.

Co-assembly components can also be entirely interdependent upon one another for gelation.[255] For example, the assembly of K or R with Fmoc-E, relies on complementary electrostatic interactions between the constituents – with the system effectively composed of a pseudo Fmoc dipeptide *via* an ionic as opposed to an amide bond.[152] In addition, in the same study, the chirality of the nanofibres was shown to be altered with different L-/D-compositions – where molecular chirality relates directly with supramolecular chirality. Here, racemic mixtures are also found to form hydrogels, but with a diminished CD signal and evidence of self sorting behaviour – or orthogonal assembly. Similarly for other systems, substituting D-alanine for L-alanine has a direct impact upon the observed supramolecular helicity,[87] with racemic mixtures exhibiting weaker rheological properties or precipitating.[80] This highlights the importance of chirality in the gelation process, and also demonstrates some of the challenges in predicting the co-assembly behaviour that will be observed.

2.8.3 Co-assembly: C-termini heterogeneity

A synergistic relationship between co-assembling aromatic peptide amphiphiles is a principle that can also be applied to C-termini modifications. For instance, it has been shown that the co-assembly of penta-fluorinated Fmoc-F and its OEG functionalised C-termini

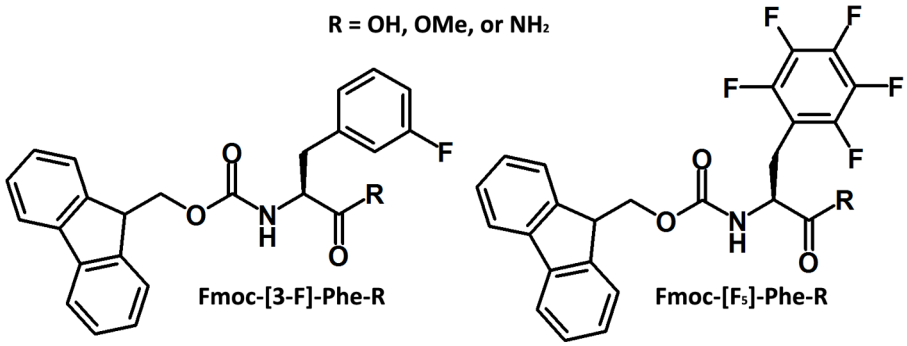

Figure 2.32 Structures of gelators used in C-termini co-assembly study.[58]

Table 2.2 Brief overview of gelation result from C-termini co-assembly study.[58]

Gelator(s)	Gel/Solution/Precipitate		Fibres observed	
	Water*	PBS pH 7.4	Water*	PBS pH 7.4
Fmoc-[3-F]-Phe-OH	Gel	Sol	Yes	Yes
Fmoc-[F_5]-Phe-OH	Gel	Sol	Yes	Yes
Fmoc-[3-F]-Phe-NH_2	Sol	Sol → Precipitate	Yes	Yes
Fmoc-[F_5]-Phe-NH_2	Sol	Sol → Precipitate	Yes	Yes
Fmoc-[3-F]-Phe-OMe	Precipitate	N/A	No	N/A
Fmoc-[F_5]-Phe-OMe	Precipitate	N/A	Yes	N/A
Fmoc-[3-F]-Phe-OH / Fmoc-[3-F]-Phe-NH_2	Gel	Gel	Yes	Yes
Fmoc-[F_5]-Phe-OH / Fmoc-[F_5]-Phe-NH_2	Gel	Gel	Yes	Yes

*pH differed but largely neutral for OMe/NH_2 and ~3.5 for COOH

equivalent, resulted in hydrogels with high elastic moduli and the ability to recover their mechanical properties.[143] In contrast, under the conditions used in this study, penta-fluorinated Fmoc-F itself only recovered 66% of its mechanical properties following the application of 100% strain, whilst the OEG analogue by itself exhibits 100% recovery but only weak gels in the first instance. Furthermore, although OEG based fibres were observed by TEM, no evidence of the pronounced helicity normally associated with these materials was inferred by CD – indicating that the OEG chains interfere with the parallel stacking conformation proposed for these systems. Upon co-assembly, the mechanical improvements were rationalised on the basis that heterogeneity helps to slow the precipitation of the penta-fluorinated Fmoc-F, which itself contributes rigidity to the co-assembly construct. In addition, the multicomponent material exhibits changes to the intensity and handedness of its CD spectrum depending upon the precise ratio used; indicating the formation of mixed fibres as opposed to self-sorting behaviour.

In another example, the co-assembly of side-chain halogenated Fmoc-phenylalanine derivatives with different C-termini was found to be useful for augmenting their respective self-assembly properties (Fig. 2.32, Table. 2.2).[58] The phenylalanine residue is too hydrophobic to undergo hydrogelation when used in conjunction with the COOMe functionality. Whereas, the corresponding amide derivatives are generally solutions, being too hydrophilic in this context to allow effective gelation. Despite this, fibrils can still be observed by TEM in each case – indicating that co-assembly with the corresponding COOH variants may allow for the tuning of these hydrophobicities. COOH derivatives themselves form hydrogels at low pH, whereas in PBS solution electrostatic repulsion of carboxylate anions compromises the mechanical properties of the hydrogel network yielding solutions. In this regard, the co-assembly of COOH and $CONH_2$ was generally found to be beneficial at high pH in PBS buffer – yielding hydrogels in each case. Hence, in this example, a non-gelating species assisted the gelation of a related molecule by helping to mitigate the effects of electrostatic repulsion; highlighting the utility of C-termini modifications within the context of co-assembly.

2.8.4 Co-assembly: self-sorting under pH control

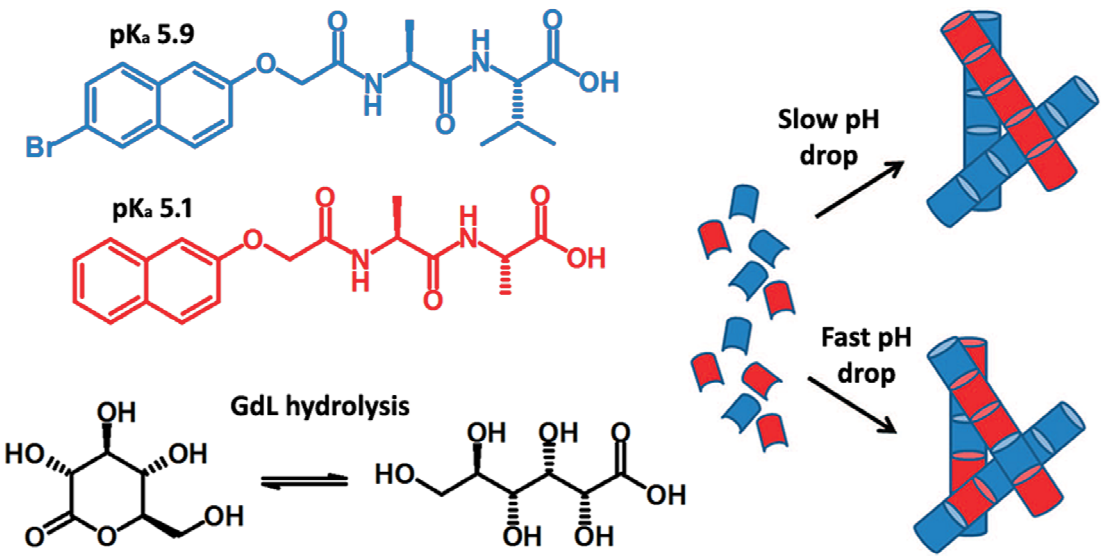

Figure 2.33 Self-sorting mechanism based on differential pK_a and corresponding gelation pH values. Slow pH drop is mediated *via* GdL hydrolysis. Adapted from.[186]

In some instances, it is possible to control the co-assembly arrangement through a judicious choice of initiation methodology, which differentially controls the assembly kinetics for different components in a mixture. For example, if the maximum gelation pH or apparent pK_a values of the co-assembly constituents are different, then it is possible to control the co-assembly arrangement through pH control (Fig. 2.33).[186] In this instance, if the pH is altered slowly – by for example utilising GdL – then the higher pK_a gelator will begin to assemble

first, as inferred by the NMR silence of this species in the supramolecular state. As the pH continues to decrease the second gelator can then assemble independently of the first, resulting in an interpenetrating network. Alternatively if the pH is lowered rapidly, then there will be insufficient opportunity for self sorting behaviour, and instead the mixed kinetic product will be attained. Hence, this illustrates that the kinetics of the initiation method can also influence the co-assembly process – potentially resulting in orthogonal assembly.

2.9 Conclusions

The self-assembly of aromatic peptide amphiphiles is based on a complex interplay of molecular, environmental, and kinetic considerations. Aromatic and peptidic functionality act in a synergistic fashion; contributing aromatic stacking and H-bonding interactions towards the self-assembly motif. Self-assembly and hydrogelation requires a balance of molecular characteristics; such as hydrophobicity, amphiphilicity, sterics, electronics, and a linear molecular geometry. In terms of the supramolecular structures associated with aromatic peptide amphiphiles; a variety of parallel, antiparallel, interlocked antiparallel, and more disordered stacking arrangements have been proposed. The adoption of a particular intermolecular stacking arrangement may depend upon a variety of factors, encompassing both the hydrogelator in question, the prevailing environmental conditions, and the degree of disorder and heterogeneity associated with the gelation methodology. Although the underlying assembly mechanisms may be similar, the emergence of a particular supramolecular structure is highly dependent upon subtle molecular alterations. For example, fibres, sheets, tubes, and spirals can be observed depending upon the sequence employed. Furthermore, a variety of higher order aggregation mechanisms have been proposed; including coiling tape and helical lamellar growth mechanisms, where the adoption of a 1D fibrous structure can be broadly explained on the basis of chirality and sterics, which normally act to disfavour extended 2D structures. Environmental factors can also have a profound impact upon the self-assembly and gelation process; with high pH (and ions) encouraging the adoption of worm-like micellar aggregates. Whilst the pH, gelator concentration, and temperature are all seen to be important factors in achieving nanoscale phase separation between the gelator and aqueous medium. Ultimately, hydrogels are kinetically-trapped meta-stable materials, and a single gelator can potentially access a variety of supramolecular structures depending upon the initiation protocol utilised. Even the adjustment of pH is a complex balance between encouraging the thermodynamically favoured aggregation of the gelator below its pK_a, and kinetic/heterogeneity considerations. The use of enzyme responsive gelation protocols allows for more direct control over the

number of fibrous nucleation sites, and the properties of the resultant materials. In addition, reversible enzymatic processes can potentially allow for dynamic hydrogel systems, whose molecular and supramolecular composition evolves over time towards a more energetically favourable state. Hence, it is only through an appreciation of molecular, supramolecular, environmental, and kinetic factors, that aromatic peptide amphiphiles can begin to be tailored for given applications in a rational and systematic fashion. While the elucidation of many of these design rules is still in its infancy, aromatic peptide amphiphile systems clearly have great potential for the preparation of minimalist, dynamic, and biocompatible materials.

2.10 References

1. J. F. Stoddart, *Angew. Chem., Int. Ed.*, 2012, **51**, 12902–12903.
2. S. Srinivasan, V. K. Praveen, R. Philip, and A. Ajayaghosh, *Angew. Chem., Int. Ed.*, 2008, **47**, 5750–5754.
3. R. J. Williams, A. M. Smith, R. Collins, N. Hodson, A. K. Das, and R. V. Ulijn, *Nat. Nanotechnol.*, 2009, **4**, 19–24.
4. R. J. Williams, R. J. Mart, and R. V. Ulijn, *Biopolymers*, 2010, **94**, 107–117.
5. B. Adhikari and B. Arindam, *J. Indian Inst. Sci.*, 2011, **91**, 471–483.
6. E. Winfree, F. Liu, L. A. Wenzler, and N. C. Seeman, *Nature*, 1998, **394**, 539–544.
7. S. M. Douglas, H. Dietz, T. Liedl, B. Högberg, F. Graf, and W. M. Shih, *Nature*, 2009, **459**, 414–418.
8. X. Li, Y. Kuang, H.-C. Lin, Y. Gao, J. Shi, and B. Xu, *Angew. Chem., Int. Ed.*, 2011, **50**, 9365–9369.
9. L. S. Birchall, S. Roy, V. Jayawarna, M. Hughes, E. Irvine, G. T. Okorogheye, N. Saudi, E. D. Santis, T. Tuttle, A. A. Edwards, and R. V. Ulijn, *Chem. Sci.*, 2011, **2**, 1349–1355.
10. R. Roytman, L. Adler-Abramovich, K. S. A. Kumar, T.-C. Kuan, C.-C. Lin, E. Gazit, and A. Brik, *Org. Biomol. Chem.*, 2011, **9**, 5755–5761.
11. N. Gour, A. K. Barman, and S. Verma, *J. Pept. Sci.*, 2012, **18**, 405–412.
12. M. Mahato, V. Arora, R. Pathak, H. K. Gautam, and A. K. Sharma, *Mol. BioSyst.*, 2012, **8**, 1742–1749.
13. X. Li, Y. Kuang, and B. Xu, *Soft Matter*, 2012, **8**, 2801–2806.
14. L. Liu, K. Busuttil, S. Zhang, Y. Yang, C. Wang, F. Besenbacher, and M. Dong, *Phys. Chem. Chem. Phys.*, 2011, **13**, 17435–17444.
15. C. Y. Xu and J. Kopecek, *Polym. Bull.*, 2007, **58**, 53–63.
16. A. Petrov and G. F. Audette, *Wiley Interdiscip. Rev.: Nanomed. Nanobiotechnol.*, 2012, **4**, 575–585.
17. R. V. Ulijn and A. M. Smith, *Chem. Soc. Rev.*, 2008, **37**, 664–675.
18. H. Wang, Z. Yang, and D. J. Adams, *Mater. Today*, 2012, **15**, 500–507.
19. E. Gazit, *Chem. Soc. Rev.*, 2007, **36**, 1263–1269.
20. J. B. Matson and S. I. Stupp, *Chem. Commun.*, 2012, **48**, 26–33.
21. S. Zhang and X. Zhao, *J. Mater. Chem.*, 2004, **14**, 2082–2086.
22. J. T. Pelton and L. R. McLean, *Anal. Biochem.*, 2000, **277**, 167–176.
23. F. Eisenhaber, B. Persson, and P. Argos, *Crit. Rev. Biochem. Mol. Biol.*, 1995, **30**, 1–94.
24. N. J. Greenfield, *Nat. Protoc.*, 2006, **1**, 2876–2890.
25. S. Toksöz and M. O. Guler, *Nano Today*, 2009, **4**, 458–469.
26. M. Biancalana, K. Makabe, A. Koide, and S. Koide, *J. Mol. Biol.*, 2008, **383**, 205–213.

27. R. V. Ulijn and D. N. Woolfson, *Chem. Soc. Rev.*, 2010, **39**, 3349–3350.
28. J. M. Fletcher, R. L. Harniman, F. R. H. Barnes, A. L. Boyle, A. Collins, J. Mantell, T. H. Sharp, M. Antognozzi, P. J. Booth, N. Linden, M. J. Miles, R. B. Sessions, P. Verkade, and D. N. Woolfson, *Science*, 2013, **340**, 595–599.
29. J. Naskar, G. Palui, and A. Banerjee, *J. Phys. Chem. B*, 2009, **113**, 11787–11792.
30. L. Zang, Y. K. Che, and J. S. Moore, *Acc. Chem. Res.*, 2008, **41**, 1596–1608.
31. S. R. Diegelmann, J. M. Gorham, and J. D. Tovar, *J. Am. Chem. Soc.*, 2008, **130**, 13840–13841.
32. W.-W. Tsai, I. D. Tevis, A. S. Tayi, H. Cui, and S. I. Stupp, *J. Phys. Chem. B.*, 2010, **114**, 14778–14786.
33. M. O. Guler, R. C. Claussen, and S. I. Stupp, *J. Mater. Chem.*, 2005, **15**, 4507–4512.
34. A. Brizard, M. Stuart, K. van Bommel, A. Friggeri, M. de Jong, and J. van Esch, *Angew. Chem., Int. Ed.*, 2008, **47**, 2063–2066.
35. G. S. Vadehra, B. D. Wall, S. R. Diegelmann, and J. D. Tovar, *Chem. Commun.*, 2010, **46**, 3947–3949.
36. P. Dastidar, *Chem. Soc. Rev.*, 2008, **37**, 2699–2715.
37. C. Subbalakshmi, S. V. Manorama, and R. Nagaraj, *J. Pept. Sci.*, 2012, **18**, 283–292.
38. V. Castelletto, G. Cheng, C. Stain, C. J. Connon, and I. W. Hamley, *Langmuir*, 2012, **28**, 11599–11608.
39. V. Castelletto, G. Cheng, B. W. Greenland, I. W. Hamley, and P. J. F. Harris, *Langmuir*, 2011, **27**, 2980–2988.
40. G. Palui, J. Nanda, S. Ray, and A. Banerjee, *Chem.–Eur. J.*, 2009, **15**, 6902–6909.
41. B. Adhikari, G. Palui, and A. Banerjee, *Soft Matter*, 2009, **5**, 3452–3460.
42. J. Nanda, B. Adhikari, S. Basak, and A. Banerjee, *J. Phys. Chem. B*, 2012, **116**, 12235–12244.
43. S. Debnath, A. Shome, S. Dutta, and P. K. Das, *Chem.–Eur. J.*, 2008, **14**, 6870–6881.
44. T. Kar, S. Dutta, and P. K. Das, *Soft Matter*, 2010, **6**, 4777–4787.
45. A. Shome, S. Dutta, S. Maiti, and P. K. Das, *Soft Matter*, 2011, **7**, 3011–3022.
46. S. K. Mandal, T. Kar, D. Das, and P. K. Das, *Chem. Commun.*, 2012, **48**, 1814–1816.
47. R. N. Mitra, D. Das, S. Roy, and P. K. Das, *J. Phys. Chem. B*, 2007, **111**, 14107–14113.
48. T. Kar, S. Debnath, D. Das, A. Shome, and P. Das, *Langmuir*, 2009, **25**, 8639–8648.
49. S. Yuran, Y. Razvag, and M. Reches, *ACS Nano*, 2012, **6**, 9559–9566.
50. R. N. Mitra, A. Shome, P. Paul, and P. K. Das, *Org. Biomol. Chem.*, 2009, **7**, 94–102.
51. R. Solaro, M. Alderighi, M. C. Barsotti, A. Battisti, M. Cifelli, P. Losi, R. D. Stefano, L. Ghezzi, and M. R. Tiné, *J. Bioact. Compat. Polym.*, 2013, **28**, 3–15.
52. A. Dehsorkhi, I. W. Hamley, J. Seitsonen, and J. Ruokolainen, *Langmuir*, 2013, **29**, 6665–6672.
53. D. J. Adams and P. D. Topham, *Soft Matter*, 2010, **6**, 3707–3721.
54. A. L. Boyle and D. N. Woolfson, *Chem. Soc. Rev.*, 2011, **40**, 4295–4306.
55. M. Zelzer and R. V. Ulijn, *Chem. Soc. Rev.*, 2010, **39**, 3351–3357.
56. S. Fleming, S. Debnath, P. W. J. M. Frederix, T. Tuttle, and R. V. Ulijn, *Chem. Commun.*, 2013, **49**, 10587–10589.
57. S. Debnath, A. Shome, D. Das, and P. K. Das, *J. Phys. Chem. B*, 2010, **114**, 4407–4415.
58. D. M. Ryan, T. M. Doran, S. B. Anderson, and B. L. Nilsson, *Langmuir*, 2011, **27**, 4029–4039.
59. M. Hughes, H. Xu, P. W. J. M. Frederix, A. M. Smith, N. T. Hunt, T. Tuttle, I. A. Kinloch, and R. V. Ulijn, *Soft Matter*, 2011, **7**, 10032–10038.
60. H. Shao and J. R. Parquette, *Chem. Commun.*, 2010, **46**, 4285–4287.
61. L. Chen, K. Morris, A. Laybourn, D. Elias, M. R. Hicks, A. Rodger, L. Serpell, and D. J. Adams, *Langmuir*, 2010, **26**, 5232–5242.

62. R. Orbach, I. Mironi-Harpaz, L. Adler-Abramovich, E. Mossou, E. P. Mitchell, V. T. Forsyth, E. Gazit, and D. Seliktar, *Langmuir*, 2012, **28**, 2015–2022.
63. A. R. Hirst, S. Roy, M. Arora, A. K. Das, N. Hodson, P. Murray, S. Marshall, N. Javid, J. Sefcik, J. Boekhoven, J. H. van Esch, S. Santabarbara, N. T. Hunt, and R. V. Ulijn, *Nat. Chem.*, 2010, **2**, 1089–1094.
64. A. M. Smith, R. F. Collins, R. V. Ulijn, and E. Blanch, *J. Raman Spectrosc.*, 2009, **40**, 1093–1095.
65. M. Zhou, A. M. Smith, A. K. Das, N. W. Hodson, R. F. Collins, R. V. Ulijn, and J. E. Gough, *Biomaterials*, 2009, **30**, 2523–2530.
66. S. Fleming, P. W. J. M. Frederix, I. Ramos-Sasselli, N. Hunt, R. V. Ulijn, and T. Tuttle, *Langmuir*, 2013, **29**, 9510–9515.
67. J. D. Hartgerink, E. Beniash, and S. I. Stupp, *Proc. Natl. Acad. Sci. U. S. A.*, 2002, **99**, 5133–5138.
68. E. Beniash, J. D. Hartgerink, H. Storrie, J. C. Stendahl, and S. I. Stupp, *Acta Biomater.*, 2005, **1**, 387–397.
69. A. Ohta, M. Shirai, T. Asakawa, and S. Miyagishi, *J. Oleo Sci.*, 2008, **57**, 659–667.
70. S. Dutta, A. Shome, S. Debnath, and P. K. Das, *Soft Matter*, 2009, **5**, 1607–1620.
71. E. T. Pashuck and S. I. Stupp, *J. Am. Chem. Soc.*, 2010, **132**, 8819–8820.
72. S. M. Standley, D. J. Toft, H. Cheng, S. Soukasene, J. Chen, S. M. Raja, V. Band, H. Band, V. L. Cryns, and S. I. Stupp, *Cancer Res.*, 2010, **70**, 3020–3026.
73. A. Pal and J. Dey, *Soft Matter*, 2011, **7**, 10369–10376.
74. A. Tan, J. Rajadas, and A. M. Seifalian, *J. Controlled Release*, 2012, **163**, 342–352.
75. C. R. Martinez and B. L. Iverson, *Chem. Sci.*, 2012, **3**, 2191.
76. H. Wang, C. Yang, M. Tan, L. Wang, D. Kong, and Z. Yang, *Soft Matter*, 2011, **7**, 3897–3905.
77. C. Tang, R. V. Ulijn, and A. Saiani, *Langmuir*, 2011, **27**, 14438–14449.
78. L. Chen, S. Revel, K. Morris, L. C. Serpell, and D. J. Adams, *Langmuir*, 2010, **26**, 13466–13471.
79. M. Hughes, P. W. J. M. Frederix, J. Raeburn, L. S. Birchall, J. Sadownik, F. C. Coomer, I.-H. Lin, E. J. Cussen, N. T. Hunt, T. Tuttle, S. J. Webb, D. J. Adams, and R. V. Ulijn, *Soft Matter*, 2012, **8**, 5595–5602.
80. Z. Yang, G. Liang, M. Ma, Y. Gao, and B. Xu, *J. Mater. Chem.*, 2007, **17**, 850–854.
81. D. J. Adams, L. M. Mullen, M. Berta, L. Chen, and W. J. Frith, *Soft Matter*, 2010, **6**, 1971–1980.
82. D. M. Ryan, S. B. Anderson, and B. L. Nilsson, *Soft Matter*, 2010, **6**, 3220–3231.
83. R. Orbach, L. Adler-Abramovich, S. Zigerson, I. Mironi-Harpaz, D. Seliktar, and E. Gazit, *Biomacromolecules*, 2009, **10**, 2646–2651.
84. Y. Huang, Z. Qiu, Y. Xu, J. Shi, H. Lin, and Y. Zhang, *Org. Biomol. Chem.*, 2011, **9**, 2149–2155.
85. J. Raeburn, A. Z. Cardoso, and D. J. Adams, *Chem. Soc. Rev.*, 2013, **42**, 5143–5156.
86. R. Vegners, I. Shestakova, I. Kalvinsh, R. M. Ezzell, and P. A. Janmey, *J. Pept. Sci.*, 1995, **1**, 371–378.
87. Y. Zhang, H. Gu, Z. Yang, and B. Xu, *J. Am. Chem. Soc.*, 2003, **125**, 13680–13681.
88. Z. Yang, H. Gu, Y. Zhang, L. Wang, and B. Xu, *Chem. Commun.*, 2004, 208–209.
89. Y. Zhang, Z. Yang, F. Yuan, H. Gu, P. Gao, and B. Xu, *J. Am. Chem. Soc.*, 2004, **126**, 15028–15029.
90. Z. Yang, H. Gu, D. Fu, P. Gao, J. K. Lam, and B. Xu, *Adv. Mater.*, 2004, **16**, 1440–1444.
91. Z. Yang and B. Xu, *Chem. Commun.*, 2004, 2424–2425.
92. M. J. Krysmann, V. Castelletto, A. Kelarakis, I. W. Hamley, R. A. Hule, and D. J. Pochan, *Biochemistry*, 2008, **47**, 4597–4605.
93. E. Gazit, *Prion*, 2007, **1**, 32–35.

94. P. Tamamis, L. Adler-Abramovich, M. Reches, K. Marshall, P. Sikorski, L. Serpell, E. Gazit, and G. Archontis, *Biophys. J.*, 2009, **96**, 5020–5029.
95. M. J. Krysmann, V. Castelletto, J. E. McKendrick, L. A. Clifton, I. W. Hamley, P. J. F. Harris, and S. A. King, *Langmuir*, 2008, **24**, 8158–8162.
96. N. S. de Groot, T. Parella, F. X. Aviles, J. Vendrell, and S. Ventura, *Biophys. J.*, 2007, **92**, 1732–1741.
97. S. Marchesan, C. D. Easton, F. Kushkaki, L. Waddington, and P. G. Hartley, *Chem. Commun.*, 2012, **48**, 2195–2197.
98. C. H. Görbitz, *Chem. Commun.*, 2006, 2332–2334.
99. L. Adler-Abramovich, M. Reches, V. L. Sedman, S. Allen, S. J. B. Tendler, and E. Gazit, *Langmuir*, 2006, **22**, 1313–1320.
100. M. Reches and E. Gazit, *Phys. Biol.*, 2006, **3**, S10–S19.
101. E. Gazit, *FASEB J.*, 2002, **16**, 77–83.
102. M. Reches, Y. Porat, and E. Gazit, *J. Biol. Chem.*, 2002, **277**, 35475–35480.
103. M. Reches and E. Gazit, *Science*, 2003, **300**, 625–627.
104. M. Reches and E. Gazit, *Nano Lett.*, 2004, **4**, 581–585.
105. M. Reches and E. Gazit, *Isr. J. Chem.*, 2005, **45**, 363–371.
106. V. Jayawarna, M. Ali, T. A. Jowitt, A. E. Miller, A. Saiani, J. E. Gough, and R. V. Ulijn, *Adv. Mater.*, 2006, **18**, 611–612.
107. A. Mahler, M. Reches, M. Rechter, S. Cohen, and E. Gazit, *Adv. Mater.*, 2006, **18**, 1365–1366.
108. Z. A. C. Schnepp, R. Gonzalez-McQuire, and S. Mann, *Adv. Mater.*, 2006, **18**, 1869–1872.
109. Z. Yang and B. Xu, *Adv. Mater.*, 2006, **18**, 3043–3046.
110. Z. Yang, G. Liang, L. Wang, and B. Xu, *J. Am. Chem. Soc.*, 2006, **128**, 3038–3043.
111. Z. Yang, G. Liang, and B. Xu, *Chem. Commun.*, 2006, 738–740.
112. S. Toledano, R. J. Williams, V. Jayawarna, and R. V. Ulijn, *J. Am. Chem. Soc.*, 2006, **128**, 1070–1071.
113. V. Jayawarna, A. Smith, J. E. Gough, and R. V. Ulijn, *Biochem. Soc. Trans.*, 2007, **35**, 535–537.
114. Z. Yang and B. Xu, *J. Mater. Chem.*, 2007, **17**, 2385–2393.
115. Z. Yang, P.-L. Ho, G. Liang, K. H. Chow, Q. Wang, Y. Cao, Z. Guo, and B. Xu, *J. Am. Chem. Soc.*, 2007, **129**, 266–267.
116. Z. Yang, G. Liang, M. Ma, Y. Gao, and B. Xu, *Small*, 2007, **3**, 558–562.
117. L. Adler-Abramovich and E. Gazit, *J. Pept. Sci.*, 2008, **14**, 217–223.
118. D. Bardelang, M. B. Zaman, I. L. Moudrakovski, S. Pawsey, J. C. Margeson, D. S. Wang, X. H. Wu, J. A. Ripmeester, C. I. Ratcliffe, and K. Yu, *Adv. Mater.*, 2008, **20**, 4517–4520.
119. L. S. Birchall, R. V. Ulijn, and S. J. Webb, *Chem. Commun.*, 2008, 2861–2863.
120. A. K. Das, R. Collins, and R. V. Ulijn, *Small*, 2008, **4**, 279–287.
121. A. M. Smith, R. J. Williams, C. Tang, P. Coppo, R. F. Collins, M. L. Turner, A. Saiani, and R. V. Ulijn, *Adv. Mater.*, 2008, **20**, 37–38.
122. Z. Yang, G. Liang, and B. Xu, *Acc. Chem. Res.*, 2008, **41**, 315–326.
123. D. J. Adams, M. F. Butler, W. J. Frith, M. Kirkland, L. Mullen, and P. Sanderson, *Soft Matter*, 2009, **5**, 1856–1862.
124. A. K. Das, A. R. Hirst, and R. V. Ulijn, *Faraday Discuss.*, 2009, **143**, 293–303.
125. J. Gao, H. Wang, L. Wang, J. Wang, D. Kong, and Z. Yang, *J. Am. Chem. Soc.*, 2009, **131**, 11286–11287.
126. Y. Gao, Y. Kuang, Z.-F. Guo, Z. Guo, I. J. Krauss, and B. Xu, *J. Am. Chem. Soc.*, 2009, **131**, 13576–13577.
127. V. Jayawarna, S. M. Richardson, A. R. Hirst, N. W. Hodson, A. Saiani, J. E. Gough, and R. V. Ulijn, *Acta Biomater.*, 2009, **5**, 934–943.

128. G. Liang, Z. Yang, R. Zhang, L. Li, Y. Fan, Y. Kuang, Y. Gao, T. Wang, W. W. Lu, and B. Xu, *Langmuir*, 2009, **25**, 8419–8422.
129. H. Shao, T. Nguyen, N. C. Romano, D. A. Modarelli, and J. R. Parquette, *J. Am. Chem. Soc.*, 2009, **131**, 16374–16376.
130. K. Thornton, A. M. Smith, C. L. R. Merry, and R. V. Ulijn, *Biochem. Soc. Trans.*, 2009, **37**, 660–664.
131. C. Tang, A. M. Smith, R. F. Collins, R. V. Ulijn, and A. Saiani, *Langmuir*, 2009, **25**, 9447–9453.
132. S. Sutton, N. L. Campbell, A. I. Cooper, M. Kirkland, W. J. Frith, and D. J. Adams, *Langmuir*, 2009, **25**, 10285–10291.
133. D. J. Adams, K. Morris, L. Chen, L. C. Serpell, J. Bacsa, and G. M. Day, *Soft Matter*, 2010, **6**, 4144–4156.
134. B. Adhikari and A. Banerjee, *Chem.–Eur. J.*, 2010, **16**, 13698–13705.
135. N. Amdursky, E. Gazit, and G. Rosenman, *Adv. Mater.*, 2010, **22**, 2311–2315.
136. L. Chen, S. Revel, K. Morris, and D. J. Adams, *Chem. Commun.*, 2010, **46**, 4267–4269.
137. L. Chen, S. Revel, K. Morris, D. G. Spiller, L. C. Serpell, and D. J. Adams, *Chem. Commun.*, 2010, **46**, 6738–6740.
138. G. Cheng, V. Castelletto, C. M. Moulton, G. E. Newby, and I. W. Hamley, *Langmuir*, 2010, **26**, 4990–4998.
139. Y. Gao, F. Zhao, Q. Wang, Y. Zhang, and B. Xu, *Chem. Soc. Rev.*, 2010, **39**, 3425–3433.
140. E. K. Johnson, D. J. Adams, and P. J. Cameron, *J. Am. Chem. Soc.*, 2010, **132**, 5130–5136.
141. M. L. Ma, Y. Kuang, Y. Gao, Y. Zhang, P. Gao, and B. Xu, *J. Am. Chem. Soc.*, 2010, **132**, 2719–2728.
142. D. M. Ryan, S. B. Anderson, F. T. Senguen, R. E. Youngman, and B. L. Nilsson, *Soft Matter*, 2010, **6**, 475–479.
143. D. M. Ryan, T. M. Doran, and B. L. Nilsson, *Chem. Commun.*, 2010, **47**, 475–477.
144. J. Ryu, S.-W. Kim, K. Kang, and C. B. Park, *Adv. Mater.*, 2010, **22**, 5537–5541.
145. J. W. Sadownik, J. Leckie, and R. V. Ulijn, *Chem. Commun.*, 2010, **47**, 728–730.
146. J. W. Sadownik and R. V. Ulijn, *Chem. Commun.*, 2010, **46**, 3481–3483.
147. H. X. Xu, A. K. Das, M. Horie, M. S. Shaik, A. M. Smith, Y. Luo, X. F. Lu, R. Collins, S. Y. Liem, A. M. Song, P. L. A. Popelier, M. L. Turner, P. Xiao, I. A. Kinloch, and R. V. Ulijn, *Nanoscale*, 2010, **2**, 960–966.
148. X.-D. Xu, C.-S. Chen, B. Lu, S.-X. Cheng, X.-Z. Zhang, and R.-X. Zhuo, *J. Phys. Chem. B*, 2010, **114**, 2365–2372.
149. X. Yan, P. Zhu, and J. Li, *Chem. Soc. Rev.*, 2010, **39**, 1877–1890.
150. Z. Yang, L. Wang, J. Wang, P. Gao, and B. Xu, *J. Mater. Chem.*, 2010, **20**, 2128–2132.
151. B. Adhikari and A. Banerjee, *Soft Matter*, 2011, **7**, 9259–9266.
152. B. Adhikari, J. Nanda, and A. Banerjee, *Soft Matter*, 2011, **7**, 8913–8922.
153. L. Chen, G. Pont, K. Morris, G. Lotze, A. Squires, L. C. Serpell, and D. J. Adams, *Chem. Commun.*, 2011, **47**, 12071–12073.
154. L. Chen, J. Raeburn, S. Sutton, D. G. Spiller, J. Williams, J. S. Sharp, P. C. Griffiths, R. K. Heenan, S. M. King, A. Paul, S. Furzeland, D. Atkins, and D. J. Adams, *Soft Matter*, 2011, **7**, 9721–9727.
155. G. Cheng, V. Castelletto, R. R. Jones, C. J. Connon, and I. W. Hamley, *Soft Matter*, 2011, **7**, 1326–1333.
156. W. Helen, P. de Leonardis, R. V. Ulijn, J. Gough, and N. Tirelli, *Soft Matter*, 2011, **7**, 1732–1740.
157. M. Ikeda, T. Tanida, T. Yoshii, and I. Hamachi, *Adv. Mater.*, 2011, **23**, 2819–2822.

158. E. K. Johnson, D. J. Adams, and P. J. Cameron, *J. Mater. Chem.*, 2011, **21**, 2024–2027.
159. T. Kar, S. K. Mandal, and P. K. Das, *Chem.–Eur. J.*, 2011, **17**, 14952–14961.
160. Y. Lin, Y. Qiao, P. Tang, Z. Li, and J. Huang, *Soft Matter*, 2011, **7**, 2762–2769.
161. Y. Liu, E. Kim, R. V. Ulijn, W. E. Bentley, and G. F. Payne, *Adv. Funct. Mater.*, 2011, **21**, 1575–1580.
162. S. Roy and A. Banerjee, *Soft Matter*, 2011, **7**, 5300–5308.
163. D. M. Ryan, T. M. Doran, and B. L. Nilsson, *Langmuir*, 2011, **27**, 11145–11156.
164. J. Shi, Y. Gao, Z. Yang, and B. Xu, *Beilstein J. Org. Chem.*, 2011, **7**, 167–172.
165. Z.-X. Tie, M. Qin, D.-W. Zou, Y. Cao, and W. Wang, *Chin. Phys. Lett.*, 2011, **28**, 028702.
166. D. J. Adams, *Macromol. Biosci.*, 2011, **11**, 160–173.
167. Z. Wang, H. Wang, W. Zheng, J. Zhang, Q. Zhao, S. Wang, Z. Yang, and D. Kong, *Chem. Commun.*, 2011, **47**, 8901–8903.
168. V. Castelletto, C. M. Moulton, G. Cheng, I. W. Hamley, M. R. Hicks, A. Rodger, D. E. López-Pérez, G. Revilla-López, and C. Alemán, *Soft Matter*, 2011, **7**, 11405–11415.
169. H.-G. Braun and A. Z. Cardoso, *Colloids Surf., B*, 2012, **97**, 43–50.
170. P. W. J. M. Frederix, R. Kania, J. A. Wright, D. A. Lamprou, R. Ulijn, C. J. Pickett, and N. T. Hunt, *Dalton Trans.*, 2012, **41**, 13112–13119.
171. M. Hughes, L. S. Birchall, K. Zuberi, L. A. Aitken, S. Debnath, N. Javid, and R. V. Ulijn, *Soft Matter*, 2012, **8**, 11565–11574.
172. D. Jiao, J. Geng, X. J. Loh, D. Das, T.-C. Lee, and O. A. Scherman, *Angew. Chem., Int. Ed.*, 2012, **51**, 9633–9637.
173. D. Li, J. Liu, L. Chu, J. Liu, and Z. Yang, *Chem. Commun.*, 2012, **48**, 6175–6177.
174. X. Mu, K. M. Eckes, M. M. Nguyen, L. J. Suggs, and P. Ren, *Biomacromolecules*, 2012, **13**, 3562–3571.
175. W. Nuansing, A. Rebollo, J. M. Mercero, J. Zuñiga, and A. M. Bittner, *J. Raman Spectrosc.*, 2012, **43**, 1397–1406.
176. J. Raeburn, T. O. McDonald, and D. J. Adams, *Chem. Commun.*, 2012, **48**, 9355–9357.
177. J. Raeburn, G. Pont, L. Chen, Y. Cesbron, R. Lévy, and D. J. Adams, *Soft Matter*, 2012, **8**, 1168–1174.
178. S. Roy, N. Javid, P. W. J. M. Frederix, D. A. Lamprou, A. J. Urquhart, N. T. Hunt, P. J. Halling, and R. V. Ulijn, *Chem.–Eur. J.*, 2012, **18**, 11723–11731.
179. S. Roy, N. Javid, J. Sefcik, P. J. Halling, and R. V. Ulijn, *Langmuir*, 2012, **28**, 16664–16670.
180. S. Roy and A. Banerjee, *RSC Adv.*, 2012, **2**, 2105–2111.
181. C. Tomasini and N. Castellucci, *Chem. Soc. Rev.*, 2012, **42**, 156–172.
182. H. Wang and Z. Yang, *Nanoscale*, 2012, **4**, 5259–5267.
183. D. M. Ryan and B. L. Nilsson, *Polym. Chem.*, 2012, **3**, 18–33.
184. Y. M. Abul-Haija, S. Roy, P. W. J. M. Frederix, N. Javid, V. Jayawarna, and R. V. Ulijn, *Small*, 2013, Advance article.
185. L. Chen, T. O. McDonald, and D. J. Adams, *RSC Adv.*, 2013, **3**, 8714–8720.
186. K. L. Morris, L. Chen, J. Raeburn, O. R. Sellick, P. Cotanda, A. Paul, P. C. Griffiths, S. M. King, R. K. O'Reilly, L. C. Serpell, and D. J. Adams, *Nat. Commun.*, 2013, **4**, 1480–1485.
187. S. K. M. Nalluri and R. V. Ulijn, *Chem. Sci.*, 2013, **4**, 3699–3705.
188. K. Thornton, Y. M. Abul-Haija, N. Hodson, and R. Ulijn, *Soft Matter*, 2013, **9**, 9430–9439.
189. M. Hughes, S. Debnath, C. W. Knapp, and R. V. Ulijn, *Biomater. Sci.*, 2013, **1**, 1138–1142.
190. S. Bai, S. Debnath, K. Gibson, B. Schlicht, L. Bayne, M. Zagnoni, and R. V. Ulijn, *Small*, 2013, n/a–n/a.

191. I.-H. Lin, L. S. Birchall, N. Hodson, R. V. Ulijn, and S. J. Webb, *Soft Matter*, 2013, **9**, 1188–1193.
192. J. Li, Y. Kuang, Y. Gao, X. Du, J. Shi, and B. Xu, *J. Am. Chem. Soc.*, 2013, **135**, 542–545.
193. J. Li, X. Li, Y. Kuang, Y. Gao, X. Du, J. Shi, and B. Xu, *Adv. Healthcare Mater.*, 2013, **2**, 1586–1590.
194. Y. Kuang, D. Yuan, Y. Zhang, A. Kao, X. Du, and B. Xu, *RSC Adv.*, 2013, **3**, 7704–7707.
195. J. Li, Y. Kuang, J. Shi, Y. Gao, J. Zhou, and B. Xu, *Beilstein J. Org. Chem.*, 2013, **9**, 908–917.
196. Y. Zhang, R. Zhou, J. Shi, N. Zhou, I. R. Epstein, and B. Xu, *J. Phys. Chem. B*, 2013, **117**, 6566–6573.
197. Y. Kuang and B. Xu, *Angew. Chem., Int. Ed.*, 2013, **52**, 6944–6948.
198. J. Li, Y. Gao, Y. Kuang, J. Shi, X. Du, J. Zhou, H. Wang, Z. Yang, and B. Xu, *J. Am. Chem. Soc.*, 2013, **135**, 9907–9914.
199. C. Ou, J. Zhang, X. Zhang, Z. Yang, and M. Chen, *Chem. Commun.*, 2013, **49**, 1853–1855.
200. J. Majumder, M. R. Das, J. Deb, S. S. Jana, and P. Dastidar, *Langmuir*, 2013, **29**, 10254–10263.
201. S. Debnath, S. Roy, and R. V. Ulijn, *J. Am. Chem. Soc.*, 2013, **135**, 16789–16792.
202. G. Scott, S. Roy, Y. M. Abul-Haija, S. Fleming, S. Bai, and R. V. Ulijn, *Langmuir*, 2013, **29**, 14321–14327.
203. Y. Zou, K. Razmkhah, N. P. Chmel, I. W. Hamley, and A. Rodger, *RSC Adv.*, 2013, **3**, 10854–10858.
204. D. E. López-Pérez, G. Revilla-López, I. W. Hamley, and C. Alemán, *Soft Matter*, 2013, **9**, 11021–11032.
205. T. Ishi-i, R. Iguchi, E. Snip, M. Ikeda, and S. Shinkai, *Langmuir*, 2001, **17**, 5825–5833.
206. G. D. Rose, A. R. Geselowitz, G. J. Lesser, R. H. Lee, and M. H. Zehfus, *Science*, 1985, **229**, 834–838.
207. R. Cowan and R. G. Whittaker, *Pept. Res.*, 1990, **3**, 75–80.
208. H. Fu, G. R. Grimsley, A. Razvi, J. M. Scholtz, and C. N. Pace, *Proteins: Struct., Funct., Bioinf.*, 2009, **77**, 491–498.
209. M. W. Pantoliano, R. C. Ladner, P. N. Bryan, M. L. Rollence, J. F. Wood, and T. L. Poulos, *Biochemistry*, 1987, **26**, 2077–2082.
210. J.-B. Guilbaud, E. Vey, S. Boothroyd, A. M. Smith, R. V. Ulijn, A. Saiani, and A. F. Miller, *Langmuir*, 2010, **26**, 11297–11303.
211. Y. Porat, A. Abramowitz, and E. Gazit, *Chem. Biol. Drug Des.*, 2006, **67**, 27–37.
212. P. W. J. M. Frederix, R. V. Ulijn, N. T. Hunt, and T. Tuttle, *J. Phys. Chem. Lett.*, 2011, **2**, 2380–2384.
213. J. H. van Esch, *Langmuir*, 2009, **25**, 8392–8394.
214. B. Ding, Y. Li, M. Qin, Y. Ding, Y. Cao, and W. Wang, *Soft Matter*, 2013, **9**, 4672–4680.
215. M. Reches and E. Gazit, *Nat. Nanotechnol.*, 2006, **1**, 195–200.
216. J. Kim, T. H. Han, Y.-I. Kim, J. S. Park, J. Choi, D. G. Churchill, S. O. Kim, and H. Ihee, *Adv. Mater.*, 2010, **22**, 583–587.
217. D. J. Welsh, P. Posocco, S. Pricl, and D. K. Smith, *Org. Biomol. Chem.*, 2013, **11**, 3177–3186.
218. J. Nanda and A. Banerjee, *Soft Matter*, 2012, **8**, 3380–3386.
219. X. Li, X. Du, J. Li, Y. Gao, Y. Pan, J. Shi, N. Zhou, and B. Xu, *Langmuir*, 2012, **28**, 13512–13517.
220. C. Tang, R. V. Ulijn, and A. Saiani, *Eur. Phys. J. E*, 2013, **36**, 111–121.
221. F. Hofmeister, *Archiv f. experiment. Pathol. u. Pharmakol.*, 1888, **24**, 247–260.

222. M. A. Greenfield, J. R. Hoffman, M. O. de la Cruz, and S. I. Stupp, *Langmuir*, 2010, **26**, 3641–3647.
223. E. T. Pashuck, H. G. Cui, and S. I. Stupp, *J. Am. Chem. Soc.*, 2010, **132**, 6041–6046.
224. A. Mata, Y. B. Geng, K. J. Henrikson, C. Aparicio, S. R. Stock, R. L. Satcher, and S. I. Stupp, *Biomaterials*, 2010, **31**, 6004–6012.
225. R. N. Shah, N. A. Shah, M. M. D. Lim, C. Hsieh, G. Nuber, and S. I. Stupp, *Proc. Natl. Acad. Sci. U. S. A.*, 2010, **107**, 3293–3298.
226. M. J. Webber, J. Tongers, M. A. Renault, J. G. Roncalli, D. W. Losordo, and S. I. Stupp, *Acta Biomater.*, 2010, **6**, 3–11.
227. H. G. Cui, M. J. Webber, and S. I. Stupp, *Biopolymers*, 2010, **94**, 1–18.
228. H. K. Kang, D. E. Kang, B. H. Boo, S. J. Yoo, J. K. Lee, and E. C. Lim, *J. Phys. Chem. A*, 2005, **109**, 6799–6804.
229. A. Barth and C. Zscherp, *Q. Rev. Biophys.*, 2002, **35**, 369–430.
230. L. Ziserman, H.-Y. Lee, S. R. Raghavan, A. Mor, and D. Danino, *J. Am. Chem. Soc.*, 2011, **133**, 2511–2517.
231. W. Edwards and D. K. Smith, *J. Am. Chem. Soc.*, 2014, **136**, 1116–1124.
232. D. K. Smith, *Chem. Soc. Rev.*, 2009, **38**, 684–694.
233. A. Aggeli, I. A. Nyrkova, M. Bell, R. Harding, L. Carrick, T. C. B. McLeish, A. N. Semenov, and N. Boden, *Proc. Natl. Acad. Sci. U. S. A.*, 2001, **98**, 11857–11862.
234. C. Yang, H. Wang, D. Li, and L. Wang, *Chin. J. Chem.*, 2013, **31**, 494–500.
235. R. J. Mart, R. D. Osborne, M. M. Stevens, and R. V. Ulijn, *Soft Matter*, 2006, **2**, 822–835.
236. G. Jia, S. Qiu, G. Li, J. Zhou, Z. Feng, and C. Li, *Sci. China Ser. B-Chem.*, 2009, **52**, 552–558.
237. J. Lowe and S. Holdcroft, *Macromolecules*, 1995, **28**, 4608–4616.
238. J. Raeburn, B. Alston, J. Kroeger, T. O. McDonald, J. R. Howse, P. J. Cameron, and D. J. Adams, *Mater. Horiz.*, 2014, **1**, 241–246.
239. P. Naumanen, P. Lappalainen, and P. Hotulainen, *J. Microsc.*, 2008, **231**, 446–454.
240. G. J. Doherty and H. T. McMahon, *Annu. Rev. Biophys.*, 2008, **37**, 65–95.
241. A. Nawrotek, M. Knossow, and B. Gigant, *J. Mol. Biol.*, 2011, **412**, 35–42.
242. J. M. Kollman, A. Merdes, L. Mourey, and D. A. Agard, *Nat. Rev. Mol. Cell Biol.*, 2011, **12**, 709–721.
243. R. V. Ulijn, *J. Mater. Chem.*, 2006, **16**, 2217–2225.
244. M. Zelzer, S. J. Todd, A. R. Hirst, T. O. McDonald, and R. V. Ulijn, *Biomater. Sci.*, 2012, **1**, 11–39.
245. Y. Chen, *Theranostics*, 2012, **2**, 139–147.
246. Y. Gao, J. Shi, D. Yuan, and B. Xu, *Nat Commun*, 2012, **3**, 1033.
247. Y. Gao, M. J. C. Long, J. Shi, L. Hedstrom, and B. Xu, *Chem. Commun.*, 2012, **48**, 8404–8406.
248. W. Zheng, J. Gao, L. Song, C. Chen, D. Guan, Z. Wang, Z. Li, D. Kong, and Z. Yang, *J. Am. Chem. Soc.*, 2013, **135**, 266–271.
249. D. Li, H. Wang, D. Kong, and Z. Yang, *Nanoscale*, 2012, **4**, 3047–3049.
250. N. Javid, S. Roy, M. Zelzer, Z. Yang, J. Sefcik, and R. V. Ulijn, *Biomacromolecules*, 2013, **14**, 4368–4376.
251. Y. Yamauchi, M. Yoshizawa, and M. Fujita, *J. Am. Chem. Soc.*, 2008, **130**, 5832–5833.
252. K. V. Rao and S. J. George, *Chem.–Eur. J.*, 2012, **18**, 14286–14291.
253. C. Wang, Y. Guo, Z. Wang, and X. Zhang, *Langmuir*, 2010, **26**, 14509–14511.
254. O. P. Lee, A. T. Yiu, P. M. Beaujuge, C. H. Woo, T. W. Holcombe, J. E. Millstone, J. D. Douglas, M. S. Chen, and J. M. J. Fréchet, *Adv. Mater.*, 2011, **23**, 5359–5363.
255. L. E. Buerkle and S. J. Rowan, *Chem. Soc. Rev.*, 2012, **41**, 6089–6102.

– Chapter 3 –

Materials and methods

3.1 Synthesis of aromatic peptide amphiphile compounds

Unless otherwise stated, all starting materials were purchased from commercial sources (e.g. Sigma Aldrich, Merck, Bachem, C S Bio Co.) and used as supplied, without any characterisation or purification. All peptide derivatives were purchased as the levo-amino acid enantiomers. The purity and/or identity of all final compounds was confirmed by HPLC (≥95%), ESI MS, and ^{1}H NMR. In addition, ^{13}C labelled final compounds were invariably assessed by ^{13}C NMR.

3.1.1 Carbonyl C=O linker (1) compounds

3.1.1.1 Common precursor: Dileucine methyl ester (LLOMe)

Dileucine methyl ester (**LLOMe**)

To a MeOH (30 mL) suspension of dileucine (300 mg, 1.2 mmol) was added thionyl chloride (262 μL, 3.6 mmol), and DMF (500 μL). The reaction mixture, which became a clear solution, was stirred at room temperature for 3 hours. The solution was concentrated *via* rotary evaporation, in order to afford the crude product, which was used without purification. ESI MS +ve $[M+H]^+$ m/z 259.05, $[M+Na]^+$ m/z 281.14

3.1.1.2 Common precursor: Dileucine tert-butyl ester (LLOtBu)

Dileucine tert-butyl ester (**LLOtBu**)

To a stirred tert-butyl acetate (7.20 mL, 53 mmol) solution of dileucine (720 mg, 2.9 mmol) at 0 ^{o}C was slowly added 70% perchloric acid (407 μL, 4.7 mmol). The reaction mixture was allowed to warm to room temperature and stirred overnight. The reaction mixture was extracted with water (x2) and HCl (x2). Potassium carbonate was added to the combined aqueous extracts until no more gas evolution was observed. The aqueous layer was extracted with ether (x2), and the organic layer dried over $MgSO_4$, and concentrated *via* rotary evaporation, in order to afford the title compound (800 mg, 90.4%).

3.1.1.3 9-Fluorenylcarbonyl tyrosine leucine (F1YL)[1]

9-Fluorenylcarbonyl tyrosine tert-butyl ester (**F1YOtBu**)

To a DCM (10 mL) solution of 9-fluorenylcarboxylic acid (400 mg, 1.9 mmol) was added HCl.tyrosine tert-butyl ester salt (678 mg, 2.5 mmol), DIPEA (1.32 mL, 7.6 mmol), and 50%

T3P solution in EtOAc (1.47 mL, 2.5 mmol). The reaction mixture was stirred at room temperature for 1.5 hours. The reaction mixture was diluted with DCM, then washed with 1 M HCl (x2), water (x2), and brine. The organic layer was isolated and concentrated *via* rotary evaporation, in order to afford the crude product. The crude product was purified *via* silica column chromatography, eluting with a 0-2% MeOH/DCM gradient, in order to afford the title compound (765 mg, 93.6%).

9-Fluorenylcarbonyl tyrosine (**F1Y**)

A 1:1 TFA/DCM (15 mL) solution of **F1YOtBu** (765 mg, 1.8 mmol) was stirred at room temperature for 3 hours. The reaction mixture was then concentrated *via* rotary evaporation. The residue was diluted with DCM, then washed with 1 M HCl (x2), water (x2), and brine. The organic layer was isolated, dried over $MgSO_4$, and concentrated *via* rotary evaporation, in order to afford the title compound (651 mg, 97.9%).

9-Fluorenylcarbonyl tyrosine leucine tert-butyl ester (**F1YLOtBu**)

The title compound (856 mg, 90.5%) was prepared (from **F1Y**) *via* a T3P mediated amide coupling, in a similar fashion to that previously described for **F1YOtBu**.

9-Fluorenylcarbonyl tyrosine leucine (**F1YL**)

The title compound (762 mg, 99.3%) was prepared (from **F1YLOtBu**) *via* a TFA mediated cleavage of a tert-butyl ester, in a similar fashion to that previously described for **F1Y**.

ESI MS +ve $[M+Na]^+$ m/z 509.15

ESI MS -ve $[M-H]^-$ m/z 485.00

^{1}H NMR (CD_3OD) δ 7.78 (t, *J* = 8.3 Hz, 2H, ArH), 7.47 (d, *J* = 7.5 Hz, 1H, ArH), 7.39 (dt, *J* = 15.8, 7.6 Hz, 2H, ArH), 7.30 (t, *J* = 7.4 Hz, 1H, ArH), 7.20 (t, *J* = 7.5 Hz, 1H, ArH), 7.07 (d, *J* = 8.5 Hz, 2H, ArH), 7.02 (d, *J* = 7.9 Hz, 1H, ArH), 6.73 (d, *J* = 8.5 Hz, 2H, ArH), 4.75-4.71 (m, 2H, ArCH/COCH), 4.50-4.46 (m, 1H, COCH), 3.16 (dd, *J* = 14.2, 4.9 Hz, 1H, $ArCH_2$), 2.86 (dd, *J* = 14.0, 10.0 Hz, 1H, $ArCH_2$), 1.73-1.61 (m, 3H, CH/CH_2), 0.94 (t, *J* = 6.2 Hz, 6H, CH_3)

^{13}C NMR (CD_3OD) δ 173.9 (C=O), 171.9 (C=O), 171.4 (C=O), 155.5 (Ar-OH), 141.5 (Ar), 141.4 (Ar), 141.3 (Ar), 141.1 (Ar), 129.5 (Ar), 127.2 (Ar), 127.2 (Ar), 127.0 (Ar), 126.5 (Ar), 124.3 (Ar), 124.0 (Ar), 119.2 (Ar), 119.1 (Ar), 114.4 (Ar), 54.1 (NHCH), 53.9 (ArCH), 50.1 (NHCH), 39.8 (CH_2), 35.9 (CH_2), 24.0 (CH), 21.5 (CH_3), 19.9 (CH_3)

3.1.1.4 9-Fluorenylcarbonyl dileucine (F1LL)

9-Fluorenylcarbonyl dileucine tert-butyl ester (**F1LLOtBu**)

The title compound (354 mg, 93.2%) was prepared (from **LLOtBu**) *via* a T3P mediated amide coupling, in a similar fashion to that previously described for **F1YOtBu**.

9-Fluorenylcarbonyl dileucine (**F1LL**)

The title compound (313 mg, 99.7%) was prepared (from **F1LLOtBu**) *via* a TFA mediated cleavage of a tert-butyl ester, in a similar fashion to that previously described for **F1Y**.

ESI MS +ve $[M+Na]^+$ m/z 459.12

ESI MS -ve $[M-H]^-$ m/z 435.10

^{1}H NMR (CD_3OD) δ 8.43 (d, *J* = 8.1 Hz, 1H, CONH), 8.33 (d, *J* = 8.1 Hz, 1H, CONH), 7.84 (dd, *J* = 7.6, 4.1 Hz, 2H, ArH), 7.58 (d, *J* = 7.5 Hz, 1H, ArH), 7.54 (d, *J* = 7.5 Hz, 1H, ArH), 7.43 (q, *J* = 6.6 Hz, 2H, ArH), 7.33 (q, *J* = 8.1 Hz, 2H, ArH), 4.87 (s, 1H, ArCH), 4.60-4.53 (m, 1H, COCH), 4.51-4.44 (m, 1H, COCH), 1.84-1.73 (m, 1H, CH), 1.71-1.56 (m, 5H, CH/CH_2), 1.02 (d, *J* = 6.5 Hz, 3H, CH_3), 0.97 (d, *J* = 6.5 Hz, 3H, CH_3), 0.90 (t, *J* = 6.4 Hz, 6H, CH_3)

^{13}C NMR (CD_3OD) δ 173.9 (C=O), 172.7 (C=O), 171.6 (C=O), 141.9 (Ar), 141.7 (Ar), 141.4 (Ar), 141.3 (Ar), 127.3 (Ar), 127.2 (Ar), 126.6 (Ar), 124.1 (Ar), 123.8 (Ar), 119.3 (Ar), 119.2 (Ar), 54.2 (NHCH), 51.3 (ArCH), 50.0 (NHCH), 40.0 (CH_2), 39.7 (CH_2), 24.1 (CH), 23.9 (CH), 21.5 (CH_3), 20.2 (CH_3), 19.9 (CH_3)

3.1.1.5 1-Pyrenylcarbonyl tyrosine leucine (P1YL)

1-Pyrenylcarbonyl tyrosine methyl ester (**P1YOMe**)

The title compound (739 mg, 86.0%) was prepared *via* a T3P mediated amide coupling, in a similar fashion to that previously described for **F1YOtBu**.

1-Pyrenylcarbonyl tyrosine (**P1Y**)

To a 1:1 THF/H_2O (10 mL) solution of **P1YOMe** (739 mg, 1.7 mmol) was added LiOH (183 mg, 4.4 mmol). The reaction mixture was stirred at room temperature for 2 hours. The reaction mixture was diluted with DCM, then washed with 1 M HCl (x2), water (x2), and brine. The organic layer was isolated and concentrated *via* rotary evaporation, in order to afford the title compound (700 mg, 98.0%).

1-Pyrenylcarbonyl tyrosine leucine methyl ester (**P1YLOMe**)

The title compound (490 mg, 53.4%) was prepared (from **P1Y**) *via* a T3P mediated amide coupling, in a similar fashion to that previously described for **F1YOtBu**.

1-Pyrenylcarbonyl tyrosine leucine (**P1YL**)

The title compound (464 mg, 97.1%) was prepared (from **P1YLOMe**) *via* LiOH methyl ester hydrolysis, in a similar fashion to that previously described for **P1Y**.

ESI MS +ve $[M+H]^+$ m/z 523.12, $[M+Na]^+$ m/z 545.14

ESI MS -ve $[M-H]^-$ m/z 521.06

^{1}H NMR ($(CD_3)_2SO$) δ 12.62 (s, 1H, COOH), 9.24 (s, 1H, ArOH), 8.79 (d, *J* = 8.6 Hz, 1H, CONH), 8.36-8.29 (m, 4H, ArH/CONH), 8.23 (q, *J* = 9.0 Hz, 2H, ArH), 8.14 (s, 2H, ArH), 8.12 (t, *J* = 7.6 Hz, 1H, ArH), 7.95 (d, *J* = 7.9 Hz, 1H, ArH), 7.24 (d, *J* = 8.4 Hz, 2H, ArH), 6.76 (d, *J* = 8.4 Hz, 2H, ArH), 4.95-4.87 (m, 1H, COCH), 4.43-4.36 (m, 1H, COCH), 3.12 (dd, *J* = 14.0, 3.6 Hz, 1H, $ArCH_2$), 2.86 (dd, *J* = 13.9, 11.0 Hz, 1H, $ArCH_2$), 1.87-1.75 (m, 1H, CH), 1.72-1.58 (m, 2H, CH_2), 0.97 (dd, *J* = 12.7, 6.6 Hz, 6H, CH_3)

^{13}C NMR ($(CD_3)_2SO$) δ 174.0 (C=O), 171.6 (C=O), 168.8 (C=O), 155.9 (ArOH), 131.8 (Ar), 131.5 (Ar), 130.7 (Ar), 130.3 (Ar), 130.2 (Ar), 128.3 (Ar), 128.2 (Ar), 127.7 (Ar), 127.7 (Ar), 127.2 (Ar), 126.5 (Ar), 125.7 (Ar), 125.5 (Ar), 125.1 (Ar), 124.9 (Ar), 124.3 (Ar), 123.6 (Ar), 123.6 (Ar), 114.9 (Ar), 55.0 (NHCH), 50.3 (NHCH), 36.4 ($ArCH_2$), 24.3 (CH_2), 22.9 (CH), 21.4 (CH_3)

3.1.1.6 1-Pyrenylcarbonyl dileucine (P1LL)

1-Pyrenylcarbonyl dileucine methyl ester (**P1LLOtBu**)

The title compound (308 mg, 75.5%) was prepared (from **LLOtBu**) *via* a T3P mediated amide coupling, in a similar fashion to that previously described for **F1YOtBu**.

1-Pyrenylcarbonyl dileucine (**P1LL**)

The title compound (257 mg, 93.5%) was prepared (from **P1LLOtBu**) *via* a TFA mediated cleavage of a tert-butyl ester, in a similar fashion to that previously described for **F1Y**.

ESI MS +ve $[M+H]^+$ m/z 473.03, $[M+Na]^+$ m/z 495.11

ESI MS -ve $[M-H]^-$ m/z 471.10

^{1}H NMR (CD_3OD) δ 8.92 (d, *J* = 7.7 Hz, 1H, CONH), 8.56 (d, *J* = 8.2 Hz, 1H, CONH), 8.48 (d, *J* = 9.2 Hz, 1H, ArH), 8.28 (t, *J* = 8.0 Hz, 3H, ArH), 8.21-8.12 (m, 4H, ArH), 8.08 (t, *J* = 7.6 Hz, 1H, ArH), 4.90-4.86 (m, 1H, COCH), 4.66-4.60 (m, 1H, COCH), 1.98-1.87 (m, 2H, CH), 1.83-1.73 (m, 4H, CH_2), 1.12 (d, *J* = 6.6 Hz, 3H, CH_3), 1.08 (d, *J* = 6.6 Hz, 3H, CH_3), 1.04 (dd, *J* = 6.6, 1.3 Hz, 6H, CH_3)

^{13}C NMR (CD_3OD) δ 174.0 (C=O), 173.1 (C=O), 171.0 (C=O), 132.0 (Ar), 130.7 (Ar), 130.3 (Ar), 130.2 (Ar), 127.8 (Ar), 127.6 (Ar), 126.4 (Ar), 125.7 (Ar), 125.0 (Ar), 124.9 (Ar), 124.1 (Ar), 123.8 (Ar), 123.6 (Ar), 123.5 (Ar), 52.1 (NHCH), 50.2 (NHCH), 39.9 (CH_2), 39.8 (CH_2), 24.3 (CH), 24.1 (CH), 21.7 (CH_3), 21.6 (CH_3), 20.3 (CH_3), 20.0 (CH_3)

3.1.1.7 1-Naphthylcarbonyl dileucine (1N1LL)

1-Naphthylcarbonyl dileucine methyl ester (**1N1LLOMe**)

To a DCM (10 mL) solution of **LLOMe** (106 mg, 0.4 mmol) was added DIPEA (244 µL, 1.4 mmol), and 1-naphthoyl chloride (90 µL, 0.6 mmol). The reaction mixture was stirred at room temperature overnight. The reaction mixture was diluted with DCM, then washed with 1 M HCl (x2), water (x2), and brine. The organic layer was isolated and concentrated *via* rotary evaporation, in order to obtain the crude product. The crude product was purified *via* silica column chromatography, eluting with a 0-1% MeOH/DCM gradient, in order to afford the title compound (147 mg, 87.1 %).

ESI MS +ve $[M+Na]^+$ m/z 435.20

1-Naphthylcarbonyl dileucine (**1N1LL**)

To a 0.5 M NaOH solution (25 mL) was added **1N1LLOMe** (147.0 mg, 0.36 mmol). The reaction mixture was stirred at 70 ^oC for 3 hours; in order to obtain an aqueous solution. After being allowed to cool, the reaction mixture was acidified using 1M HCl, and the resulting precipitate extracted with DCM. The DCM solution was then concentrated *via* rotary evaporation, in order to afford the title compound (135 mg, 95.0 %).

ESI MS +ve $[M+Na]^+$ m/z 421.20

ESI MS -ve $[M-H]^-$ m/z 397.07

^1H NMR ($CDCl_3$) δ 8.27-8.22 (m, 1H, ArH), 7.91 (d, *J* = 8.5 Hz, 1H, ArH), 7.88-7.84 (m, 1H, ArH), 7.61 (d, *J* = 7.0 Hz, 1H, ArH), 7.58-7.49 (m, 3H, ArH/CONH), 7.42 (t, *J* = 7.7 Hz, 1H, ArH), 7.20 (d, *J* = 8.7 Hz, 1H, ArH), 4.94-4.86 (m, 1H, CHCO), 4.65-4.58 (m, 1H, CHCO), 1.82-1.56 (m, 6H, CH/CH_2), 1.00 (dd, *J* = 8.4, 6.3 Hz, 6H, CH_3), 0.93 (d, *J* = 6.2 Hz, 6H, CH_3)

3.1.1.8 9-Anthrylcarbonyl dileucine (A1LL)

9-Anthrylcarbonyl dileucine methyl ester (**A1LLOMe**)

To a DCM (10 mL) solution of 9-anthrylcarboxylic acid (133 mg, 0.6 mmol) was added thionyl chloride (44 µL, 0.6 mmol), and DMF (200 µL). The reaction mixture was stirred at room temperature for 30 minutes, before the addition of **LLOMe** (106 mg, 0.4 mmol) and DIPEA (418 µL, 2.4 mmol), after which the reaction mixture was left to stir overnight. The reaction mixture was diluted with DCM, then washed with 1 M HCl (x2), water (x2), and brine. The organic layer was isolated and concentrated *via* rotary evaporation, in order to obtain the crude product. The crude product was purified *via* silica column chromatography, eluting with a 0-1% MeOH/DCM gradient, in order to afford the title compound (142 mg, 75.1 %).

ESI MS +ve $[M+Na]^+$ m/z 485.20

9-Anthrylcarbonyl dileucine (**A1LL**)

The title compound (24.8 mg, 18.0 %) was prepared (from **A1LLOMe**) *via* NaOH methyl ester hydrolysis, in a similar fashion to that previously described for **1N1LL**.

ESI MS +ve $[M+Na]^+$ m/z 471.20

ESI MS -ve $[M-H]^-$ m/z 447.13

^{1}H NMR ($CDCl_3$) δ 8.45 (s, 1H, ArH), 8.03-7.92 (m, 4H, ArH), 7.53-7.42 (m, 4H, ArH/CONH), 7.11 (s, 1H, ArH), 6.83 (s, 1H, ArH), 5.02-4.94 (m, 1H, COCH), 4.74-4.64 (m, 1H, CHCO), 1.88-1.56 (m, 6H, CH/CH_2), 1.08-0.90 (m, 12H, CH_3)

3.1.1.9 Biphenyl-3-carbonyl dileucine (3B1LL)

Biphenyl-3-carbonyl dileucine (**3B1LL**)

The title compound (40.0 mg, 38.4 %) was prepared *via* an acid chloride amide coupling, in a similar fashion to that previously described for **1N1LLOMe**.

ESI MS +ve $[M+Na]^+$ m/z 447.20

ESI MS -ve $[M-H]^-$ m/z 423.13

^{1}H NMR ($CDCl_3$) δ 8.07 (s, 1H, ArH), 7.81 (d, *J* = 7.7 Hz, 1H, ArH), 7.73 (d, *J* = 7.7 Hz, 1H, ArH), 7.61 (d, *J* = 7.4 Hz, 2H, ArH), 7.57-7.44 (m, 4H, ArH/CONH), 7.41-7.36 (m, 1H, ArH), 7.24-7.16 (br s, 1H, ArH), 4.96-4.88 (m, 1H, CHCO), 4.67-4.59 (m, 1H, CHCO), 1.81-1.55 (m, 6H, CH/CH_2), 0.98-0.94 (m, 6H, CH_3), 0.88 (t, *J* = 6.3 Hz, 6H, CH_3)

3.1.1.10 Biphenyl-4-carbonyl dileucine (4B1LL)

Biphenyl-4-carbonyl dileucine (**4B1LL**)

The title compound (35.2 mg, 33.8 %) was prepared *via* an acid chloride amide coupling, in a similar fashion to that previously described for **1N1LLOMe**.

ESI MS +ve $[M+Na]^+$ m/z 447.27

ESI MS -ve $[M-H]^-$ m/z 423.20

^{1}H NMR ($CDCl_3$) δ 7.91 (d, *J* = 8.0 Hz, 2H, ArH), 7.62 (dd, *J* = 17.4, 7.7 Hz, 4H, ArH), 7.49-7.34 (m, 4H, ArH/CONH), 4.97-4.89 (m, 1H, CHCO), 4.67-4.58 (m, 1H, CHCO), 1.82-1.55 (m, 6H, CH/CH_2), 1.01-0.94 (m, 6H, CH_3), 0.92-0.84 (m, 6H, CH_3)

3.1.2 Methylcarbonyl $CH_2C{=}O$ linker (2) compounds

3.1.2.1 9-Fluorenylmethylcarbonyl tyrosine leucine (F2YL)[1]

Tert-butyl carbonyl tyrosine leucine methyl ester (**BocYLOMe**)

The title compound (499 mg, 85.9%) was prepared *via* a T3P mediated amide coupling, in a

similar fashion to that previously described for **F1YOtBu**.

Tyrosine leucine methyl ester (**YLOMe**)

The title compound (110 mg, 29.2%) was prepared (from **BocYLOMe**) *via* a TFA mediated cleavage of a tert-butyl carbamate, in a similar fashion to that previously described for **F1Y**.

9-Fluorenylmethylcarbonyl tyrosine leucine methyl ester (**F2YLOMe**)

The title compound (115 mg, 62.6%) was prepared (from **YLOMe**) *via* a T3P mediated amide coupling, in a similar fashion to that previously described for **F1YOtBu**.

ESI MS +ve $[M+Na]^+$ m/z 537.27

ESI MS -ve $[M-H]^-$ m/z 513.13

^{1}H NMR (CD_3OD) δ 7.76 (dd, *J* = 7.6, 2.6 Hz, 2H, ArH), 7.41 (d, *J* = 7.4 Hz, 1H, ArH), 7.34 (q, *J* = 6.6 Hz, 2H, ArH), 7.28-7.18 (m, 3H, ArH), 7.13 (d, *J* = 8.5 Hz, 2H, ArH), 6.72 (d, *J* = 8.6 Hz, 2H, ArH), 4.81 (dd, *J* = 9.6, 5.6 Hz, 1H, CH), 4.53 (dd, *J* = 9.5, 5.7 Hz, 1H, CH), 4.32 (t, *J* = 7.5 Hz, 1H, CH), 3.71 (s, 3H, OCH_3), 3.08 (dd, *J* = 13.9, 5.6 Hz, 1H, $ArCH_2$), 2.79 (dd, *J* = 14.1, 9.6 Hz, 1H, $ArCH_2$), 2.63 (dd, *J* = 14.6, 7.2 Hz, 1H, $ArCH_2$), 2.55 (dd, *J* = 14.7, 7.8 Hz, 1H, $ArCH_2$), 1.81-1.60 (m, 3H, CH/CH_2), 0.98 (dd, *J* = 12.0, 6.6 Hz, 6H, CH_3)

9-Fluorenylmethylcarbonyl tyrosine leucine (**F2YL**)

The title compound (53.2 mg, 96.3%) was prepared (from **F2YLOMe**) *via* LiOH methyl ester hydrolysis, in a similar fashion to that previously described for **P1Y**.

ESI MS +ve $[M+H]^+$ m/z 501.00, $[M+Na]^+$ m/z 523.16

ESI MS -ve $[M-H]^-$ m/z 499.14

^{1}H NMR (CD_3OD) δ 8.37 (d, *J* = 8.4 Hz, 1H, CONH), 7.75 (dd, *J* = 7.5, 3.0 Hz, 2H, ArH), 7.41-7.30 (m, 3H, ArH), 7.24 (td, *J* = 7.5, 1.1 Hz, 1H, ArH), 7.21-7.18 (m, 2H, ArH), 7.14 (d, *J* = 8.5 Hz, 2H, ArH), 6.73 (d, *J* = 8.5 Hz, 2H, ArH), 4.84-4.81 (m, 1H, ArCH), 4.56-4.49 (m, 1H, CHCO), 4.31 (t, *J* = 7.4 Hz, 1H, CHCO), 3.14 (dd, *J* = 14.2, 4.6 Hz, 1H, $ArCH_2$), 2.79 (dd, *J* = 14.1, 10.1 Hz, 1H, $ArCH_2$), 2.63 (dd, *J* = 14.7, 7.1 Hz, 1H, $ArCH_2$), 2.53 (dd, *J* = 14.6, 7.9 Hz, 1H, $ArCH_2$), 1.85-1.74 (m, 1H, CH), 1.70 (t, *J* = 7.3 Hz, 2H, CH_2), 1.00 (dd, *J* = 10.7, 6.5 Hz, 6H, CH_3)

3.1.2.2 9-Fluorenylmethylcarbonyl dileucine (F2LL)

9-Fluorenylmethylcarbonyl dileucine (**F2LL**)

In a fritted column, Wang resin (500 mg, 0.6 mmol) was washed with DMF (x4). A DMF solution of Fmoc-L (972 mg, 2.8 mmol) and pyridine (365 μL, 4.5 mmol) was then added to the resin. DBC (394 μL, 2.8 mmol) was then added to the resin slurry, which was agitated

overnight. The resin was then washed with DMF (x4). 20% piperidine in DMF was added to the resin, which was agitated for 30 minutes. The resin was then washed with DMF (x4). A DMF solution of Fmoc-L (583 mg, 1.7 mmol), DIPEA (479 μL, 2.8 mmol), and HBTU (605 mg, 2.9 mmol) was then added to resin, which was agitated for an hour. The resin was then washed with DMF (x4). 20% piperidine in DMF was added to the resin, which was agitated for 30 minutes. The resin was then washed with DMF (x4). A DMF solution of 9-Fluoreneacetic acid (370 mg, 1.7 mmol), DIPEA (479 μL, 2.8 mmol), and HBTU (396 mg, 1.0 mmol) was then added to resin, which was agitated for an hour. The resin was then washed with DMF (x4) and DCM (x4). A 95:5 TFA:water solution was added to the resin, which was agitated overnight. The resin was then washed with DCM (x4), and the filtrate collected, and concentrated under vacuum. The residue was then swirled with diethyl ether, which was subsequently decanted off (x3). The residue was then concentrated under vacuum in order to afford the title compound (66.7 mg, 24.7%).

ESI MS +ve $[M+H]^+$ m/z 451.00, $[M+Na]^+$ m/z 473.20

ESI MS -ve $[M-H]^-$ m/z 449.13

^{1}H NMR (CD_3OD) δ 8.33 (d, *J* = 8.1 Hz, 1H, CONH), 8.11 (d, *J* = 7.6 Hz, 1H, CONH), 7.79 (d, *J* = 7.5 Hz, 2H, ArH), 7.53 (dd, *J* = 12.3, 7.1 Hz, 2H, ArH), 7.38 (t, *J* = 7.4 Hz, 2H, ArH), 7.29 (qd, *J* = 7.9, 1.1 Hz, 2H, ArH), 4.62-4.49 (m, 2H, CHCO), 4.40 (t, *J* = 7.5 Hz, 1H, ArCH), 2.74 (dd, *J* = 14.5, 7.2 Hz, 1H, CH_2CO), 2.61 (dd, *J* = 14.6, 7.8 Hz, 1H, CH_2CO), 1.88-1.51 (m, 6H, CH/CH_2), 1.02-0.96 (m, 12H, CH_3)

3.1.2.3 9-Fluorenylmethylcarbonyl diphenylalanine (F2FF)

9-Fluorenylmethylcarbonyl diphenylalanine (**F2FF**)

The title compound (144 mg, 44.9 %) was prepared *via* SPPS, in a similar fashion to that previously described for **F2LL**.

ESI MS +ve $[M+H]^+$ m/z 518.93, $[M+Na]^+$ m/z 541.13

ESI MS -ve $[M-H]^-$ m/z 517.07

^{1}H NMR (CD_3OD) δ 8.25-8.19 (m, CONH) 7.74 (dd, *J* = 7.9, 2.3 Hz, 2H, ArH), 7.36-7.12 (m, 16H, ArH), 4.90-4.86 (m, 1H, CHCO), 4.73-4.69 (m, 1H, CHCO), 4.27 (t, *J* = 7.5 Hz, 1H, ArCH), 3.25 (dd, *J* = 13.8, 5.3 Hz, 1H, $ArCH_2$), 3.17 (dd, *J* = 14.1, 5.0 Hz, 1H, $ArCH_2$), 3.06 (dd, *J* = 14.0, 8.1 Hz, 1H, $ArCH_2$), 2.84 (dd, *J* = 13.9, 10.0 Hz, 1H, $ArCH_2$), 2.57 (dd, *J* = 14.7, 7.0 Hz, 1H, $ArCH_2$), 2.47 (dd, *J* = 14.8, 7.9 Hz, 1H, $ArCH_2$)

3.1.2.4 9-Fluorenylmethylcarbonyl phenylalanine leucine (F2FL)

9-Fluorenylmethylcarbonyl phenylalanine leucine (**F2FL**)

The title compound (157 mg, 52.2 %) was prepared *via* SPPS, in a similar fashion to that

previously described for **F2LL**.

ESI MS +ve $[M+H]^+$ m/z 485.00, $[M+Na]^+$ m/z 507.13

ESI MS -ve $[M-H]^-$ m/z 483.13

^{1}H NMR ($CDCl_3$) δ 7.72 (d, *J* = 7.4 Hz, 2H, ArH), 7.42-7.30 (m, 4H, ArH), 7.27-7.16 (m, 7H, ArH), 6.75 (d, *J* = 8.4 Hz, 1H, CONH), 6.66 (d, *J* = 7.9 Hz, 1H, CONH), 4.95-4.87 (m, 1H, CHCO), 4.56-4.43 (m, 1H, CHCO), 4.40 (t, *J* = 7.1 Hz, 1H, ArCH), 3.02 (dd, *J* = 7.1, 3.4 Hz, 2H, $ArCH_2$), 2.61 (dd, *J* = 7.2, 2.4 Hz, 2H, CH_2CO), 1.72-1.51 (m, 3H, CH/CH_2), 0.94 (dd, *J* = 6.2, 2.7 Hz, 6H, CH_3)

3.1.2.5 9-Fluorenylmethylcarbonyl phenylalanine tyrosine (F2FY)

9-Fluorenylmethylcarbonyl phenylalanine tyrosine (**F2FY**)

The title compound (26.8 mg, 8.1 %) was prepared *via* SPPS, in a similar fashion to that previously described for **F2LL**.

ESI MS +ve $[M+H]^+$ m/z 534.93, $[M+Na]^+$ m/z 557.13

ESI MS -ve $[M-H]^-$ m/z 533.07

^{1}H NMR (CD_3OD) δ 8.22 (d, *J* = 8.5 Hz, 1H, CONH), 7.74 (dd, *J* = 7.5, 2.5 Hz, 2H, ArH), 7.38-7.12 (m, 11H, ArH), 7.09 (d, *J* = 8.5 Hz, 2H, ArH), 6.72 (d, *J* = 8.5 Hz, 2H, ArH), 4.90-4.86 (m, 1H, CHCO), 4.64 (dd, *J* = 8.0, 5.1 Hz, 1H, CHCO), 4.29 (t, *J* = 7.5 Hz, 1H, ArCH), 3.16 (dt, *J* = 14.1, 5.1 Hz, 2H, $ArCH_2$), 2.97 (dd, *J* = 14.0, 8.0 Hz, 1H, $ArCH_2$), 2.83 (dd, *J* = 14.1, 10.0 Hz, 1H, $ArCH_2$), 2.59 (dd, *J* = 14.7, 7.1 Hz, 1H, $ArCH_2$), 2.46 (dd, *J* = 14.7, 8.0 Hz, 1H, $ArCH_2$)

3.1.2.6 9-Fluorenylmethylcarbonyl dialanine (F2AA)[2,3]

9-Fluorenylmethylcarbonyl alanine methyl ester (**F2AOMe**)

The title compound (434 mg, 77.1%) was prepared *via* a T3P mediated amide coupling, in a similar fashion to that previously described for **F1YOtBu**.

9-Fluorenylmethylcarbonyl alanine (**F2A**)

The title compound (381 mg, 91.9%) was prepared (from **F2AOMe**) *via* LiOH methyl ester hydrolysis, in a similar fashion to that previously described for **P1Y**.

9-Fluorenylmethylcarbonyl dialanine methyl ester (**F2AAOMe**)

The title compound (428 mg, 87.2 %) was prepared (from **F2A**) *via* a T3P mediated amide coupling, in a similar fashion to that previously described for **F1YOtBu**.

^{1}H NMR ($CDCl_3$) δ 7.78 (d, *J* = 7.3 Hz, 2H, ArH), 7.51 (dd, *J* = 7.4, 4.2 Hz, 2H, ArH), 7.40 (t, *J* = 7.7 Hz, 2H, ArH), 7.34-7.29 (m, 2H, ArH), 6.65 (d, *J* = 7.6 Hz, 1H, CONH), 5.98 (d, *J*

= 7.4 Hz, 1H, CONH), 4.61-4.52 (m, 2H, CHCO), 4.50 (t, *J* = 7.1 Hz, 1H, ArCH), 3.77 (s, 3H, OCH_3), 2.71 (dd, *J* = 14.8, 7.0 Hz, 1H, CH_2), 2.71 (dd, *J* = 14.8, 7.3 Hz, 1H, CH_2), 1.45 (d, *J* = 7.2 Hz, 3H, CH_3), 1.34 (d, *J* = 7.0 Hz, 3H, CH_3)

9-Fluorenylmethylcarbonyl dialanine (**F2AA**)

The title compound (402 mg, 97.5%) was prepared (from **F2AAOMe**) *via* LiOH methyl ester hydrolysis, in a similar fashion to that previously described for **P1Y**.

ESI MS +ve $[M+H]^+$ m/z 366.98, $[M+Na]^+$ m/z 389.13

ESI MS -ve $[M-H]^-$ m/z 365.05

^{1}H NMR (CD_3OD) δ 7.79 (d, *J* = 7.5 Hz, 2H, ArH), 7.54 (d, *J* = 7.5 Hz, 1H, ArH), 7.51 (d, *J* = 7.6 Hz, 1H, ArH), 7.37 (t, *J* = 7.4 Hz, 2H, ArH), 7.29 (q, *J* = 6.8 Hz, 2H, ArH), 4.53 (q, *J* = 7.1 Hz, 1H, COCH), 4.46 (q, *J* = 7.3 Hz, 1H, COCH), 4.41 (t, *J* = 7.5 Hz, 1H, ArCH), 2.66 (dd, *J* = 14.6, 7.3 Hz, 1H, CH_2), 2.60 (dd, *J* = 14.6, 7.9 Hz, 1H, CH_2), 1.47 (d, *J* = 7.3 Hz, 3H, CH_3), 1.39 (d, *J* = 7.2 Hz, 3H, CH_3)

3.1.2.7 1-Pyrenylmethylcarbonyl tyrosine leucine (P2YL)

1-Pyrenylmethylcarbonyl tyrosine methyl ester (**P2YOMe**)

The title compound (1.62 g, 88.1%) was prepared *via* a T3P mediated amide coupling, in a similar fashion to that previously described for **F1YOtBu**.

1-Pyrenylmethylcarbonyl tyrosine (**P2Y**)

The title compound (1.39 g, 96.7%) was prepared (from **P2YOMe**) *via* LiOH methyl ester hydrolysis, in a similar fashion to that previously described for **P1Y**.

1-Pyrenylmethylcarbonyl tyrosine leucine methyl ester (**P2YLOMe**)

The title compound (1.37 g, 76.1%) was prepared (from **P2Y**) *via* a T3P mediated amide coupling, in a similar fashion to that previously described for **F1YOtBu**.

1-Pyrenylmethylcarbonyl tyrosine leucine (**P2YL**)

The title compound (1.30 mg, 97.2%) was prepared (from **P2YLOMe**) *via* LiOH methyl ester hydrolysis, in a similar fashion to that previously described for **P1Y**.

ESI MS +ve $[M+H]^+$ m/z 536.93, $[M+Na]^+$ m/z 559.13

^{1}H NMR (CD_3OD) δ 8.22 (d, *J* = 8.0 Hz, 1H, CONH), 8.21 (d, *J* = 7.7 Hz, 2H, ArH), 8.12 (d, *J* = 7.8 Hz, 1H, ArH), 8.08 (d, *J* = 7.1 Hz, 4H, ArH), 8.02 (t, *J* = 7.7 Hz, 1H, ArH), 7.91 (d, *J* = 8.1 Hz, 1H, CONH), 7.81 (d, *J* = 7.8 Hz, 1H, ArH), 6.93 (d, *J* = 8.4 Hz, 2H, ArH), 6.56 (d, *J* = 8.5 Hz, 2H, ArH), 4.75-4.68 (m, 1H, CHCO), 4.47-4.40 (m, 1H, CHCO), 4.25

(s, 2H, $ArCH_2$), 3.05 (dd, *J* = 13.9, 4.8 Hz, 1H, $ArCH_2$), 2.81 (dd, *J* = 14.0, 9.3 Hz, 1H, $ArCH_2$), 1.63-1.52 (m, 3H, CH/CH_2), 0.84-0.81 (m, 6H, CH_3)

3.1.2.8 1-Pyrenylmethylcarbonyl dileucine (P2LL)

1-Pyrenylmethylcarbonyl dileucine methyl ester (**P2LLOMe**)

The title compound (211 mg, 69.0%) was prepared (from **LLOMe**) *via* a T3P mediated amide coupling, in a similar fashion to that previously described for **F1YOtBu**.

1-Pyrenylmethylcarbonyl dileucine (**P2LL**)

The title compound (194 mg, 94.8%) was prepared (from **P2LLOMe**) *via* LiOH methyl ester hydrolysis, in a similar fashion to that previously described for **P1Y**.

ESI MS +ve $[M+Na]^+$ m/z 509.07

ESI MS -ve $[M-H]^-$ m/z 485.13

^1H NMR (CD_3OD) δ 8.32 (d, *J* = 9.4 Hz, 1H, ArH), 8.21 (d, *J* = 7.9 Hz, 2H, ArH), 8.16 (dd, *J* = 11.4, 8.6 Hz, 2H, ArH), 8.07 (s, 2H, ArH), 8.02 (dd, *J* = 14.6, 7.7 Hz, 2H, ArH), 4.56-4.50 (m, 1H, COCH), 4.43-4.37 (m, 1H, COCH), 4.33 (s, 2H, $ArCH_2$), 1.71-1.44 (m, 6H, CH/CH_2), 0.90 (dd, *J* = 14.9, 6.2 Hz, 6H, CH_3), 0.80-0.73 (m, 6H, CH_3)

3.1.2.9 1-Naphthylmethylcarbonyl tyrosine leucine (1N2YL)

1-Naphthylmethylcarbonyl tyrosine leucine (**1N2YL**)

The title compound (137 mg, 49.2%) was prepared *via* SPPS, in a similar fashion to that previously described for **F2LL**.

ESI MS +ve $[M+H]^+$ m/z 463.00, $[M+Na]^+$ m/z 485.13

^1H NMR (CD_3OD) δ 7.89-7.77 (m, 3H, ArH), 7.51-7.44 (m, 2H, ArH), 7.39 (dd, *J* = 8.1, 7.1 Hz, 1H, ArH), 7.26 (d, *J* = 6.9 Hz, 1H, ArH), 6.91 (d, *J* = 8.4 Hz, 2H, ArH), 6.61 (d, J= 8.4 Hz, 2H, ArH), 4.70-4.64 (m, 1H, COCH), 4.46-4.40 (m, 1H, COCH), 3.97 (s, 2H, $ArCH_2$), 3.03 (dd, *J* = 14.0, 4.8 Hz, 1H, $ArCH_2$), 2.79 (dd, *J* = 14.0, 9.3 Hz, 1H, $ArCH_2$), 1.69-1.54 (m, 3H, CH/CH_2), 0.90 (dd, *J* = 10.0, 5.9 Hz, 6H, CH_3)

3.1.2.10 1-Naphthylmethylcarbonyl dileucine (1N2LL)

1-Naphthylmethylcarbonyl dileucine methyl ester (**1N2LLOMe**)

The title compound (132 mg, 76.0%) was prepared (from **LLOMe**) *via* a T3P mediated amide coupling, in a similar fashion to that previously described for **F1YOtBu**.

1-Naphthylmethylcarbonyl dileucine (**1N2LL**)

The title compound (122 mg, 95.6%) was prepared (from **1N2LLOMe**) *via* LiOH methyl ester hydrolysis, in a similar fashion to that previously described for **P1Y**.

ESI MS +ve $[M+H]^+$ m/z 413.10, $[M+Na]^+$ m/z 435.19

^{1}H NMR (CD_3OD) δ 8.10-8.03 (m, 1H, ArH), 7.89 (d, *J* = 7.6 Hz, 1H, ArH), 7.84-7.79 (m, 1H, ArH), 7.56-7.42 (m, 4H, ArH), 4.53-4.37 (m, 2H, COCH), 4.06 (s, 2H, $ArCH_2$), 1.68-1.49 (m, 6H, CH/CH_2), 0.94-0.84 (m, 12H, CH_3)

3.1.2.11 2-Naphthylmethylcarbonyl tyrosine leucine (2N2YL)

2-Naphthylmethylcarbonyl tyrosine leucine (**2N2YL**)

The title compound (172 mg, 61.8%) was prepared *via* SPPS, in a similar fashion to that previously described for **F2LL**.

ESI MS +ve $[M+H]^+$ m/z 463.00, $[M+Na]^+$ m/z 485.13

^{1}H NMR (CD_3OD) δ 7.85-7.73 (m, 3H, ArH), 7.63 (s, 1H, ArH), 7.50-7.42 (m, 2H, ArH), 7.23 (dd, *J* = 8.4, 1.5 Hz, 1H, ArH), 7.00 (d, *J* = 8.4 Hz, 2H, ArH), 6.62 (d, J= 8.4 Hz, 2H, ArH), 4.67 (dd, J= 9.4, 4.8 Hz, 1H, COCH), 4.44-4.38 (m, 1H, COCH), 3.66 (d, *J* = 8.5 Hz, 2H, $ArCH_2$), 3.10 (dd, *J* = 14.2, 4.8 Hz, 1H, $ArCH_2$), 2.81 (dd, *J* = 14.1, 9.5 Hz, 1H, $ArCH_2$), 1.68-1.54 (m, 3H, CH/CH_2), 0.88 (dd, *J* = 8.1, 5.8 Hz, 6H, CH_3)

3.1.2.12 2-Naphthylmethylcarbonyl dileucine (2N2LL)

2-Naphthylmethylcarbonyl dileucine methyl ester (**2N2LLOMe**)

The title compound (124 mg, 71.2%) was prepared (from **LLOMe**) *via* a T3P mediated amide coupling, in a similar fashion to that previously described for **F1YOtBu**.

2-Naphthylmethylcarbonyl dileucine (**2N2LL**)

The title compound (115 mg, 96.1%) was prepared (from **2N2LLOMe**) *via* LiOH methyl ester hydrolysis, in a similar fashion to that previously described for **P1Y**.

ESI MS +ve $[M+H]^+$ m/z 413.10, $[M+Na]^+$ m/z 435.19

^{1}H NMR (CD_3OD) δ 7.87-7.77 (m, 4H, ArH), 7.51-7.42 (m, 3H, ArH), 4.53-4.37 (m, 2H, COCH), 3.73 (s, 2H, $ArCH_2$), 1.73-1.47 (m, 6H, CH/CH_2), 0.98-0.80 (m, 12H, CH_3)

3.1.3 Methoxycarbonyl $CH_2OC{=}O$ linker (3) compounds

3.1.3.1 9-Fluorenylmethoxycarbonyl tyrosine leucine (F3YL)[1,4]

9-Fluorenylmethoxycarbonyl tyrosine leucine tert-butyl ester (**F3YLOtBu**)

The title compound (796 mg, 70.1 %) was prepared *via* a T3P mediated amide coupling, in a similar fashion to that previously described for **F1YOtBu**.

9-Fluorenylmethoxycarbonyl tyrosine leucine (**F3YL**)

The title compound (658 mg, 91.7 %) was prepared (from **F3YLOtBu**) *via* a TFA mediated

cleavage of a tert-butyl ester, in a similar fashion to that previously described for **F1Y**.

ESI MS +ve $[M+H]^+$ m/z 517.13, $[M+Na]^+$ m/z 539.20

ESI MS -ve $[M-H]^-$ m/z 514.87

^{1}H NMR (CD_3OD) δ 7.80 (d, J= 7.5 Hz, 2H, ArH), 7.59 (d, *J* = 7.4 Hz, 2H, ArH), 7.39 (t, *J* = 7.4 Hz, 2H, ArH), 7.31 (q, *J* = 7.1 Hz, 2H, ArH), 7.11 (d, *J* = 8.3 Hz, 2H, ArH), 6.71 (d, *J* = 8.3 Hz, 2H, ArH), 4.46 (t, *J* = 7.3 Hz, 1H, ArCH), 4.43-4.36 (m, 1H, COCH), 4.32 (dd, *J* = 9.9, 6.8 Hz, 1H, COCH), 4.24-4.14 (m, 2H, CH_2O), 3.08 (dd, *J* = 13.9, 4.7 Hz, 1H, CH_2Ar), 2.78 (dd, *J* = 14.0, 9.7 Hz, 1H, CH_2Ar), 1.75-1.62 (m, 3H, CH/CH_2), 0.94 (dd, *J* = 8.2, 6.3 Hz, 6H, CH_3)

^{13}C NMR ($(CD_3)_2SO$) 172.7 (C=O), 170.8 (C=O), 154.8 (OC=O), 153.8 (Ar-OH), 141.9 (Ar), 139.1 (Ar), 128.0 (Ar), 125.9 (Ar), 125.3 (Ar), 124.8 (Ar), 122.9 (Ar), 117.5 (Ar), 112.8 (Ar), 64.6 (CH_2O), 54.5 (NHCH), 54.4 (NHCH), 48.9 (ArCH), 38.5 (CH_2), 34.9 (CH_2), 22.6 (CH), 20.0 (CH_3), 18.6 (CH_3)

3.1.3.2 9-Fluorenylmethoxycarbonyl leucine-1-^{13}C leucine (F3L*L)

9-Fluorenylmethoxycarbonyl leucine-1-^{13}C (**F3L***)

To water (6 mL) was added leucine-1-^{13}C (500 mg, 3.78 mmol), and triethylamine (528 μL, 3.78 mmol). Separately, Fmoc-NHS ester (1.28 g, 3.78 mmol) was dissolved in MeCN (5 mL). The two solutions were mixed, and the pH raised to 9.0 *via* the dropwise addition of triethylamine. The reaction mixture was stirred at room temperature for 1.5 hours. The reaction mixture was acidified with 1M HCl and extracted with EtOAc. The organic layer was dried over $MgSO_4$ and concentrated under vacuum in order to afford the title compound (1.20 g, 89.5 %).

^{1}H NMR (CD_3OD) δ 7.80 (d, *J* = 7.6 Hz, 2H, ArH), 7.69 (t, *J* = 7.3 Hz, 2H, ArH), 7.40 (t, *J* = 7.4 Hz, 2H, ArH), 7.32 (tt, *J* = 7.5, 1.1 Hz, 2H, ArH), 4.37 (d, *J* = 7.1 Hz, 2H, ArCH/CH_2), 4.26-4.18 (m, 2H, CH_2/CHCO), 1.78-1.69 (m, 1H, CH), 1.64 (td, *J* = 7.3, 2.5 Hz, 2H, CH_2), 0.97 (dd, *J* = 12.6, 6.5 Hz, 6H, CH_3)

9-Fluorenylmethoxycarbonyl leucine-1-^{13}C leucine tert-butyl ester (**F3L*LOtBu**)

The title compound (1.70 g, 95.8 %) was prepared (from **F3L***) ***via*** a T3P mediated amide coupling, in a similar fashion to that previously described for **F1YOtBu**.

9-Fluorenylmethoxycarbonyl leucine-1-^{13}C leucine (**F3L*L**)

The title compound (1.50 g, 98.7 %) was prepared (from **F3L*LOtBu**) *via* a TFA mediated cleavage of a tert-butyl ester, in a similar fashion to that previously described for **F1Y**.

ESI MS +ve $[M+H]^+$ m/z 468.13, $[M+Na]^+$ m/z 490.27

^{1}H NMR (CD_3OD) δ 7.81 (d, *J* = 7.5 Hz, 2H, ArH), 7.68 (t, *J* = 7.4 Hz, 2H, ArH), 7.40 (t, *J* = 7.5 Hz, 2H, ArH), 7.32 (tt, *J* = 7.5, 1.3 Hz, 2H, ArH), 4.46 (td, *J* = 7.4, 2.5 Hz, 1H, ArCH), 4.39 (d, *J* = 6.9 Hz, 2H, CH_2O), 4.26-4.19 (m, 2H, CHCO), 1.78-1.52 (m, 6H, CH/CH_2), 0.99-0.89 (m, 12H, CH_3)

^{13}C NMR (CD_3OD) δ 173.5 (^{13}C=O)

3.1.3.3 9-Fluorenylmethoxycarbonyl leucine leucine-1-^{13}C leucine (F3LL*L)

Leucine-1-^{13}C tert butyl ester (**L*OtBu**)

The title compound (381 mg, 53.5 %) was prepared *via* formation of a tert-butyl ester, in a similar fashion to that previously described for **LLOtBu**.

^{1}H NMR ($CDCl_3$) δ 3.37 (dt, *J* = 8.3, 5.6 Hz, 1H, CHCO), 1.86-1.77 (m, 3H, CH/CH_2), 1.48 (s, 9H, CH_3), 0.95 (dd, *J* = 9.2, 6.6 Hz, 6H, CH_3)

9-Fluorenylmethoxycarbonyl leucine leucine-1-^{13}C tert-butyl ester (**F3LL*OtBu**)

The title compound (785 mg, 96.3 %) was prepared (from **L*OtBu**) *via* a T3P mediated amide coupling, in a similar fashion to that previously described for **F1YOtBu**.

9-Fluorenylmethoxycarbonyl leucine leucine-1-^{13}C (**F3LL***)

The title compound (687 mg, 98.0 %) was prepared (from **F3LL*OtBu**) *via* a TFA mediated cleavage of a tert-butyl ester, in a similar fashion to that previously described for **F1Y**.

9-Fluorenylmethoxycarbonyl leucine leucine-1-^{13}C leucine tert-butyl ester (**F3LL*LOtBu**)

The title compound (699 mg, 74.8 %) was prepared (from **F3LL***) ***via*** a T3P mediated amide coupling, in a similar fashion to that previously described for **F1YOtBu**.

9-Fluorenylmethoxycarbonyl leucine leucine-1-^{13}C leucine (**F3LL*L**)

The title compound (604 mg, 94.6 %) was prepared (from **F3LL*LOtBu**) *via* a TFA mediated cleavage of a tert-butyl ester, in a similar fashion to that previously described for **F1Y**.

ESI MS +ve $[M+H]^+$ m/z 581.20, $[M+Na]^+$ m/z 603.33

^{1}H NMR (CD_3OD) δ 8.21-8.16 (m, CONH), 8.04 (d, *J* = 7.9 Hz, CONH), 7.82 (d, *J* = 7.5 Hz, 2H, ArH), 7.70-7.65 (m, 2H, ArH), 7.41 (t, J= 7.4 Hz, 2H, ArH), 7.32 (tt, *J* = 7.5, 1.1 Hz, 2H, ArH), 4.52-4.34 (m, 4H, $ArCH/CHCO/OCH_2$), 4.24 (t, *J* = 6.8 Hz, 1H, CHCO), 4.19 (t, *J* = 7.6 Hz, 1H, CHCO), 1.76-1.52 (m, 9H, CH/CH_2), 0.99-0.88 (m, 18H, CH_3)

^{13}C NMR (CD_3OD) δ 172.5 (^{13}C=O)

3.1.3.4 9-Fluorenylmethoxycarbonyl alanine-1-^{13}C alanine (F3A*A)[3]

9-Fluorenylmethoxycarbonyl alanine-1-^{13}C (**F3A***)

The title compound (800 mg, 92.3 %) was prepared *via* Fmoc protection, in a similar fashion to that previously described for **F3L***.

9-Fluorenylmethoxycarbonyl alanine-1-^{13}C alanine tert-butyl ester (**F3A*AOtBu**)

The title compound (1.03 g, 77.2 %) was prepared (from **F3A***) *via* a T3P mediated amide coupling, in a similar fashion to that previously described for **F1YOtBu**.

9-Fluorenylmethoxycarbonyl alanine-1-^{13}C alanine (**F3A*A**)

The title compound (839 mg, 92.9 %) was prepared (from **F3A*AOtBu**) *via* a TFA mediated cleavage of a tert-butyl ester, in a similar fashion to that previously described for **F1Y**.

ESI MS +ve $[M+H]^+$ m/z 384.07, $[M+Na]^+$ m/z 406.20

^{1}H NMR (CD_3OD) δ 7.81 (d, *J* = 7.5 Hz, 2H, ArH), 7.68 (t, *J* = 8.0 Hz, 2H, ArH), 7.40 (t, *J* = 7.4 Hz, 2H, ArH), 7.33 (td, *J* = 7.4, 0.9 Hz, 2H, ArH), 4.44-4.34 (m, 3H, CHCO/CH_2O), 4.24 (t, *J* = 6.9 Hz, 1H, ArCH), 4.21-4.15 (m, 1H, CHCO), 1.42 (d, *J* = 7.2 Hz, 3H, CH_3), 1.37 (dd, *J* = 6.9, 4.4 Hz, 3H, CH_3)

^{13}C NMR (CD_3OD) δ 173.4 (^{13}C=O)

3.1.3.5 1-Pyrenylmethoxycarbonyl dileucine (P3LL)

1-Pyrenylmethoxycarbonyl dileucine (**P3LL**)

To a THF (15 mL) solution of 1-pyrenemethanol (300 mg, 1.3 mmol) was added DIPEA (270 μL, 1.6 mmol) and 4-nitrophenyl chloroformate (260 mg, 1.3 mmol). The reaction mixture was stirred at room temperature for 15 minutes. Dileucine (316 mg, 1.3 mmol) was added, and the reaction mixture refluxed overnight. The reaction mixture was diluted with DCM, then washed with 1 M HCl (x2), water (x2), and brine. The organic layer was isolated and concentrated *via* rotary evaporation, in order to afford the crude product. The crude product was purified *via* silica column chromatography, eluting with a 0-2% MeOH/DCM gradient, in order to afford the title compound (64.8 mg, 10.0%). At all stages of the preparation glassware was wrapped in tinfoil to avoid potential photocleavage of the product.[5]

ESI MS +ve $[M+Na]^+$ m/z 525.05

^{1}H NMR (CD_3OD) δ 8.37 (d, *J* = 9.2 Hz, 1H, ArH), 8.25 (dd, *J* = 7.5, 3.9 Hz, 2H, ArH), 8.20 (d, *J* = 8.4 Hz, 2H, ArH), 8.14-8.07 (m, 3H, ArH), 8.05 (t, *J* = 7.6 Hz, 1H, ArH), 5.84 (s, 2H, $ArCH_2O$), 4.50-4.42 (m, 1H, COCH), 4.31-4.23 (m, 1H, COCH), 1.77-1.48 (m, 6H,

CH/CH_2), 0.94 (d, *J* = 6.7 Hz, 6H, CH_3), 0.90 (dd, *J* = 13.2, 6.2 Hz, 6H, CH_3)

3.1.3.6 1-Pyrenylmethoxycarbonyl tyrosine leucine (P3YL)

Tert-butyl carbonyl tyrosine leucine tert-butyl ester (**BocYLOtBu**)

The title compound (779 mg, 97.3%) was prepared *via* a T3P mediated amide coupling, in a similar fashion to that previously described for **F1YOtBu**.

Tyrosine leucine (**YL**)

The title compound (507 mg, 99.6%) was prepared (from **BocYLOtBu**) *via* a TFA mediated cleavage of a tert-butyl ester and carbamate, in a similar fashion to that previously described for **F1Y**.

1-Pyrenylmethoxycarbonyl tyrosine leucine (**P3YL**)

The title compound (60.0 mg, 6.3%) was prepared (from **YL**) *via* 4-nitrophenyl chloroformate mediated carbamate formation, in a similar fashion to that previously described for **P3LL**.

ESI MS +ve $[M+Na]^+$ m/z 575.08

^{1}H NMR (CD_3OD) δ 8.28-8.21 (m, 3H, ArH), 8.19-8.14 (m, 2H, ArH), 8.12-8.02 (m, 3H, ArH), 7.97 (d, *J* = 7.7 Hz, 1H, ArH), 7.09 (d, *J* = 8.4 Hz, 2H, ArH), 6.70 (d, *J* = 8.4 Hz, 2H, ArH), 5.74 (d, *J* = 9.5 Hz, 2H, $ArCH_2O$), 4.50-4.41 (m, 2H, COCH), 3.09 (dd, *J* = 14.1, 4.7 Hz, 1H, $ArCH_2$), 2.76 (dd, *J* = 14.1, 9.7 Hz, 1H, $ArCH_2$), 1.74-1.61 (m, 3H, CH/CH_2), 0.92 (dd, *J* = 9.8, 6.2 Hz, 6H, CH_3)

3.1.4 Ethylcarbonyl $(CH_2)_2C=O$ linker (4) compounds

3.1.4.1 Common precursor: 1-Naphthylpropanoic acid (1N4)

1-Naphthylethanol mesylate ester (**1N4OMs**)

A DCM (20 mL) solution of 1-naphthylethanol (1.00 g, 5.8 mmol) was cooled to 0 ^oC in an ice bath. To this was added triethylamine (1.21 mL, 8.7 mmol), before the dropwise addition of methanesulfonyl chloride (494 µl, 6.4 mmol). The reaction mixture was then stirred for an hour whilst being allowed to warm to room temperature. The reaction mixture was washed with HCl (x2), $NaHCO_3$ (x2), water (x2), dried over $MgSO_4$, and concentrated *via* rotary evaporation in order to afford the crude product (1.42 g, 97.7%).

1-Naphthylethylnitrile (**1N4CN**)

To a DMSO (15 mL) solution of **1N4OMs** (1.42 g, 5.7 mmol) was added sodium cyanide (292 mg, 6.0 mmol). The reaction mixture was then stirred, and heated at 90 ^oC for 4 hours.

The reaction mixture was then partitioned between DCM and water. The organic layer was isolated, dried over $MgSO_4$, and concentrated *via* rotary evaporation in order to afford the crude product. The crude product was purified *via* silica column chromatography, eluting with a 5-25% EtOAc/Hexane gradient, in order to afford the title compound (635 mg, 61.8%).

1-Naphthylpropanoic acid (**1N4**)

To an ethanol (10 mL) solution of **1N4CN** (635 mg, 3.5 mmol) was added 1 M KOH solution (40 mL). The reaction mixture was then stirred, and refluxed for 72 hours. The reaction mixture was acidified using 1M HCl, which caused precipitation to occur. The organics were extracted using DCM, which was dried over $MgSO_4$, and concentrated *via* rotary evaporation in order to afford the title compound (689 mg, 98.2%).

^{1}H NMR ($CDCl_3$) δ 8.06 (d, *J* = 8.4 Hz, 1H, ArH), 7.90 (d, *J* = 7.9 Hz, 1H, ArH), 7.77 (d, *J* = 7.8 Hz, 1H, ArH), 7.59-7.50 (m, 2H, ArH), 7.46-7.38 (m, 2H, ArH), 3.50-3.45 (m, 2H, $ArCH_2$), 2.89-2.84 (m, 2H, $COCH_2$)

3.1.4.2 1-Naphthylethylcarbonyl tyrosine leucine (1N4YL)

1-Naphthylethylcarbonyl tyrosine methyl ester (**1N4YOMe**)

The title compound (499 mg, 88.2%) was prepared (from **1N4**) *via* a T3P mediated amide coupling, in a similar fashion to that previously described for **F1YOtBu**.

1-Naphthylethylcarbonyl tyrosine (**1N4Y**)

The title compound (460 mg, 95.9%) was prepared (from **1N4YOMe**) *via* LiOH methyl ester hydrolysis, in a similar fashion to that previously described for **P1Y**.

1-Naphthylethylcarbonyl tyrosine leucine methyl ester (**1N4YLOMe**)

The title compound (522 mg, 84.0%) was prepared (from **1N4Y**) *via* a T3P mediated amide coupling, in a similar fashion to that previously described for **F1YOtBu**.

1-Naphthylethylcarbonyl tyrosine leucine (**1N4YL**)

The title compound (444 mg, 87.5%) was prepared (from **1N4YLOMe**) *via* LiOH methyl ester hydrolysis, in a similar fashion to that previously described for **P1Y**.

ESI MS +ve $[M+H]^+$ m/z 477.02, $[M+Na]^+$ m/z 499.17

ESI MS -ve $[M-H]^-$ m/z 475.09

^{1}H NMR (CD_3OD) δ 8.21 (d, *J* = 8.2 Hz, 1H, CONH), 8.06 (d, *J* = 8.6 Hz, 1H, ArH), 7.97 (d, *J* = 8.4 Hz, 1H, CONH), 7.87 (d, *J* = 8.4 Hz, 1H, ArH), 7.73 (d, *J* = 8.2 Hz, 1H, ArH),

7.54 (td, *J* = 7.6, 1.6 Hz, 1H, ArH), 7.48 (td, *J* = 7.4, 1.4 Hz, 1H, ArH), 7.38-7.34 (m, 1H, ArH), 7.26 (d, *J* = 6.8 Hz, 1H, ArH), 7.01 (d, *J* = 8.5 Hz, 2H, ArH), 6.68 (d, *J* = 8.5 Hz, 2H, ArH), 4.70-4.63 (m, 1H, CHCO), 4.49-4.43 (m, 1H, CHCO), 3.28 (td, *J* = 7.8, 2.9 Hz, 2H, $ArCH_2$), 3.03 (dd, *J* = 14.1, 5.0 Hz, 1H, $ArCH_2$), 2.76 (dd, *J* = 14.1, 9.2 Hz, 1H, $ArCH_2$), 2.60 (t, *J* = 7.5 Hz, 2H, CH_2CO), 1.76-1.61 (m, 3H, CH/CH_2), 0.95 (dd, *J* = 12.8, 6.3 Hz, 6H, CH_3)

3.1.4.3 1-Naphthylethylcarbonyl dileucine (1N4LL)

1-Naphthylethylcarbonyl leucine methyl ester (**1N4LOMe**)

The title compound (409 mg, 83.4%) was prepared (from **1N4**) *via* a T3P mediated amide coupling, in a similar fashion to that previously described for **F1YOtBu**.

1-Naphthylethylcarbonyl leucine (**1N4L**)

The title compound (388 mg, 99.0%) was prepared (from **1N4LOMe**) *via* LiOH methyl ester hydrolysis, in a similar fashion to that previously described for **P1Y**.

1-Naphthylethylcarbonyl dileucine methyl ester (**1N4LLOMe**)

The title compound (438 mg, 80.3%) was prepared (from **1N4L**) *via* a T3P mediated amide coupling, in a similar fashion to that previously described for **F1YOtBu**.

1-Naphthylethylcarbonyl dileucine (**1N4LL**)

The title compound (405 mg, 95.6%) was prepared (from **1N4LLOMe**) *via* LiOH methyl ester hydrolysis, in a similar fashion to that previously described for **P1Y**.

ESI MS +ve $[M+H]^+$ m/z 427.05, $[M+Na]^+$ m/z 449.21

ESI MS -ve $[M-H]^-$ m/z 425.13

^1H NMR (CD_3OD) δ 8.18 (d, *J* = 8.1 Hz, 1H, CONH), 8.14 (d, *J* = 8.2 Hz, 1H, ArH), 8.03 (d, *J* = 7.9 Hz, 1H, CONH), 7.87 (d, *J* = 8.1 Hz, 1H, ArH), 7.74 (dd, *J* = 6.8, 2.6 Hz, 1H, ArH), 7.55 (td, *J* = 7.6, 1.5 Hz, 1H, ArH), 7.49 (td, *J* = 7.4, 1.2 Hz, 1H, ArH), 7.41-7.36 (m, 2H, ArH), 4.48-4.40 (m, 2H, CHCO), 3.42 (td, *J* = 7.7, 3.1 Hz, 2H, $ArCH_2$), 2.69 (t, *J* = 7.7 Hz, 2H, CH_2CO), 1.80-1.68 (m, 1H, CH/CH_2), 1.68-1.63 (m, 2H, CH/CH_2), 1.58-1.42 (m, 3H, CH/CH_2), 0.96 (dd, *J* = 16.0, 6.5 Hz, 6H, CH_3), 0.89 (dd, *J* = 10.6, 6.2 Hz, 6H, CH_3)

3.1.4.4 Common precursor: 2-Naphthylpropanoic acid (2N4)

2-Naphthylethanol mesylate ester (**2N4OMs**)

The title compound (1.40 g, 96.3%) was prepared *via* formation of the mesylate ester, in a similar fashion to that previously described for **1N4OMs**.

2-Naphthylethylnitrile (**2N4CN**)

The title compound (746 mg, 73.6%) was prepared (from **2N4OMs**) *via* nucleophilic addition of cyanide, in a similar fashion to that previously described for **1N4CN**.

2-Naphthylpropanoic acid (**2N4**)

The title compound (814 mg, 98.8%) was prepared (from **2N4CN**) *via* nitrile hydrolysis, in a similar fashion to that previously described for **1N4**.

^{1}H NMR ($CDCl_3$) δ 7.85-7.78 (m, 3H, ArH), 7.69 (s, 1H, ArH), 7.51-7.43 (m, 2H, ArH), 7.37 (dd, *J* = 8.4, 1.6 Hz, 1H, ArH), 3.15 (t, *J* = 7.8 Hz, 2H, $ArCH_2$), 2.80 (t, *J* = 7.8 Hz, 2H, $COCH_2$)

3.1.4.5 2-Naphthylethylcarbonyl tyrosine leucine (2N4YL)

2-Naphthylethylcarbonyl tyrosine methyl ester (**2N4YOMe**)

The title compound (665 mg, 88.2%) was prepared (from **2N4**) *via* a T3P mediated amide coupling, in a similar fashion to that previously described for **F1YOtBu**.

2-Naphthylethylcarbonyl tyrosine (**2N4Y**)

The title compound (623 mg, 97.3%) was prepared (from **2N4YOMe**) *via* LiOH methyl ester hydrolysis, in a similar fashion to that previously described for **P1Y**.

2-Naphthylethylcarbonyl tyrosine leucine methyl ester (**2N4YLOMe**)

The title compound (548 mg, 65.2%) was prepared (from **2N4Y**) *via* a T3P mediated amide coupling, in a similar fashion to that previously described for **F1YOtBu**.

2-Naphthylethylcarbonyl tyrosine leucine (**2N4YL**)

The title compound (473 mg, 88.9%) was prepared (from **2N4YLOMe**) *via* LiOH methyl ester hydrolysis, in a similar fashion to that previously described for **P1Y**.

ESI MS +ve $[M+H]^+$ m/z 477.02, $[M+Na]^+$ m/z 499.17

ESI MS -ve $[M-H]^-$ m/z 475.09

^{1}H NMR (CD_3OD) δ 8.19 (d, *J* = 8.2 Hz, 1H, CONH), 7.97 (d, *J* = 8.1 Hz, 1H, CONH), 7.82-7.73 (m, 3H, ArH), 7.61 (s, 1H, ArH), 7.47-7.39 (m, 2H, ArH), 7.30 (dd, *J* = 8.5, 1.8 Hz, 1H, ArH), 7.00 (d, *J* = 8.5 Hz, 2H, ArH), 6.66 (d, *J* = 8.5 Hz, 2H, ArH), 4.67-4.60 (m, 1H, CHCO), 4.48-4.41 (m, 1H, CHCO), 3.06-2.96 (m, 3H, $ArCH_2$), 2.76 (dd, *J* = 14.1, 9.1 Hz, 1H, $ArCH_2$), 2.60-2.54 (m, 2H, CH_2CO), 1.74-1.55 (m, 3H, CH/CH_2), 0.92 (dd, *J* = 14.9, 6.3 Hz, 6H, CH_3)

3.1.4.6 2-Naphthylethylcarbonyl dileucine (2N4LL)

2-Naphthylethylcarbonyl leucine methyl ester (**2N4LOMe**)

The title compound (535 mg, 81.8%) was prepared (from **2N4**) *via* a T3P mediated amide coupling, in a similar fashion to that previously described for **F1YOtBu**.

2-Naphthylethylcarbonyl leucine (**2N4L**)

The title compound (486 mg, 94.9%) was prepared (from **2N4LOMe**) *via* LiOH methyl ester hydrolysis, in a similar fashion to that previously described for **P1Y**.

2-Naphthylethylcarbonyl dileucine methyl ester (**2N4LLOMe**)

The title compound (451 mg, 66.0%) was prepared (from **2N4L**) *via* a T3P mediated amide coupling, in a similar fashion to that previously described for **F1YOtBu**.

2-Naphthylethylcarbonyl dileucine (**2N4LL**)

The title compound (422 mg, 96.6%) was prepared (from **2N4LLOMe**) *via* LiOH methyl ester hydrolysis, in a similar fashion to that previously described for **P1Y**.

ESI MS +ve $[M+H]^+$ m/z 426.99, $[M+Na]^+$ m/z 449.21

ESI MS -ve $[M-H]^-$ m/z 425.19

^{1}H NMR (CD_3OD) δ 8.15 (d, *J* = 8.1 Hz, 1H, CONH), 7.98 (d, *J* = 8.0 Hz, 1H, CONH), 7.83-7.77 (m, 3H, ArH), 7.67 (s, 1H, ArH), 7.47-7.37 (m, 3H, ArH), 4.46-4.35 (m, 2H, CHCO), 3.10 (t, *J* = 7.4 Hz, 2H, $ArCH_2$), 2.73-2.60 (m, 2H, CH_2CO), 1.77-1.65 (m, 1H, CH), 1.64-1.59 (m, 2H, CH_2), 1.50-1.37 (m, 2H, CH_2), 1.31-1.21 (m, 1H, CH), 0.93 (dd, *J* = 18.4, 6.5 Hz, 6H, CH_3), 0.72 (dd, *J* = 17.7, 6.6 Hz, 6H, CH_3)

3.1.4.7 Common precursor: 9-Fluorenylpropanoic acid (F4)[1]

9-Fluorenylpropanoate methyl ester (**F4OMe**)

A DMSO (20 mL) solution of fluorene (1.00 g, 6.0 mmol) was cooled to 0 ^oC in an ice bath, and stirred under nitrogen. To this was added 60% NaH dispersion in mineral oil (313 mg, 7.8 mmol), and the reaction mixture stirred for 40 minutes, before the subsequent addition of methyl 3-bromopropionate (985 μL, 9.0 mmol). After being allowed to warm to room temperature, the reaction mixture was stirred for a further hour, before being quenched by the slow addition of MeOH. The reaction mixture was then partitioned between DCM and 1 M HCl solution. The organic layer was isolated, dried over $MgSO_4$, and concentrated *via* rotary evaporation in order to afford the crude product. The crude product was purified by silica column chromatography, eluting with 2% MeOH/DCM in order to afford the title compound (297 mg, 19.6%).

9-Fluorenylpropanoic acid (**F4**)

The title compound (260 mg, 92.7%) was prepared (from **F4OMe**) *via* LiOH methyl ester hydrolysis, in a similar fashion to that previously described for **P1Y**.

^{1}H NMR ($CDCl_3$) δ 7.77 (d, *J* = 7.4 Hz, 2H, ArH), 7.52 (d, *J* = 7.6 Hz, 2H, ArH), 7.40 (t, *J* = 7.2 Hz, 2H, ArH), 7.33 (td, *J* = 7.4, 1.2 Hz, 2H, ArH), 4.11 (t, *J* = 5.2 Hz, 1H, ArCH), 2.49-2.42 (m, 2H, CH_2), 2.04-1.98 (m, 2H, CH_2)

^{13}C NMR ($CDCl_3$) δ 178.3 (COOH), 145.3 (ArH), 141.0 (ArH), 126.9 (ArH), 126.6 (ArH), 123.8 (ArH), 119.5 (ArH), 45.5 (ArCH), 28.5 (CH_2), 26.8 (CH_2)

3.1.4.8 9-Fluorenylethylcarbonyl tyrosine leucine (F4YL)[1]

9-Fluorenylethylcarbonyl tyrosine methyl ester (**F4YOMe**)

The title compound (211 mg, 93.3%) was prepared (from **F4**) *via* a T3P mediated amide coupling, in a similar fashion to that previously described for **F1YOtBu**.

9-Fluorenylethylcarbonyl tyrosine (**F4Y**)

The title compound (202 mg, 99.0%) was prepared (from **F4YOMe**) *via* LiOH methyl ester hydrolysis, in a similar fashion to that previously described for **P1Y**.

9-Fluorenylethylcarbonyl tyrosine leucine methyl ester (**F4YLOMe**)

The title compound (120 mg, 45.0%) was prepared (from **F4Y**) *via* a T3P mediated amide coupling, in a similar fashion to that previously described for **F1YOtBu**.

9-Fluorenylethylcarbonyl tyrosine leucine (**F4YL**)

The title compound (114 mg, 97.3%) was prepared (from **F4YLOMe**) *via* LiOH methyl ester hydrolysis, in a similar fashion to that previously described for **P1Y**.

ESI MS +ve $[M+H]^+$ m/z 515.20, $[M+Na]^+$ m/z 537.27

ESI MS -ve $[M-H]^-$ m/z 513.20

^{1}H NMR (CD_3OD) δ 8.18 (d, *J* = 8.0 Hz, 1H, CONH), 7.83 (d, *J* = 8.3 Hz, 1H, CONH), 7.76 (d, *J* = 7.7 Hz, 2H, ArH), 7.51 (dd, *J* = 13.9, 7.2 Hz, 2H, ArH), 7.38-7.27 (m, 4H, ArH), 7.01 (d, *J* = 8.5 Hz, 2H, ArH), 6.65 (d, *J* = 8.6 Hz, 2H, ArH), 4.58-4.50 (m, 1H, CHCO), 4.43-4.36 (m, 1H, CHCO), 3.94 (t, *J* = 5.5 Hz, 1H, ArCH), 3.00 (dd, *J* = 14.1, 5.0 Hz, 1H, CH_2), 2.66 (dd, *J* = 14.0, 9.5 Hz, 1H, CH_2), 2.25-2.18 (m, 2H, CH_2), 1.94-1.80 (m, 2H, CH_2), 1.70-1.56 (m, 3H, CH/CH_2), 0.89 (dd, *J* = 16.1, 6.3 Hz, 6H, CH_3)

^{13}C NMR (CD_3OD) 173.8 (C=O), 173.6 (C=O), 172.0 (C=O), 155.3 (Ar-OH), 145.8 (Ar), 140.6 (Ar), 129.4 (Ar), 127.3 (Ar), 126.3 (Ar), 126.2 (Ar), 123.7 (Ar), 118.9 (Ar), 114.2

(Ar), 53.9 (NHCH), 50.1 (NHCH), 45.7 (ArCH), 39.8 (CH_2), 36.0 (CH_2), 30.5 (CH_2), 27.8 (CH_2), 24.0 (CH), 21.4 (CH_3), 20.0 (CH_3)

3.1.4.9 9-Fluorenylethylcarbonyl dileucine (F4LL)

9-Fluorenylethylcarbonyl leucine methyl ester (**F4LOMe**)

The title compound (182 mg, 91.4%) was prepared (from **F4**) *via* a T3P mediated amide coupling, in a similar fashion to that previously described for **F1YOtBu**.

9-Fluorenylethylcarbonyl leucine (**F4L**)

The title compound (170 mg, 97.0%) was prepared (from **F4LOMe**) *via* LiOH methyl ester hydrolysis, in a similar fashion to that previously described for **P1Y**.

9-Fluorenylethylcarbonyl dileucine methyl ester (**F4LLOMe**)

The title compound (140 mg, 60.5%) was prepared (from **F4L**) *via* a T3P mediated amide coupling, in a similar fashion to that previously described for **F1YOtBu**.

9-Fluorenylethylcarbonyl dileucine (**F4LL**)

The title compound (133 mg, 97.9%) was prepared (from **F4LLOMe**) *via* LiOH methyl ester hydrolysis, in a similar fashion to that previously described for **P1Y**.

ESI MS +ve $[M+Na]^+$ m/z 487.27

^{1}H NMR ($CDCl_3$) δ 7.76 (d, *J* = 7.3 Hz, 2H, ArH), 7.52 (t, *J* = 7.7 Hz, 2H, ArH), 7.39 (t, *J* = 7.2 Hz, 2H, ArH), 7.32 (tt, *J* = 7.4, 1.2 Hz, 2H, ArH), 7.00 (d, *J* = 8.2 Hz, 1H, CONH), 6.38 (d, *J* = 8.6 Hz, 1H, CONH), 4.59-4.48 (m, 2H, CHCO), 4.07 (t, *J* = 5.3 Hz, 1H, ArCH), 2.48-2.34 (m, 2H, CH_2), 1.90-1.84 (m, 2H [obscured], CH_2), 1.70-1.59 (m, 2H, CH/CH_2), 1.58-1.48 (m, 3H, CH/CH_2), 1.43-1.32 (m, 1H, CH/CH_2), 0.93-0.83 (m, 12H, CH_3)

^{13}C NMR (CD_3OD) 173.9 (C=O), 173.8 (C=O), 172.9 (C=O), 145.9 (Ar), 140.7 (Ar), 126.4 (Ar), 126.2 (Ar), 123.7 (Ar), 118.9 (Ar), 51.1 (NHCH), 51.0 (NHCH), 45.8 (ArCH), 39.8 (CH_2), 30.4 (CH_2), 27.7 (CH_2), 24.0 (CH), 21.5 (CH_3), 20.2 (CH_3), 19.9 (CH_3)

3.1.4.10 Common precursor: 1-Pyrenylpropanoic acid (P4)[6]

1-Pyrenylethanol (**P4OH**)

A THF (20 mL) solution of 1-pyreneacetic acid (1.5 g, 5.8 mmol) was cooled to 0 ^oC in an ice bath, and stirred under nitrogen. To this was added 2.0 M $LiAlH_4$ THF solution (5.8 mL, 11.5 mmol), and the reaction mixture stirred under nitrogen for 2 hours before being quenched by the slow addition of EtOAc. The reaction mixture was washed with HCl (x2), dried over $MgSO_4$, and concentrated *via* rotary evaporation in order to afford the crude

product (1.38 g, 97.2%).

1-Pyrenylethanol mesylate ester (**P4OMs**)

The title compound (1.79 g, 98.5%) was prepared (from **P4OH**) *via* formation of the mesylate ester, in a similar fashion to that previously described for **1N4OMs**.

1-Pyrenylethylnitrile (**P4CN**)

The title compound (609 mg, 43.2%) was prepared (from **P4OMs**) *via* nucleophilic addition of cyanide, in a similar fashion to that previously described for **1N4CN**.

1-Pyrenylpropanoic acid (**P4**)

The title compound (624 mg, 95.4%) was prepared (from **P4CN**) *via* nitrile hydrolysis, in a similar fashion to that previously described for **1N4**.

^{1}H NMR (CD_3OD) δ 8.34 (d, *J* = 9.2 Hz, 1H, ArH), 8.22-8.12 (m, 4H, ArH), 8.05 (s, 2H, ArH), 8.00 (t, *J* = 7.6 Hz, 1H, ArH), 7.95 (d, *J* = 7.9 Hz, 1H, ArH), 3.71-3.65 (m, 2H, $ArCH_2$), 2.88-2.82 (m, 2H, $COCH_2$)

3.1.4.11 1-Pyrenylethylcarbonyl tyrosine leucine (P4YL)[6]

1-Pyrenylethylcarbonyl tyrosine methyl ester (**P4YOMe**)

The title compound (468 mg, 94.8%) was prepared (from **P4**) *via* a T3P mediated amide coupling, in a similar fashion to that previously described for **F1YOtBu**.

1-Pyrenylethylcarbonyl tyrosine (**P4Y**)

The title compound (440 mg, 97.0%) was prepared (from **P4YOMe**) *via* LiOH methyl ester hydrolysis, in a similar fashion to that previously described for **P1Y**.

1-Pyrenylethylcarbonyl tyrosine leucine methyl ester (**P4YLOMe**)

The title compound (430 mg, 75.7%) was prepared (from **P4Y**) *via* a T3P mediated amide coupling, in a similar fashion to that previously described for **F1YOtBu**.

1-Pyrenylethylcarbonyl tyrosine leucine (**P4YL**)

The title compound (400 mg, 95.4%) was prepared (from **P4YLOMe**) *via* LiOH methyl ester hydrolysis, in a similar fashion to that previously described for **P1Y**.

ESI MS +ve $[M+H]^+$ m/z 551.00, $[M+Na]^+$ m/z 573.15

ESI MS -ve $[M-H]^-$ m/z 549.13

^{1}H NMR (CD_3OD) δ 8.31 (d, *J* = 9.3 Hz, 1H, ArH), 8.22-8.13 (m, 3H, ArH), 8.10 (d, *J* = 7.9

Hz, 1H, ArH), 8.04 (s, 2H, ArH), 8.01 (t, *J* = 7.6 Hz, 1H, ArH), 7.82 (d, *J* = 7.9 Hz, 1H, ArH), 6.97 (d, *J* = 8.5 Hz, 2H, ArH), 6.64 (d, *J* = 8.5 Hz, 2H, ArH), 4.72-4.65 (m, 1H, CHCO), 4.48-4.42 (m, 1H, CHCO), 3.54 (t, *J* = 7.8 Hz, 2H, $ArCH_2$), 3.01 (dd, *J* = 14.1, 5.1 Hz, 1H, $ArCH_2$), 2.78-2.68 (m, 3H, $ArCH_2/CH_2CO$), 1.74-1.56 (m, 3H, CH/CH_2), 0.93 (dd, *J* = 9.7, 6.2 Hz, 6H, CH_3)

^{13}C NMR ($(CD_3)_2SO$) 171.4 (C=O), 171.1 (C=O), 171.0 (C=O), 155.7 (Ar-OH), 135.7 (Ar), 130.8 (Ar), 130.4 (Ar), 130.2 (Ar), 129.3 (Ar), 128.0 (Ar), 127.9 (Ar), 127.4 (Ar), 127.3 (Ar), 127.0 (Ar), 126.5 (Ar), 126.1 (Ar), 124.9 (Ar), 124.8 (Ar), 124.1 (Ar), 124.1 (Ar), 123.2 (Ar), 114.8 (Ar), 53.9 (NHCH), 50.5 (NHCH), 37.2 (CH_2), 37.1 (CH_2), 36.8 (CH_2), 28.7 (CH_2), 24.3 (CH), 22.9 (CH_3), 21.5 (CH_3)

3.1.4.12 1-Pyrenylethylcarbonyl dileucine (P4LL)

1-Pyrenylethylcarbonyl leucine methyl ester (**P4LOMe**)

The title compound (431 mg, 98.2%) was prepared (from **P4**) *via* a T3P mediated amide coupling, in a similar fashion to that previously described for **F1YOtBu**.

1-Pyrenylethylcarbonyl leucine (**P4L**)

The title compound (401 mg, 96.4%) was prepared (from **P4LOMe**) *via* LiOH methyl ester hydrolysis, in a similar fashion to that previously described for **P1Y**.

1-Pyrenylethylcarbonyl dileucine methyl ester (**P4LLOMe**)

The title compound (302 mg, 56.8%) was prepared (from **P4L**) *via* a T3P mediated amide coupling, in a similar fashion to that previously described for **F1YOtBu**.

1-Pyrenylethylcarbonyl dileucine (**P4LL**)

The title compound (283 mg, 96.2%) was prepared (from **P4LLOMe**) *via* LiOH methyl ester hydrolysis, in a similar fashion to that previously described for **P1Y**.

ESI MS +ve $[M+H]^+$ m/z 501.03, $[M+Na]^+$ m/z 523.19

ESI MS -ve $[M-H]^-$ m/z 499.17

^1H NMR (CD_3OD) δ 8.40 (d, *J* = 9.3 Hz, 1H, ArH), 8.23-8.18 (m, 2H, ArH), 8.18-8.13 (m, 2H, ArH), 8.06 (s, 2H, ArH), 8.02 (t, *J* = 7.6 Hz, 1H, ArH), 7.94 (d, *J* = 7.8 Hz, 1H, ArH), 4.46-4.32 (m, 2H, CHCO), 3.76-3.66 (m, 2H, $ArCH_2$), 2.81 (t, *J* = 7.6 Hz, 2H, CH_2CO), 1.78-1.66 (m, 1H, CH/CH_2), 1.65-1.59 (m, 2H, CH/CH_2), 1.45-1.37 (m, 1H, CH/CH_2), 1.36-1.27 (m, 1H, CH/CH_2), 1.20-1.08 (m, 1H, CH/CH_2), 0.93 (dd, *J* = 14.0, 6.5 Hz, 6H, CH_3), 0.66 (t, *J* = 6.3 Hz, 6H, CH_3)

3.1.4.13 1-Pyrenylethylcarbonyl serine (P4S)[6]

1-Pyrenylethylcarbonyl O-tert-Butyl-serine tert-butyl ester (**P4S(OtBu)OtBu**)

The title compound (967 mg, 87.5%) was prepared (from **P4**) *via* a T3P mediated amide coupling, in a similar fashion to that previously described for **F1YOtBu**.

1-Pyrenylethylcarbonyl serine (**P4S**)

The title compound (591 mg, 80.1%) was prepared (from **P4S(OtBu)OtBu**) *via* a TFA mediated cleavage of a tert-butyl ester and ether, in a similar fashion to that previously described for **F1Y**.

ESI MS +ve $[M+H]^+$ m/z 362.13, $[M+Na]^+$ m/z 384.13

ESI MS -ve $[M-H]^-$ m/z 360.00

^{1}H NMR (CD_3OD) δ 8.38 (d, *J* = 9.3 Hz, 1H, ArH), 8.21-8.11 (m, 4H, ArH), 8.04 (s, 2H, ArH), 8.00 (t, *J* = 7.6 Hz, 1H, ArH), 7.95 (d, *J* = 7.8 Hz, 1H, ArH), 4.56 (t, *J* = 4.6 Hz, 1H, CHCO), 3.89 (dd, *J* = 11.3, 5.0 Hz, 1H, CH_2O), 3.80 (dd, *J* = 11.2, 4.1 Hz, 1H, CH_2O), 3.72-3.66 (m, 2H, $ArCH_2$), 2.84 (td, *J* = 8.1, 1.7 Hz, 2H, CH_2CO)

^{13}C NMR ($(CD_3)_2SO$) 172.0 (C=O), 171.5 (C=O), 135.8 (Ar), 130.8 (Ar), 130.4 (Ar), 129.4 (Ar), 128.0 (Ar), 127.4 (Ar), 127.3 (Ar), 126.5 (Ar), 126.1 (Ar), 124.9 (Ar), 124.8 (Ar), 124.2 (Ar), 124.1 (Ar), 123.3 (Ar), 61.4 (CH_2), 54.6 (NHCH), 37.0 (CH_2), 28.6 (CH_2)

3.1.5 Methoxymethylcarbonyl $CH_2OCH_2C{=}O$ linker (5) compounds

3.1.5.1 1-Naphthylmethoxymethylcarbonyl dileucine (1N5LL)

1-Naphthylmethoxyacetic acid (**1N5**)

To a THF (20 mL) solution of 1-naphthalenemethanol (273 mg, 1.7 mmol) was added bromoacetic acid (200 mg, 1.4 mmol), and 60% sodium hydride dispersion in mineral oil (127 mg, 3.2 mmol). The reaction mixture was initially stirred under nitrogen at 0 ^oC for 10 minutes, before being allowed to warm to room temperature and stirred for a further 3 hours. The reaction mixture was quenched by the dropwise addition of methanol, and concentrated *via* rotary evaporation. The residue was partitioned between 1 M HCl and DCM, and the organic layer isolated, dried over $MgSO_4$, and concentrated *via* rotary evaporation in order to afford the crude product. The crude product was purified *via* silica column chromatography, eluting with 50% EtOAc/Hexane, in order to afford the title compound (206 mg, 66.1 %).

1-Naphthylmethoxymethylcarbonyl dileucine methyl ester (**1N5LLOMe**)

The title compound (310 mg, 71.4%) was prepared (from **1N5** and **LLOMe**) *via* a T3P mediated amide coupling, in a similar fashion to that previously described for **F1YOtBu**.

ESI MS +ve $[M+Na]^+$ m/z 479.27

ESI MS -ve $[M-H]^-$ m/z 455.07

^{1}H NMR ($CDCl_3$) δ 8.11 (d, *J* = 8.3 Hz, 1H, ArH), 7.91-7.82 (m, 2H, ArH), 7.59-7.50 (m, 2H, ArH), 7.48-7.42 (m, 2H, ArH), 6.94 (d, *J* = 8.6 Hz, 1H, CONH), 6.77 (d, *J* = 8.0 Hz, 1H, CONH), 5.09 (d, *J* = 12.0 Hz, 1H, $ArCH_2$), 4.98 (d, *J* = 12.0 Hz, 1H, $ArCH_2$), 4.60-4.48 (m, 2H, COCH), 4.04 (s, 2H, OCH_2), 3.72 (s, 3H, OCH_3), 1.69-1.38 (m, 6H, CH/CH_2), 0.91-0.87 (m, 12H, CH_3)

1-Naphthylmethoxymethylcarbonyl dileucine (**1N5LL**)

The title compound (294 mg, 97.7%) was prepared (from **1N5LLOMe**) *via* LiOH methyl ester hydrolysis, in a similar fashion to that previously described for **P1Y**.

ESI MS +ve $[M+Na]^+$ m/z 465.27

ESI MS -ve $[M-H]^-$ m/z 441.00

^{1}H NMR (CD_3OD) δ 8.40 (d, *J* = 8.1 Hz, 1H, CONH), 8.23 (d, *J* = 8.4 Hz, 1H, ArH), 7.94-7.87 (m, 2H, ArH), 7.68 (d, *J* = 8.5 Hz, 1H, CONH), 7.61-7.51 (m, 3H, ArH), 7.51-7.45 (m, 1H, ArH), 5.16 (d, *J* = 12.0 Hz, 1H, $ArCH_2$), 5.04 (d, *J* = 12.0 Hz, 1H, $ArCH_2$), 4.56-4.49 (m, 1H, COCH), 4.48-4.41 (m, 1H, COCH), 4.07 (d, *J* = 6.5 Hz, 2H, OCH_2), 1.78-1.61 (m, 3H, CH/CH_2), 1.60-1.41 (m, 3H, CH/CH_2), 0.97-0.89 (m, 12H, CH_3)

3.1.5.2 2-Naphthylmethoxymethylcarbonyl dileucine (2N5LL)

2-Naphthylmethoxyacetic acid (**2N5**)

The title compound (211 mg, 67.7%) was prepared *via* nucleophilic addition of an alkoxide, in a similar fashion to that previously described for **1N5**.

2-Naphthylmethoxymethylcarbonyl dileucine methyl ester (**2N5LLOMe**)

The title compound (284 mg, 63.9%) was prepared (from **2N5** and **LLOMe**) *via* a T3P mediated amide coupling, in a similar fashion to that previously described for **F1YOtBu**.

^{1}H NMR ($CDCl_3$) δ 7.88-7.81 (m, 3H, ArH), 7.78 (s, 1H, ArH), 7.53-7.43 (m, 3H, ArH), 7.09 (d, *J* = 8.7 Hz, 1H, CONH), 6.93 (d, *J* = 8.0 Hz, 1H, CONH), 4.73 (d, *J* = 8.8 Hz, 2H, $ArCH_2$), 4.65-4.55 (m, 2H, COCH), 4.02 (d, *J* = 5.9 Hz, 2H, OCH_2), 3.72 (s, 3H, OCH_3), 1.77-1.50 (m, 6H, CH/CH_2), 0.94 (dd, *J* = 6.2, 4.7 Hz, 6H, CH_3), 0.90 (d, *J* = 6.1 Hz, 6H, CH_3)

2-Naphthylmethoxymethylcarbonyl dileucine (**2N5LL**)

The title compound (197 mg, 71.5 %) was prepared (from **2N5LLOMe**) *via* LiOH methyl ester hydrolysis, in a similar fashion to that previously described for **P1Y**.

ESI MS +ve $[M+Na]^+$ m/z 465.20

ESI MS -ve $[M-H]^-$ m/z 441.13

^{1}H NMR (CD_3OD) δ 8.44 (d, *J* = 8.0 Hz, 1H, CONH), 7.91-7.85 (m, 4H, ArH), 7.83 (d, *J* = 8.3 Hz, 1H, CONH), 7.54 (dd, *J* = 8.4, 1.7 Hz, 1H, ArH), 7.52-7.48 (m, 2H, ArH), 4.79 (d, *J* = 6.6 Hz, 2H, $ArCH_2$), 4.61-4.54 (m, 1H, COCH), 4.50-4.43 (m, 1H, COCH), 4.06 (s, 2H, OCH_2), 1.79-1.56 (m, 6H, CH/CH_2), 0.98-0.91 (m, 12H, CH_3)

3.1.5.3 9-Anthrylmethoxymethylcarbonyl dileucine (A5LL)

9-Anthrylmethoxyacetic acid (**A5**)

The title compound (234 mg, 60.9%) was prepared *via* nucleophilic addition of an alkoxide, in a similar fashion to that previously described for **1N5**.

9-Anthrylmethoxymethylcarbonyl dileucine methyl ester (**A5LLOMe**)

The title compound (322 mg, 72.5%) was prepared (from **A5** and **LLOMe**) *via* a T3P mediated amide coupling, in a similar fashion to that previously described for **F1YOtBu**.

^{1}H NMR ($CDCl_3$) δ 8.49 (s, 1H, ArH), 8.34 (d, *J* = 8.5 Hz, 2H, ArH), 8.03 (d, *J* = 8.4 Hz, 2H, ArH), 7.60-7.54 (m, 2H, ArH), 7.52-7.46 (m, 2H, ArH), 6.89 (d, *J* = 8.5 Hz, 1H, CONH), 6.75 (d, *J* = 8.0 Hz, 1H, CONH), 5.58 (q, *J* = 11.8 Hz, 2H, $ArCH_2$), 4.58-4.44 (m, 2H, COCH), 4.11 (d, *J* = 1.6 Hz, 2H, OCH_2), 3.70 (s, 3H, OCH_3), 1.67-1.33 (m, 6H, CH/CH_2), 0.87 (d, *J* = 5.8 Hz, 6H, CH_3), 0.84 (dd, *J* = 6.5, 1.6 Hz, 6H, CH_3)

9-Anthrylmethoxymethylcarbonyl dileucine (**A5LL**)

The title compound (228 mg, 72.7 %) was prepared (from **A5LLOMe**) *via* LiOH methyl ester hydrolysis, in a similar fashion to that previously described for **P1Y**.

ESI MS +ve $[M+Na]^+$ m/z 515.27

ESI MS -ve $[M-H]^-$ m/z 491.20

^{1}H NMR (CD_3OD) δ 8.57 (s, 1H, ArH), 8.49 (d, *J* = 8.8 Hz, 2H, ArH), 8.39 (d, *J* = 8.0 Hz, 1H, CONH), 8.08 (d, *J* = 8.4 Hz, 2H, ArH), 7.65 (d, *J* = 8.3 Hz, 1H, CONH), 7.62-7.57 (m, 2H, ArH), 7.54-7.49 (m, 2H, ArH), 5.67 (d, *J* = 1.0 Hz, 2H, $ArCH_2$), 4.55-4.48 (m, 1H, COCH), 4.47-4.40 (m, 1H, COCH), 4.16 (d, *J* = 10.1 Hz, 2H, OCH_2), 1.77-1.39 (m, 6H, CH/CH_2), 0.96-0.87 (m, 12H, CH_3)

3.1.5.4 Common precursor: 1-Pyrenylmethoxyacetic acid (P5)

1-Pyrenylmethoxyacetic acid (**P5**)

The title compound (59.1 mg, 14.1%) was prepared *via* nucleophilic addition of an alkoxide, in a similar fashion to that previously described for **1N5**.

^{1}H NMR (CD_3OD) δ 8.54 (d, *J* = 9.3 Hz, 1H, ArH), 8.26-8.21 (m, 2H, ArH), 8.20-8.16 (m, 2H, ArH), 8.11-8.01 (m, 4H, ArH), 5.34 (s, 2H, $ArCH_2$), 4.26 (s, 2H, CH_2)

3.1.5.5 1-Pyrenylmethoxymethylcarbonyl tyrosine leucine (P5YL)

1-Pyrenylmethoxymethylcarbonyl tyrosine methyl ester (**P5YOMe**)

The title compound (235 mg, 81.1%) was prepared (from **P5**) *via* a T3P mediated amide coupling, in a similar fashion to that previously described for **F1YOtBu**.

1-Pyrenylmethoxymethylcarbonyl tyrosine (**P5Y**)

The title compound (218 mg, 95.6%) was prepared (from **P5YOMe**) *via* LiOH methyl ester hydrolysis, in a similar fashion to that previously described for **P1Y**.

1-Pyrenylmethoxymethylcarbonyl tyrosine leucine methyl ester (**P5YLOMe**)

The title compound (230 mg, 84.4%) was prepared (from **P5Y**) *via* a T3P mediated amide coupling, in a similar fashion to that previously described for **F1YOtBu**.

1-Pyrenylmethoxymethylcarbonyl tyrosine leucine (**P5YL**)

The title compound (221 mg, 98.5%) was prepared (from **P5YLOMe**) *via* LiOH methyl ester hydrolysis, in a similar fashion to that previously described for **P1Y**.

ESI MS +ve $[M+Na]^+$ m/z 589.33

ESI MS -ve $[M-H]^-$ m/z 565.20

^{1}H NMR (CD_3OD) δ 8.37 (d, *J* = 9.2 Hz, 1H, ArH), 8.29-8.18 (m, 4H, ArH), 8.12 (d, *J* = 1.1 Hz, 2H, ArH), 8.05 (t, *J* = 7.6 Hz, 1H, ArH), 7.98 (d, *J* = 7.8 Hz, 1H, ArH), 6.98 (d, *J* = 8.5 Hz, 2H, ArH), 6.60 (d, *J* = 8.6 Hz, 2H, ArH), 5.23 (d, *J* = 10.5 Hz, 2H, $ArCH_2O$), 4.74-4.67 (m, 1H, CHCO), 4.49-4.43 (m, 1H, CHCO), 4.10 (d, *J* = 15.2 Hz, 1H, OCH_2), 4.00 (d, *J* = 15.2 Hz, 1H, OCH_2), 3.09 (dd, *J* = 14.0, 5.1 Hz, 1H, $ArCH_2$), 2.81 (dd, *J* = 14.1, 8.7 Hz, 1H, $ArCH_2$), 1.74-1.61 (m, 3H, CH/CH_2), 0.92 (dd, *J* = 11.1, 6.2 Hz, 6H, CH_3)

3.1.5.6 1-Pyrenylmethoxymethylcarbonyl dileucine (P5LL)

1-Pyrenylmethoxymethylcarbonyl dileucine methyl ester (**P5LLOMe**)

The title compound (63.3 mg, 58.6%) was prepared (from **P5** and **LLOMe**) *via* a T3P mediated amide coupling, in a similar fashion to that previously described for **F1YOtBu**.

^{1}H NMR ($CDCl_3$) δ 8.35 (d, *J* = 9.2 Hz, 1H, ArH), 8.25-8.21 (m, 2H, ArH), 8.20-8.15 (m, 2H, ArH), 8.12-8.02 (m, 3H, ArH), 7.98 (d, *J* = 7.8 Hz, 1H, ArH), 6.96 (d, *J* = 8.4 Hz, 1H, CONH), 6.59 (d, *J* = 8.1 Hz, 1H, CONH), 5.36 (d, *J* = 11.9 Hz, 1H, $ArCH_2$), 5.24 (d, *J* = 11.9 Hz, 1H, $ArCH_2$), 4.61-4.54 (m, 1H, COCH), 4.51-4.43 (m, 1H, COCH), 4.12 (s, 2H,

OCH_2), 3.73 (s, 3H, OCH_3), 1.68-1.26 (m, 6H, CH/CH_2), 0.89 (d, J = 6.2 Hz, 6H, CH_3), 0.81 (dd, J = 6.5, 4.1 Hz, 6H, CH_3)

1-Pyrenylmethoxymethylcarbonyl dileucine (**P5LL**)

The title compound (52.9 mg, 85.8 %) was prepared (from **P5LLOMe**) *via* LiOH methyl ester hydrolysis, in a similar fashion to that previously described for **P1Y**.

ESI MS +ve $[M+Na]^+$ m/z 539.33

ESI MS -ve $[M-H]^-$ m/z 515.20

^1H NMR (CD_3OD) δ 8.48 (d, J = 9.3 Hz, 1H, ArH), 8.38 (d, J = 8.0 Hz, 1H, CONH), 8.27-8.18 (m, 4H, ArH), 8.12-8.02 (m, 4H, ArH), 7.70 (d, J = 8.3 Hz, 1H, CONH), 5.42 (d, J = 11.9 Hz, 1H, $ArCH_2$), 5.27 (d, J = 11.9 Hz, 1H, CH_2), 4.52-4.40 (m, 2H, COCH), 4.15 (d, J = 8.6 Hz, 2H, OCH_2), 1.76-1.59 (m, 3H, CH/CH_2), 1.55-1.33 (m, 3H, CH/CH_2), 0.91 (dd, J = 14.8, 6.4 Hz, 6H, CH_3), 0.78 (dd, J = 12.7, 6.1 Hz, 6H, CH_3)

3.2 Hydrogel preparation protocols

Note that for all the hydrogel preparation protocols, care must be taken throughout the NaOH and HCl/NaH_2PO_4 addition, to ensure that the pH value remains less than 10.5 to prevent the base catalysed loss of Fmoc functionality (if present).[7]

3.2.1 Dropwise pH method

The peptide derivative was suspended in 1 mL of doubly distilled (ddH_2O), to give 20 mmol/L. Dissolution was achieved *via* sonication and the addition of 0.5 M NaOH solution (50 μL). 1 M HCl was then added dropwise while the sample underwent repeated sonication, vortexing, and rest periods until the sample was self-supporting upon vial inversion. Note that this methodology – though simple – does not yield the most reproducible results,[8,9] as if the 1M HCl is added too quickly sample inhomogeneity and/or precipitation can result.

3.2.2 Phosphate buffered hydrogels

For the single component systems; gelator/surfactant (20 μmol) was suspended in 807 μL of double-distilled water (ddH_2O). For the co-assembly systems, gelator(s)/surfactant(s) (20 μmol of each) were suspended in 787 μL of double-distilled water (ddH_2O). For the single component systems, in the first instance, 25 μL of 1 M NaOH was added. For the co-assembly samples 45 μL of 1 M NaOH is required to account for the additional 20 μmol of carboxylic acid present. In each case, the mixture is sonicated to give a clear solution. An additional, 68 μL of 1 M NaOH and 100 μL of 1M NaH_2PO_4 were added together and the

mixture vortexed briefly to give a 100 mM phosphate buffered hydrogel with a final pH of ~7.3. For the lower pH systems, the final pH can be decreased by 1 M HCl addition. For FTIR samples, the above procedure was followed, using deuterium oxide (D_2O) in place of water; though a negligible number of protons will be present from the non-deuterated NaOH, NaH_2PO_4, and the gelator and/or surfactant compound(s) themselves. In addition, to minimize water content, the low pH deuterated FTIR samples were prepared by decreasing the initial concentration of NaOH (instead of neutralizing with HCl) – this alternate methodology requires more vortexing and sonication to achieve similar levels of dissolution and consequent homogeneity in the gel state.

3.2.3 HQ electrochemical hydrogel coating

3.2.3.1 Pre-gelation coating solutions

The *gelator* (Fmoc-F or Pyr-YL) and *surfactant* (Fmoc-S) if applicable were suspended in 0.5 mL of double distilled water (ddH_2O), to give 5 mmol/L of each component. 18 μL of 0.5 M NaOH solution was added, and the mixture sonicated to give a clear solution (e.g. ~pH 9-10). For the Pyr-YL based systems, 5 μL of 1 M NaH_2PO_4 solution was added. In all cases the pH was then adjusted *via* the dropwise addition of 1 M HCl to achieve a final pH value of either 6.7 (Pyr-YL and Pyr-YL/Fmoc-S) or 8.0 (Fmoc-F). Hydroquinone was then added to the solution, so as to achieve a 50 mM concentration. Due to the auto-oxidation of hydroquinone, once prepared the solutions were used within a few hours.

3.2.3.2 Bulk coating procedure

A strip of paper ~1.5 cm in width was wrapped around folded-back strands of copper cable such that only a single copper strand was exposed at one end. Another copper cable with all strands exposed, was then attached to the first using electrical tape. Crocodile clips were used to connect the copper cables to a Precision Gold M105 multimeter operating in ohmmeter mode, such that the single copper strand would act as an anode, whilst the unmodified cable would act as the cathode or counter electrode. The anode and cathode were inserted into an eppendorf containing the coating solution (see above), such that both were submerged. Here, the length of the anode (copper strand determined to have a thickness on the order of 200 μm and assumed to be cylindrical) and the resistance scale setting on the multimeter could be adjusted to afford rudimentary control over the applied current density. The applied current was measured by a second Iso-Tech IDM 71 multimeter, connected in series, operating in ammeter mode. In each case the current was applied for four minutes, and the coating subsequently assessed visually and under UV irradiation.

3.2.3.3 MEA platinisation and electrochemical coating procedure

The MEA array was connected to a custom made PCB with switches for addressing individual nodes on the array. The current source used was a Yokogawa GS610, operating under galvanostatic control in all cases. For platinisation, a standard 1% platinic chloride ($PtCl_6H_2$) and 0.08% lead acetate ($Pb(OAc)_2$) aqueous solution was utilised; selected nodes acted as cathodes, with an 80 nA current applied per electrode for 2 minutes and 20 seconds. For Pyr-YL hydrogel coatings, the previously described gelator coating solution was utilised; selected nodes acted as anodes, with an 8 nA current applied per electrode for 4 minutes.

3.3 Characterisation techniques

3.3.1 Fourier transform infrared spectroscopy

Gels were prepared as described above, using D_2O in place of water. However, a negligible number of protons will be present from the non-deuterated NaOH, HCl/NaH_2PO_4, and the gelator compounds themselves. Hence, broad baseline-type absorptions from HOD or H_2O were generally in the amide I region. Spectra were recorded on a Bruker Vertex 70 spectrometer averaging 25 scans per sample at a resolution of 1 cm^{-1}. Samples were sandwiched between two 2 mm CaF_2 windows separated with a 25 μm PTFE spacer.

3.3.2 Fluorescence emission spectroscopy

Spectra were recorded on a Jasco FP-6500 spectrofluorometer, with emission measured perpendicular to the excitation light. 2 mL samples were transferred into cuvettes with a path length of 1 cm. An excitation wavelength of 295 nm was used, and the emission intensity recorded in the range between 300 and 600 nm. An excitation and emission bandwidth of 3 nm was utilised, while the fluorometer sensitivity was altered to as to attain a well defined spectrum in each case.

3.3.3 Circular dichroism

In order to obtain homogeneous samples and acceptable HT signals, it was necessary to use a range of concentrations (5-15 mM), due to the viscous nature and high absorption of the gels. Samples were pipetted into a 0.2 mm cell. Spectra were measured between 200 and 400 nm on a Jasco J600 spectropolarimeter with 1 s integrations, a step size of 1 nm and a single acquisition with a slit width of 1 nm. Note that for co-assembly samples, since pyrene absorption dominates; for the purposes of calculating the molar ellipticity, the concentration of fluorophore present (e.g. either pyrene or fluorene) was used. For example, a 20 mM/20 mM co-assembly sample would be defined as: 20 mM if an Fmoc and pyrene based

component were both present; or 40 mM if both species possessed the same fluorophore.

3.3.4 Atomic force microscopy

20 µl of a 2 mM solution, was placed on a trimmed, freshly cleaved mica sheet attached to an AFM support stub, which was left to air-dry overnight in a dust-free environment, prior to imaging. The images were obtained by scanning the mica surface in air under ambient conditions using a Veeco MultiMode with NanoScope IIID Controller Scanning Probe Microscope (Digital Instruments, Santa Barbara, CA, USA; Veeco software Version 6.14r1) operated in tapping mode. The AFM measurements were obtained using a sharp silicon probe (TESP; nominal length (lnom) = 125 µm, width (wnom) = 40 µm, tip radius (Rnom) = 8 nm, resonant frequency (nom) = 320 kHz, spring constant (knom) = 42 N m^{-1}; Veeco Instruments SAS, Dourdan, France), and AFM scans were taken at 512 x 512 pixels resolution. Typical scanning parameters were as follows: tapping frequency 308 kHz, integral and proportional gains 0.3 and 0.5, respectively, set point 0.5 – 0.8 V and scanning speed 1.0 Hz. The images were analyzed using Veeco Image Analysis software Version 6.14r1.

3.3.5 Rheology

To assess the mechanical properties of the hydrogels, dynamic frequency sweep experiments were carried out on a strain-controlled rheometer (Malvern Kinexus Pro) using a parallel-plate geometry (20 mm) with a 0.50 mm gap. To ensure the measurements were made in the linear viscoelastic regime, a strain sweep (1 Hz) was performed. The dynamic modulus of the hydrogel was measured as a frequency function (~0.2 %, see appendices), where the frequency sweeps were carried out between 0.1 and 100 Hz. Note that at frequencies > 10 Hz, the extrusion of water and the consequently increased concentration of the samples, generally results in a sharp increase in the respective moduli values.

3.3.6 Scanning electron microscopy

SEM images of the MEA device were recorded using an FEI Quanta 250 field-emission gun environmental scanning electron microscope (FEG-ESEM) (courtesy of Dr Paul Edwards, Semiconductor spectroscopy & devices, Dept. of Physics).

3.3.7 Brightfield and fluorescence microscopy

MEA coatings were assessed using a Zeiss Imager A1 microscope operated in brightfield (100 W halogen lamp) and epifluorescence (50 W mercury lamp) modes. For epifluorescence a standard DAPI filter insert was used. In all cases, images were captured

using a Canon Powershot G6 camera.

3.3.8 Impedance measurements

For impedance measurements an Iso-Tech LCR Meter LCR821 was used with an operating voltage of 0.1 V. For bulk hydrogel measurements a probe was inserted into the existing gel and impedance measured over the frequency range 12-2x10^5 Hz. For MEA impedance measurements, individual nodes were measured using custom made PCB apparatus with switches for addressing individual nodes on the array. Throughout the MEA impedance measurements, coatings were stabilised[10] in 100 mM pH 5.0 sodium phosphate buffer - identical conditions were used for the measurement of platinised and uncoated nodes.

3.3.9 High performance liquid chromatography

The co-assembled Pyr-YL/Fmoc-S bulk electrochemical hydrogel coating was scrapped off into an HPLC vial and diluted with 50% acetonitrile/water. A Dionex P680 HPLC system equipped with a Macherey-Nagel C18 column of 250 mm length, 4.6 mm internal diameter and 5 mm particle size was used with a gradient of 20% acetonitrile/water at 4 minutes to 80% acetonitrile/water at 31 minutes. With each run lasting a total of 46 minutes, using a flow rate of 1 mL min^{-1}, and a detection wavelength of 280 nm.

3.4 References

1. S. Fleming, S. Debnath, P. W. J. M. Frederix, T. Tuttle, and R. V. Ulijn, *Chem. Commun.*, 2013, **49**, 10587–10589.
2. I. R. Sasselli, *MSc Thesis Univeristy Strathclyde*, 2012.
3. S. Fleming, P. W. J. M. Frederix, I. Ramos-Sasselli, N. Hunt, R. V. Ulijn, and T. Tuttle, *Langmuir*, 2013, **29**, 9510–9515.
4. S. Roy, N. Javid, P. W. J. M. Frederix, D. A. Lamprou, A. J. Urquhart, N. T. Hunt, P. J. Halling, and R. V. Ulijn, *Chem. – Eur. J.*, 2012, **18**, 11723–11731.
5. S. Okada, S. Yamashita, T. Furuta, and M. Iwamura, *Photochem. Photobiol.*, 1995, **61**, 431–434.
6. S. Fleming, S. Debnath, P. W. J. M. Frederix, N. T. Hunt, and R. V. Ulijn, *Biomacromolecules*, 2014, **15**, 1171–1184.
7. C. Tang, A. M. Smith, R. F. Collins, R. V. Ulijn, and A. Saiani, *Langmuir*, 2009, **25**, 9447–9453.
8. D. J. Adams, M. F. Butler, W. J. Frith, M. Kirkland, L. Mullen, and P. Sanderson, *Soft Matter*, 2009, **5**, 1856–1862.
9. W. Helen, P. de Leonardis, R. V. Ulijn, J. Gough, and N. Tirelli, *Soft Matter*, 2011, **7**, 1732–1740.
10. Y. Liu, E. Kim, R. V. Ulijn, W. E. Bentley, and G. F. Payne, *Adv. Funct. Mater.*, 2011, **21**, 1575–1580.

– Chapter 4 –

Assessing the utility of FTIR in β-sheet type H-bonding structure elucidation

4.1 Abstract

β-Sheets are a commonly found structural motif in self-assembling aromatic peptide amphiphiles, and their characteristic "amide I" infrared absorption bands are routinely used to support the formation of supramolecular structure. In this chapter, we assess the utility of IR spectroscopy as a structural diagnostic tool for this class of self-assembling systems. Using various Fmoc and analogous Fmc functionalised dipeptides as examples, we show that the origin of the band around 1680-1695 cm^{-1} in FTIR spectra, which was previously assigned to an antiparallel β-sheet conformation, is in fact absorption of the stacked carbamate group in Fmoc-peptides. IR spectra from ^{13}C-labeled samples also support our conclusions.

4.2 Introduction

Infrared spectroscopy is well-established as a useful technique to assist in the determination of secondary structure elements in proteins, specifically in the amide I region (1600-1700 cm^{-1}), which is sensitive to hydrogen-bonding patterns found in α-helices and β-sheets.[1–7] Recently, IR spectroscopy has been utilized to help characterize the supramolecular structure of self-assembling nanostructures composed of oligopeptides. It is theoretically possible to differentiate between infinite parallel and antiparallel β-sheets, the former typically showing a single band at approximately 1615-1640 cm^{-1} and the latter having an additional component near 1685 cm^{-1}.

This practice of using models developed for the secondary structure determination of proteins may not be valid for interpreting the infrared spectra of LMW hydrogels. In examples that consist of 7-29 amino acid residues,[8–11] typically a 1615 cm^{-1} amide I peak and a much weaker 1680 cm^{-1} peak are observed - characteristic of proteins with an antiparallel β-sheet structure. However, the presence of β-sheets has also been reported for a class of LMW gelators composed from various short (e.g., di- and tri-) peptides capped at the N-terminus with an aromatic group - most commonly the Fmoc moiety.[12–21] The assignment of infrared bands that are apparently analogous to those seen in longer peptides is often used as a key piece of evidence to support an antiparallel β-sheet structure. While the absorption bands of LMW gelators resemble β-sheet signals in terms of line position, the relative

infrared peak intensities for these materials are not always typical of that found for longer peptides or indeed proteins.[22] Significant variation in the intensity of the 1690 cm^{-1} band has been observed, with this band often being of similar or greater magnitude compared to the lower frequency (1615-1640 cm^{-1}) amide I contribution,[14,19,20,23,24] which is higher than expected for even a perfect antiparallel β-sheet.[4–6] Additionally, the relative intensity of the 1690 cm^{-1} band is observed to decrease as the ratio of amide to carbamate groups increases in longer Fmoc-peptide examples.[18,21] This is not consistent with what would be expected if this peak is truly indicative of an antiparallel β-sheet in these systems, especially since the longer chain length would be more likely to increase the ν ∥ component (see Fig. 4.1), rather than decrease it. The ambiguity surrounding these assignments has led to doubt regarding the presence of antiparallel β-sheet structures in spite of infrared evidence suggesting this conformation, with authors increasingly wary of applying traditional protein secondary structure interpretations.[25–27] For instance, in spite of IR evidence for "antiparallel" β-sheets, parallel β-sheet structures have been proposed based on X-ray diffraction data,[26] and a recent experimental and computational study has suggested a polyproline II conformation,[27] which lacks significant hydrogen bonding between residues.

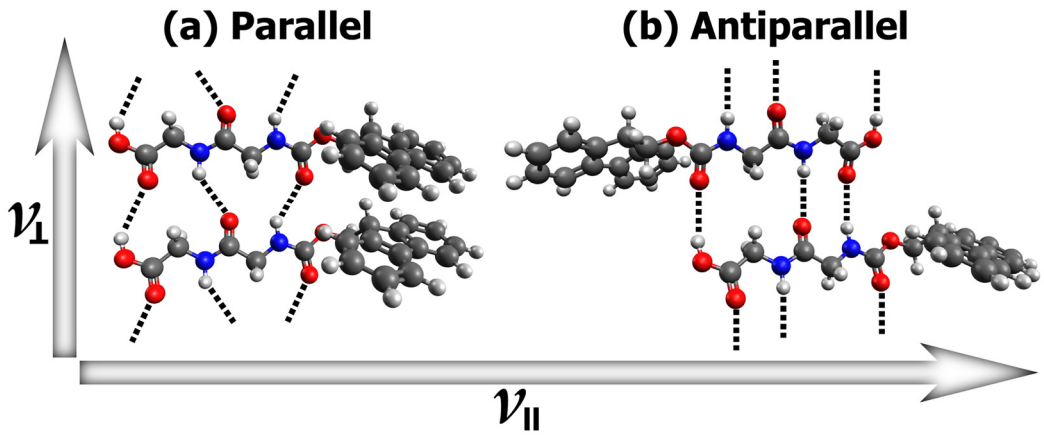

Figure 4.1 (a) Parallel and (b) Antiparallel models showing potential β-sheet hydrogen bonding patterns for a generic aromatic dipeptide amphiphile – side chains omitted for clarity, so nominally Fmoc-GG. Arrows show the direction of parallel (∥) and perpendicular (⊥) excitons as discussed in the text.

Additionally, we have previously observed the absence of the 1690 cm^{-1} peak,[28] in hydrogels assembled from non-Fmoc aromatic dipeptides that lack the carbamate group. The carbamate group is known to absorb IR light in the 1685-1730 cm^{-1} range,[29–33] including a report by Nuansing et al. on Fmoc-FG powders,[34] which shows contributions significantly higher than the 1650 cm^{-1} absorption for free amide groups. For these reasons, it is important to assess the diagnostic value of the amide I infrared region for these systems.

In the general case of antiparallel β-sheets, the low-frequency component (1615-1640 cm^{-}

[1]) arises from interstrand delocalization and mode coupling (ν⊥, see Fig. 4.1), which shifts the mode to lower wavenumbers as strands become more aligned and the number of strands per sheet increases.[4,5] In contrast, the frequency of the high wavenumber peak (1680-1695 cm^{-1}) is generally independent of the number of strands and originates from vibrational excitons that run along a particular β-strand (ν ||, Fig. 4.1).[4] As a consequence, the transition dipole moment along the strands will be relatively small for short peptide β-sheet strands (≤3 amino acids), and it is conceivable that this peak may not be resolvable in spectra of their supramolecular structures. Moreover, in cases of β-sheets of finite size, correctly determining the presence of a parallel or antiparallel structure can be challenging; as disorder or twists, which may be expected for short, flexible peptides, can severely diminish the delocalization of vibrational modes and therefore broaden or shift optical transitions.[1,35–37]

In this chapter we examine the amide I infrared bands of various hydrogels capped with either **Fmoc** or **Fmc** (or **F3** and **F2**, respectively, according to nomenclature adopted in Chapter 3) at the N-terminus. **Fmc** was utilized as a close analogue for the **Fmoc** moiety but crucially lacks the carbamate oxygen and is instead linked to the dipeptide sequence via an amide bond (see Fig. 4.2). A range of common dipeptide sequences were considered (Fig. 4.2),[14,38–42] in order to investigate and confirm the generality of any trends observed using FTIR spectroscopy and isotope labelling. However, particular focus was given to the Fmoc-dialanine (**Fmoc-AA**) and Fmc-dialanine (**Fmc-AA**) systems; as alanine is the simplest chiral amino acid and consequently dialanine based aromatic peptide amphiphiles have been the subject of recent computational studies.[27,43]

4.3 Results and discussion

Hydrogels were prepared via the dropwise addition (see Chapter 3, section 3.2.1) of 1 M HCl to 20 mM solutions of the gelator compound in D_2O at an initial pH of ~9 and a final pH of ~4-7 (Table 4.1). Note that this methodology – though simple – does not yield the most reproducible results,[44,45] as if the 1M HCl is added too quickly sample inhomogeneity and/or precipitation can result.

In an effort to elucidate the mechanisms responsible for the FTIR features generally observed in corresponding **Fmoc** and **Fmc** systems, a variety of **Fmoc** and **Fmc** functionalised dipeptide gelators were examined in this study (Fig. 4.2). While it should be acknowledged that different linkers can potentially have a non-trivial impact upon the self-assembly and gelation of aromatic peptide amphiphiles (see Chapter 5).[28] Due to the structural similarity between corresponding **Fmoc** and **Fmc** molecules, it is reasonable to assume that similar supramolecular H-bonding arrangements and corresponding FTIR results

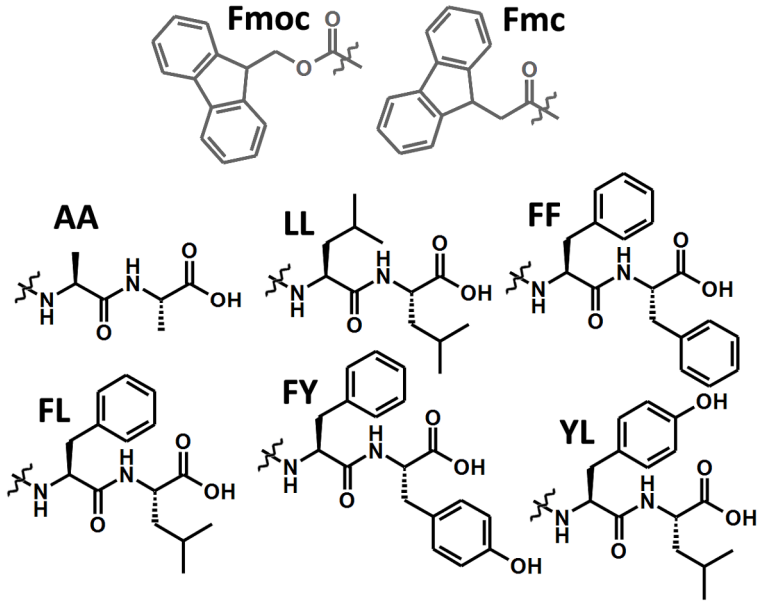

Figure 4.2 Molecular structures the gelators utilised in this study.

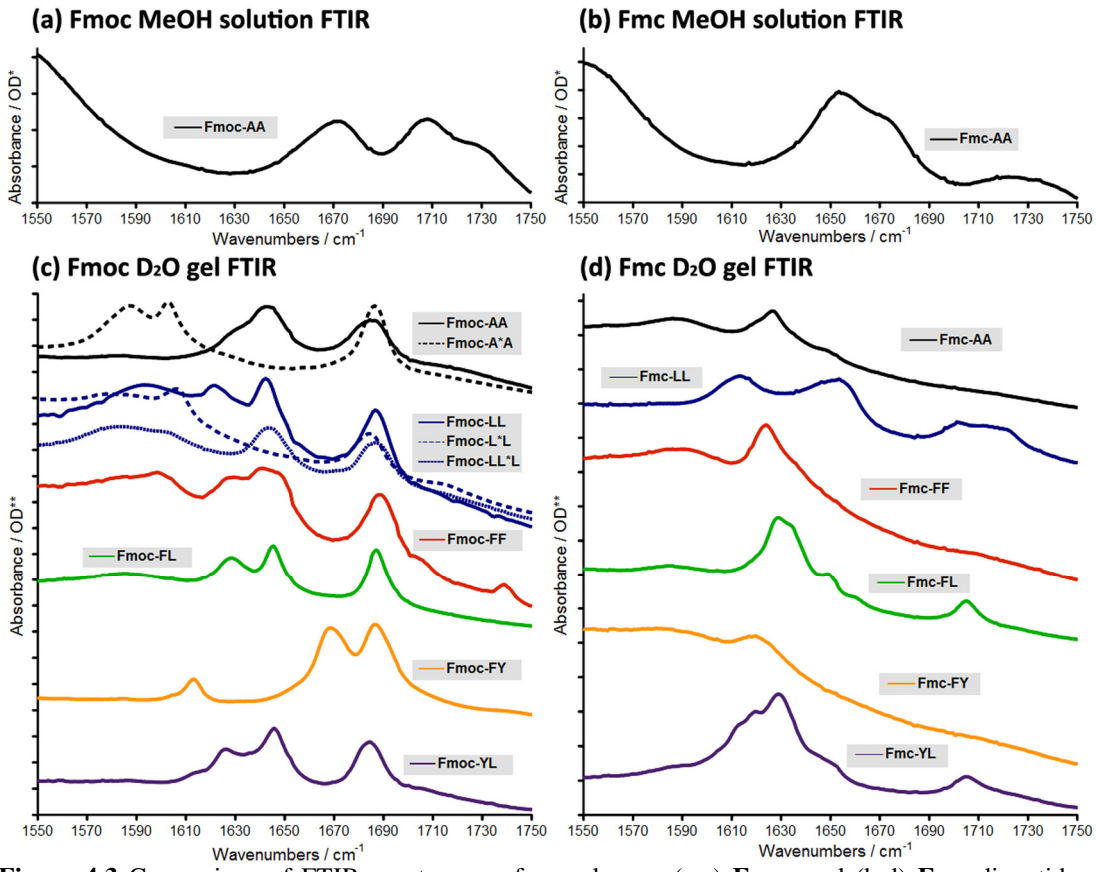

Figure 4.3 Comparison of FTIR spectra seen for analogous (a,c) **Fmoc** and (b,d) **Fmc** dipeptides. Spectra vertically offset for clarity: *each division corresponds with 0.02 units; **each division corresponds with 0.2 units.

should be observed – particularly if the accepted ν⊥ and ν∥ amide I assignments are correct. However, an initial comparison of the FTIR spectra of **Fmoc** and **Fmc** gels reveals clear differences between these species (Fig. 4.3). In particular the 1685 cm^{-1} band traditionally

associated with an antiparallel β-sheet type H-bonding arrangement is absent for the **Fmc** based systems. Hence, we instead attribute this absorption to the carbamate moiety present for the **Fmoc** materials.[34]

4.3.1 Degree of ionisation

In some of the spectra, a broad contribution around 1590 cm^{-1} is discernible, which indicates that a fraction of terminal carboxylic acid groups remain deprotonated, in line with other aromatic peptide amphiphile based gels.[22,46] Also note that the high wavenumber absorption (~1705 cm^{-1}) seen in the FTIR spectra of **Fmc-LL**, **Fmc-FL**, and **Fmc-YL** is assigned to the terminal protonated carboxylic acid group and should not be confused with the carbamate absorption.[34] The 1705 cm^{-1} peak may also be present in some of the **Fmoc** systems, such as **Fmoc-FF**, where it is partially obscured by the carbamate band. Hence, the presence of the 1705 cm^{-1} contribution is likely to be dependant upon both the hydrogel pH value and the apparent pK_a of the gelator in question; where the apparent pK_a has been previously found to be largely dependant upon the C log P value, with the apparent pK_a and maximum gelation pH broadly increasing with hydrophobicity.[47,41] Using the dropwise HCl method, sample reproducibility can be an issue, in addition, the gelation properties of these materials can vary when using D_2O instead of water - thus the quoted pH values (Table 4.1) are likely to differ from the pH/pD of the samples used in FTIR experiments. Hence, the prominence of the 1705 cm^{-1} in certain spectra indicates that the pH of these samples was lower than necessary to achieve gelation, with some degree of precipitation and loss of β-sheet type structure likely.[22]

Table 4.1 pH and C log P values of gelators

	Fmoc		Fmc	
	pH*	C log P**	pH*	C log P**
AA	4.9	2.47	4.1	2.03
YL	5.1	4.68	5.2	4.12
LL	6.3	4.82	5.5	4.33
FY	4.9	4.83	5.0	4.38
FL	6.1	5.04	6.0	4.61
FF	6.4	5.28	5.4	4.76

*pH measured in hydrogel (H_2O) samples and hence may differ from pH/pD of deuterated gels (D_2O) used for the FTIR study. **Using online program at Virtual Computational Chemistry Laboratory

4.3.2 Fmoc based gels

The FTIR spectra of the **Fmoc** dipeptide systems display varying degrees of associated disorder. For example, the **Fmoc-AA** gel (Fig. 4.3(c)) shows a characteristic amide I band centred around 1640 cm^{-1}, which clearly has at least two overlapping contributions, indicating substantial inhomogeneity associated with the amide I arrangement. In

comparison, **Fmoc-LL**, **Fmoc-FF**, **Fmoc-FL**, and **Fmoc-YL** all exhibit more clearly separated amide I bands; with a contribution at ~1625 cm^{-1} that is assigned to an ordered β-sheet type H-bonding arrangement, as well as major absorptions at ~1640 cm^{-1} that are indicative of relatively disordered H-bonded stacks.[22,28] The tails of these FTIR absorption bands also extend beyond 1650 cm^{-1}, which is usually attributed to "random coil" conformation in protein spectroscopy. In short peptides, this is more commonly assigned to disordered[48] or unstacked[46] amide groups, indicating imperfect sheet stacking or partial polyproline II conformation.[27,48,46] These broad convoluted amide I peaks, despite the presence of only a single amide group, demonstrate that there are at least two distinct supramolecular populations associated with these **Fmoc** systems. Furthermore, in contrast to the other **Fmoc** based gels, **Fmoc-FY** exhibits a small peak at 1615 cm^{-1} and a broad contribution around 1670 cm^{-1}. Given the relatively opaque appearance of the **Fmoc-FY** gel (Fig. 4.4), this suggests that material is precipitating out to a greater extent, resulting in a far more pronounced splitting of the amide I peak. Hence, the **Fmoc** materials exhibit several amide I bands indicative of H-bonding stack size inhomogeneity – suggesting some degree of precipitation, as evidenced by the aforementioned 1705 cm^{-1} peak that is partly obscured in the Fmoc-FF spectrum, for example.

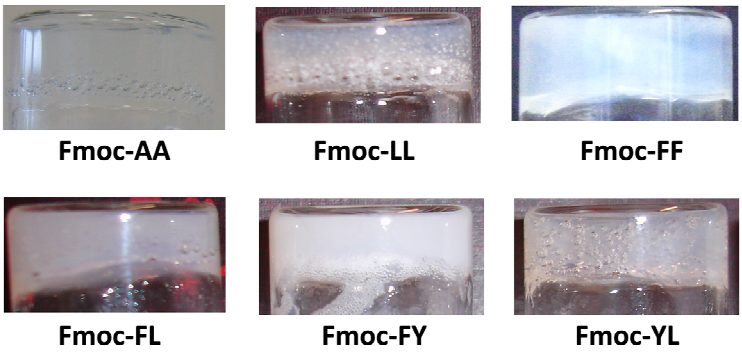

Figure 4.4 Appearance of the Fmoc based gels.

While the extent of implied amide I disorder appears to vary considerably between the gelators, and is also likely to be affected by the nature of the gelation protocol utilised,[14,49] there is generally less variation in the frequency associated with the carbamate moiety. The relative consistency of this absorption frequency (~1685 cm^{-1}) is likely a consequence of the carbamate being adjacent to the supramolecular interlocked aromatic stacking arrangement.[19] Hence, there is potentially a greater degree of freedom associated with single amide group of the **Fmoc** based gelators – thus accounting for the pronounced split amide I peaks exhibited by several of the **Fmoc** systems. Furthermore, both the amide I and carbamate bands are consistently observed to be of a similar intensity, which is not expected for antiparallel β-sheets, but is characteristic for Fmoc-dipeptide hydrogels,[22] and evidently this supports the

carbamate assignment.

4.3.3 Fmc based gels

For the **Fmc** based systems (Fig. 4.3(d)), we observe that in comparison to the **Fmoc** hydrogels, there is generally less associated amide I inhomogeneity, with a greater proportion of amide I contributions now at lower wavenumbers. This general observation is attributed to the additional amide group now adjacent to the aromatic, which similar to the carbamate also likely has less freedom and hence less variability in its H-bonding arrangement. For instance, **Fmc-AA**, exhibits a peak at 1625 cm^{-1}, whose non-Gaussian shape suggests that this is the convolution of two close absorption bands (i.e. there are two amide groups). Similarly, **Fmc-FF** and **Fmc-FY** each demonstrate an amide I peak centred around 1625 cm^{-1}, consistent with β-sheet type structure[22] with only weak contributions at higher (e.g. 1650 cm^{-1}) wavenumbers .

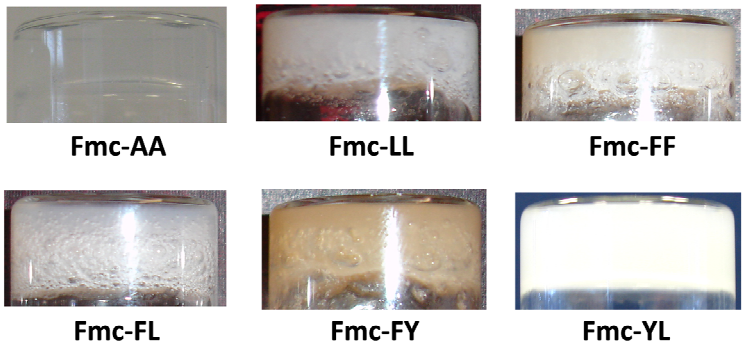

Figure 4.5 Appearance of the Fmc based gels.

In contrast, the analogous **Fmc-LL**, **Fmc-FL**, and **Fmc-YL** gels exhibit more complex amide I bands. **Fmc-LL** shows broad amide I bands at 1615 and 1650 cm^{-1}, indicative of a β-sheet type arrangement and a relatively disordered conformation, respectively. In this **Fmc-LL** example, the disordered 1650 cm^{-1} band is relatively prominent. Whilst, **Fmc-FL** demonstrates a convoluted amide I band at 1630 cm^{-1}, in addition to a small peak around 1650 cm^{-1} from disordered or relatively unstacked amide groups. Similarly, **Fmc-YL** shows overlapping 1615, 1620, and 1630 cm^{-1} amide I contributions and a shoulder that extends beyond 1650 cm^{-1}. The apparent disorder present in the **Fmc-LL**, **Fmc-FL**, and **Fmc-YL** systems is also accompanied by the aforementioned 1705 cm^{-1} peak, and for **Fmc-LL**, additional higher wavenumber contributions. This indicates that the observed amide I band disorder, correlates with the partial precipitation of these systems.

Overall however, the **Fmc** systems consistently demonstrate the absence of the 1685 cm^{-1} peak, which is characteristic of the corresponding **Fmoc** based gels. Assuming that the self-assembly of analogous **Fmoc** and **Fmc** systems proceed in a similar fashion, these results

would again indicate the 1685 cm^{-1} peak is more likely a consequence of carbamate moiety absorption, rather than the ν || component of antiparallel β-sheets, as the latter is expected to be of negligible intensity for very short peptide chains.

4.3.4 Methanol solutions

The carbamate assignment is confirmed by the spectra of **Fmoc-AA** and **Fmc-AA** in neat methanol at the same concentration (Fig. 4.3(a,b)). Despite the absence of gelation or any apparent self-assembly in this solvent – and the consequently higher wavenumber absorptions compared to the corresponding D_2O gels – it is clear that the spectrum of **Fmoc-AA** shows distinctly separate bands at 1670 and 1708 cm^{-1} assigned to the respective amide I and carbamate absorptions, whereas **Fmc-AA** shows two overlapping amide I bands around 1652 and 1670 cm^{-1} from the two respective amide groups. Furthermore, in both experimental spectra a band is present at 1730 cm^{-1} due to the carboxylic acid terminal group. Note that a weak methanol absorption is responsible for the sloped background below 1600 cm^{-1}.

It is also apparent that the absorption of **Fmoc-AA** and **Fmc-AA** in methanol solution has a much lower intensity due to the lack of the cooperative effect (note the difference in scale between Figures 4.3(a,b) and 4.3(c,d)), but the relative intensities of the bands are preserved. This indicates that, in the gel state, both the ~1625-1640 cm^{-1} amide band and the 1685 cm^{-1} carbamate band of **Fmoc** based gels are equally enhanced as part of the β-sheet structure, which again suggests that interstrand delocalization is responsible in each case, rather than the ν || and ν ⊥ components.

4.3.5 ^{13}C labelled gelators

Conclusive evidence for the assignment of the 1685 cm^{-1} peak to the carbamate group was given by the IR spectrum of ^{13}C labelled **Fmoc-A*A**, **Fmoc-L*L**,[50] and **Fmoc-LL*L**[15,38] gels, whereby the amide carbonyl closest to the C-terminus was modified (Fig. 4.6). This procedure typically red-shifts the vibrational frequency of affected H-bonded carbonyl groups by 40-43 cm^{-1} (e.g., ref [51]). Figure 4.3 shows that, in comparison with unlabelled **Fmoc-AA**, only the lower frequency band moves from about 1640 to 1600 cm^{-1}, while the position of the 1685 cm^{-1} peak remains unaffected, in agreement with its different chemical nature. Similarly, for **Fmoc-L*L**, the ~1685 cm^{-1} carbamate band is preserved, whilst the previously observed amide I bands are shifted to around 1605 cm^{-1} – thus further confirming the assignment of these respective peaks. In the case of **Fmoc-LL*L**, we now possess carbamate, amide I, and ^{13}C amide I groups all in a single system. Correspondingly, the 1685 cm^{-1}, 1640 cm^{-1}, and 1600 cm^{-1} bands are now observed simultaneously, although the latter

peak is partially obscured with a broad 1585 cm^{-1} contribution from a portion of carboxylate anions.[22] Hence, it is clear that the 1685 cm^{-1} vibration corresponds to the carbamate moiety, and hence is not associated with an antiparallel β-sheet arrangement for these aromatic peptide amphiphile systems. However, this does not necessarily preclude the antiparallel structure, since for short dipeptide sequences, one would anticipate that the ν ∥ component (Fig. 4.1) should be minimal.[1]

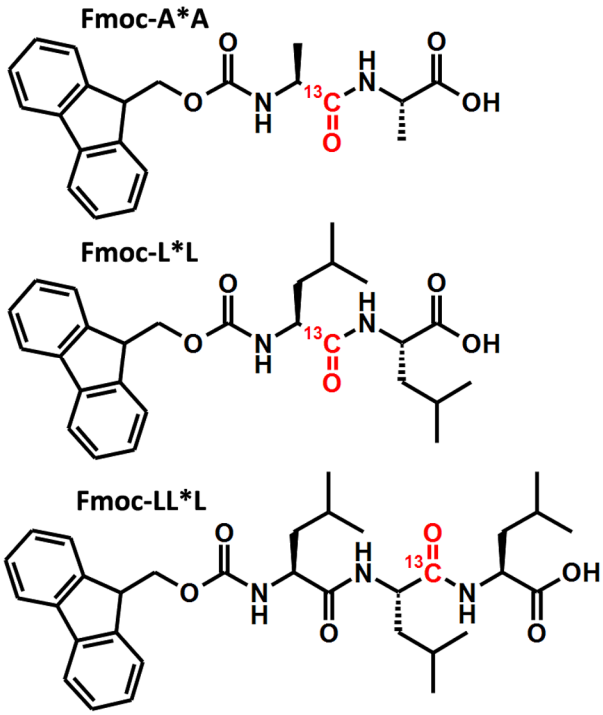

Figure 4.6 Molecular structures of the ^{13}C labelled **Fmoc-A*A**, **Fmoc-L*L**, and **Fmoc-LL*L** hydrogelators.

4.4 Conclusions

In summary, we have demonstrated that for self-assembling Fmoc-containing peptides the presence of two separate peaks in the amide I region of the IR is not indicative of antiparallel β-sheets. Instead, results show that it is the presence of the carbamate moiety that is responsible for the 1685 cm^{-1} peak observed in these systems rather than a ν ∥ component. A similar peak pattern can thus be expected for, for example, Cbz functionalised peptides. As a consequence, neither parallel nor antiparallel β-sheets can be ruled out as potential supramolecular structures on the basis of infrared spectroscopy alone. Recent computational work also qualitatively agrees with the experimental results presented here.[43,52] In any case, this work mainly indicates that a more cautious interpretation of infrared results of short peptides will be required in the future but does not necessarily alter the conclusions of the parallel,[26] antiparallel,[19] or polyproline II models[27] proposed for specific cases. Ultimately, the unambiguous determination of a parallel or antiparallel supramolecular conformation

will likely require the culmination of a variety of experimental techniques including, for example, vibrational circular dichroism,[36,53,54] multidimensional IR,[5,55,56] and solid state NMR.[57]

4.5 References

1. A. Barth and C. Zscherp, *Q. Rev. Biophys.*, 2002, **35**, 369–430.
2. R. V. Rughani and J. P. Schneider, *MRS Bull.*, 2008, **33**, 530–535.
3. H. Yan, H. Frielinghaus, A. Nykanen, J. Ruokolainen, A. Saiani, and A. F. Miller, *Soft Matter*, 2008, **4**, 1313–1325.
4. C. Lee and M. Cho, *J. Phys. Chem. B*, 2004, **108**, 20397–20407.
5. S. Hahn, S.-S. Kim, C. Lee, and M. Cho, *J. Chem. Phys.*, 2005, **123**, 084905.
6. Z. Ganim, H. S. Chung, A. W. Smith, L. P. DeFlores, K. C. Jones, and A. Tokmakoff, *Acc. Chem. Res.*, 2008, **41**, 432–441.
7. C. M. Cheatum, A. Tokmakoff, and J. Knoester, *J. Chem. Phys.*, 2004, **120**, 8201–8215.
8. R. V. Rughani, D. A. Salick, M. S. Lamm, T. Yucel, D. J. Pochan, and J. P. Schneider, *Biomacromolecules*, 2009, **10**, 1295–1304.
9. T. J. Measey and R. Schweitzer-Stenner, *J. Am. Chem. Soc.*, 2006, **128**, 13324–13325.
10. T. J. Measey, K. B. Smith, S. M. Decatur, L. Zhao, G. Yang, and R. Schweitzer-Stenner, *J. Am. Chem. Soc.*, 2009, **131**, 18218–18219.
11. J. P. Schneider, D. J. Pochan, B. Ozbas, K. Rajagopal, L. Pakstis, and J. Kretsinger, *J. Am. Chem. Soc.*, 2002, **124**, 15030–15037.
12. H. Shao and J. R. Parquette, *Chem. Commun.*, 2010, **46**, 4285–4287.
13. R. Orbach, I. Mironi-Harpaz, L. Adler-Abramovich, E. Mossou, E. P. Mitchell, V. T. Forsyth, E. Gazit, and D. Seliktar, *Langmuir*, 2012, **28**, 2015–2022.
14. A. R. Hirst, S. Roy, M. Arora, A. K. Das, N. Hodson, P. Murray, S. Marshall, N. Javid, J. Sefcik, J. Boekhoven, J. H. van Esch, S. Santabarbara, N. T. Hunt, and R. V. Ulijn, *Nat. Chem.*, 2010, **2**, 1089–1094.
15. H. X. Xu, A. K. Das, M. Horie, M. S. Shaik, A. M. Smith, Y. Luo, X. F. Lu, R. Collins, S. Y. Liem, A. M. Song, P. L. A. Popelier, M. L. Turner, P. Xiao, I. A. Kinloch, and R. V. Ulijn, *Nanoscale*, 2010, **2**, 960–966.
16. V. Jayawarna, S. M. Richardson, A. R. Hirst, N. W. Hodson, A. Saiani, J. E. Gough, and R. V. Ulijn, *Acta Biomater.*, 2009, **5**, 934–943.
17. S. Debnath, A. Shome, D. Das, and P. K. Das, *J. Phys. Chem. B*, 2010, **114**, 4407–4415.
18. R. J. Williams, A. M. Smith, R. Collins, N. Hodson, A. K. Das, and R. V. Ulijn, *Nat. Nanotechnol.*, 2009, **4**, 19–24.
19. A. M. Smith, R. J. Williams, C. Tang, P. Coppo, R. F. Collins, M. L. Turner, A. Saiani, and R. V. Ulijn, *Adv. Mater.*, 2008, **20**, 37–38.
20. V. Castelletto, G. Cheng, B. W. Greenland, I. W. Hamley, and P. J. F. Harris, *Langmuir*, 2011, **27**, 2980–2988.
21. X.-D. Xu, C.-S. Chen, B. Lu, S.-X. Cheng, X.-Z. Zhang, and R.-X. Zhuo, *J. Phys. Chem. B*, 2010, **114**, 2365–2372.
22. C. Tang, A. M. Smith, R. F. Collins, R. V. Ulijn, and A. Saiani, *Langmuir*, 2009, **25**, 9447–9453.
23. C. Tang, R. V. Ulijn, and A. Saiani, *Langmuir*, 2011, **27**, 14438–14449.
24. R. Orbach, L. Adler-Abramovich, S. Zigerson, I. Mironi-Harpaz, D. Seliktar, and E. Gazit, *Biomacromolecules*, 2009, **10**, 2646–2651.
25. G. Cheng, V. Castelletto, C. M. Moulton, G. E. Newby, and I. W. Hamley, *Langmuir*, 2010, **26**, 4990–4998.
26. M. Ikeda, T. Tanida, T. Yoshii, and I. Hamachi, *Adv. Mater.*, 2011, **23**, 2819–2822.

27. X. Mu, K. M. Eckes, M. M. Nguyen, L. J. Suggs, and P. Ren, *Biomacromolecules*, 2012, **13**, 3562–3571.
28. S. Fleming, S. Debnath, P. W. J. M. Frederix, T. Tuttle, and R. V. Ulijn, *Chem. Commun.*, 2013, **49**, 10587–10589.
29. A. Paquet, *Can. J. Chem.*, 1982, **60**, 976–980.
30. K. Isama, S. Kojima, and A. Nakamura, *J. Biomed. Mater. Res.*, 1993, **27**, 539–545.
31. B. J. Egner and M. Bradley, *Drug Discovery Today*, 1997, **2**, 102–109.
32. A. F. Jalbout, L. Xin-Hua, B. Trzaskowski, and H. Raissi, *Eclética Quím.*, 2006, **31**, 53–62.
33. N. Spegazzini, H. W. Siesler, and Y. Ozaki, *J. Phys. Chem. A*, 2011, **115**, 8832–8844.
34. W. Nuansing, A. Rebollo, J. M. Mercero, J. Zuñiga, and A. M. Bittner, *J. Raman Spectrosc.*, 2012, **43**, 1397–1406.
35. H. Torii and M. Tasumi, *J. Chem. Phys.*, 1992, **96**, 3379–3387.
36. J. Kubelka and T. A. Keiderling, *J. Am. Chem. Soc.*, 2001, **123**, 12048–12058.
37. H. Torii and M. Tasumi, *J. Raman Spectrosc.*, 1998, **29**, 81–86.
38. A. K. Das, R. Collins, and R. V. Ulijn, *Small*, 2008, **4**, 279–287.
39. V. Jayawarna, M. Ali, T. A. Jowitt, A. E. Miller, A. Saiani, J. E. Gough, and R. V. Ulijn, *Adv. Mater.*, 2006, **18**, 611–612.
40. Y. Zhang, H. Gu, Z. Yang, and B. Xu, *J. Am. Chem. Soc.*, 2003, **125**, 13680–13681.
41. D. J. Adams, L. M. Mullen, M. Berta, L. Chen, and W. J. Frith, *Soft Matter*, 2010, **6**, 1971–1980.
42. S. Roy, N. Javid, P. W. J. M. Frederix, D. A. Lamprou, A. J. Urquhart, N. T. Hunt, P. J. Halling, and R. V. Ulijn, *Chem.–Eur. J.*, 2012, **18**, 11723–11731.
43. S. Fleming, P. W. J. M. Frederix, I. Ramos-Sasselli, N. Hunt, R. V. Ulijn, and T. Tuttle, *Langmuir*, 2013, **29**, 9510–9515.
44. D. J. Adams, M. F. Butler, W. J. Frith, M. Kirkland, L. Mullen, and P. Sanderson, *Soft Matter*, 2009, **5**, 1856–1862.
45. W. Helen, P. de Leonardis, R. V. Ulijn, J. Gough, and N. Tirelli, *Soft Matter*, 2011, **7**, 1732–1740.
46. P. W. J. M. Frederix, R. Kania, J. A. Wright, D. A. Lamprou, R. Ulijn, C. J. Pickett, and N. T. Hunt, *Dalton Trans.*, 2012, **41**, 13112–13119.
47. L. Chen, S. Revel, K. Morris, L. C. Serpell, and D. J. Adams, *Langmuir*, 2010, **26**, 13466–13471.
48. M. Hughes, P. W. J. M. Frederix, J. Raeburn, L. S. Birchall, J. Sadownik, F. C. Coomer, I.-H. Lin, E. J. Cussen, N. T. Hunt, T. Tuttle, S. J. Webb, D. J. Adams, and R. V. Ulijn, *Soft Matter*, 2012, **8**, 5595–5602.
49. S. Roy, N. Javid, J. Sefcik, P. J. Halling, and R. V. Ulijn, *Langmuir*, 2012, **28**, 16664–16670.
50. A. M. Smith, R. F. Collins, R. V. Ulijn, and E. Blanch, *J. Raman Spectrosc.*, 2009, **40**, 1093–1095.
51. A. Blume, W. Huebner, and G. Messner, *Biochemistry*, 1988, **27**, 8239–8249.
52. I. R. Sasselli, *MSc Thesis, Univeristy of Strathclyde*, 2012.
53. T. J. Measey and R. Schweitzer-Stenner, *J. Am. Chem. Soc.*, 2011, **133**, 1066–1076.
54. R. Schweitzer-Stenner, *J. Phys. Chem. B*, 2012, **116**, 4141–4153.
55. A. M. Woys, A. M. Almeida, L. Wang, C.-C. Chiu, M. McGovern, J. J. de Pablo, J. L. Skinner, S. H. Gellman, and M. T. Zanni, *J. Am. Chem. Soc.*, 2012, **134**, 19118–19128.
56. N. T. Hunt, *Chem. Soc. Rev.*, 2009, **38**, 1837–1848.
57. Y. Masuda, A. Nakanishi, R. Ohashi, K. Takegoshi, T. Shimizu, T. Shirasawa, and K. Irie, *Biosci., Biotechnol., Biochem.*, 2008, **72**, 2170–2175.

– Chapter 5 –

The impact of the linker upon gelation properties and supramolecular structure

5.1 Abstract

In this study, we identify the molecular characteristics of aromatic dipeptide amphiphiles, and attempt to elucidate the design rules vital for achieving supramolecular aggregation and hydrogelation for a subset of compounds. In particular, the impact of the linker between the aromatic moiety and dipeptide sequence will be considered. Successful gelators are assessed firstly on the basis of their gelation pH, and rheological properties. In addition, gels are also characterised by AFM, FTIR, CD, and fluorescence; so as to comprehensively assess the supramolecular fibres, β-sheet content, and aromatic stacking interactions which underpin the self assembly process. Overall, this study demonstrates a clear dependence upon the precise linker utilised - this will help to facilitate the design and tailoring of potential gelators in future.

5.2 Introduction

Much work has been carried out in an attempt to rationalise and control, both the self assembly process and resultant properties of aromatic peptide amphiphile based hydrogel materials.[1] One of the most common strategies for elucidating aromatic peptide amphiphile design rules is by making changes to the molecular structure. For example, the peptide sequence can be defined by synthetic means,[2–7] or alternatively prepared *via* an enzymatic (e.g. thermolysin) reversed hydrolysis mechanism.[8–10] Here, the self-assembly initiation method utilised, can have an impact upon the properties of the resultant materials,[11] with the initiation method affecting the kinetics of the self-assembly process. As a consequence, the relative thermodynamic stability of the kinetically trapped hydrogel network can vary considerably. Although these effects are outside the scope of this study, it should be noted that the molecular structure associated with the hydrogelator is an important but not an all encompassing parameter.

In terms of the molecular structure, altering the peptide gives access to all of the diverse chemical functionality associated with amino acids,[12] either to simply tailor the hydrophobicity of the amphiphile, or to introduce more specific interactions, between for example charged or H-bonding residues. At the N-terminus a variety of aromatic moieties have been studied: such as phenyl, naphthalene, pyrene, azobenzene, and anthracene, but the

Fmoc group is overwhelmingly the most common.[3,6,13–16] Furthermore, peptide and aromatic components have been altered with various ring substituents, where the augmented electronic, hydrophobic, and steric properties of the ring system can have an impact upon the precise aromatic stacking interactions and resultant supramolecular properties.[4,17] In addition, the effect of the C-termini modifications has also been investigated, with the common carboxylic acid functionality substituted with methyl ester or amide groups, this change in the solubility and amphiphilicity has a dramatic effect on the self-assembly of these materials.[18] Hence, by making relatively minor alterations to the molecular structure of aromatic peptide amphiphiles it is possible to attain a variety of nanoscale morphologies including: fibres, tubes, sheets, and spheres.[19–21,9] Furthermore, for a subset of gelators it has been possible to correlate the gelation pH with calculated log P values.[4,7,22,23] Thus, it is clear that there is the potential for the development of design rules, which attempt to elucidate the relationship between molecular structure, supramolecular organisation, and the resultant physical properties of these hydrogel materials.

In terms of the molecular structure, altering the peptide gives access to all of the diverse chemical functionality associated with amino acids,[12] either to simply tailor the hydrophobicity of the amphiphile, or to introduce more specific interactions, between for example charged or H-bonding residues. At the N-terminus a variety of aromatic moieties have been studied: such as phenyl, naphthalene, pyrene, azobenzene, and anthracene, but the Fmoc group is overwhelmingly the most common.[3,6,13–16] Furthermore, peptide and aromatic components have been altered with various ring substituents, where the augmented electronic, hydrophobic, and steric properties of the ring system can have an impact upon the precise aromatic stacking interactions and resultant supramolecular properties.[4,17] In addition, the effect of the C-termini modifications has also been investigated, with the common carboxylic acid functionality substituted with methyl ester or amide groups, this change in the solubility and amphiphilicity has a dramatic effect on the self-assembly of these materials.[18] Hence, by making relatively minor alterations to the molecular structure of aromatic peptide amphiphiles it is possible to attain a variety of nanoscale morphologies including: fibres, tubes, sheets, and spheres.[19–21,9] Furthermore, for a subset of gelators it has been possible to correlate the gelation pH with calculated log P values.[4,7,22,23] Thus, it is clear that there is the potential for the development of design rules, which attempt to elucidate the relationship between molecular structure, supramolecular organisation, and the resultant physical properties of these hydrogel materials.

To this end, we have identified the three distinct regions[24] within our gelator molecules (excluding the C-terminus which remained unfunctionalised in this study); the N-terminal

aromatic component, (di)peptide sequence, and the nature of the linker which combines the two. In the current chapter, we have varied these three parameters in a systematic fashion; but with particular emphasis on the linker,[3,25] the influence of which has been somewhat neglected in the past. It is believed that by using a consistent gelation protocol the kinetic effects of the initiation process can be largely discounted in this study, with the final pH being the main determinant of the hydrogel properties.[26] Hence, the focus of this study will be on the molecular considerations.

5.3 Results and discussion

To ascertain the molecular-supramolecular relationships within aromatic dipeptide amphiphile hydrogelators, the molecule was considered to consist of three separate entities (Fig. 5.1). Previous work has described the hydrogelation properties of Fmoc-LL (**F3LL**)[27] and Fmoc-YL (**F3YL**)[28] in some detail. Hence, LL and YL were chosen as model dipeptides in our study; broadly covering typical hydrophobic sequences, whilst tyrosine is also an aromatic residue believed to have a role in stabilising β-sheet fibrils.[29] In addition, we sought to alter the aromatic component, utilising several functionalities such as: fluorene, naphthalene, and pyrene, which provides continuity with our previous work and also addresses the impact of additional aromaticity. However, our focus was to investigate the role of the linker section by replacing the methoxycarbonyl (carbamate) with alternative amide linkers of varying lengths. The methoxycarbonyl (**3**) linker has been shown to be an optimal choice for fluorenyl YL compounds; hence the ubiquity of the N-termini Fmoc group.[25] Extrapolating from this, we hypothesised that achieving the correct linker length and a rigidity/flexibility balance may be a more general parameter to consider for aromatic dipeptide amphiphile gelators.

5.3.1 Linker flexibility

The linker segments were ultimately derived from the popular methoxycarbonyl (**3** - specifically Fmoc) motif. From least to most flexible: the minimal carbonyl (**1**) linker segment; for methylcarbonyl (**2**) the methoxy oxygen has been removed, in ethylcarbonyl (**4**) the methoxy oxygen has been replaced with a methylene unit, and finally for methoxymethylcarbonyl (**5**) a methylene unit has been inserted between the methoxy oxygen and the carbonyl. In terms of the linker segments **1-5** (Fig. 5.1), self-assembly trends are believed to correlate with the flexibility or degrees of freedom associated with a particular motif.[25] Hence, as the linker length is increased additional orientations become available – which may or may not facilitate supramolecular organisation. However, as seen with

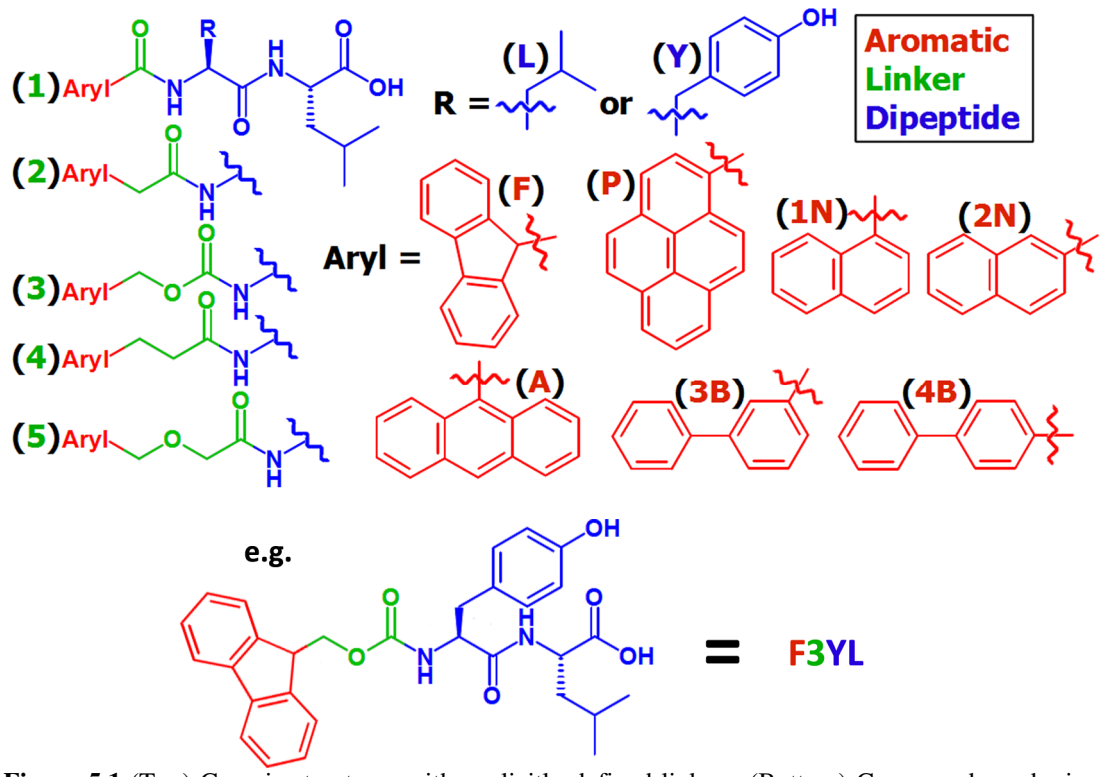

Figure 5.1 (Top) Generic structures with explicitly defined linkers. (Bottom) Compound numbering system example.

fluorenyl YL analogues,[25] the methoxycarbonyl (**3**) linker does not adhere to the apparently intuitive relationship that holds for the amide linkers. On the basis of linker length alone, one would expect the methoxycarbonyl (**3**) linker to be broadly equivalent to the ethylcarbonyl (**4**) linker, but this is not the case.

The key difference may be rationalised on the basis of a difference in the flexibility (entropy) associated with the carbamate moiety of **F3YL**, as the lone pairs on the methoxy oxygen, can potentially donate electron density to the adjacent carbonyl giving rise to a partial double bond (Fig. 5.2). Given the increased electronegativity of oxygen compared to nitrogen, this resonance form is not likely to be as significant as the analogous resonance structure that is well documented to restrict amide bond rotation.[30,31] In addition, the methoxy oxygen is a potential H-bond acceptor, which could also have implications for the relative assembly characteristics of these materials. Thus throughout this study the methoxycarbonyl (**3**) linker compounds should be considered separately from their amide equivalents, since the increased rigidity associated with the carbamate moiety likely precludes the elucidation of a simple relation between the two types of linkers.

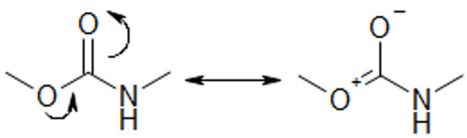

Figure 5.2 A resonance structure associated with the carbamate group.

5.3.2 Synthesis

For the most part, syntheses consist of repeated amide couplings and a C-termini deprotection strategy (see section 5.3.2.1). The most challenging synthetic aspect was the incorporation of a particular linker segment. Naturally, for the methoxycarbonyl linker (**3**) variants, Fmoc amino acids are commercially available, however, the corresponding Pmoc analogues had to be prepared (see section 5.3.2.2). Pyrenyl, naphthyl, and fluorenyl variants of the carboxylate and acetic acid precursors of the respective **1** and **2** linker compounds were commercially available. However, corresponding propanoic acid (**4**) and methoxyacetic acid (**5**) linker precursors had to be prepared using various methodologies (see section 5.3.2.3).

5.3.2.1 Amide couplings

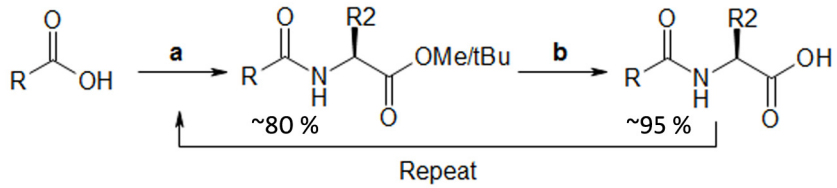

Scheme 5.1 (a) T3P, DIPEA, protected amino acid, DCM; (b) LiOH, THF/H_2O or TFA/DCM for methyl or tert butyl ester respectively.

Compounds were prepared via a solution phase synthetic scheme - similar to previously reported methods.[32,3,33–35] Amide couplings were followed by one of two deprotection strategies depending upon the lability of other functionalities (Scheme 5.1). In addition, the choice of amide coupling reagent was also important; as in our hands we often found the common HBTU[19] reagent unsatisfactory during the aryl linker coupling to the first amino acid. Presumably, these limitations arise from steric requirements around the aromatic moiety, and consequently T3P was selected as our coupling reagent of choice.

5.3.2.2 Pmoc

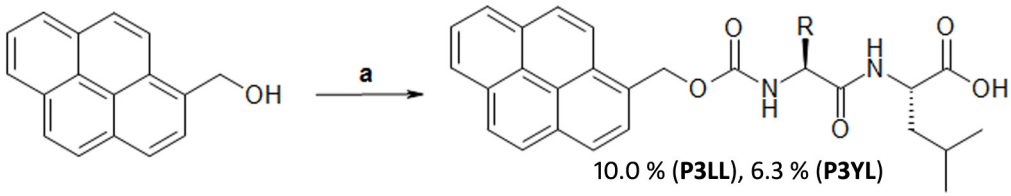

Scheme 5.2 (a) (i) 4-nitrophenyl chloroformate, DIPEA, THF; and (ii) dipeptide.

Due to the potentially photolytic[36] nature of the Pmoc (**P3LL** and **P3YL**)[37] functionality, a synthetic scheme was devised whereby the aromatic alcohol, carbamate linker, and dipeptide were combined in a one-pot synthesis (Scheme. 5.2). This reaction was poor yielding (e.g. 10%), possibly due to steric hindrance around the pyrene 4-nitrophenyl intermediate – the

presence of which was inferred by TLC before addition of the dipeptide. However, despite the poor yield, a sufficient quantity of material was obtained for study in each case.

5.3.2.3 Propanoic acid and methoxyacetic acid precursors

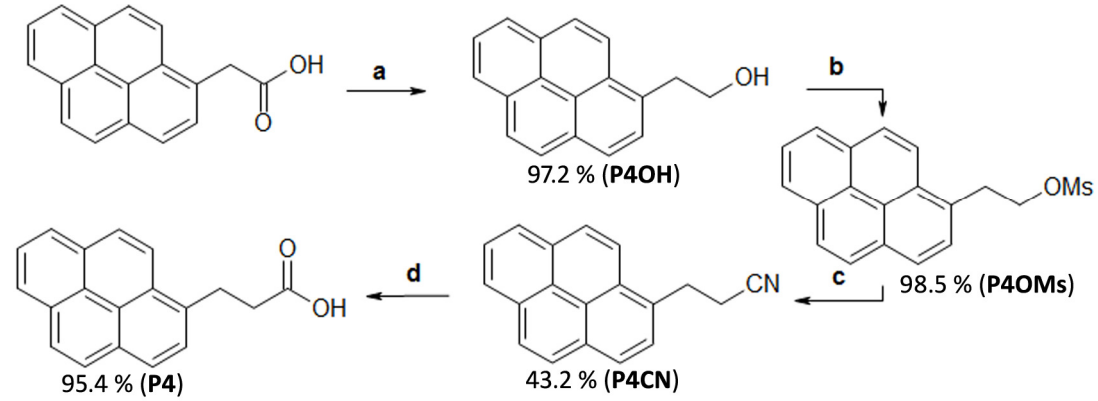

Scheme 5.3 (a) $LiAlH_4$, THF, 0 °C; (b) Mesyl chloride, triethylamine, DCM; (c) NaCN, DMSO, 80 °C; and (d) KOH aqueous reflux.

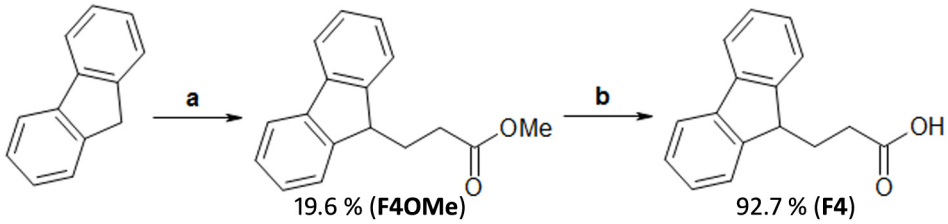

Scheme 5.4 (a) NaH, methyl 3-bromopropionate, DMSO, 0 °C; and (b) LiOH, THF/H_2O.

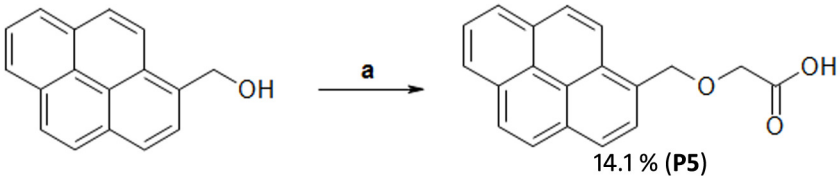

Scheme 5.5 (a) NaH, bromoacetic acid, THF, 0 °C.

Compounds containing the ethyl amide linker (**4**) had to be prepared via one of two routes (Scheme 5.3 or 5.4). 1-pyrenylpropanoic acid was prepared from the corresponding acetic acid, which was reduced to the alcohol, converted to a mesylate ester, which was displaced with cyanide, and finally hydrolysed to prepare the homologous carboxylic acid. Note that an equivalent synthetic methodology was also used to prepare corresponding naphthyl compounds. However, this route proved unsuitable for the fluorene analogue, due to the acidity and reactivity of the ArylCH proton position. Hence, 9-fluorenylpropanoic acid was synthesized from fluorene, which was deprotonated, giving 9-fluorenylpropanoate methyl ester via bromide displacement, subsequent methyl ester hydrolysis yielded the final product. This fluorene scheme was poor yielding (~15% over 2 steps) due to the competing formation of the di-substituted product.

Methoxyacetic acid linker (**5**) based compounds were similarly prepared via the

deprotonation of the corresponding alcohol (Scheme. 5.5). Note that an equivalent synthetic methodology was also used to prepare corresponding naphthyl compounds. However, this route proved unsuitable for the fluorenyl analogues; in this instance, an alternative route was not devised.

5.3.3 Preliminary gelation results

The hydrogelation of each system was attempted in 100 mM phosphate buffer under a range of pH conditions (see later, sections 5.3.4.1 and 5.3.5.1). A subset of the aromatic peptide amphiphiles formed stable hydrogels (Table. 5.1, black font) as determined by vial inversion. In line with expectations, the successful gelators included the previously studied **F3LL** (Fmoc-LL) and **F3YL** (Fmoc-YL) compounds,[28,27] in addition to a variety of pyrene and other fluorene based systems. In comparison, all naphthalene, bi-phenyl, and anthracene compounds that were tested precipitated.

Table 5.1 Preliminary gelation results

	Linker 1	Linker 2	Linker 3	Linker 4	Linker 5
9-Fluorenyl LL	**F1LL**	**F2LL**	**F3LL**	F4LL	-
9-Fluorenyl YL	**F1YL**	**F2YL**	**F3YL**	**F4YL**	-
1-Pyrenyl LL	P1LL	**P2LL**	**P3LL**	P4LL*	P5LL
1-Pyrenyl YL	**P1YL**	**P2YL**	**P3YL**	**P4YL**	P5YL*
1-Naphthalyl LL	1N1LL	1N2LL	-	1N4LL	1N5LL
1-Naphthalyl YL	-	1N2YL	-	1N4YL	-
2-Naphthalyl LL	-	2N2LL	-	2N4LL	2N5LL
2-Naphthalyl YL	-	2N2YL	-	2N4YL	-
9-Anthracenyl LL	A1LL	-	-	-	A5LL
3-Bi-phenyl LL	3B1LL	-	-	-	-
4-Bi-phenyl LL	4B1LL	-	-	-	-

NB – Stable hydrogel systems indicated by black font, those in grey failed to form stable hydrogels, whilst those with an asterisk displayed apparent self-assembly properties. Bold border indicates the linkers and aromatics which will be the focus of the remainder of this chapter.

In the case of bi-phenyl derivatives, the perpendicular arrangement of the aromatic rings may preclude stable aromatic stacking arrangements vital for supramolecular assembly. Although not covered extensively in this study, 9-anthracene has independently been found to fail to form hydrogels in the past,[16] we hypothesize that this may be a consequence of the steric hindrance associated with the 9-substituted ring. Furthermore, despite the fact that

naphthalene gelators, including naphthylmethylcarbonyl (**N2**) derivatives, have been reported previously,[13,34,38,39] other studies have shown a strong dependence upon the linker utilised, with the naphthoxymethylcarbonyl moiety found to be a more optimal choice on account of a more linear molecular conformation.[3]

Hence, while some of these aromatics are potentially of interest when used in conjunction with alternative linkers or peptide sequences, the remainder of this study will instead focus on fluorenyl and pyrenyl examples; these will be considered separately from one another for ease of interpretation.

5.3.4 Fluorenyl systems

5.3.4.1 Gelation results and rheological properties

To ascertain the quality of the stable gels, both the gelation pH and rheological results were considered. The gelation pH is an important indicator of the relative ease of gelation; with apparent pK_a values previously found to correlate with C log P values.[4,40] Hence, a relatively low minimum gelation pH associated with a given gelator implies either that fibre formation is less favourable, or that individual fibres fail to coalesce with one another on account of electrostatic repulsion. There is also literature evidence for the existence of worm like micellar aggregation (with COOH groups assumed to be deprotonated and solvent facing) at high pH values.[41] Meanwhile, rheological moduli provide a measure of the macroscale strength of the hydrogel network, in particular it is the ratio between the elastic (G') and viscous (G") moduli which defines a viscoelastic gel; where the elastic (solid) component must be greater than the viscous (liquid) component. In addition, the stable range of the frequency sweep indicates the point at which the gel network is unable to recover fast enough, and G' and G" values begin to deviate from the average values quoted for the linear region. It should be noted that the mechanical properties are difficult to compare between gelators with different quoted pH values – i.e. if a system is said to gel at pH 6.5 that implies it would be a solution at higher pH values.

Table 5.2 Fluorenyl systems: Gelation pH and rheological properties summary

System	pH[a]	G' / Pa	G'' / Pa	Stable Freq / Hz
F1YL	7.3 (gel)	20 ± 2	6.5 ± 1.5	0.1 – 4.0
F2YL	6.5 (gel)	230 ± 30	50 ± 10	0.1 – 4.0
F3YL	7.3 (gel)	390 ± 70	190 ± 20	0.1 – 5.0
F4YL	6.0 (gel)	320 ± 20	55 ± 9	0.1 – 5.0
F1LL	7.3 (gel)	460 ± 45	100 ± 20	0.1 – 12.6
F2LL	6.5 (gel)	840 ± 70	120 ± 40	0.1 – 7.9
F3LL	7.0 (gel)	110 ± 20	25 ± 10	0.1 – 10.0

[a]Gelation initially attempted at ~7.3 before reattempting at lower pH values if required.

With the exception of **F4LL**, all the fluorenyl compounds studied were found to form hydrogels at a 20 mM concentration in 100 mM phosphate buffer. However, the buffer pH required for gelation and the corresponding rheological properties of the gels differ considerably between systems (Table 5.2, and Appendices Figs. A.3-A.9).

For the YL based fluorenyl hydrogelators, the gelation trends with respect to the linker are clear. **F2YL** and **F4YL** form hydrogels at the relatively acidic pH 6.5 and pH 6.0 respectively. Whereas in comparison, **F1YL** and **F3YL** successfully formed hydrogels at pH 7.3 – which was the highest pH attempted in this study. Of the physiological pH hydrogels, **F3YL** was found to exhibit an elastic modulus of ~390 Pa, whereas **F1YL** was over an order of magnitude less rigid with an elastic modulus of ~20 Pa. **F2YL** and **F4YL** exhibited elastic moduli of ~230 Pa and ~320 Pa respectively, and in addition exhibited a larger elastic : viscous moduli ratio compared to gels **F1YL** and **F3YL**. However, these properties are difficult to directly compare due to differences in the required gelation pH – at pH 7.3 systems **F2YL** and **F4YL** were solutions. These initial gelation results indicate that the choice of linker does have a significant impact upon the properties of these materials. Interestingly on the basis of these results **F3YL** is the strongest gelator at physiological pH. The amide based linker analogues show a correlation between pH and linker length, with the shorter linkers being more optimal at high pH compared to longer equivalents. These trends lend some credence to the notion that **F3YL** behaves more like **F1YL** because the carbamate is a relatively rigid linker on account of resonance arguments.

The LL based fluorenyl systems appear to exhibit similar patterns with respect to the linker segment utilised. For example, the longest linker compound, **F4LL**, precipitated because it lacks the correct balance for effective aqueous self assembly; at least partly on account of an overly flexible linker. Similarly, **F2LL** requires a maximum hydrogelation pH of 6.5, compared to 7.3 and 7.0 for the respective **F1LL** and **F3LL** systems. Interestingly, for the dileucine examples, the minimal amide linker compound **F1LL** provides a more effective balance for gelation than the corresponding carbamate linker **F3LL** system – which is also reflected in a higher elastic modulus value (460 Pa versus 110 Pa). Hence, while the fluorenyl LL gelation results broadly mirror those of the corresponding YL systems, they also indicate that the optimal linker segment may switch between **1** and **3** depending upon the hydrophobic/-philic balance as a result of the precise dipeptide sequence under investigation.

In summary, as seen previously,[28,27] the Fmoc hydrogels form at physiological pH values. Overall **F3YL** (Fmoc-YL) gels at a higher pH value and is more rigid than the analogous **F3LL** (Fmoc-LL); here the less hydrophobic YL dipeptide sequence provides a more

effective balance for gelation; this result does not follow the trend expected based on C log P values.[4] In terms of the amide linkers (**1**, **2**, and **4**), there appears to be a clear correlation between the linker length, and the resultant properties of the hydrogels. For instance, the fluorene gelators appear to require an increasingly low gelation pH as the linker length is increased. There is also an influence from dipeptide sequence, where for example, the LL derivative **F1LL** exhibits a greatly increased stiffness compared with the corresponding YL based **F1YL**. However, the YL dipeptide motif accommodates a wider array of linkers. So overall, fluorene gelation is facilitated by shorter, or more rigid, amide linkers. However, the YL sequence is more capable of supporting the hydrogelation of the longer, less optimal, linker segments compared to the LL dipeptide motif.

5.3.4.2 Fluorescence emission spectroscopy

Fluorescence emission was utilised as a means of inferring the extent and orientations of aromatic stacking interactions within the supramolecular structures. The majority of the fluorene hydrogels show multiple peaks associated with excimer formation, indicating the presence of different orientations within the structure, from relatively disordered aromatic stacking interactions (Fig. 5.3).[42–44]

For the YL based fluorenyl hydrogels (Fig. 5.3(a)) the most significant excimer redshift – indicative of extensive aromatic stacking interactions[42,44] – is exhibited by **F3YL**, with an emission maximum around 450 nm. In comparison, **F2YL** and **F4YL**, show multiple excimer bands around 380 and 400 nm – suggestive of less efficient aromatic overlap, previously attributed to antiparallel and parallel dimers.[25,44] Similar bands are also observed for **F3YL**, but these are largely masked by the main 450 nm excimer peak. These prominent multiple peaks may be a consequence of these **2** and **4** linkers facilitating a multitude of stacking orientations – as opposed to a more consistent intermolecular arrangement. Interestingly, **F1YL** does not show any excimer formation, instead only the redshift relative to the dilute solution spectrum (330 nm versus 315 nm) is observed. Hence, an extended J-aggregate is not inferred for this material. This is thought to be a consequence of the **1** linker being too short to allow orientation of the fluorenyl groups for effective aromatic stacking interactions. Generally, aromatic stacking is believed to be dominated by extended antiparallel fluorenyl–fluorenyl interactions,[45] however, alternative less-aggregated fluorenyl arrangements and fluorenyl–tyrosine interactions are also likely to contribute to some extent. Overall, the amide linker trends are less clear, but evidently the Fmoc derivative **F3YL** is found to exhibit the most extensive aromatic stacking arrangement on account of a relatively long but sufficiently rigid linker segment that allows a more stable and consistent aromatic stacking arrangement.

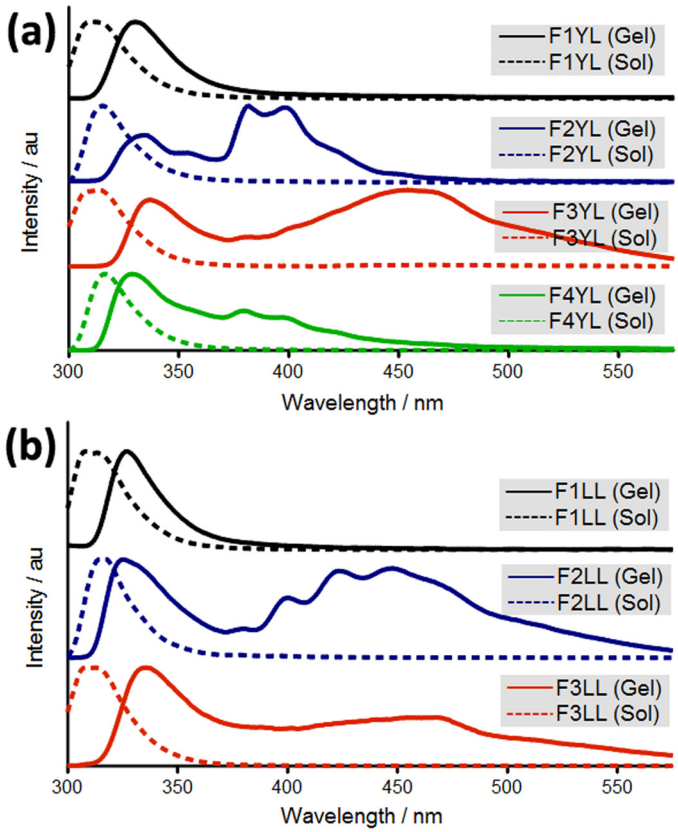

Figure 5.3 Fluorescence emission spectra of fluorenyl hydrogels and their corresponding dilute solutions: (a) tyrosine leucines; and (b) dileucines.

Some similar trends are also observed for the corresponding fluorenyl LL systems (Fig. 5.3(b)). As seen for **F1YL**, the minimal linker compound **F1LL** similarly does not exhibit significant excimer formation. This observation suggests that aromatic stacking interactions are also not prominent for this system, as the rigid **1** linker is thought to restrict the favourable molecular and supramolecular orientations of the fluorene moiety, resulting in relatively simple fluorescence spectra. Perhaps for these **1** linker examples, hydrophobic interactions in conjunction with β-sheet type H-bonding formation provides a sufficient basis for robust self assembly. In contrast; the **F2LL** and **F3LL** hydrogels each display a redshifted monomer emission that is accompanied by various excimer contributions - indicative of extensive aromatic stacking interactions. As seen for other systems, **F2LL** exhibits multiple contributions at 380, 400, and 425 nm, but unlike the corresponding **F2YL** gel, **F2LL** also shows a prominent 450 nm band. Hence, this difference supports the notion that intercalation of the tyrosine residues is responsible for some of the observed disruption to the interlocked fluorenyl-fluorenyl stacking arrangement.[45] Overall, the extent of fluorenyl stacking interactions and the degree of associated disorder seems to correlate strongly with the choice of linker, which likely influences the precise stacking arrangement(s) available to the gelator in question.

5.3.4.3 Circular dichroism

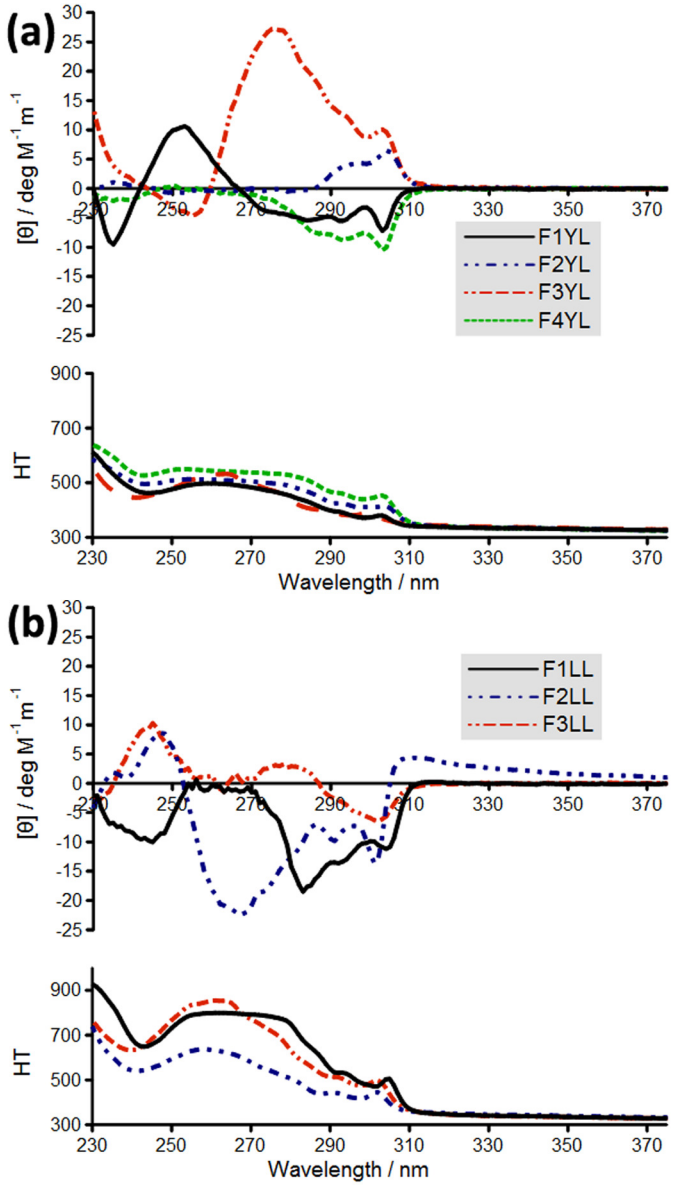

Figure 5.4 Circular dichroism and corresponding high tension voltage spectra of the various fluorenyl systems: (a) tyrosine leucines; and (b) dileucines.

CD was used to help ascertain the presence of chirality associated with the supramolecular fibres. At high pH (e.g. 10.5) values, where samples lacked any apparent self-assembly and gelation, samples were found to be CD silent. CD was performed on subgelation concentrations of the hydrogelators; this was found to be necessary to achieve homogeneity throughout the sample cell. In addition, this methodology attempts to minimize the influence of an excessive HT signal, potential linear dichroism, and any scattering effects. Due to excessive absorption and the relative weakness of the circular dichroism observed on a molar basis,[46,47] it was not possible to consistently record a CD spectrum covering the wavelength range relevant to the β-sheet organization.[15,48,49] Despite this limitation, it is possible to

observe the substantial induced chirality associated with the aromatic portion of the gelator molecules.[50] For the fluorenyl systems a peak at ~305 nm is typically observed, in addition to shorter wavelength signals which potentially have a contribution from the tyrosine residues of the YL gelators (Fig. 5.4).[28,51]

For the YL based fluorenyl systems (Fig. 5.4(a)), **F3YL** and **F4YL** exhibit a stronger molar ellipticity than the other systems in terms of the magnitude of the 305 nm absorption. In addition, **F3YL** also demonstrates substantial absorption bands at 275 nm, which may have some contribution from the tyrosine residue.[51] In terms of the direction associated with the amide based linkers, it is of note that the handedness of the 305 nm peak switches between positive and negative as methylene units are added. This indicates that the length of the alkyl chain is having a direct effect upon the fluorenyl conformation, and the precise supramolecular chirality adopted. **F3YL** appears to have a positive 305 nm peak similar to **F2YL**, which is interesting since both compounds possess a single methylene associated with their linker segments. These results again show the importance of the linker towards the self-assembly of these materials, and again suggest that **F3YL** adopts a relatively ordered supramolecular arrangement. Here, the linker length/flexibility may be influencing the precise stacking arrangement associated with these systems as additional methylene and/or oxygen units alter the relative orientation between the peptide and aromatic segments.[52]

All of the LL based fluorenyl systems (Fig. 5.4(b)) adopt a negative CD signal, in contrast to the fluorenyl YL gelators where the linker appeared to have an effect on the observed supramolecular handedness. Given that this linker dependence is not apparent for the fluorenyl LL gelators, we propose that it is the relative orientation between the fluorene and tyrosine fluorophores that influences the observed handedness.

In previous studies, handedness is seen to often be dependant not only of the structure of the gelator but also upon the precise hydrogelation initiation technique employed – such as enzymatic versus pH control.[28,11,53] Hence, we believe that a multitude of stacking arrangements and consequent supramolecular chiralities are possible. Ultimately the predominance of a particular structure is thought to be dependant upon both thermodynamic and kinetic factors. Molecular structure is a single consideration in a complex interplay of variables which will ultimately dictate the precise self-assembly arrangement adopted.

5.3.4.4 Infrared absorption spectroscopy

In general, the FTIR of the gels (in D_2O) demonstrates the coupling of well aligned H-bonded amide I modes at ~1625 cm^{-1}.[54,40,55] However, the precise frequency and relative intensity varies considerably between the gelators (Fig. 5.5) . With some examples exhibiting multiple overlapping peaks, which is indicative of inhomogeneity arising from a variety of

H-bonding stack sizes. In addition, the most apparent linker-dependent observation is the presence of the higher wavenumber band at ~1685 cm^{-1}, which corresponds with the carbamate moiety of **3** analogues.[55] The amide I and carbamate peaks are both indicative of the enhancement of these vibrational modes within an ordered β-sheet type H-bonding arrangement.[56,54,32,2,28,11]

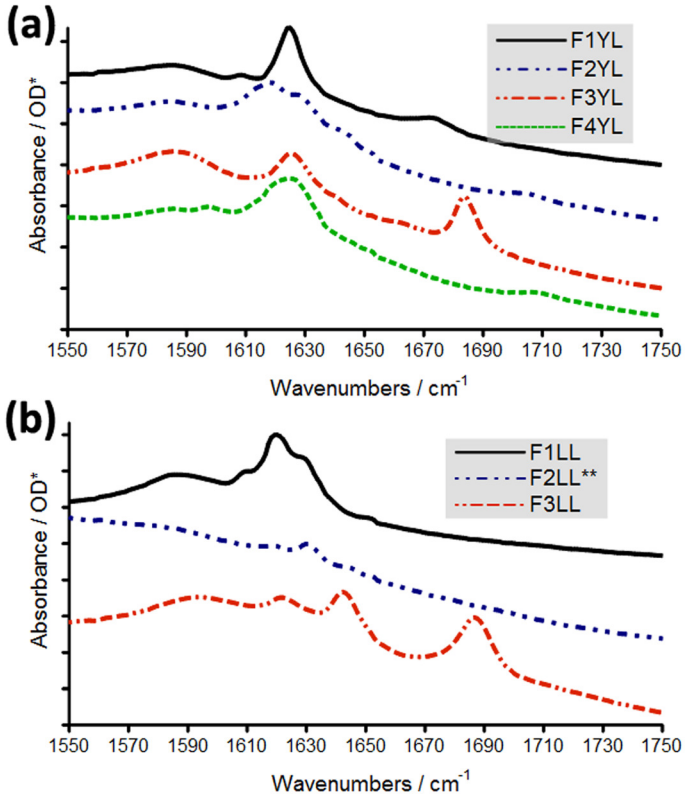

Figure 5.5 Amide I region of the infrared spectra for fluorenyl gelators: (a) tyrosine leucines; and (b) dileucines. *Optical density has been shifted for clarity, each division corresponds to 0.1 units. **Viscous solution in D_2O.

Infrared absorption spectroscopy (Fig. 5.5(a)) of the YL based fluorenyl gels (in D_2O) in each case shows the amide I band around 1625 cm^{-1}, associated with the increase in peak intensity due to the coupling of well-aligned H-bonded amide modes.[55,54,40] However, the degree of apparent inhomogeneity associated with these materials varies considerably. While **F3YL** and **F1YL** in particular exhibit relatively sharp well defined peaks, **F2YL** and **F4YL** demonstrate broader overlapping bands, suggestive of a variety of H-bonding stack sizes.[57,58] These observations appear to qualitatively correlate with the required gelation pH in each case, suggesting more disorder associated with the lower pH hydrogels. In addition, it should be noted that **F3YL** shows an additional band at 1685 cm^{-1} that is associated with the peak intensity enhancement of the aligned vibrational modes belonging to the carbamate moiety.[55] As such this additional band is not believed to infer a distinct H-bonding arrangement associated with this material. Hence, the relation between linker length and H-bonding

inhomogeneity correlates well with the fluorenyl YL based gelators being dependent upon a shorter or more rigid linker segment.

However, the linker trends observed for the YL variants do not appear to hold for the corresponding fluorenyl LL systems (Fig. 5.5(b)). In contrast to **F3YL**, **F3LL** displays a more dominant peak at 1645 cm^{-1}, which corresponds with a more disordered arrangement associated with the amide groups.[58] The corresponding amide linker based gelators also show substantial disorder in their FTIR spectra. For instance, **F1LL** exhibits a variety of overlapping amide I bands from 1610-1630 cm^{-1}, indicative of substantial inhomogeneity. In addition, **F2LL** displays various weak amide I peaks, however this result may be related to the fact that this system only yielded a viscous solution when using deuterated water. Regardless, the LL sequence appears to consistently result in increased disorder associated with the H-bonding arrangements of these fluorenyl systems. This is proposed to be a consequence of the tyrosine residue playing a role in better defining the preferred orientation of the amino acid side chains within the interlocked β-sheet type arrangement,[45,19] whereas the more uniform LL sequence is less likely to consistently adopt a given side chain arrangement (based solely on being either the first or second leucine residue).

5.3.4.5 Atomic force microscopy

AFM images (Fig. 5.6) show the presence of nanoscale fibres within the hydrogel matrix of all the gelators studied. The fibres or bundles of fibres observed in these systems vary in size, but are typically about 40-200 nm in width, a result which is broadly consistent with nanofibre dimensions seen in similar materials.[59,28,60]

Significant differences were observed between the YL based fluorenyl systems, with **F2YL** showing very few fibres by AFM compared to the corresponding **F3YL** and **F4YL** samples. **F3YL** and **F4YL** each demonstrate dense fibrous assemblies composed from a multitude of overlapping individual fibres. This suggests a high propensity for fibre formation in these systems. However, these morphologies are not all homogeneous, for instance, **F4YL** shows substantial variability in the fibre diameters (e.g. ~80-250 nm) with the larger examples appearing helical; this is likely due to the further aggregation of elementary fibres via coiling mechanisms. In addition, no fibres were seen to be present in the corresponding **F1YL** system, which instead exhibited a more amorphous structure featuring lumpy spherical aggregates. Given the inflexibility of the **1** linker, it is likely that there is substantial disorder associated with fluorene stacking. It is possible that **F1YL** adopts a hydrogel network which is interlaced with a high proportion of micellar type aggregates. Hence, although fibres are the dominant, almost ubiquitous morphology, there appears to be the potential for a variety of other aggregation mechanisms throughout the

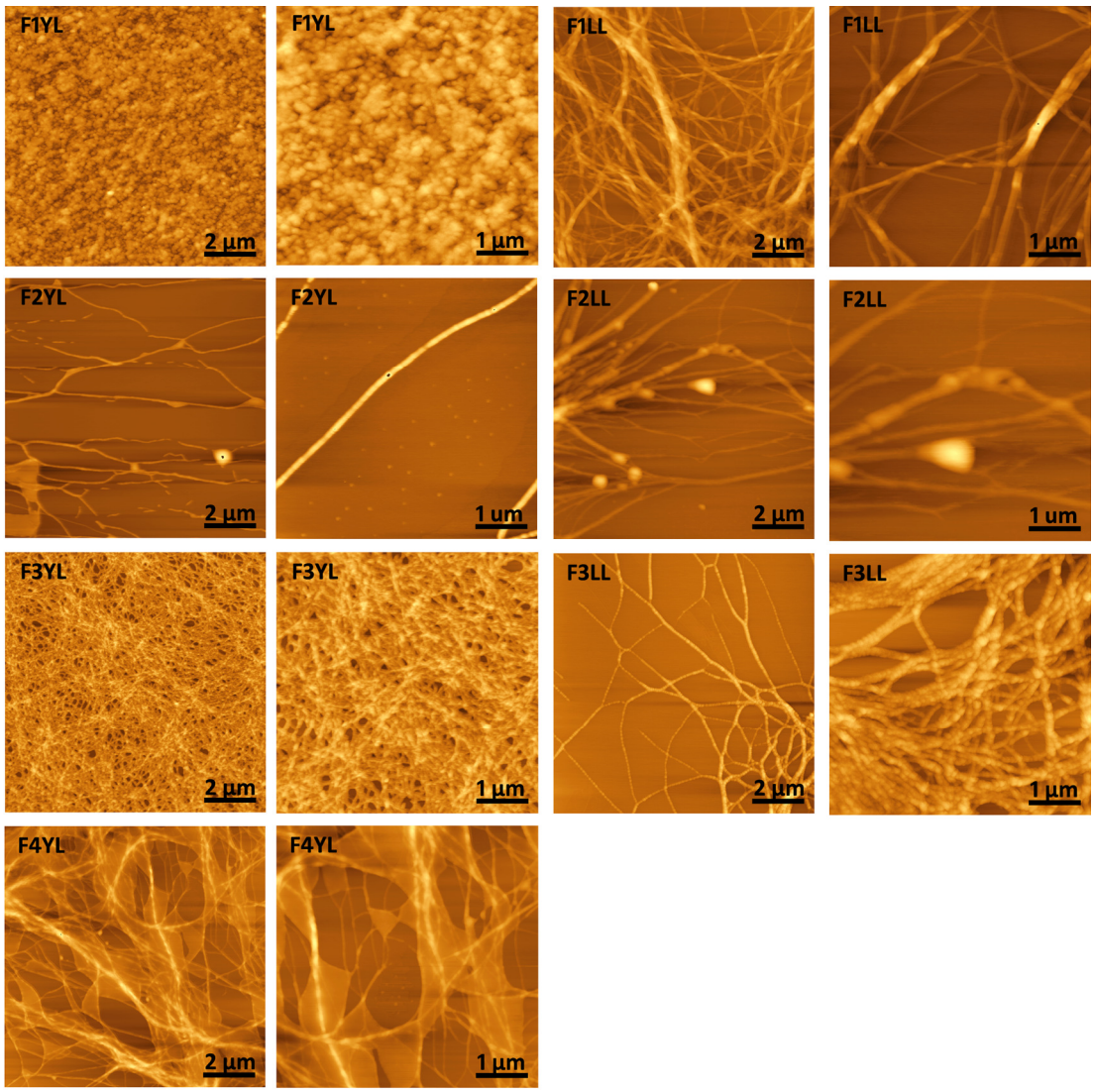

Figure 5.6 AFM images of all fluorenyl systems with 2 and 1 µm scale bars.

supramolecular constructs. This again reflects the structural inhomogeneity previously inferred by FTIR and fluorescence.

In terms of the fluorenyl LL examples, AFM similarly shows substantial variability between systems with different linkers. For instance, **F1LL** exhibits the greatest propensity for fibre formation, and also appears to show elementary fibres interweaving with one another and combining to form larger fibrous structures. Furthermore, **F2LL** and **F3LL** also show the presence of fibres – though those of **F2LL** appear to be more discontinuous and less prevalent than many of the others systems described here. Overall, the AFM results should be interpreted with caution, as they are highly dependent upon the dried sample preparation, and as such are not necessarily representative of the fibrous morphologies present in the gel state. Nevertheless, under the dried sample preparation conditions utilised, the choice of linker appears to have a substantial effect on the overall fibrous morphology,

although a correlation with the corresponding spectroscopic results is unclear.

5.3.4.6 Summary

High pH/physiological gelation of fluorenyl based systems is facilitated by short and/or rigid linkers such as carbonyl (**1**) and methoxycarbonyl (**3**). Comparing the spectroscopic results, it becomes clear that the implied extent of aromatic stacking interactions does not always correlate with the extent of H-bonding seen by FTIR. For instance, **F1YL** shows a strong well-defined amide I peak, but little excimer formation by fluorescence emission. Whereas other systems such as **F2LL** and **F3LL** shows an extensive excimer band, but only a relatively weak or disordered amide I contribution by FTIR – indicative of substantial H-bonding inhomogeneity. In contrast, **F2YL** and **F4YL** exhibit moderate excimer redshifts and broad amide I contributions with a fair degree of disorder. Only in examples that possess optimal peptide and linker segments, such as **F3YL**,[25] do both processes appear to manifest strongly within the same system. Hence, these results indicate that only with certain linker dependant molecular orientations are aromatic peptide amphiphiles able to adopt a robust aromatic stacking and H-bonding arrangement – this is perhaps linked to the respective distances required for β-sheets (~4.5 A) and aromatic stacking (~3.5 Å).[45] Overall, we also find that that when a compromise must be made the YL derivatives are more prone disruption of fluorenyl-fluorenyl aromatic stacking interactions (Fig. 5.3), whilst in contrast the LL derivatives have more disordered H-bonding interactions (Fig. 5.5). These trends are attributed to tyrosine residue intercalation and a more random side chain orientation, for YL and LL fluorenyl systems, respectively.

5.3.5 Pyrenyl systems

5.3.5.1 Gelation results and rheological properties

Similar to the fluorenyl materials, the self-assembly and gelation properties of the pyrenyl based systems were initially assessed by gelation pH and rheology if applicable (Table 5.3, and Appendices Figs. A.10-A.15).

In terms of the hydrogelation properties of the pyrenyl YL based compounds, there are several points to note. For instance, **P5YL** forms a particulate gel as opposed to a single continuous phase (Fig. 5.7). This is presumed to be a consequence of the ether (**5**) linkage allowing excessive degrees of freedom, such that the molecules are unable to adopt a consistent stacking arrangement. The additional (or shifted) H-bonding acceptor may also be a factor in perturbing the stacking arrangement of this system. In contrast, the other compounds all form stable homogeneous hydrogels. For example, the **P1YL** and **P2YL** systems each exhibit a gelation pH of 7.0 and similar rheological properties to one another.

However, the optimal hydrogelator in terms of the maximum required gelation pH is the **P4YL** system, which possesses a relatively flexible linker. In direct contrast, the carbamate linker based compound, **P3YL**, exhibits a relatively acidic required gelation pH of 5.5; indicating that for pyrenyl based materials sufficient flexibility is important. Hence, these results suggest that for pyrenyl based hydrogel systems, longer or more flexible linkers are preferable - although generally there is less variation than that observed for the equivalent fluorenyl based materials.

Table 5.3 Pyrenyl systems: Gelation pH and rheological properties summary

System	pH[a]	G' / Pa	G'' / Pa	Stable Freq / Hz
P1YL	7.0 (gel)	290 ± 50	60 ± 20	0.1 – 12.6
P2YL	7.0 (gel)	310 ± 35	35 ± 5	0.1 – 5.0
P3YL	5.5 (gel)	300 ± 35	40 ± 3.5	0.1 – 12.6
P4YL	7.3 (gel)	190 ± 30	45 ± 20	0.1 – 15.8
P5YL	7.0 (parts)[c]	-	-	-
P2LL	7.3 (gel)	60 ± 7	10 ± 2	0.1 – 3.2
P3LL	6.5 (gel)	8 ± 1	1.5 ± 0.5	0.1 – 3.2
P4LL	7.3 (meta)[b]	-	-	-

[a]Gelation initially attempted at ~7.3 before reattempting at lower pH values if required. [b]Metastable collapsing hydrogel. [c]Particulate gel solution.

For the pyrenyl systems, the hydrophobic LL sequence is detrimental to the gelation and self-assembly properties. For instance, the most rigid and most flexible **P1LL** and **P5LL** systems both precipitated, indicating that there is little linker length/flexibility tolerance. In addition, **P4LL** forms a hydrogel initially, but over the course of 7 hours proceeds to collapse to form a small fragile pellet that retains the shape of the container (Fig. 5.8, and supplementary video). The metastable[61] **P4LL** is thought to be a consequence of the LL dipeptide causing hydrophobic collapse of the supramolecular structure, resulting in the expulsion of water. Although syneresis of aromatic peptide amphiphile hydrogels has been reported previously,[7] to our knowledge this is the most extreme example of this process. Hydrophobicity is clearly a factor in the precipitation or collapse of the LL based pyrenyl systems, however, these phenomena are also evidently dependant on the linker in question - given that the related **P2LL** and **P3LL** systems do form stable gels. Similar to the YL systems, the carbamate linker system **P3LL** only gels at a relatively acidic pH of 6.5, and exhibits an elastic modulus of just 8 Pa. In comparison, the **P2LL** hydrogelator is a more optimal choice in terms of linker, with a physiological gelation pH of 7.3, and an elastic modulus of 60 Pa – though this is still a fairly weak gel compared to many of the pyrenyl YL systems. Hence, the pyrenyl LL gelation trends with respect to the choice of linker are less clear, as the hydrophobicity of these compounds limits our ability to discriminate between

different linkers. However, as for the pyrenyl YL materials, a physiological gelation pH is facilitated by amide (e.g. **2** and **4**(metastable)) as opposed to carbamate (**3**) linkers.

In summary, carbamate linker pyrene compounds, **P3LL** and **P3YL**, only gel at a relatively acidic pH, with **P3LL** demonstrating an elastic modulus over an order of magnitude less than the more robust hydrogels. Pyrene may have more specific aromatic stacking requirements, on account of its increased planarity and steric bulk compared to fluorene. The corresponding amide linker pyrene amphiphiles exhibit a distinct relationship with respect to gelation properties and amide linker length. For pyrene, physiological gelation is favoured by longer linker lengths, with the necessary gelation pH generally observed to decrease slightly as the linker length decreases (e.g. from **P4YL** to **P2YL**). This apparent preference for more flexible linkers is in direct contrast to fluorenyl examples, however, there is generally less variation in the physical properties observed for the pyrenyl systems with regards to linker dependence. In this respect, hydrophobicity has a significant role for the pyrenyl systems, with the hydrophobic LL sequence clearly not conducive to effective gelation with only a single stable pyrene amide linker example.

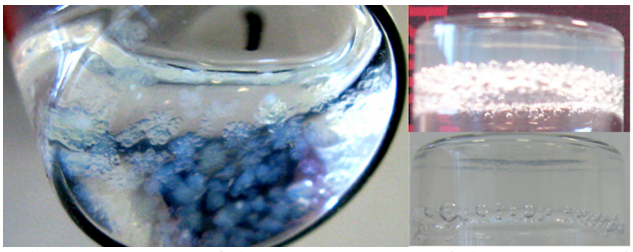

Figure 5.7 (left) Particulate appearance of the **P5YL** system; (right) representative hydrogel examples (top) **P4YL**, (bottom) **F4YL**. Similar in appearance to other hydrogel systems.

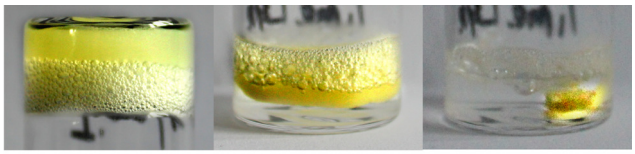

Figure 5.8 Collapse of the metastable **P4LL** hydrogel over time. Contrast adjusted for clarity.

5.3.5.2 Fluorescence emission spectroscopy

Unsurprisingly, the pyrenyl gelators (Fig. 5.9) display a more extensive excimer redshift than the corresponding fluorenyl systems (Fig. 5.3), which is characteristic of the presence of extensive aromatic stacking interactions within the supramolecular aggregates. In addition, the pyrene based materials generally exhibit complete quenching of their characteristic monomer emission.[62,63] This suggests that as would be expected in moving from fluorene to pyrene; gelation is increasingly dominated by the aromatic interactions.

For YL based pyrenyl gels, **P1YL** and **P2YL** demonstrate the least pronounced redshift in their excimer emission, with fluorescence intensity concentrated around 418 nm (Fig.

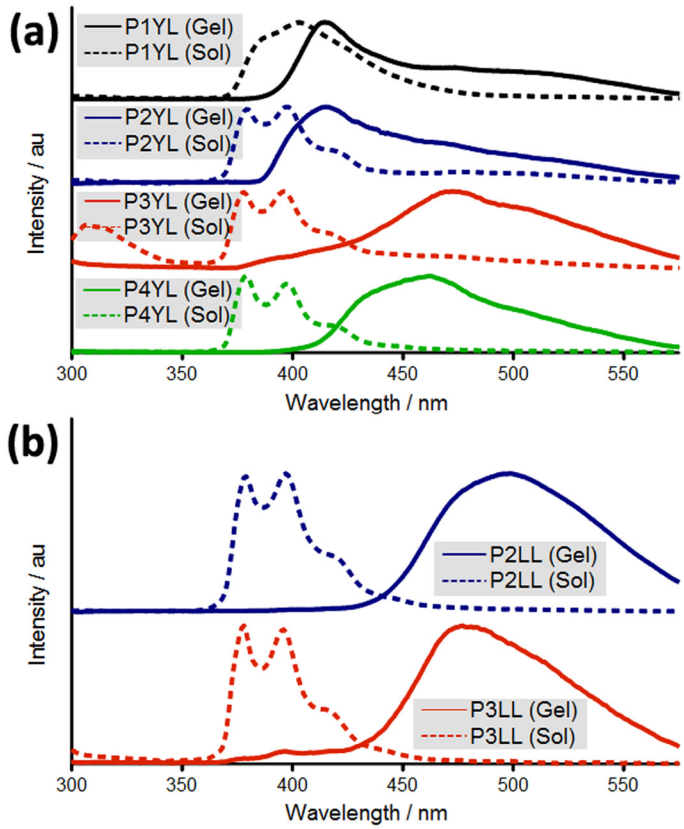

Figure 5.9 Fluorescence emission spectra of pyrenyl hydrogels and their corresponding dilute solutions: (a) tyrosine leucines; and (b) dileucines.

5.9(a)). This 418 nm peak corresponds with the shoulder seen in the dilute pyrene solution spectra,[64,65] suggesting less aromatic stacking interactions due to a lack of linker flexibility. This is a similar result to that seen previously for the **1** linker fluorenes (section 5.3.4.2). In addition, the **P1YL** solution spectrum is red-shifted with respect to the other pyrenyl solution spectra, and exhibits poorly defined peaks. This may also be a consequence of the inflexibility associated with this molecule, possibly resulting in an intramolecular interaction with the adjacent tyrosine residue, or alternatively conjugation with the carbonyl group may be a factor. In the **P2YL** hydrogel, the conformational restrictions arising from a short linker may also result in increased disorder associated with the aromatic stacking interactions, with the tyrosine residues possibly interacting with pyrene in an intermolecular fashion.[45] In contrast, the **P3YL** and **P4YL** systems consistently show a pronounced broad excimer redshift upon hydrogel formation. We also observe complete quenching of the characteristic dilute solution spectra peaks; this suggests extensive aromatic stacking interactions throughout their respective supramolecular networks. Hence, for the pyrene YL gelators, sufficient linker length appears to be the main factor in determining whether pronounced excimer formation will be observed.

In contrast to what is observed for pyrene YL systems, both **P2LL** and **P3LL** demonstrate

a pronounced broad excimer redshift upon hydrogel formation (Fig. 5.9(b)). The **P2LL** and **P3LL** systems exhibit maxima at around 490 and 475 nm, whereas the related **P2YL**, **P3YL**, and **P4YL** hydrogels exhibit their main peaks at 418, 475 and 460 nm respectively. This provides additional evidence that it is the intercalation of the tyrosine residues that contributes to the disruption of pyrene-pyrene stacking interactions, here, longer linkers appear to mitigate this effect to some extent. Hence, for the pyrenyl based materials, the fluorescence emission of the LL derivatives are not influenced by the linker segment to the same extent as the equivalent YL systems.

5.3.5.3 Circular dichroism

Pyrene generally shows well defined peaks at ~330 and ~350 nm. However, these peaks change in wavelength, intensity, and handedness depending upon the linker and peptide components (Fig. 5.10). The observed circular dichroism associated with the pyrene moiety is consistently stronger on a molar basis than that seen previously for fluorene (Fig. 5.4) - this general observation may indicate that pyrene stacking is more specific and less disordered.

There is considerable variation in the circular dichroism observed for the YL based pyrenyl systems (Fig. 5.10(a)). **P1YL** displays a strong positive CD signal, which is also significantly blue shifted relative to the other systems. However, this observation undoubtedly ties in with the previously discussed fluorescence emission of both gel and solution, which also demonstrated unusual characteristics. Again this can be ascribed to the rigidity of this particular molecule's linker segment, which could certainly have implications for aromatic stacking interactions and supramolecular chirality - potentially via intercalation of the tyrosine residues. On the other hand, **P3YL** shows relatively weak circular dichroism - a result which is presumably a consequence of the rigidity associated with the methoxycarbonyl (**3**) linker inhibiting the supramolecular chiral organisation of peptide and aromatic. In contrast, **P2YL** and **P4YL** adopt similar CD profiles in terms of possessing a negative signal and moderate intensity. This indicates that these materials assume analogous supramolecular structures whose organisation is facilitated by the longer amide linkers.

For the LL based pyrenyl systems (Fig. 5.10(b)), **P2LL** demonstrates a relatively weak circular dichroism signal in the pyrene region. In contrast, **P3LL** demonstrates a strong positive CD signal; a complete reversal of the previously described chirality of **P2YL** and **P4YL**. Although it is not immediately obvious why **P2LL** and **P3LL** should exhibit characteristics that do not reflect those of their YL equivalents (**P2YL** and **P3YL**), there is a possible role for tyrosine intercalation in determining the overall supramolecular chirality.[45] Overall, the linker and peptide segments both contribute towards the observed

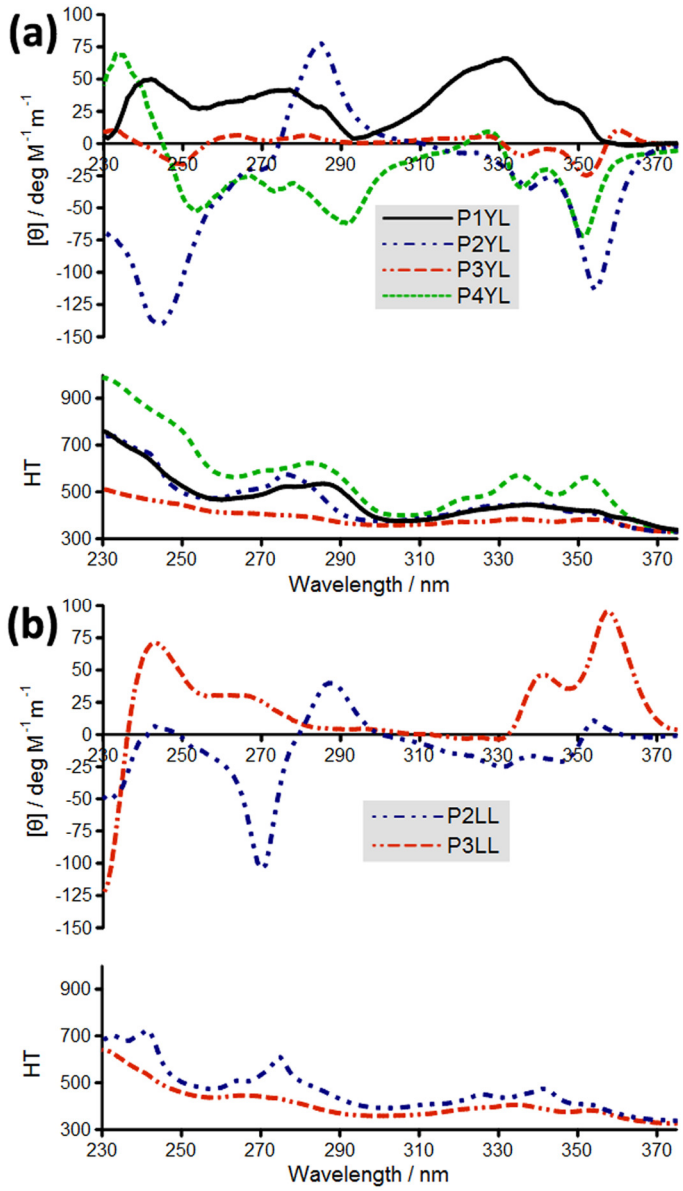

Figure 5.10 Circular dichroism and corresponding high tension voltage spectra of the various pyrenyl systems: (a) tyrosine leucines; and (b) dileucines.

supramolecular chirality of these pyrenyl based gelators. Given that the supramolecular helicity ultimately originates from the molecular chirality of the peptide component, it is perhaps unsurprising that the trends seen for the LL and YL gelators do not necessarily correlate with one another.

5.3.5.4 Infrared absorption spectroscopy

Several trends are apparent with respect to the FTIR spectra of YL based pyrenyl gels in D_2O (Fig. 5.11(a)). For example, **P3YL**, exhibits a relatively high wavenumber amide I band at 1645 cm^{-1}. The apparent disorder associated with **P3YL**, is related to the rigidity of the methoxycarbonyl linker, restricting self-assembly in the peptide domain. However, the

additional oxygen atom may also provide potential H-bonding stacking arrangements that perturb the overall supramolecular structure. In comparison, the amide linker based gelators **P1YL**, **P2YL**, and **P4YL** all show amide I bands in the ~1620 cm^{-1} region, typically associated with an extended β-sheet type H-bonding arrangement. Varying degrees of inhomogeneity are observed for these systems, with the majority exhibiting some higher wavenumber contributions. The **P1YL** peak is somewhat less broad than the other systems, suggesting a more ordered H-bonding arrangement. In this case, the short rigid conjugated carbonyl (**1**) linker that precludes optimal aromatic stacking, benefits assembly of the peptide segment. Hence, these results indicate that for the pyrenyl systems, short or more rigid linkers preclude optimal assembly for both the aromatic and peptide domains.

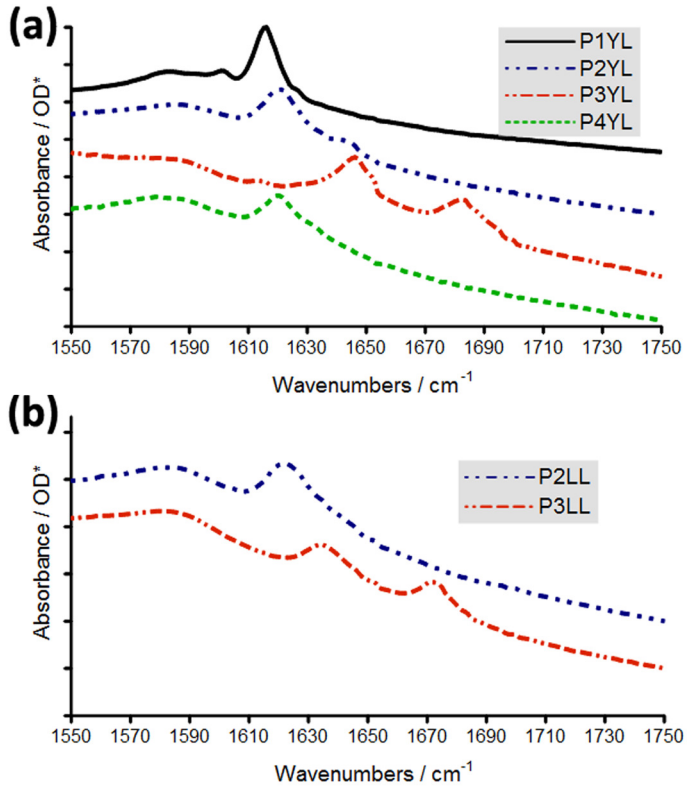

Figure 5.11 Amide I region of the infrared spectra for pyrenyl gelators: (a) tyrosine leucines; and (b) dileucines. *Optical density has been shifted for clarity, each division corresponds to 0.1 units. **Viscous solution in D_2O.

For the pyrenyl LL systems (Fig. 5.11(b)), similar to **P3YL**, **P3LL** is observed to demonstrate a relatively high wavenumber amide I band at 1635 cm^{-1}. In addition, what is assumed to be the carbamate peak of **P3LL** appears at ~1675 cm^{-1}, which is approximately 10 cm^{-1} lower than that exhibited by the other **3** analogues. This apparent shift is another indication that the precise H-bonding arrangement around the carbamate moiety can be different for these pyrene based systems. In contrast, the **P2LL** system exhibits a band at ~1620 cm^{-1} similar to that observed for the corresponding **P2YL** gel. Overall, it can be

surmised that for both LL and YL pyrenyl gels, the carbamate linker results in substantial disorder associated with the H-bonding arrangement, with (longer) amide linkers providing a more effective balance for self-assembly.

5.3.5.5 Atomic force microscopy

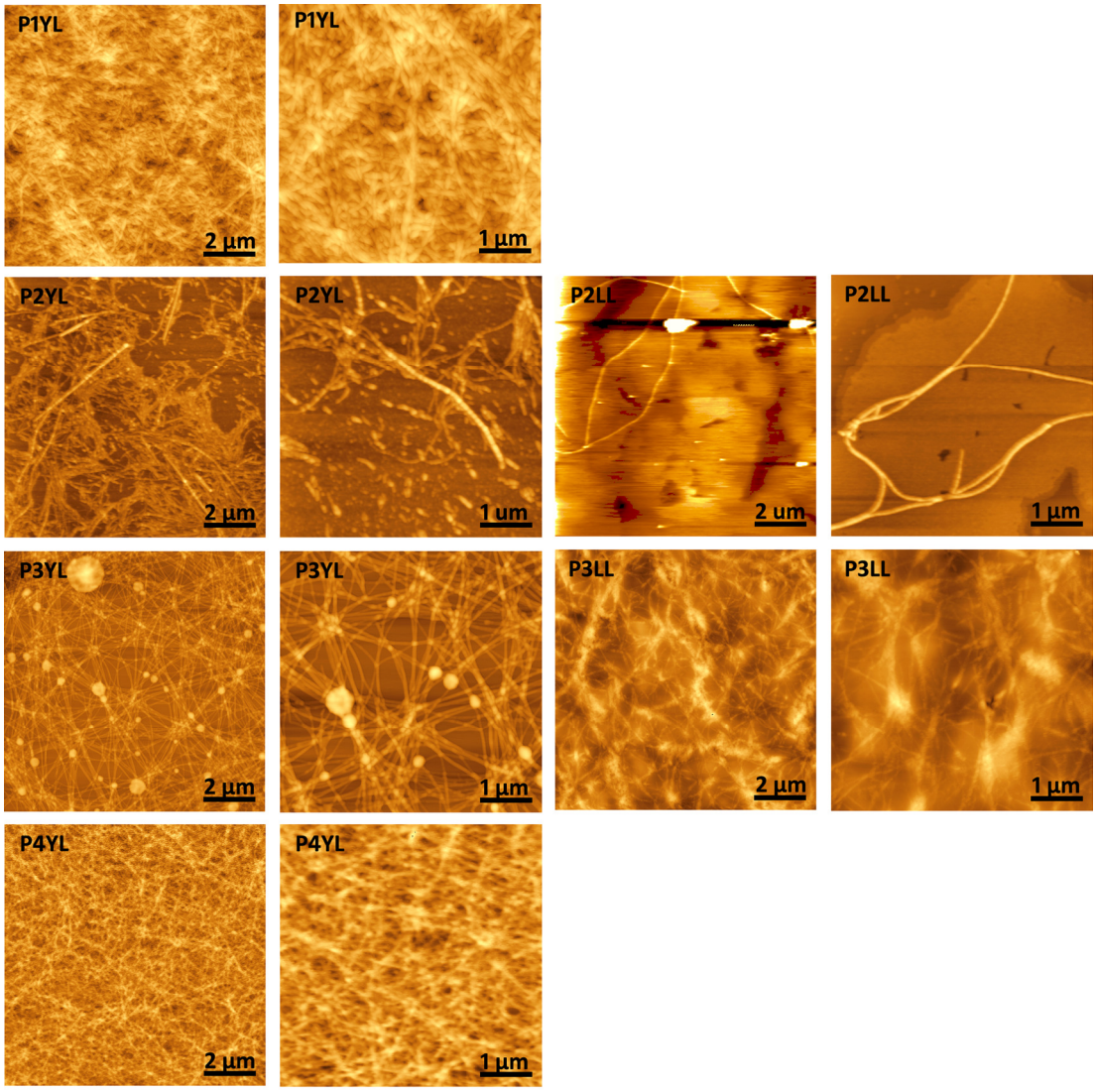

Figure 5.12 AFM images of all pyrenyl systems with 2 and 1 µm scale bars.

P1YL, **P3YL** and **P4YL** all demonstrate dense fibrous assemblies composed from a multitude of overlapping individual fibres by AFM. This suggests a high propensity for fibre formation in these systems. However, these morphologies are not all homogeneous across the sample, as **P3YL** exhibits spherical structures that intersect the overlapping fibres, which could indicate the presence of crystallinity associated with this system. In addition, **P2YL** also exhibits fibres – though they appear to be relatively short and less prevalent than the others YL systems described here. Hence, as seen for the fluorenyl materials, substantial differences are observed between these pyrenyl YL systems, though rationalising these

differences is difficult.

The morphology of pyrenyl LL materials is also affected by the choice of linker segment. With **P2LL** demonstrating the presence of isolated fibres, while **P3LL** appears to exhibit a dense fibrous assembly composed from a multitude of overlapping individual fibres – though the resolution of these images is poor. As stated before, AFM is of limited diagnostic value as the preparation of these dried sample films is subject to features not found in the gel state materials. Nonetheless, the morphology of the network appears to have substantial variability, depending upon the hydrogel system studied.

5.3.5.6 Summary

In contrast to the fluorenyl systems, pyrenyl based materials appear to display a preference for relatively flexible linkers. We can hypothesise that the additional flexibility provided by the CH position on fluorene, provides a more effective means of achieving a conformation which is conducive to self assembly with short or more rigid linker like carbonyl (**1**) or methoxycarbonyl (**3**). For example, the rigid **P1YL** system shows strong/sharp amide I modes and a pronounced, if distorted, positive CD signal. This is indicative of an extensive H-bonding arrangement and chiral supramolecular organisation. Despite this, the rigid linker is apparently not conducive to extensive aromatic stacking interactions. In comparison, the rigid, but longer, **P3LL** and **P3YL** examples exhibit extensive aromatic stacking interactions by fluorescence emission spectroscopy. However, for **P3LL** we observe a distinct H-bonding arrangement associated with carbamate group of this material by FTIR. In addition, **P3YL** exhibits an inferred random coil type H-bonding structures by FTIR; with this lack of order associated with the peptide also reflected in the much weaker circular dichroism. Hence, while for **P1YL** it is aromatic stacking interactions that suffer; for **P3LL** and **P3YL**, it is the β-sheet type H-bonding formation that fails to effectively reconcile with the aromatic stacked arrangement. In each case, this is likely a consequence of insufficient linker flexibility acting to disfavour the optimal orientations, intermolecular distances and consequent assembly in both the aromatic and peptidic domains. In contrast, the **P4YL** hydrogelator variant possesses a suitable balance of hydrophobics/-philics, aromatic stacking, and linker flexibility to also facilitate β-sheet type H-bonding formation, and resultant hydrogelation at a physiological pH. The self-assembly of aromatic peptide amphiphiles can thus be considered to have two main contributors; aromatic stacking and peptidic H-bonding interactions. In general terms, as anticipated, replacing fluorene with pyrene results in more extensive aromatic stacking interactions. In addition, the YL sequence appears to offer a better balance for H-bonding and gelation, with the LL sequence seen to be more prone to precipitation. However, the influence of these aspects cannot be considered in isolation, and

evidently the linker segment between these molecular domains is key.

5.4 Conclusions

In summary, we have reported on the effects of a systematic variation of the aromatic, linker, and dipeptide domains of this class of small molecule hydrogelators. Overall, results suggest the existence of an optimal but distinct linker flexibility trend for the respective fluorene and pyrene gelator classes – based on the peptide sequences tested here. The linker must not be too rigid to preclude the conformation required for simultaneous aromatic stacking and β-sheet type H-bonding formation. However, equally important is the need to avoid an excessive degree of freedom, particularly in hydrophobic examples where precipitation is an all too viable alternative to gelation. As proposed previously,[25] short (e.g. **1**) and/or relatively rigid (e.g. **3**) linkers, appear to facilitate the physiological pH gelation of the fluorenyl systems. In contrast, pyrene gelators exhibit a preference for longer, more flexible, amide linkers (e.g. **4**), with methoxycarbonyl (**3**) observed to be a particularly poor choice in terms of minimum gelation pH and/or mechanical properties. Presumably this difference is a consequence of pyrene's increased planarity and steric requirements, which mean that a more flexible linkage is required for effective orientation in both the dipeptide β-sheet type and aromatic stacked supramolecular self assembly domains. These differential linker preferences that depend upon the aromatic moiety, clearly demonstrate that the distinct structural features cannot be considered in isolation.

This is further exemplified as the YL hydrogelators consistently have a better balance for hydrogelation, with LL often unsuitable, particularly for pyrene based materials. This is evidenced nicely by the collapsing **P4LL**, which seems to be exhibiting a metastable hydrogel state, en route to a fragile pellet – an "unconventional" precipitation process. In contrast, the equivalent **P4YL** system forms a stable hydrogel under identical conditions. FTIR, fluorescence, and CD have respectively inferred the importance of β-sheet type H-bonding formation, aromatic stacking interactions, and supramolecular chirality in the self-assembly of these materials. These disparate aspects of the supramolecular structure are seen to be strongly influenced by the choice of linker, which indicates that this is a key variable in the self assembly process. This primarily appears to depend on the linker length/flexibility, which is thought to influence the available orientations and intermolecular distances of the peptide and aromatic assembly. However, the potential H-bonding accepting oxygen of the methoxy (**3**) moiety may also be a factor in influencing the overall stacking arrangement. The disorder associated with many of the studied systems is likely to be highly dependent upon the gelation protocol utilized as well as the molecular structure of gelator itself, as

ultimately rapid hydrogelation will result in kinetically favoured supramolecular structures, as opposed to the thermodynamic product. The increased contribution of aromatic stacking interactions towards the integrity of the supramolecular structures of pyrene based gelators, suggests that similar materials could potentially find optoelectronic applications which utilise this extended aromatic aggregation mechanism. It is hoped that this work will aid in the future development process, of novel, small molecule hydrogelators.

5.5 References

1. J. H. van Esch, *Langmuir*, 2009, **25**, 8392–8394.
2. R. Orbach, I. Mironi-Harpaz, L. Adler-Abramovich, E. Mossou, E. P. Mitchell, V. T. Forsyth, E. Gazit, and D. Seliktar, *Langmuir*, 2012, **28**, 2015–2022.
3. Z. Yang, G. Liang, M. Ma, Y. Gao, and B. Xu, *J. Mater. Chem.*, 2007, **17**, 850–854.
4. L. Chen, S. Revel, K. Morris, L. C. Serpell, and D. J. Adams, *Langmuir*, 2010, **26**, 13466–13471.
5. R. Orbach, L. Adler-Abramovich, S. Zigerson, I. Mironi-Harpaz, D. Seliktar, and E. Gazit, *Biomacromolecules*, 2009, **10**, 2646–2651.
6. Y. Huang, Z. Qiu, Y. Xu, J. Shi, H. Lin, and Y. Zhang, *Org. Biomol. Chem.*, 2011, **9**, 2149–2155.
7. D. J. Adams, L. M. Mullen, M. Berta, L. Chen, and W. J. Frith, *Soft Matter*, 2010, **6**, 1971–1980.
8. A. K. Das, R. Collins, and R. V. Ulijn, *Small*, 2008, **4**, 279–287.
9. M. Hughes, P. W. J. M. Frederix, J. Raeburn, L. S. Birchall, J. Sadownik, F. C. Coomer, I.-H. Lin, E. J. Cussen, N. T. Hunt, T. Tuttle, S. J. Webb, D. J. Adams, and R. V. Ulijn, *Soft Matter*, 2012, **8**, 5595–5602.
10. A. K. Das, A. R. Hirst, and R. V. Ulijn, *Faraday Discuss.*, 2009, **143**, 293–303.
11. S. Roy, N. Javid, J. Sefcik, P. J. Halling, and R. V. Ulijn, *Langmuir*, 2012, **28**, 16664–16670.
12. P. W. J. M. Frederix, R. V. Ulijn, N. T. Hunt, and T. Tuttle, *J. Phys. Chem. Lett.*, 2011, **2**, 2380–2384.
13. J. Shi, Y. Gao, Z. Yang, and B. Xu, *Beilstein J. Org. Chem.*, 2011, **7**, 167–172.
14. D. M. Ryan, S. B. Anderson, F. T. Senguen, R. E. Youngman, and B. L. Nilsson, *Soft Matter*, 2010, **6**, 475–479.
15. M. L. Ma, Y. Kuang, Y. Gao, Y. Zhang, P. Gao, and B. Xu, *J. Am. Chem. Soc.*, 2010, **132**, 2719–2728.
16. L. Chen, S. Revel, K. Morris, and D. J. Adams, *Chem. Commun.*, 2010, **46**, 4267–4269.
17. D. M. Ryan, S. B. Anderson, and B. L. Nilsson, *Soft Matter*, 2010, **6**, 3220–3231.
18. D. M. Ryan, T. M. Doran, S. B. Anderson, and B. L. Nilsson, *Langmuir*, 2011, **27**, 4029–4039.
19. M. Hughes, H. Xu, P. W. J. M. Frederix, A. M. Smith, N. T. Hunt, T. Tuttle, I. A. Kinloch, and R. V. Ulijn, *Soft Matter*, 2011, **7**, 10032–10038.
20. M. Zelzer and R. V. Ulijn, *Chem. Soc. Rev.*, 2010, **39**, 3351–3357.
21. M. Hughes, L. S. Birchall, K. Zuberi, L. A. Aitken, S. Debnath, N. Javid, and R. V. Ulijn, *Soft Matter*, 2012, **8**, 11565–11574.
22. C. Tang, R. V. Ulijn, and A. Saiani, *Langmuir*, 2011, **27**, 14438–14449.
23. C. Tang, R. V. Ulijn, and A. Saiani, *Eur. Phys. J. E*, 2013, **36**, 111–121.
24. P. Dastidar, *Chem. Soc. Rev.*, 2008, **37**, 2699–2715.
25. S. Fleming, S. Debnath, P. W. J. M. Frederix, T. Tuttle, and R. V. Ulijn, *Chem. Commun.*, 2013, **49**, 10587–10589.

26. J. Raeburn, G. Pont, L. Chen, Y. Cesbron, R. Lévy, and D. J. Adams, *Soft Matter*, 2012, **8**, 1168–1174.
27. A. M. Smith, R. F. Collins, R. V. Ulijn, and E. Blanch, *J. Raman Spectrosc.*, 2009, **40**, 1093–1095.
28. A. R. Hirst, S. Roy, M. Arora, A. K. Das, N. Hodson, P. Murray, S. Marshall, N. Javid, J. Sefcik, J. Boekhoven, J. H. van Esch, S. Santabarbara, N. T. Hunt, and R. V. Ulijn, *Nat. Chem.*, 2010, **2**, 1089–1094.
29. M. Biancalana, K. Makabe, A. Koide, and S. Koide, *J. Mol. Biol.*, 2008, **383**, 205–213.
30. W. D. Phillips, *J. Chem. Phys.*, 1955, **23**, 1363–1364.
31. A. H. Lewin and M. Frucht, *Org. Magn. Reson.*, 1975, **7**, 206–225.
32. L. Chen, K. Morris, A. Laybourn, D. Elias, M. R. Hicks, A. Rodger, L. Serpell, and D. J. Adams, *Langmuir*, 2010, **26**, 5232–5242.
33. Y. Zhang, H. Gu, Z. Yang, and B. Xu, *J. Am. Chem. Soc.*, 2003, **125**, 13680–13681.
34. G. Liang, Z. Yang, R. Zhang, L. Li, Y. Fan, Y. Kuang, Y. Gao, T. Wang, W. W. Lu, and B. Xu, *Langmuir*, 2009, **25**, 8419–8422.
35. D. J. Adams, M. F. Butler, W. J. Frith, M. Kirkland, L. Mullen, and P. Sanderson, *Soft Matter*, 2009, **5**, 1856–1862.
36. M. Ikeda, T. Tanida, T. Yoshii, and I. Hamachi, *Adv. Mater.*, 2011, **23**, 2819–2822.
37. S. Okada, S. Yamashita, T. Furuta, and M. Iwamura, *Photochem. Photobiol.*, 1995, **61**, 431–434.
38. Z. Yang, G. Liang, M. Ma, Y. Gao, and B. Xu, *Small*, 2007, **3**, 558–562.
39. Z. Yang, G. Liang, and B. Xu, *Chem. Commun.*, 2006, 738–740.
40. C. Tang, A. M. Smith, R. F. Collins, R. V. Ulijn, and A. Saiani, *Langmuir*, 2009, **25**, 9447–9453.
41. L. Chen, G. Pont, K. Morris, G. Lotze, A. Squires, L. C. Serpell, and D. J. Adams, *Chem. Commun.*, 2011, **47**, 12071–12073.
42. H. K. Kang, D. E. Kang, B. H. Boo, S. J. Yoo, J. K. Lee, and E. C. Lim, *J. Phys. Chem. A*, 2005, **109**, 6799–6804.
43. Z. Yang, H. Gu, Y. Zhang, L. Wang, and B. Xu, *Chem. Commun.*, 2004, 208–209.
44. Z. Yang, H. Gu, D. Fu, P. Gao, J. K. Lam, and B. Xu, *Adv. Mater.*, 2004, **16**, 1440–1444.
45. A. M. Smith, R. J. Williams, C. Tang, P. Coppo, R. F. Collins, M. L. Turner, A. Saiani, and R. V. Ulijn, *Adv. Mater.*, 2008, **20**, 37–38.
46. E. T. Pashuck, H. G. Cui, and S. I. Stupp, *J. Am. Chem. Soc.*, 2010, **132**, 6041–6046.
47. M. O. Guler, R. C. Claussen, and S. I. Stupp, *J. Mater. Chem.*, 2005, **15**, 4507–4512.
48. S. Marchesan, C. D. Easton, F. Kushkaki, L. Waddington, and P. G. Hartley, *Chem. Commun.*, 2012, **48**, 2195–2197.
49. N. J. Greenfield, *Nat. Protoc.*, 2006, **1**, 2876–2890.
50. N. Yan, Z. Xu, K. K. Diehn, S. R. Raghavan, Y. Fang, and R. G. Weiss, *Langmuir*, 2013, **29**, 793–805.
51. S. Bhattacharjee, G. Tóth, S. Lovas, and J. D. Hirst, *J. Phys. Chem. B*, 2003, **107**, 8682–8688.
52. E. Longo, A. Orlandin, F. Mancin, P. Scrimin, and A. Moretto, *ACS Nano*, 2013.
53. S. Roy, N. Javid, P. W. J. M. Frederix, D. A. Lamprou, A. J. Urquhart, N. T. Hunt, P. J. Halling, and R. V. Ulijn, *Chem.–Eur. J.*, 2012, **18**, 11723–11731.
54. H. Shao and J. R. Parquette, *Chem. Commun.*, 2010, **46**, 4285–4287.
55. S. Fleming, P. W. J. M. Frederix, I. Ramos-Sasselli, N. Hunt, R. V. Ulijn, and T. Tuttle, *Langmuir*, 2013, **29**, 9510–9515.
56. H. X. Xu, A. K. Das, M. Horie, M. S. Shaik, A. M. Smith, Y. Luo, X. F. Lu, R. Collins, S. Y. Liem, A. M. Song, P. L. A. Popelier, M. L. Turner, P. Xiao, I. A. Kinloch, and R. V. Ulijn, *Nanoscale*, 2010, **2**, 960–966.
57. G. Cheng, V. Castelletto, C. M. Moulton, G. E. Newby, and I. W. Hamley, *Langmuir*, 2010, **26**, 4990–4998.

58. X. Mu, K. M. Eckes, M. M. Nguyen, L. J. Suggs, and P. Ren, *Biomacromolecules*, 2012, **13**, 3562–3571.
59. V. Jayawarna, S. M. Richardson, A. R. Hirst, N. W. Hodson, A. Saiani, J. E. Gough, and R. V. Ulijn, *Acta Biomater.*, 2009, **5**, 934–943.
60. E. T. Pashuck and S. I. Stupp, *J. Am. Chem. Soc.*, 2010, **132**, 8819–8820.
61. J. R. Moffat and D. K. Smith, *Chem. Commun.*, 2008, 2248–2250.
62. A. B. P. Gursharan Bains, *Molecules*, 2011, **16**, 7909–7935.
63. D. J. Welsh, P. Posocco, S. Pricl, and D. K. Smith, *Org. Biomol. Chem.*, 2013, **11**, 3177–3186.
64. E. Miller and D. Jóźwik-Styczyńska, *Spectrochim. Acta, Part A*, 2009, **72**, 312–321.
65. E. C. Buruiana, T. Buruiana, and L. Hahui, *J. Photochem. Photobiol., A*, 2007, **189**, 65–72.

– Chapter 6 –

Insights into the co-assembly of *gelators* and *surfactants*

6.1 Abstract

The co-assembly of small molecules is a useful means of increasing the complexity and functionality of their resultant supramolecular constructs in a modular fashion. In this study, we explore the assembly and co-assembly of serine surfactants and tyrosine-leucine hydrogelators; capped at the N-termini with either Fmoc or 1-pyrenylethylcarbonyl. These systems all exhibit self-assembly processes which are influenced by aromatic stacking interactions, while the hydrogelators also exhibit β-sheets type arrangements which reinforce their supramolecular structures. We provide evidence for three distinct supramolecular co-assembly models; cooperative, disruptive and orthogonal. The co-assembly mode adopted depends upon whether the individual constituents; (I) are sufficiently different, such that effective segregation and orthogonal assembly occurs; (II) adhere to a communal mode of self-assembly; or (III) act to compromise the assembly of one another via incorporation and disruption. We find that greater scope for controllable co-assembly exists within orthogonal systems; which show minimal relative changes in the native gelator structure by FTIR, CD, and fluorescence spectroscopy. This is indicative of the segregation of orthogonal co-assembly constituents into distinct domains; where surfactant chemical functionality is presented at the surface of the gelator's supramolecular fibres. Overall, this work provides new insights into the design of modular co-assembly systems, which have the potential to augment the chemical and physical properties of existing gelator systems.

6.2 Introduction

Owing to their high water content; rheological properties that can mimic those of a variety of tissues;[1,2] and bio-inspired chemical functionality; hydrogels have the potential to be utilized in a variety of biomedical applications, such as controlled drug delivery devices[3,4] and cell culture[5,6]. In addition, the supramolecular aromatic stacking interactions that are central to the self-assembly of aromatic peptide amphiphiles, may lead to the development of soft optoelectronic devices which possess some degree of electro-conductivity.[7–11]

When considering the hydrogel's supramolecular architecture, it is desirable to control the stiffness,[12,13] topology,[14–17] aromatic interactions,[7–11] and the presentation of (bio-)chemical functionality[5,18–20] at the surface. These aspects are particularly important considerations for

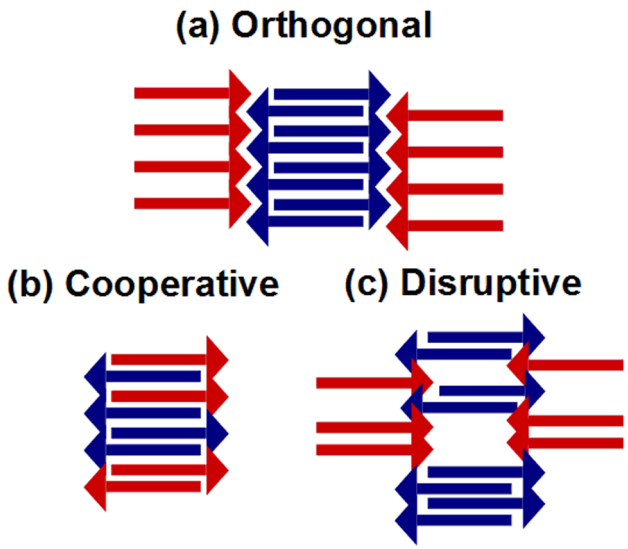

Figure 6.1 Conceptual diagram illustrating different possible co-assembly modes; (a) orthogonal self-assembly, where blue and red building blocks segregate into distinct structural components; (b) cooperative self-assembly, where building blocks both adhere to a common mode of self-assembly; and (c) disruptive self-assembly, where partial incorporation and mismatches between building blocks result in the occurrence of defects/discontinuities in the structure.

the development of biocompatible materials, which can help bridge the gap between biology and technology.[21] Due to the likely competing requirements for a particular application that interfaces a device with biology, it is desirable to be able to tailor the properties of existing gelator systems. In general terms, co-assembly is a potentially useful means of augmenting materials in a modular fashion.[22–26]

For example, using co-assembly it is possible to incorporate a bioactive peptide within a mixed hydrogel structure to improve cell culture viability.[27] In addition, mixed/cooperative (Fig. 6.1) co-assembly between donor and acceptor molecules is a useful means of achieving supramolecular charge transfer structures for optoelectronic applications.[28–30] However the co-assembly of different molecules can potentially result in other arrangements, besides a simple mixed/cooperative structure (Fig. 6.1).[31]

There has been much recent interest in the development of so-called "orthogonal" co-assembly, or self-sorting behaviour.[32–36] In these systems, individual constituents such as gelators and surfactants, are able to assemble independently in the presence of one another. This orthogonal assembly process can potentially result in various architectures such as interpenetrating networks, or mixed fibrous structures with domains or layers consisting of predominately one of the individual components. This phase separation behaviour can be a consequence of intermolecular interactions or environmental effects, such as pH.[32,34,37] Such hybrid systems can potentially exhibit characteristics neither system could achieve in isolation.[35] This associated increase in complexity is a desirable development in the field of small-molecule self-assembly,[38] where the chemical and/or physical properties of existing

supramolecular materials can be combined synergistically.

In an effort to start elucidating co-assembly design rules, we herein report on the development of gelators based on pyrene peptide amphiphiles,[39–41] studied together with analogous Fmoc-capped compounds,[42–52] see Fig. 6.2. Both Fmoc-YL[53] (**F3YL**) and Pyr-YL (**P4YL**) have been found to gel at a physiological pH. The corresponding Fmoc-S[5] and Pyr-S (**P4S**) surfactant compounds were chosen because Fmoc-S has been previously found to improve cell viability on Fmoc-FF based hydrogels. In this chapter, *gelators* are distinguished by their ability to form a β-sheet type H-bonding arrangement, whereas surfactant self-assembly is governed solely by aromatic stacking and hydrophobic/hydrophilic considerations. Hence, in our study the influence of the peptide and aromatic upon supramolecular co-assembly structures can be investigated in a systematic fashion.

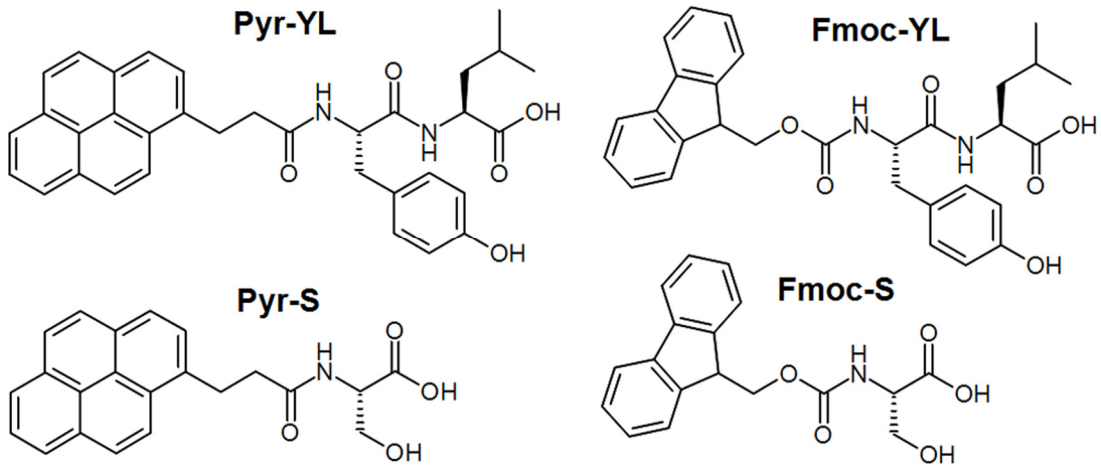

Figure 6.2 Structures of the gelator (YL) and surfactant (S) molecules.

This chapter first discusses the proposed models for each of the individual systems, followed by a detailed examination of the different combinations of Fmoc- and pyrene compounds by infrared, fluorescence and circular dichroism spectroscopy, atomic force microscopy and rheology. The results are organized according to the corresponding characterization techniques utilized, with a separate subsection for systems proposed to follow a particular model. This approach facilitates comparison between the proposed supramolecular structures within the context of the experimental techniques.

6.3 Results and discussion

Gelators Fmoc-YL[53,54] and Pyr-YL were chosen for this study on account of their ability to form hydrogels at a physiological pH. The surfactant Fmoc-S along with the analogous Pyr-S, were selected in order to explore the effects of co-assembly with micellar components.[5]

These gelator and surfactant compounds (Fig. 6.2) enable a comparison of the variation in both peptide and aromatic moieties. Note that despite the nomenclature adopted in this chapter, the surfactant Pyr-S is capable of gelation at a relatively acidic pH. In the first instance, individual gelator and surfactant molecules were considered, before undertaking a systematic analysis of their co-assembly characteristics. All systems were initially prepared at 20 mM or 20 mM:20 mM concentrations in 100 mM phosphate buffer. In addition, although not investigated here, it is likely that Pyr-YL and Fmoc-YL gelators can adopt (worm-like) micellar structures under high pH (e.g. 10.5) conditions.[55,56]

6.3.1 Proposed models

The adoption of a particular arrangement is believed to be determined primarily by the similarity between individual components in terms of both aromatic and peptidic intermolecular interactions. In order to facilitate interpretation of the experimental results, hypothesized models (Fig. 6.3) are first presented for each of the individual or co-assembly systems. Note that these are idealized cartoons for the purposes of interpretation.

6.3.1.1 Gelators

Fmoc-YL[53] and related aromatic peptide amphiphile based hydrogelators have been previously shown to give an antiparallel β-sheet type H-bonding arrangement (Fig. 6.3(a)), which is then interlocked via aromatic stacking interactions.[53,57,7,58,59] The influence of the peptide also results in a chiral supramolecular organization.[60] The resultant fibres subsequently aggregate further and form a supramolecular network, thus accounting for their viscoelastic properties. Hence, the analogous Pyr-YL system is proposed to self-assemble in a similar fashion.

6.3.1.2 Surfactants

Fmoc-S[5] and Pyr-S surfactant-like molecules are hypothesized to assemble into spherical (Fig. 6.3(b), left) and/or worm-like (Fig. 6.3(b), right) micelles[56,61,62] respectively, owing to the amphiphilic nature of their molecular structures. In contrast to the previously described gelators, an extensive internal H-bonding structure is not expected for these molecules, with their relatively hydrophilic amino acid side chain functionality.

6.3.1.3 Orthogonal co-assembly

Orthogonal co-assembly is believed to be most likely for the respective Pyr-YL/Fmoc-S and Fmoc-YL/Pyr-S systems; where the corresponding co-assembly partners possess different aromatic and peptide parts. Hence, there is expected to be relatively little interaction between the two components (Fig. 6.1(a), 6.3(c)) with orthogonal systems forming the aromatic

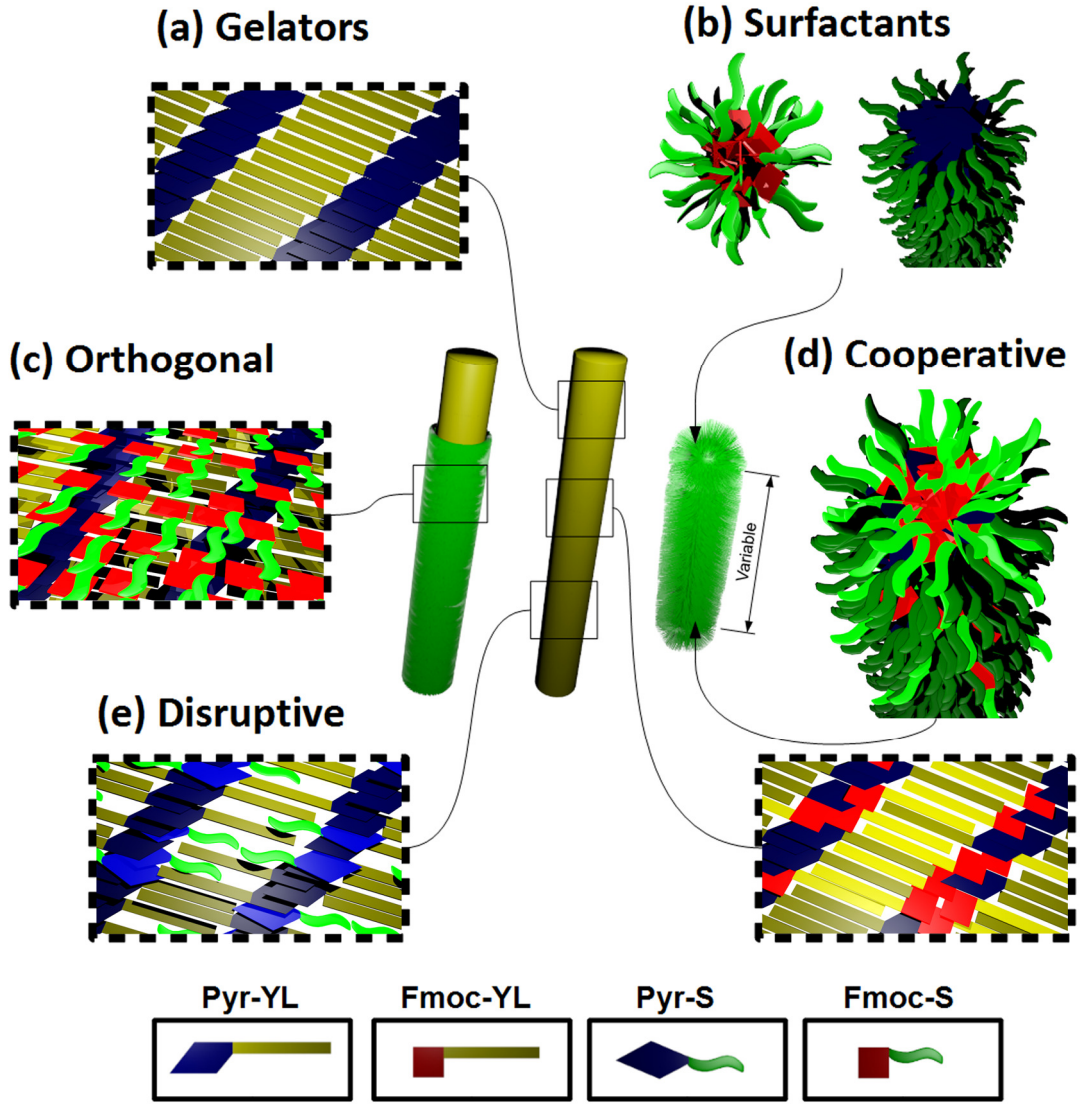

Figure 6.3 Proposed supramolecular models for: (a) The gelators Pyr-YL and (Fmoc-YL); (b) The surfactants Fmoc-S and Pyr-S; (c) Orthogonal Pyr-YL/Fmoc-S and (Fmoc-YL/Pyr-S); (d) Cooperative Pyr-YL/Fmoc-YL and Pyr-S/Fmoc-S; and (e) Disruptive Pyr-YL/Pyr-S and (Fmoc-YL/Fmoc-S). The legend (bottom) defines the simplified molecular structures utilized in these models. Within each co-assembly cartoon one component is highlighted for clarity.

stacked, β-sheet reinforced YL fibres discussed previously. Provided that these fibres are sufficiently stable, the surfactant molecules can potentially coat the YL fibres, without significant incorporation into the aforementioned aromatic stacks, or β-sheet type structures. This orthogonal model is a potentially useful co-assembly mechanism, as in principle it should allow the furnishing of a supramolecular fibre with a variety of chemical functionality[5] which is presented at the fibre-aqueous interface.

The complete segregation of co-assembly constituents into interpenetrating networks of single component fibres has also been referred to as orthogonal.[33,34,32,36] Hence, it should be clarified that the so-called orthogonal systems presented herein, are only such from the

perspective of the underlying YL fibres – in this model, micelles are not believed to exist independently of the main fibrous assembly.

6.3.1.4 Cooperative co-assembly

Cooperative co-assembly (Fig. 6.1(b)) systems are hypothesized to follow either a mixed aromatic stacked β-sheet type arrangement (Fig. 6.3(d), top), or a mixed micellar organisation (Fig. 6.3(d), bottom), respectively. This cooperative mode of assembly is believed to be facilitated by the Pyr-YL/Fmoc-YL and Pyr-S/Fmoc-S systems, when molecules which possess similar individual supramolecular arrangements – on account of their peptidic functionality – are combined within a single structure.

6.3.1.5 Disruptive co-assembly

In contrast to cooperative co-assembly, disruptive co-assembly is hypothesized to occur when the individual constituents possess the same aromatic moiety, but differ in their ability to form a β-sheet type H-bonding arrangement (e.g. Pyr-YL/Pyr-S and Fmoc-YL/Fmoc-S). For this scenario, there is a high propensity for aromatic stacking interactions between constituents, but the surfactant will likely be unable to contribute to the β-sheet type mode of assembly utilized by the gelator molecules (Fig. 6.1(c), 6.3(e)).

6.3.1.6 Other potential co-assembly arrangements

Besides the co-assembly arrangements presented in Fig. 6.3, there are other supramolecular arrangements which can be considered. More traditional orthogonal arrangements such as interpenetrating fibrous networks,[34] and fibres mixed with micellar structures are distinct possibilities.[35,33] Where appropriate, these alternatives will also be considered within the context of the experimental results.

6.3.2 Infrared absorption spectroscopy

6.3.2.1 Gelators

Infrared spectra of the deuterated gels show an amide I peak at 1625 cm^{-1} for Fmoc-YL and 1620 cm^{-1} for Pyr-YL (Fig. 6.4(a)). Furthermore, an additional 1684 cm^{-1} peak is seen for the Fmoc-YL gelator, attributed to the presence of the carbamate moiety.[63,64] The intensity and definition associated with these peaks is indicative of the enhancement of the respective carbonyl vibrational modes that occurs within the ordered β-sheet type H-bonding arrangement. For both gelators, the amide peak has a smaller component towards higher frequencies, which may be attributed to inhomogeneity associated with the H-bonding stack sizes. A broad peak is observed around 1586 cm^{-1}, which corresponds to the presence of the carboxylate anion, which shows a fraction of the C-termini remains deprotonated at the

sample pH (~7.3).

6.3.2.2 Surfactants

The surfactant systems show the typically broad infrared absorption bands associated with an unstructured H-bonding arrangement that features extensive solvent interactions (Fig. 6.4(b)). For both samples, the carboxylate band (1586 cm^{-1} for Pyr-S and 1596 cm^{-1} for Fmoc-S) has a more prominent presence than in the gelator samples. In Fmoc-S, a broad band around 1680 cm^{-1} is assigned to unstructured carbamate groups. A weak band, analogously assigned to unstructured amide groups, can be distinguished in the Pyr-S spectrum around 1640 cm^{-1}. As expected for both these single amino acid amphiphile systems: the absence of a cooperatively enhanced H-bonding arrangement confirms that the Pyr-S hydrogel represents a distinct self-assembly mode, likely driven only by hydrophobic interactions between the pyrene moieties.[56,61,65]

6.3.2.3 Orthogonal co-assembly

The proposed orthogonal co-assembly systems exhibit spectra (Fig. 6.4(c)) that resemble those of their corresponding *gelator* components (Fig. 6.4(a)). In addition, the prominent carbamate peak around 1685 cm^{-1} specifically requires that the Fmoc-YL β-sheet type H-bonding structure is present within the Fmoc-YL/Pyr-S mixed assembly. No such peak was observed in the Pyr-YL/Fmoc-S spectrum (Fig. 6.4(c)); this result indicates that as expected the carbamate groups of the surfactant molecules do not form an extended H-bonding stack within the Pyr-YL/Fmoc-S co-assembly system. For the Pyr-YL/Fmoc-S system, the broad 1676 cm^{-1} contribution in the surfactant spectrum disappears, while a weak band rises at 1666 cm^{-1}, which may be attributed to inclusion of the carbamate moiety on the surface of an Fmoc-dipeptide fibrous core.

6.3.2.4 Cooperative co-assembly

The spectrum for the Pyr-YL/Fmoc-YL co-assembly (Fig. 6.4(d)) closely resembles a linear combination (Appendices, Fig A.16) of its individual components. The 1620 cm^{-1} amide I peak is significantly larger than the carbamate peak as expected from the 3:1 ratio of amide to carbamate moieties present in the mixed system. Note that the strong absorption in the amide I region occurs as a consequence of the excitonic coupling effect only seen for well-ordered amide groups like in a β-sheet-type structure.[64] Therefore, these observations indicate that the propensity to form β-sheet structures is not influenced by the different aromatic moieties. However, these FTIR results cannot distinguish between a cooperative co-assembly and a completely segregated co-assembly mode where a block co-assembly or separate Fmoc-YL and Pyr-YL fibres are present; although this self-sorting can often only be

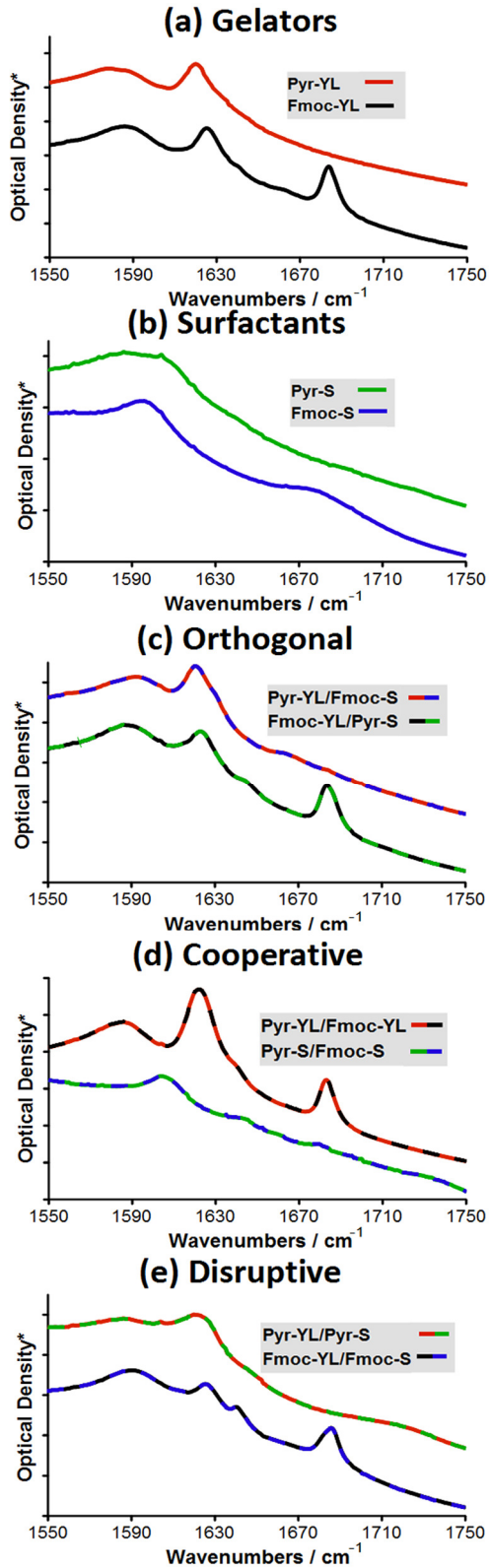

Figure 6.4 Amide I FTIR spectra of: (a) The gelators Pyr-YL and Fmoc-YL; (b) The surfactants Fmoc-S and Pyr-S; (c) Orthogonal Pyr-YL/Fmoc-S and Fmoc-YL/Pyr-S ; (d) Cooperative Pyr-YL/Fmoc-YL and Pyr-S/Fmoc-S; and (e) Disruptive Pyr-YL/Pyr-S and Fmoc-YL/Fmoc-S. *Spectra have been vertically offset for clarity; each division corresponds to 0.1 units.

achieved for molecules that gelate under different environmental conditions, such as pH.[34]

Pyr-S/Fmoc-S (Fig. 6.4(d)) exhibits only weak, broad infrared bands in the amide I region. Compared to a linear combination of the two individual components, a broad band centred around 1643 cm^{-1} was observed, which indicates Pyr-S molecules with their amide bonds in a randomly structured configuration. The 1676 cm^{-1} IR absorption, assigned to the Fmoc-S carbamate groups, weakens slightly in the co-assembled gel; relative to what would be expected from a linear combination of the individual components (Appendices, Fig A.16), pointing to a change in the Fmoc-S state.

6.3.2.5 Disruptive co-assembly

The proposed disruptive co-assembly systems show clear differences from the spectral sum of their components (Appendices, Fig A.16). For instance, Fmoc-YL/Fmoc-S exhibits a more distinct amide I peak around 1640 cm^{-1} (Fig. 6.4(e)); the emergence of this significant contribution, while the lower frequency band decreases in intensity, can be assigned to a less extended secondary structure. The amide I region of the Pyr-YL/Pyr-S system (Fig. 6.4(e)) exhibits two close bands around 1620 and 1626 cm^{-1}, compared to a relatively strong 1620 cm^{-1} band with a tail towards 1630 cm^{-1} that is assigned to inhomogeneity for the Pyr-YL (Fig. 6.4(a)) and Pyr-YL/Fmoc-S (Fig. 6.4(c)) systems. This could be explained by two different types of linear amide stacks, while the inhomogeneous component also appears to still be present. These differences in the FTIR of the Fmoc-YL/Fmoc-S and Pyr-YL/Pyr-S systems suggest that the surfactant component is having an impact on the β-sheet type H-bonding formation associated with the dipeptide.

6.3.3 Fluorescence emission spectroscopy

Fluorescence emission was utilized as a means of inferring the extent and orientations of aromatic stacking interactions within each of the supramolecular constructs (Fig. 6.5). The dilute solution spectra of materials consisting of Fmoc constituents (e.g. Fig. 6.5(a), lower panel, faded line) show a band with contributions around 306 and 315 nm, with a tail extending beyond 350 nm.[66,67] Dilute pyrene amphiphile solutions (e.g. Fig. 6.5(a), upper panel, faded line) exhibit multiple distinct bands at 380, 398, and 418 nm.[68,69,62] Hence, the non-overlapping emission profiles of fluorene and pyrene should allow the monitoring of the individual constituents within co-assembly systems with mixed fluorophores. However, at gelation concentrations pyrene completely quenches the fluorene peaks (Fig. 6.5(c,d)), due to its absorption at the fluorene emission wavelengths.[70] The %max intensities of characteristic monomer emissions are utilized in Fig. 6.6, to provide an indication of the CAC in these systems. Above the CAC, excimer peak(s) become apparent, and as the concentration is increased the excimer becomes gradually more intense than the corresponding monomeric

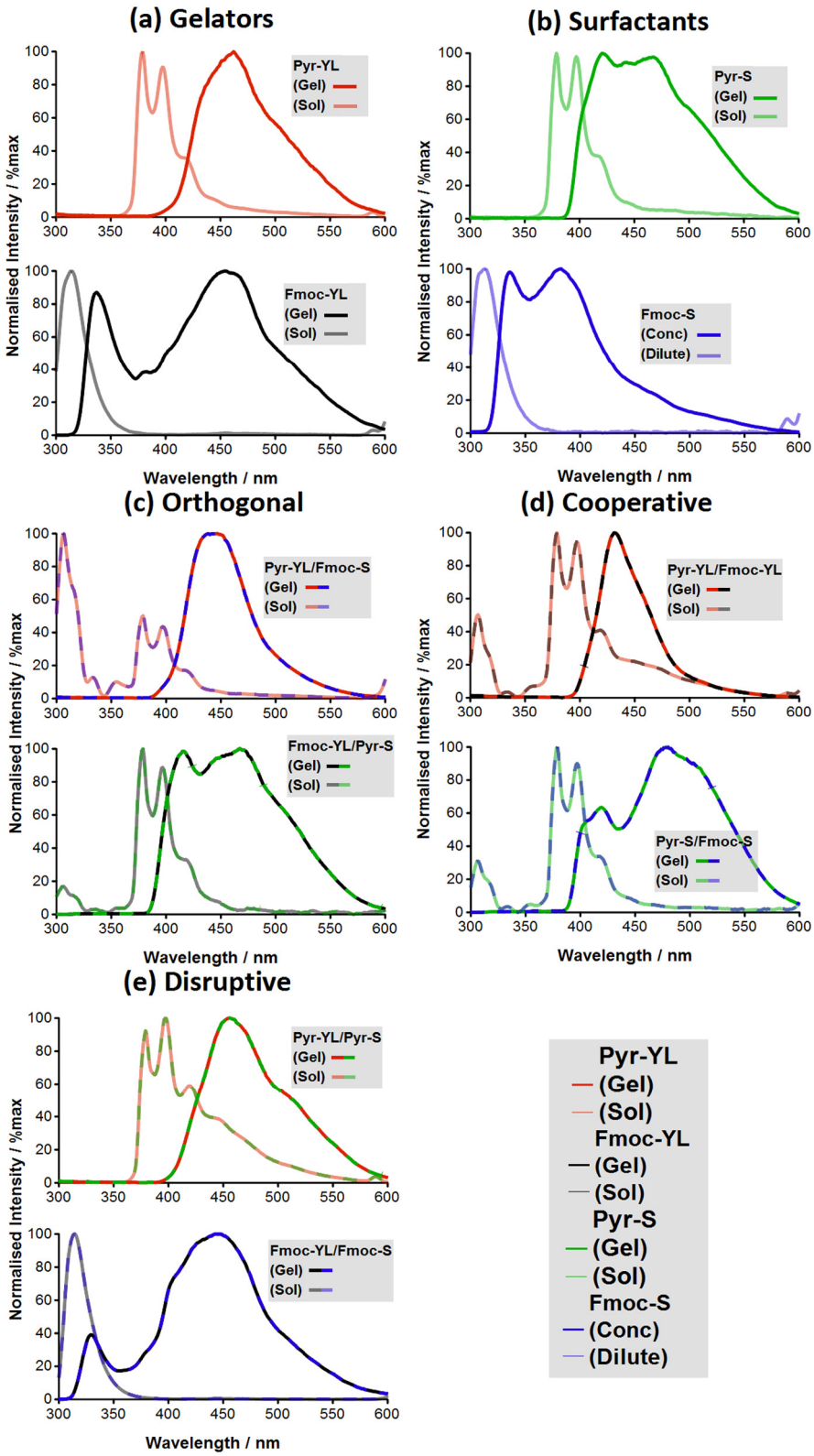

Figure 6.5 Fluorescence emission spectra of: (a) The gelators Pyr-YL and Fmoc-YL; (b) The surfactants Fmoc-S and Pyr-S; (c) Orthogonal Pyr-YL/Fmoc-S and Fmoc-YL/Pyr-S; (d) Cooperative Pyr-YL/Fmoc-YL and Pyr-S/Fmoc-S; and (e) Disruptive Pyr-YL/Pyr-S and Fmoc-YL/Fmoc-S. Note legend descriptions – Gel/Conc @ 20 mM of each constituent, Sol/Dilute @ ~0.16 mM of each constituent.

emission. The concentration at which the excimer and monomeric emissions are equal is indicated in Fig. 6.6 (Xs) and it is primarily these 50%max values that are used to compare the various systems. However, it should be noted that the initial aggregates detected at very low concentrations may differ from the supramolecular structures found in the gel state.[71] The data in utilized in Fig. 6.6 originates from extracted Gaussians (see Appendices, section A.3.2).

6.3.3.1 Gelators

The gelators Pyr-YL and Fmoc-YL demonstrate substantially redshifted emission when compared to their corresponding dilute solutions. This is indicative of aromatic stacking interactions within the hydrogel network and resulting intermolecular energy transfer.[72,73] The Pyr-YL hydrogel in particular exhibits a continuous broad emission profile, with complete quenching of its characteristic monomer peaks (Fig. 6.5(a)).[74] In comparison the Fmoc-YL system displays the presence of various aggregates other than the main excimer peak. This would suggest that not all of the fluorene segments are effectively incorporated into the supramolecular structure. This observation suggests that fluorenes can exist in a multitude of different conformations, with varying degrees of disorder.[75–77] In terms of the 50%max intensities (Fig. 6.6(a)), we observe a clear transition at approximately 0.7 mM; where pyrene's monomeric emission becomes increasingly quenched as the concentration is increased and the broad excimer emission becomes dominant. In contrast, the fluorene monomer contributions at <320 nm markedly shift to higher wavelengths at ~4 mM. In addition, the fluorene excimer emission at 454 nm only becomes the dominant feature at the 20 mM gelation concentration (see Appendices, section A.3.2). Hence, while aromatic stacking helps drive Pyr-YL assembly, for Fmoc-YL these interactions are weaker as would be anticipated. Overall, fluorescence emission spectroscopy confirms the presence of supramolecular aggregates within the YL hydrogelator assemblies. However, this aspect of the self-assembly mechanism is more prominent for the Pyr-YL system, as may be expected on account of its increased aromaticity.

6.3.3.2 Surfactants

Compared to the Pyr-YL system, Pyr-S displays a marginally more pronounced excimer redshift (Fig. 6.5(b)), exhibiting a maximum at approximately 466-475 nm compared with 453-462 nm for Pyr-YL (see also Appendices, section A.3.2). Lacking a β-sheet like H-bonding arrangement; the assembly of the Pyr-S molecules is entirely dependant upon aromatic stacking interactions. The fact that Pyr-S exhibits a larger redshift than Pyr-YL is believed to be a consequence of a β-sheet type formation in the latter, altering the optimal

orientation of the aromatic stacking interactions. Furthermore, besides the broad Pyr-S excimer band, we also observe a peak at 418 nm. This feature of the emission spectrum indicates that there are additional supramolecular arrangements associated with the Pyr-S surfactant molecules that are less strongly bound to each other; perhaps loosely aggregating on the surface of the main assembly. This observation contrasts with the comparatively well defined stacks present in the Pyr-YL supramolecular structures. In addition, the Pyr-S excimer does not persist to be the main peak below concentrations of 1.5 mM; which coincides with the predominance of the monomeric pyrene emissions (e.g. 380 nm) (Fig. 6.6(b)). Hence, it can be surmised that the Pyr-S forms aggregates which are less persistent at lower concentrations since these structures lack the additional stabilization afforded by β-sheet formation. Nonetheless, at higher concentrations the %max intensity of the higher wavelength contributions indicates the formation of extended 1D nanostructures. This observation, combined with the inferred disorder and solvation associated with H-bonding of the serine residues by FTIR, suggests that worm like micelles are prevalent in the Pyr-S system. Here the planarity of the pyrene ring predisposes the formation of extended 1D structures as opposed to the related spherical micelles. Worm like micelle structures have also been recently reported in the literature for Fmoc-FF and other peptide amphiphile systems at high pH.[61,78]

In contrast, the Fmoc-S surfactant exhibits the least prominent excimer redshift (Fig. 6.5(b)). This observation suggests that the self-assembly mode adopted by Fmoc-S does not feature the extended 1D aromatic stacking interactions seen for the other individual systems, which would be consistent with the spherical micelle model. Besides the modest excimer redshift, we also observe the existence of multiple peaks from alternative fluorene orientations.[65] Moreover, the fact that the fluorene group features a non-aromatic bridgehead carbon atom, may put some geometrical constraints on the extended stacking of Fmoc-groups when not assisted by a beta sheet configuration of an appended peptide; which could account for some of the spectral differences between Fmoc-S and the analogous 1D Pyr-S system.

6.3.3.3 Orthogonal co-assembly

When moving to the co-assembled systems, it was found that the excimer redshift of Pyr-YL/Fmoc-S is similar to that of pure Pyr-YL (Fig. 6.5(c)), as also seen for FTIR, although the loss of some %max intensity at higher wavelengths is observed. This suggests that intercalation of fluorene is not occurring to a great extent within the aromatic pyrene stacks. The fluorescence versus concentration data of the pyrene and fluorene constituents illustrates that within the co-assembly system an energy transfer from fluorene to pyrene takes place;

with monomeric fluorene at 306 nm only dominating at concentrations under 0.1 mM (Fig. 6.6(c)). Similarly for Fmoc-YL/Pyr-S co-assembly, we observe the preservation of the excimer redshift (Fig. 6.5(c)) associated with Pyr-S structures, unlike the FTIR which was dominated by Fmoc-YL H-bonding. These complementary observations suggest that the Pyr-S molecules retain significant pyrene stacking interactions in the co-assembly structure; hence intercalation with Fmoc-YL is not inferred. This is consistent with the proposed orthogonal coating mechanism, or it could alternatively suggest self-separation whereby the respective Fmoc-YL and Pyr-S fibrous structures exist independently of one another. Further evidence for the orthogonal coating mode of assembly is provided in the circular dichroism section, see below. In Fmoc-YL/Pyr-S, the fluorene to pyrene energy transfer mechanism is seen to be significant even at the lowest concentrations (Fig. 6.6(c)). These observations suggest that even at low concentrations Fmoc-YL and Pyr-S remain in close proximity through aggregation, allowing comprehensive energy transfer. Overall, the largely preserved pyrene excimer redshifts suggests that Fmoc-YL/Pyr-S and Pyr-YL/Fmoc-S each adhere to an orthogonal co-assembly arrangement (Fig. 6.1(a), 6.3(c)), due to the differential modes of peptide and aromatic assembly exhibited by each of their constituents.

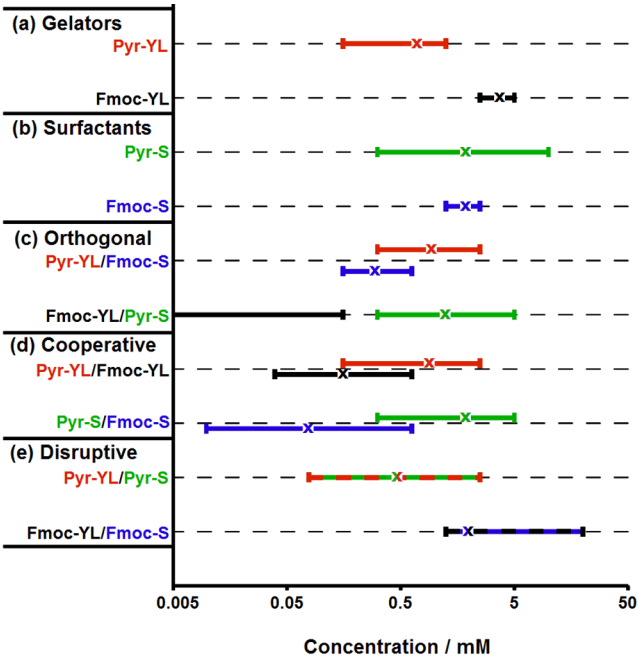

Figure 6.6 Summary of the fluorescence intensity versus concentration data of each system. Where "X" indicates the concentration at which Pyr (380 nm) or Fmoc (306 or <320 nm) monomer emission intensity is 50%, while the lines show the full 0-100% range of the sigmoidal region of the graphs (see Appendices, section A.3.2).

6.3.3.4 Cooperative co-assembly

In the Pyr-YL/Fmoc-YL system the excimer redshift (Fig. 6.5(d)) is less pronounced than for pure Pyr-YL gel; exhibiting a narrower band than either Pyr-YL or Pyr-YL/Fmoc-S. This is

thought to be caused by extensive intercalation of Pyr-YL and Fmoc-YL aromatic stacked β-sheet structures, which acts to curtail the extended pyrene intermolecular energy transfer seen in other systems. Even so, it is likely that discrete sections of stacked pyrene and Fmoc exist, with intercalation between the two a random occurrence rather than an alternating pattern. In conjunction with the previously observed cooperatively enhanced FTIR absorptions, these results are consistent with a mixed cooperative structure as opposed to an interpenetrating network of separate Pyr-YL and Fmoc-YL fibres. This mixed structure does not appear to be detrimental to the resilience of the supramolecular constructs; hence, aggregation and quenching of the 380 nm monomeric pyrene emission (Fig. 6.6(d)) occurs at a similar concentration to that observed for Pyr-YL alone. In addition, the 380 peak's %max intensity decreases upon the appearance of the 306 nm fluorene peak, as also for Pyr-YL/Fmoc-S (see Appendices, section A.3.2). This is thought to be a consequence of reduced energy transfer between fluorophores, as the aggregates do not persist to same extent at lower concentrations (<0.1 mM).

For the co-surfactant Pyr-S/Fmoc-S hydrogel the excimer redshift (Fig. 6.5(d)) is similar to that of Pyr-S. This suggests that the co-assembly consists of extensive 1D aromatic stacking interactions within a cooperative worm-like micelle structure, similar to that proposed for Pyr-S. Hence, despite the presence of Fmoc-S, extensive pyrene stacking interactions within these structures is observed. In addition, we also see the preservation of the typical Pyr-S 50%max (Fig. 6.6(d)). Interestingly however, upon altering the concentration we observe the fluorene monomer only dominating at the very lowest concentration (~5 nM). This robust Fmoc-S to Pyr-S energy transfer mechanism indicates that these components remain in mixed aggregates irrespective of concentration. This suggests that as the concentration is lowered, mixed spherical micelle structures are likely to exist, which continue to mediate the energy transfer mechanism between fluorene and pyrene fluorophores. However, these spherical micelles result in a loss of 1D stacking interactions and therefore show a relatively low pyrene excimer redshift (see Appendices, section A.3.2). Thus, these results suggest that while Pyr-YL/Fmoc-YL and Pyr-S/Fmoc-S each exist in cooperative co-assembly structures, the co-surfactant system shows that co-assembly has a relatively small impact upon extended Pyr-S stacking in the gel state. This may be evidence of some segregation between components within the Pyr-S/Fmoc-S structure, or this may be facilitated by the relatively disordered nature of the proposed worm-like micelle construct.

6.3.3.5 Disruptive co-assembly

The Pyr-YL/Pyr-S excimer redshift (Fig. 6.5(e)) suggests that this system adopts a structure more in line with that seen for Pyr-YL; hence the aromatic stacked β-sheet type H-bonding

structure is present, as opposed to the worm-like micelle structure proposed for Pyr-S. This observation was also supported by FTIR, which suggested a cooperatively enhanced, albeit disrupted, H-bonding arrangement. This system also exhibits a gradual increase in the wavelength of the dominant peak as the concentration is increased, as opposed to more stable excimer redshift seen for individual Pyr-YL and Pyr-S systems (see Appendices, section A.3.2), thus suggesting that this represents a convolution of the two separate profiles as the co-assembly of Pyr-YL and Pyr-S results in a mixed structure, which is subject to considerable disruption (Fig. 6.1(e), 6.3(e)).

For the Fmoc-YL/Fmoc-S system, fluorescence emission spectra (Fig. 6.5(e)) are similar to those seen previously for Fmoc-YL; possessing an initial excimer redshift more in line with the Fmoc-YL structure. Thus, this system is also thought to adopt the aromatic stacked, β-sheet type reinforced fibrous structures seen previously for the YL gelators. This was also inferred from the disrupted, but present, cooperatively enhanced FTIR absorptions. Hence, we believe this Fmoc-YL type structure also features intercalation of Fmoc-S into the 1D aromatic stacking arrangement. This is supported by the much longer and distorted sigmoidal region of the fluorescence versus concentration graph, which shows a two-step change in the fluorene monomer intensity as Fmoc-S is increasingly incorporated into the Fmoc-YL aromatic stack as the concentration is increased (Fig. 6.6(e), see Appendices, section A.3.2). This is significant when compared to the much sharper transitions seen previously for the individual Fmoc-YL and Fmoc-S systems (Fig. 6.6(a,b), see Appendices, section A.3.2).

6.3.4 Circular dichroism

CD was used to help ascertain the presence of chirality associated with the supramolecular fibres (Fig. 6.7). Due to the viscous nature of these materials, CD was performed on subgelation concentrations of the hydrogelators; this was found to be necessary to achieve homogeneity throughout the sample cell. This methodology also attempts to minimize the influence of an excessive HT voltage, potential linear dichroism, and any scattering effects. Previous work on aromatic peptide amphiphiles found that self-assembly (as determined by pK_a shifts) is sensitive to the concentration.[79] It is for this reason that all concentrations used for CD were still significantly greater than the CAC, as defined by fluorescence data (Fig. 6.6). Hence, we are assuming that the supramolecular structures present at these subgelation concentrations are largely representative of those found in the gel state – e.g. isolated fibres. In addition, due to excessive absorption and the relative weakness of the circular dichroism observed on a molar basis,[12,41] it was not possible to consistently record a CD spectrum covering the wavelength range relevant to the β-sheet organization.[80–82] Despite this

limitation and the fact that the aromatic groups are not chiral by themselves, it is possible to observe the substantial supramolecular chirality associated with the stacking of the aromatic portion of the studied molecules.[40]

6.3.4.1 Gelators

Pyr-YL in particular shows well defined peaks at 330 and 350 nm; these consistently exhibit a negative CD signal (Fig. 6.7(a)). In comparison, Fmoc-YL demonstrates a positive CD peak at ~305 nm, in addition to strong shorter wavelength signals centred around 275 nm which potentially have a contribution from the tyrosine residues.[53,83] Thus, it has been ascertained that both the Fmoc-YL and Pyr-YL fibres have an associated supramolecular chirality.

6.3.4.2 Surfactants

Similarly, Pyr-S exhibits characteristic pyrene peaks at around 330 and 350 nm, but in contrast to Pyr-YL, now a positive signal is observed for these peaks (Fig. 6.7(b)), providing further evidence that the Pyr-S gel doesn't conform to the aromatic-stacked, β-sheet like H-bonding reinforced model of Pyr-YL. Instead proposed individual worm like micelles are believed to coil around one another in an arrangement determined by the chirality of the external serine residues. On the other hand, Fmoc-S, which is believed to form spherical micelles, as expected does not exhibit a significant CD signal. The absence of CD signals that are typical of fibre formation is consistent with the spherical micelle model for Fmoc-S. These results validate the previous fluorescence emission observations that only suggested an extended 1D structure for the Pyr-S system.

6.3.4.3 Orthogonal co-assembly

Co-assembly of Pyr-YL/Fmoc-S results in a negative CD signal associated with the pyrene arrangement, similar in handedness and intensity to that observed for Pyr-YL (Fig. 6.7(c)), as seen previously from FTIR and fluorescence emission spectroscopy. In contrast, co-assembly of Fmoc-YL/Pyr-S gives a weakly negative pyrene CD signal, in addition to a reversal of handedness for the remainder of the spectra, when compared to that seen for Pyr-S alone. The observation that the associated supramolecular chirality of the Pyr-YL structure is relatively unaffected by the Fmoc-S co-assembly, is thought to support the notion of an orthogonal co-assembly mechanism (Fig. 6.1(a), 6.3(c)). However, it is also observed that the 335 and 355 nm peaks have changed slightly in relative magnitude and wavelength – hence, the Fmoc-S coating is likely having some effect upon the chiral pyrenyl arrangement. For Fmoc-YL/Pyr-S, we see a significant change in the supramolecular chirality from that observed for the worm-like micelle structures; this result rules out the possibility of an

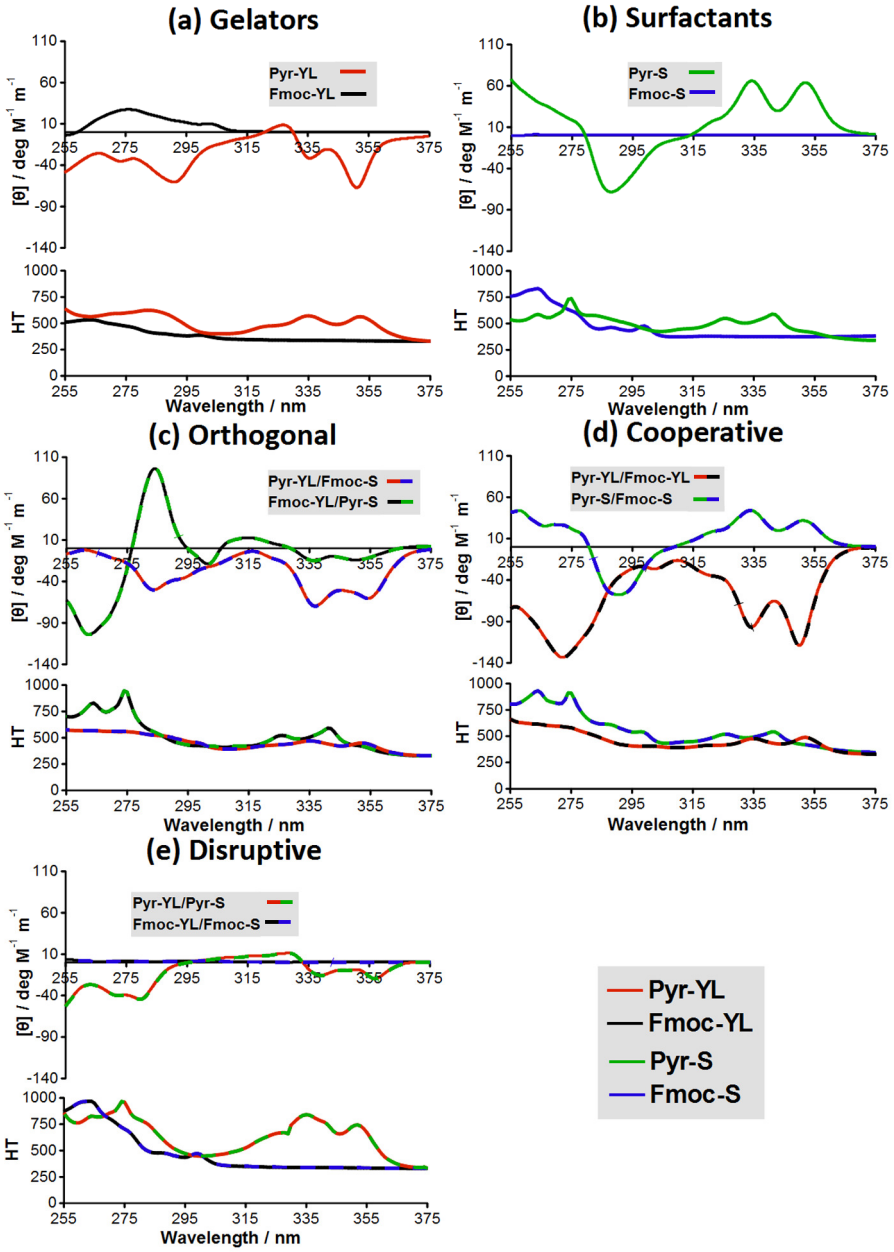

Figure 6.7 CD spectra (top panels) and corresponding HT spectra (bottom panels). (a) The gelators Pyr-YL and Fmoc-YL; (b) The surfactants Fmoc-S and Pyr-S; (c) Orthogonal Pyr-YL/Fmoc-S and Fmoc-YL/Pyr-S; (d) Cooperative Pyr-YL/Fmoc-YL and Pyr-S/Fmoc-S; and (e) Disruptive Pyr-YL/Pyr-S and Fmoc-YL/Fmoc-S.

Fmoc-YL/Pyr-S interpenetrating fibrous network. While CD is consistent with Pyr-S adhering to the Fmoc-YL fibres (as opposed to following its own independent self-assembly mode) this result does not in itself preclude disruptive co-assembly. However, because significant intercalation between fluorene and pyrene is not inferred from fluorescence data (Fig. 6.5), this mechanism is deemed to be orthogonal, with the Pyr-S adhering to the Fmoc-YL fibre surface to shield the hydrophobic pyrene moiety, whilst exposing the hydrophilic serine residue to the aqueous environment. Thus, the native Fmoc-YL and Pyr-YL aromatic

stacked β-sheet structures are believed to exist intact underneath their respective Pyr-S or Fmoc-S serine coatings; as also evidenced by FTIR, which showed preservation of their β-sheet type structures (Fig. 6.4).

6.3.4.4 Cooperative co-assembly

The Pyr-S/Fmoc-S system exhibits a spectrum which is fairly consistent with that previously observed for Pyr-S alone (Fig. 6.7(d)). In particular, the characteristic positive 330 and 350 nm pyrene signals are preserved. This provides further indication that the surfactant-like nature of both Fmoc-S and Pyr-S acts to facilitate the formation of structures which are akin to those previously observed for Pyr-S. For the co-assembling YL amphiphiles, the presence of Fmoc-YL appears to enhance the negative Pyr-YL CD signals, suggesting aromatic stacked β-sheets that compliment one another. In conjunction with previous fluorescence emission data that suggested extensive intercalation between fluorophores; the enhanced CD signal further supports a mixed cooperative structure as opposed to an interpenetrating network. However, for the Pyr-YL/Fmoc-YL system, we also observe a change in the Fmoc-YL 305 and 275 nm peaks, from positive to negative. This may be indicative of Fmoc-YL following a stacking arrangement specific to Pyr-YL, or alternatively pyrene's absorption may dominate that of Fmoc. In any case, these results suggest a mixed co-assembly mechanism (Fig. 6.1(b)) for Pyr-YL/Fmoc-YL and Pyr-S/Fmoc-S; in each case gelators or surfactants cooperatively assemble within their common peptide determined mode of self-assembly.

6.3.4.5 Disruptive co-assembly

Co-assembly between Pyr-YL and Pyr-S results in a diminished negative pyrene CD signal, suggesting that their respective modes of self-assembly act to compromise one another (Fig. 6.7(e)). Ultimately, the negative CD signal reasserts that it is Pyr-YL, the gelator, which dictates the co-assembly between the two molecules. In addition, co-assembly of Fmoc-YL/Fmoc-S, is characterized by a loss of Fmoc-YL's positive 305 and 275 nm signals. Hence, both of the mixed peptide common aromatic co-assembly partners exhibit an apparent disruption in the supramolecular structure, as was previously suggested based on FTIR evidence. We believe that this effect is particularly prominent for these co-assembly partners because the supramolecular chirality originates from the chiral peptide segment of these molecules. Hence, intercalation between the identical aromatic segments of these molecules, which adhere to entirely disparate modes of self-assembly, results in disruption of the supramolecular β-sheet type structure, and consequently a diminished CD spectrum, compared to that previously obtained from the individual gelator components.

6.3.5 Atomic force microscopy

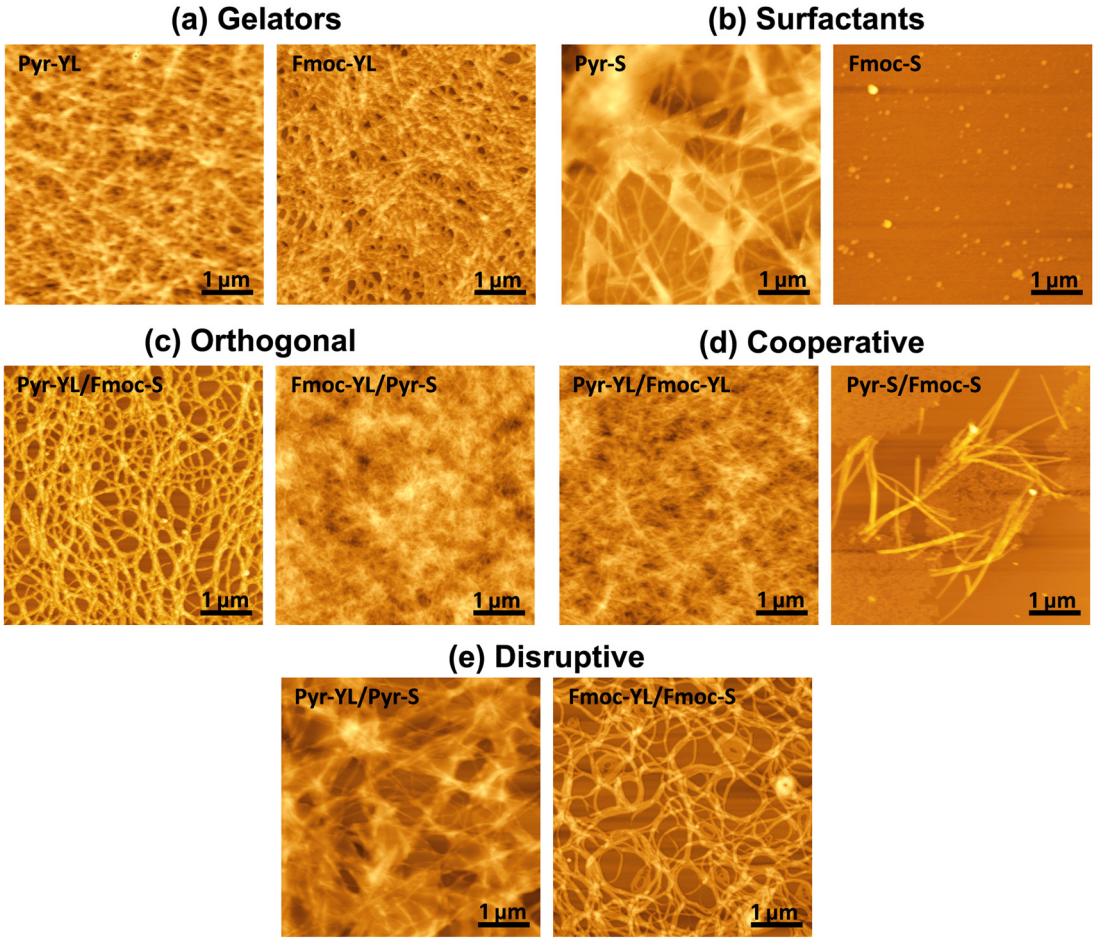

Figure 6.8 AFM of: (a) The gelators Pyr-YL and Fmoc-YL; (b) The surfactants Fmoc-S and Pyr-S; (c) Orthogonal Pyr-YL/Fmoc-S and Fmoc-YL/Pyr-S; (d) Cooperative Pyr-YL/Fmoc-YL and Pyr-S/Fmoc-S; and (e) Disruptive Pyr-YL/Pyr-S and Fmoc-YL/Fmoc-S.

6.3.5.1 Gelators

Atomic force microscopy was used to examine the fibre morphology of the gelator systems (Fig. 6.8(a)). Both of the YL hydrogelators show the presence of dense fibrous assemblies, which was anticipated for these aromatic stacked, β-sheet reinforced fibrous networks. The (bundles of) fibres observed in these systems vary in size, but are typically about 40-200 nm in width. Care should be taken with quantitative feature size interpretation of these AFM images, which may depend on AFM sample preparation. However, the fibre sizes observed here are broadly consistent with nanofibre dimensions seen in similar materials.[53,5,84] The varying fibre diameters observed is also consistent with the supramolecular inhomogeneity previously inferred by FTIR and fluorescence.

6.3.5.2 Surfactants

Atomic force microscopy shows the absence of any fibres for the Fmoc-S system, instead exhibiting spherical structures, which may be from micellar aggregates (Fig. 6.8(b)). The

surfactant Pyr-S shows fibres, but in comparison to the gelators appears more heterogeneous; indicating increased disorder associated with the system, and thus reflecting the proposed worm-like micelle nature of the species.

6.3.5.3 Orthogonal co-assembly

Fmoc-YL/Pyr-S shows the presence of dense fibrous networks by AFM, which also characterized the individual Fmoc-YL material (Fig. 6.8(c)). We also note that the fibrous network appears finer than that of the individual Fmoc-YL system. These results indicate that Pyr-S is having an impact on the macroscale Fmoc-YL fibres, as opposed to forming distinct structures of its own. The observed fibres most likely form via the aggregation of more elementary supramolecular structures. The observation of thinner fibres may then relate to reduced aggregation of the elementary Fmoc-YL fibrils as a consequence of an increased negative charge from the Pyr-S coating on the fibre surface. Hence, this result is consistent with the orthogonal coating mechanism and also demonstrates the absence of an interpenetrating network morphology.

Co-assembly of Pyr-YL and Fmoc-S results in a fibre morphology which appears to be homogeneous along the length of the fibre, which is consistent with interfacial assembly of Fmoc-S. In this case, co-assembly does not result in significant changes to the fibre morphology of the native Pyr-YL gelator. In contrast to Pyr-S, Fmoc-S does not natively form fibres or 1D aromatic stacking interactions and thus may have less relative influence over the corresponding gelator's fibre morphology.

6.3.5.4 Cooperative co-assembly

Pyr-S/Fmoc-S forms truncated fibres on the order of 2 μm in length (Fig. 6.8(d)), whereas individually Pyr-S showed much longer fibres; at least on the scale of the recorded AFM images. This is hypothesized to be a consequence of Fmoc-S rich areas, with a tendency to form spherical aggregates, capping the ends of the Pyr-S dominated worm-like micelle structures. This model is consistent with CD that previously showed marginally less intense positive Pyr-S peaks, which could indicate a shorter 1D nanoscale structure. Hence, this co-assembly arrangement could be considered to be disruptive in terms of the overall network morphology. If accurate, this model is also an example of the effective segregation of components within these size limited, supramolecular structures, which would account somewhat for the preserved Pyr-S fluorescence excimer redshift. Such an assembly mechanism makes sense within the context of these serine surfactants whose self-assembly is most strongly influenced by aromatic stacking, since no scope for β-sheet type organization exists.

In contrast, Pyr-YL/Fmoc-YL shows the presence of dense fibrous networks. This demonstrates again that co-assembly can work if there is sufficient commonality between constituents, such that they adhere to similar modes of supramolecular assembly, and are thus able to accommodate one another to an extent. The observation of only a single population of morphologies implies that Pyr-YL and Fmoc-YL do form mixed cooperative fibres as opposed to an interpenetrating network - this was also previously suggested by spectroscopic evidence.

6.3.5.5 Disruptive co-assembly

In terms of fibre morphology, the Pyr-YL/Pyr-S co-assembly system appears to exhibit the intermittent fibrous and disordered regions which previously characterized the Pyr-S surfactant (Fig. 6.8(e)). This further supports the notion that Pyr-S is acting to perturb the standard β-sheet type H-bonding and fibre formation associated with Pyr-YL alone. The related Fmoc-YL/Fmoc-S system shows fibres with a consistent tendency to form into spiral structures. This also hints at the idea that the Fmoc-S is having a disruptive effect on the 1D Fmoc-YL structure. Thus for each of the proposed co-assembly systems possessing components with a common aromatic moiety, AFM images suggest that the inclusion of an intercalating surfactant does have an influence on supramolecular structure and the observed fibre morphology; a result consistent with the disruptive model (Fig. 6.1(c), 6.3(e)).

6.3.6 Rheology and gelation results

Rheology and gelation results are presented for each of the systems in turn. Note that the pH values reported for each system in Table 6.1 apply throughout the text. All systems were initially prepared in 100 mM phosphate buffer at pH 7.3, before the pH was lowered *via* the addition of 1 M HCl if required for gelation (Fmoc-S excepted) as determined by vial inversion test. Hence, rheological properties can only be meaningfully compared for systems at the same pH – i.e. lower pH systems were solutions at pH 7.3 value. However, we believe that over our limited 7.3 to 5.0 pH range, the reported supramolecular structures are broadly representative – with the pH influencing surface charge and the likelihood of forming a continuous hydrogel network as opposed to isolated fibres in solution.[55] Also note that, at frequencies greater than the stable ranges reported in Table 6.1, the extrusion of water and the consequent breakdown of the hydrogel network and concentration of the sample, generally results in a sharp increase in the respective moduli values (Appendices, section A.3.3).[5]

6.3.6.1 Gelators

In terms of their material properties (Table 6.1 and Appendices, section A.3.3), both Fmoc-YL and Pyr-YL demonstrate gelation at a physiological pH. The rheological properties the Pyr-YL system demonstrates a relatively low[85,12,5] G' of approximately 190 Pa. In addition, Pyr-YL also shows a relatively large stable frequency sweep range – where elastic (G') and viscous (G") moduli remain largely constant. Comparing rheological properties, it becomes clear that Fmoc-YL does not form a particularly robust gel, as it exhibits a small elastic (G') to viscous (G") modulus ratio. These moduli values differ from some previously reported Fmoc-YL gels with G' sometimes in excess of 1000 Pa, however this parameter is found to vary greatly depending upon salts, pH, concentration, and the precise method of preparation employed.[86,54] Fmoc-YL also exhibits a more brief stable frequency sweep range. In addition, the fact that G'' > G' at some higher frequencies (Appendices, section A.3.3) indicates that in these instances gel network is unable to recover on this timescale – as also evidenced by the relatively large phase angle associated with Fmoc-YL and similarly affected systems (Appendices, section A.3.3). Furthermore, it can also be observed that the Pyr-YL more readily recovers its ability to withstand vial inversion, simply after the mechanical stresses associated with transferring samples using a spatula. So it can be surmised that Fmoc-YL forms a more rigid, but brittle hydrogel. The increased aromaticity of Pyr-YL is thought to be responsible for the more robust mechanical properties and recovery of Pyr-YL compared to the Fmoc-YL hydrogelator system.

6.3.6.2 Surfactants

Fmoc-S forms a solution, and as such no gelation pH or rheology data is applicable (Table 6.1 and Appendices, section A.3.3). Pyr-S forms gels, but at a more acidic pH than Pyr-YL; a lower gelation pH implies that greater protonation is needed to facilitate self-assembly and consequently increased interconnectivity between fibres. This makes sense within the context of a worm-like micelle model, whose carboxylates at the aqueous interface will preclude further aggregation and effective gelation - unless a sufficient number are protonated, or divalent cations are used for cross-linking.[56] In terms of its rheological properties, Pyr-S has a relatively low elastic modulus, and a short stable frequency sweep range. These are unsurprising observations, since evidently Pyr-S lacks the additional structural integrity afforded by β-sheet type H-bonding formation. Hence, Pyr-S is believed to follow an entirely different self-assembly mode from the related Pyr-YL gelator.

6.3.6.3 Orthogonal co-assembly

In terms of material properties (Table 6.1 and Appendices, section A.3.3), Fmoc-YL/Pyr-S

Table 6.1 Gelation pH and Rheology Data

	System	pH (Gel/Sol)	G' / Pa	G'' / Pa	Stable Freq / Hz
Gelators	Pyr-YL	7.3 (Gel)	190 ± 30	45 ± 20	0.1-15.8
	Fmoc-YL	7.3 (Gel)	390 ± 70	190 ± 20	0.1-5.0
Surfactants	Pyr-S	6.5 (Gel)*	58 ± 5	8 ± 3	0.1-2.5
	Fmoc-S	7.3 (Sol)	-	-	-
Orthogonal	Pyr-YL/Fmoc-S	7.3 (Gel)	160 ± 20	30 ± 14	0.1-15.8
	Fmoc-YL/Pyr-S	7.3 (Gel)	450 ± 100	70 ± 20	0.1-15.8
Cooperative	Pyr-YL/Fmoc-YL	7.3 (Gel)	27 ± 5	10 ± 4	0.1-1.6
	Pyr-S/Fmoc-S	5.0 (Gel)*	980 ± 230	200 ± 180	0.1-31.6
Disruptive	Pyr-YL/Pyr-S	6.0 (Gel)*	290 ± 27	60 ± 15	0.1-15.8
	Fmoc-YL/Fmoc-S	7.0 (Gel)*	26 ± 3	5 ± 0.6	0.1-2.0

*These systems are solutions at pH 7.3 as defined by vial inversion test. **Quoted moduli values are averages over the stable frequency range.

and Pyr-YL/Fmoc-S both gel under physiological pH conditions, as did their individual Fmoc-YL and Pyr-YL hydrogels. Furthermore, Pyr-YL and the co-assembled Pyr-YL/Fmoc-S system display very similar rheological properties. The co-assembly system shows the characteristically large stable frequency sweep range and the elastic (G') and viscous (G'') moduli remain largely consistent with those of the Pyr-YL material. Hence, Fmoc-S does not appear to interfere with Pyr-YL's material properties; this would be expected if the proposed orthogonal mechanism is accurate. Co-assembly between Fmoc-YL and Pyr-S appears to result in relatively robust mechanical properties, exceeding both Fmoc-YL and Pyr-YL in the magnitude and ratio of the respective moduli, and equalling the stable frequency sweep range of Pyr-YL. This observed change in the mechanical properties of Fmoc-YL, also reflects the apparent morphological changes seen by AFM (Fig. 6.8(a,c)). The pH and rheological results suggest that robust co-assembly is facilitated when both aromatic and peptide components are sufficiently different such that segregation between components is able to occur. This prevents mismatches from occurring between the β-sheet type H-bonding or indeed the aromatic stacking interactions, which are both crucial to stable gel formation. Ultimately, this is also a vital prerequisite for the orthogonal co-assembly model, where the intermingling of components is undesirable.

6.3.6.4 Cooperative co-assembly

Pyr-S/Fmoc-S is only capable of gelation at pH 5, which is over a pH unit lower than the individual Pyr-S worm-like micelle hydrogel (Table 6.1 and Appendices, section A.3.3). This illustrates the impact of the previously observed (by AFM) fibre truncation upon the overall network integrity of the hydrogel, which now requires substantial protonation and interconnectivity for effective gelation. In terms of rheology, the Pyr-S/Fmoc-S hydrogel is surprising robust when comparing its stable frequency sweep range and moduli magnitude to the other systems. However, the low gelation pH requirement indicates that of all the systems studied, Pyr-S/Fmoc-S has the least propensity for gelation; to reiterate, Pyr-S/Fmoc-S is a solution at pH 7.3 value. For the co-gelators, the relative weakness of the Fmoc-YL hydrogel is also inherited by the co-assembled Pyr-YL/Fmoc-YL system which also demonstrates a brief stable frequency sweep range. In addition, we also observe low elastic and viscous moduli accompanied by a low moduli ratio; this suggests that the mixed system is significantly less rigid and less robust than the individual Fmoc-YL component alone. This compromising of Pyr-YL's mechanical properties suggests – in agreement with what was observed by fluorescence and CD - that complete segregation of Pyr-YL and Fmoc-YL fibres doesn't occur. Instead Fmoc-YL is thought to hinder Pyr-YL assembly via effective incorporation into the β-sheet type H-bonding arrangement, but is then subsequently unable to fulfil pyrene's aromatic stacking requirements. The discrete pyrene and fluorene aromatic assemblies are believed to result in an overall structure which contains aromatic stacking mismatches, resulting in more structural "defects" and consequently weaker fibres. Ultimately, the mixed cooperative supramolecular structure compromises the mechanical properties of the network at the macroscale.

6.3.6.5 Disruptive co-assembly

The hydrogelation of Pyr-YL/Pyr-S only occurs at pH 6, which is significantly lower than the physiological Pyr-YL hydrogel (Table 6.1 and Appendices, section A.3.3). If Pyr-S was merely a spectator, then the gelation pH of the mixed system would not be expected to change; this is strong evidence that Pyr-S is incorporating itself into the Pyr-YL structure. A lower gelation pH implies that greater protonation and consequently increased interconnectivity between fibres is required for effective gelation. We hypothesize that strong pyrene stacking interactions imply that effective segregation doesn't occur between Pyr-YL and Pyr-S molecules in the co-assembly state. Consequently, Pyr-S intercalates the Pyr-YL aromatic stacked, H-bonding reinforced, fibrous assembly (Fig. 6.3(e)). Owing to serine's inability to form a β-sheet type arrangement, this has the effect of compromising the Pyr-YL structure; in a process analogous to having missing rungs in a ladder. In addition, the

relatively weak rheological properties of the Fmoc-YL hydrogel appear to be compounded by co-assembly with Fmoc-S, which results in over an order of magnitude drop in the respective moduli. Furthermore, the stable frequency sweep range decreases. We hypothesize that the Fmoc-YL gel is weakened by Fmoc-S co-assembly in much the same way as the Pyr-YL/Pyr-S system: fluorene stacking interactions between components result in the YL β-sheet type structure being distorted by the serine residues. These observations indicate that disruptive co-assembly (Fig. 6.1(c), 6.3(e)) has a profound impact on the structural integrity of these materials. A conclusion that is also supported by the apparently disrupted FTIR and CD spectra. Hence, these systems represent a failure of the co-assembly components to either structurally segregate, or accommodate one another by effectively following a common self-assembly mechanism.

6.4 Conclusions

In summary, based on spectroscopic, morphological, and mechanical properties, we propose three distinct co-assembly models. Cooperative co-assembly occurs between the molecules in this study that share their propensity to adopt the β-sheet type H-bonding mode of supramolecular self-assembly. In this case, either a mixed serine micellar model or a mixed YL aromatic stacked, H-bonding reinforced structure is adhered to. Furthermore, by tailoring the constituents ratio in the Pyr-S/Fmoc-S system, it is anticipated control over micellar dimensions is possible. Disruptive co-assembly is proposed to take place with systems that only share the same aromatic moiety. This results in substantial intercalation of the serine constituent, which ultimately compromises the structural integrity of the YL β-sheet type arrangement. Finally, attaining effective structural segregation between hydrogel components is a prerequisite for the orthogonal co-assembly model. This is only readily achievable if the aromatic and peptide segments of each component are sufficiently different such that partial incorporation and disruption of their respective supramolecular structures does not occur. The orthogonal co-assembly mechanism is potentially useful for cell culture applications that require the chemical functionalisation of fibre surfaces, without affecting the material properties of an existing gelator system. The other co-assembly paradigms could also find utility; however, the disruption of the underlying gelator structure will likely make tailoring gels for a given application more complex, with several variables to consider. In general, upon substituting Fmoc for pyrene there is an increase in the aromatic stacking contribution in terms of the factors driving the aromatic dipeptide amphiphile assembly. Consequently, the pyrene based materials have a greater potential for exhibiting electro-conductive properties. Overall this study provides new insights into the design of co-

assembly structures based upon aromatic peptide amphiphiles. The rules of thumb that result provide a potentially useful design paradigm, which may allow the formation of fibrous materials furnished with (bio)chemical functionality. In more general self-assembly terms, orthogonal assembly or the phase separation of nanoscale structures is facilitated by dissimilar co-assembly constituents; this is analogous to the bulk phase separation that can occur between (for example) polar and non-polar solvents.

6.5 References

1. D. E. Discher, D. J. Mooney, and P. W. Zandstra, *Science*, 2009, **324**, 1673–1677.
2. J. H. Collier, *Soft Matter*, 2008, **4**, 2310–2315.
3. N. M. Sangeetha and U. Maitra, *Chem. Soc. Rev.*, 2005, **34**, 821–836.
4. J. K. Oh, R. Drumright, D. J. Siegwart, and K. Matyjaszewski, *Prog. Polym. Sci.*, 2008, **33**, 448–477.
5. V. Jayawarna, S. M. Richardson, A. R. Hirst, N. W. Hodson, A. Saiani, J. E. Gough, and R. V. Ulijn, *Acta Biomater.*, 2009, **5**, 934–943.
6. O. Z. Fisher, A. Khademhosseini, R. Langer, and N. A. Peppas, *Acc. Chem. Res.*, 2010, **43**, 419–428.
7. H. X. Xu, A. K. Das, M. Horie, M. S. Shaik, A. M. Smith, Y. Luo, X. F. Lu, R. Collins, S. Y. Liem, A. M. Song, P. L. A. Popelier, M. L. Turner, P. Xiao, I. A. Kinloch, and R. V. Ulijn, *Nanoscale*, 2010, **2**, 960–966.
8. L. Zang, Y. K. Che, and J. S. Moore, *Acc. Chem. Res.*, 2008, **41**, 1596–1608.
9. S. R. Diegelmann, J. M. Gorham, and J. D. Tovar, *J. Am. Chem. Soc.*, 2008, **130**, 13840–13841.
10. W.-W. Tsai, I. D. Tevis, A. S. Tayi, H. Cui, and S. I. Stupp, *J. Phys. Chem. B.*, 2010, **114**, 14778–14786.
11. Y. Yamauchi, M. Yoshizawa, and M. Fujita, *J. Am. Chem. Soc.*, 2008, **130**, 5832–5833.
12. E. T. Pashuck, H. G. Cui, and S. I. Stupp, *J. Am. Chem. Soc.*, 2010, **132**, 6041–6046.
13. M. A. Greenfield, J. R. Hoffman, M. O. de la Cruz, and S. I. Stupp, *Langmuir*, 2010, **26**, 3641–3647.
14. M. J. Dalby, *Med. Eng. Phys.*, 2005, **27**, 730–742.
15. M. J. López-Bosque, E. Tejeda-Montes, M. Cazorla, J. Linacero, Y. Atienza, K. H. Smith, A. Lladó, J. Colombelli, E. Engel, and A. Mata, *Nanotechnology*, 2013, **24**, 255305.
16. E. Tejeda-Montes, K. H. Smith, M. Poch, M. J. López-Bosque, L. Martín, M. Alonso, E. Engel, and A. Mata, *Acta Biomater.*, 2012, **8**, 998–1009.
17. S. Al-Haque, J. W. Miklas, N. Feric, L. L. Y. Chiu, W. L. K. Chen, C. A. Simmons, and M. Radisic, *Macromol. Biosci.*, 2012, **12**, 1342–1353.
18. M. J. Webber, J. Tongers, M. A. Renault, J. G. Roncalli, D. W. Losordo, and S. I. Stupp, *Acta Biomater.*, 2010, **6**, 3–11.
19. A. L. Prieto, G. M. Edelman, and K. L. Crossin, *Proc. Natl. Acad. Sci. U. S. A.*, 1993, **90**, 10154 –10158.
20. D. N. Woolfson and Z. N. Mahmoud, *Chem. Soc. Rev.*, 2010, **39**, 3464–3479.
21. S. Brahim and A. Guiseppi-Elie, *Electroanalysis*, 2005, **17**, 556–570.
22. A. R. Hirst and D. K. Smith, *Chem.–Eur. J.*, 2005, **11**, 5496–5508.
23. W. Edwards and D. K. Smith, *J. Am. Chem. Soc.*, 2014, **136**, 1116–1124.
24. M. M. Smith, W. Edwards, and D. K. Smith, *Chem. Sci.*, 2013, **4**, 671–676.
25. J. G. Hardy, A. R. Hirst, and D. K. Smith, *Soft Matter*, 2012, **8**, 3399–3406.
26. W. Edwards and D. K. Smith, *J. Am. Chem. Soc.*, 2013, **135**, 5911–5920.

27. M. Zhou, A. M. Smith, A. K. Das, N. W. Hodson, R. F. Collins, R. V. Ulijn, and J. E. Gough, *Biomaterials*, 2009, **30**, 2523–2530.
28. K. V. Rao and S. J. George, *Chem.–Eur. J.*, 2012, **18**, 14286–14291.
29. C. Wang, Y. Guo, Z. Wang, and X. Zhang, *Langmuir*, 2010, **26**, 14509–14511.
30. J. R. Moffat and D. K. Smith, *Chem. Commun.*, 2008, 2248–2250.
31. H. A. Behanna, K. Rajangam, and S. I. Stupp, *J. Am. Chem. Soc.*, 2007, **129**, 321–327.
32. J. R. Moffat and D. K. Smith, *Chem. Commun.*, 2009, 316–318.
33. A. Heeres, C. van der Pol, M. Stuart, A. Friggeri, B. L. Feringa, and J. van Esch, *J. Am. Chem. Soc.*, 2003, **125**, 14252–14253.
34. K. L. Morris, L. Chen, J. Raeburn, O. R. Sellick, P. Cotanda, A. Paul, P. C. Griffiths, S. M. King, R. K. O'Reilly, L. C. Serpell, and D. J. Adams, *Nat. Commun.*, 2013, **4**, 1480–1485.
35. A. Brizard, M. Stuart, K. van Bommel, A. Friggeri, M. de Jong, and J. van Esch, *Angew. Chem., Int. Ed.*, 2008, **47**, 2063–2066.
36. M. M. Smith and D. K. Smith, *Soft Matter*, 2011, **7**, 4856–4860.
37. A. C. Coleman, J. M. Beierle, M. C. A. Stuart, B. Maciá, G. Caroli, J. T. Mika, D. J. van Dijken, J. Chen, W. R. Browne, and B. L. Feringa, *Nat. Nanotechnol.*, 2011, **6**, 547–552.
38. J. F. Stoddart, *Angew. Chem., Int. Ed.*, 2012, **51**, 12902–12903.
39. B. Adhikari, J. Nanda, and A. Banerjee, *Chem.–Eur. J.*, 2011, **17**, 11488–11496.
40. N. Yan, Z. Xu, K. K. Diehn, S. R. Raghavan, Y. Fang, and R. G. Weiss, *Langmuir*, 2013, **29**, 793–805.
41. M. O. Guler, R. C. Claussen, and S. I. Stupp, *J. Mater. Chem.*, 2005, **15**, 4507–4512.
42. R. Orbach, I. Mironi-Harpaz, L. Adler-Abramovich, E. Mossou, E. P. Mitchell, V. T. Forsyth, E. Gazit, and D. Seliktar, *Langmuir*, 2012, **28**, 2015–2022.
43. G. Cheng, V. Castelletto, C. M. Moulton, G. E. Newby, and I. W. Hamley, *Langmuir*, 2010, **26**, 4990–4998.
44. G. Cheng, V. Castelletto, R. R. Jones, C. J. Connon, and I. W. Hamley, *Soft Matter*, 2011, **7**, 1326–1333.
45. D. J. Adams and P. D. Topham, *Soft Matter*, 2010, **6**, 3707–3721.
46. D. J. Adams, L. M. Mullen, M. Berta, L. Chen, and W. J. Frith, *Soft Matter*, 2010, **6**, 1971–1980.
47. M. Hughes, P. W. J. M. Frederix, J. Raeburn, L. S. Birchall, J. Sadownik, F. C. Coomer, I.-H. Lin, E. J. Cussen, N. T. Hunt, T. Tuttle, S. J. Webb, D. J. Adams, and R. V. Ulijn, *Soft Matter*, 2012, **8**, 5595–5602.
48. Y. Gao, F. Zhao, Q. Wang, Y. Zhang, and B. Xu, *Chem. Soc. Rev.*, 2010, **39**, 3425–3433.
49. Z. Yang, L. Wang, J. Wang, P. Gao, and B. Xu, *J. Mater. Chem.*, 2010, **20**, 2128–2132.
50. D. M. Ryan and B. L. Nilsson, *Polym. Chem.*, 2012, **3**, 18–33.
51. D. M. Ryan, S. B. Anderson, and B. L. Nilsson, *Soft Matter*, 2010, **6**, 3220–3231.
52. D. M. Ryan, T. M. Doran, S. B. Anderson, and B. L. Nilsson, *Langmuir*, 2011, **27**, 4029–4039.
53. A. R. Hirst, S. Roy, M. Arora, A. K. Das, N. Hodson, P. Murray, S. Marshall, N. Javid, J. Sefcik, J. Boekhoven, J. H. van Esch, S. Santabarbara, N. T. Hunt, and R. V. Ulijn, *Nat. Chem.*, 2010, **2**, 1089–1094.
54. S. Roy, N. Javid, J. Sefcik, P. J. Halling, and R. V. Ulijn, *Langmuir*, 2012, **28**, 16664–16670.
55. C. Tang, A. M. Smith, R. F. Collins, R. V. Ulijn, and A. Saiani, *Langmuir*, 2009, **25**, 9447–9453.
56. L. Chen, G. Pont, K. Morris, G. Lotze, A. Squires, L. C. Serpell, and D. J. Adams, *Chem. Commun.*, 2011, **47**, 12071–12073.
57. A. M. Smith, R. J. Williams, C. Tang, P. Coppo, R. F. Collins, M. L. Turner, A. Saiani, and R. V. Ulijn, *Adv. Mater.*, 2008, **20**, 37–38.
58. S. Debnath, A. Shome, D. Das, and P. K. Das, *J. Phys. Chem. B*, 2010, **114**, 4407–4415.

59. J. Nanda and A. Banerjee, *Soft Matter*, 2012, **8**, 3380–3386.
60. B. Adhikari, J. Nanda, and A. Banerjee, *Soft Matter*, 2011, **7**, 8913–8922.
61. J. Raeburn, G. Pont, L. Chen, Y. Cesbron, R. Lévy, and D. J. Adams, *Soft Matter*, 2012, **8**, 1168–1174.
62. D. J. Welsh, P. Posocco, S. Pricl, and D. K. Smith, *Org. Biomol. Chem.*, 2013, **11**, 3177–3186.
63. W. Nuansing, A. Rebollo, J. M. Mercero, J. Zuñiga, and A. M. Bittner, *J. Raman Spectrosc.*, 2012, **43**, 1397–1406.
64. S. Fleming, P. W. J. M. Frederix, I. Ramos-Sasselli, N. Hunt, R. V. Ulijn, and T. Tuttle, *Langmuir*, 2013, **29**, 9510–9515.
65. J. W. Sadownik, J. Leckie, and R. V. Ulijn, *Chem. Commun.*, 2010, **47**, 728–730.
66. D. L. Horrocks and W. G. Brown, *Chem. Phys. Lett.*, 1970, **5**, 117–119.
67. S. Roy and A. Banerjee, *Soft Matter*, 2011, **7**, 5300–5308.
68. E. Miller and D. Jóźwik-Styczyńska, *Spectrochim. Acta, Part A*, 2009, **72**, 312–321.
69. E. C. Buruiana, T. Buruiana, and L. Hahui, *J. Photochem. Photobiol., A*, 2007, **189**, 65–72.
70. G. Basu Ray, I. Chakraborty, and S. P. Moulik, *J. Colloid Interface Sci.*, 2006, **294**, 248–254.
71. X. Yan, Y. Cui, Q. He, K. Wang, J. Li, W. Mu, B. Wang, and Z. Ou-yang, *Chemistry – A European Journal*, 2008, **14**, 5974–5980.
72. K. J. Channon, G. L. Devlin, and C. E. MacPhee, *J. Am. Chem. Soc.*, 2009, **131**, 12520–12521.
73. L. Chen, S. Revel, K. Morris, and D. J. Adams, *Chem. Commun.*, 2010, **46**, 4267–4269.
74. A. B. P. Gursharan Bains, *Molecules*, 2011, **16**, 7909–7935.
75. Z. Yang, H. Gu, D. Fu, P. Gao, J. K. Lam, and B. Xu, *Adv. Mater.*, 2004, **16**, 1440–1444.
76. H. K. Kang, D. E. Kang, B. H. Boo, S. J. Yoo, J. K. Lee, and E. C. Lim, *J. Phys. Chem. A*, 2005, **109**, 6799–6804.
77. Z. Yang, H. Gu, Y. Zhang, L. Wang, and B. Xu, *Chem. Commun.*, 2004, 208–209.
78. L. Chen, T. O. McDonald, and D. J. Adams, *RSC Adv.*, 2013, **3**, 8714–8720.
79. C. Tang, R. V. Ulijn, and A. Saiani, *Eur. Phys. J. E*, 2013, **36**, 111–121.
80. S. Marchesan, C. D. Easton, F. Kushkaki, L. Waddington, and P. G. Hartley, *Chem. Commun.*, 2012, **48**, 2195–2197.
81. M. L. Ma, Y. Kuang, Y. Gao, Y. Zhang, P. Gao, and B. Xu, *J. Am. Chem. Soc.*, 2010, **132**, 2719–2728.
82. N. J. Greenfield, *Nat. Protoc.*, 2006, **1**, 2876–2890.
83. S. Bhattacharjee, G. Tóth, S. Lovas, and J. D. Hirst, *J. Phys. Chem. B*, 2003, **107**, 8682–8688.
84. E. T. Pashuck and S. I. Stupp, *J. Am. Chem. Soc.*, 2010, **132**, 8819–8820.
85. J. K. Kretsinger, L. A. Haines, B. Ozbas, D. J. Pochan, and J. P. Schneider, *Biomaterials*, 2005, **26**, 5177–5186.
86. S. Roy, N. Javid, P. W. J. M. Frederix, D. A. Lamprou, A. J. Urquhart, N. T. Hunt, P. J. Halling, and R. V. Ulijn, *Chem.–Eur. J.*, 2012, **18**, 11723–11731.

– Chapter 7 –

Self-assembled hydrogels: coated micro electrode array towards neuron device interfaces

7.1 Abstract

Within the context of micro electrode arrays (MEAs) used for the electrical characterisation of neurons; functionalising said electrode surfaces with hydrogel coatings is potentially a useful means of improving cell adhesion and consequently electrical signal fidelity. To this end, the anodic oxidation of hydroquinone is utilised as the basis for an electrochemical hydrogel deposition process that has been demonstrated in the bulk with the Fmoc-F, Pyr-YL, and Pyr-YL/Fmoc-S systems. Similarly the Pyr-YL coating has been successfully applied to MEA devices, as confirmed by fluorescence microscopy. Preliminary MEA impedance measurements show that the hydrogel coated electrodes exhibit impedances similar to those of the uncoated device, but thus far demonstrate higher impedances than electrodes that have been electroplated with platinum. Hence, further work is required in future in order to optimise the coating process and lower corresponding impedances, to allow for eventual application as a neuron device interface.

7.2 Introduction

The electronic stimulation and/or monitoring of neurons has many important laboratory applications, such as gaining an increased understanding of network development or neuron degeneration processes.[1–3] Micro electrode arrays (MEAs) provide a useful device for the study of neurons, whereby the electrodes are approximately on the same scale as the cells (e.g. tens of microns), such that an individual neuron can in principle by addressed by one or more electrodes.[4,5] The electrodes are normally ITO based, but are subsequently electroplated with a relatively inert metal such as platinum in order to provide a conductive medium with a high surface area for neuronal contact, thus ensuring an efficacious signal-to-noise ratio. However, the use of such hard electrode substrates is in no way representative of the native extracellular environment of neurons.[6] In this respect, coating the electrode surfaces with a hydrogel could potentially provide a relatively biocompatible device interface, and encourage neuron-device interaction – thus improving signal fidelity.

Hydrogels are composed of an extensive 3D array capable of retaining a large quantity (e.g. ~99%) of water within the structure; in this respect hydrogels can be considered as simple mimics of the extra cellular matrix.[7,8] In addition, the presence of substantial

supramolecular aromatic stacking interactions, may lend itself well to the development of soft optoelectronic devices.[9–14] As discussed in chapter 6, the orthogonal co-assembly of Pyr-YL/Fmoc-S could be of utility in offering a potentially conductive pyrene stacked core, with biocompatible hydrophilic serine functionality at the surface. This Pyr-YL/Fmoc-S co-assembly motif is proposed to be of interest within the context of hydrogel coated MEA devices for the neuron device interface. However, while it is also possible to covalently functionalise surfaces with biocompatible peptidic functionality,[15,16] selectively coating a MEA surface with self-assembled peptide-based hydrogels is a potential challenge. Nevertheless, the formation of aromatic peptide amphiphile based supramolecular materials is usually reversible with changes in pH. Hence, the localised surface gelation of aromatic peptide amphiphile systems can be readily achieved by for example coupling to an electrochemical oxidative process that releases protons – inducing a local decrease in pH and gelation at the electrode surface.[17–19]

Hence, we herein report on work towards the establishment of a protocol for coating MEA surfaces with co-assembled aromatic peptide amphiphile hydrogels; composed of a potentially conductive fibrous core with biocompatible functionality at the surface. In addition, the efficacy of the coated MEA is assessed in terms of its impedance, particularly at 1 kHz, which is relevant for working towards potential neuronal applications in the future.[20]

Note that at the time of writing, the co-assembly coating and impedance optimisation work is at a preliminary stage. Additionally, electro-conducting polymers including polyacetylene have been shown to require doping with additives such as iodine, in order to achieve substantial levels of electro-conductivity.[21] Similarly, the conductivity of iodine can be increased *via* the addition of aromatic compounds such as naphthalene and pyrene.[22] Furthermore, the conductivity of supramolecular organogels based on readily oxidised tetrathiafulvalene derivatives is also dependant upon doping with iodine in order to yield a mixed valence state.[23,24] Hence, it is likely that significant levels of conductivity are attainable with the current hydrogel system only after iodine doping and/or the addition of more readily oxidised (and intercalated[25,26]) aromatic additives.

7.3 Results and discussion

Pyr-YL (**P4YL**) and the Pyr-YL/Fmoc-S systems (Fig. 7.1(a)) were selected for this study on account of their ability to form an orthogonal core-shell self-assembled structure (Fig. 7.1(b), see chapter 6), whereby Pyr-YL provides a fibrous core and Fmoc-S a hydrophilic biocompatible coating at the fibre surface.[8,27] Here, the Pyr-YL forms an antiparallel H-bonding arrangement, interlocked via extensive pyrenyl stacking interactions along the fibre

axis (Fig. 7.1(c)). Hence, this supramolecular motif provides some degree of electro-conductivity as previously demonstrated for Fmoc-LLL,[9] where the increased aromaticity of pyrene compared to fluorene should improve this effect. In addition, the nanoscale topography generally associated with aromatic peptide amphiphile hydrogels should provide a high surface area.

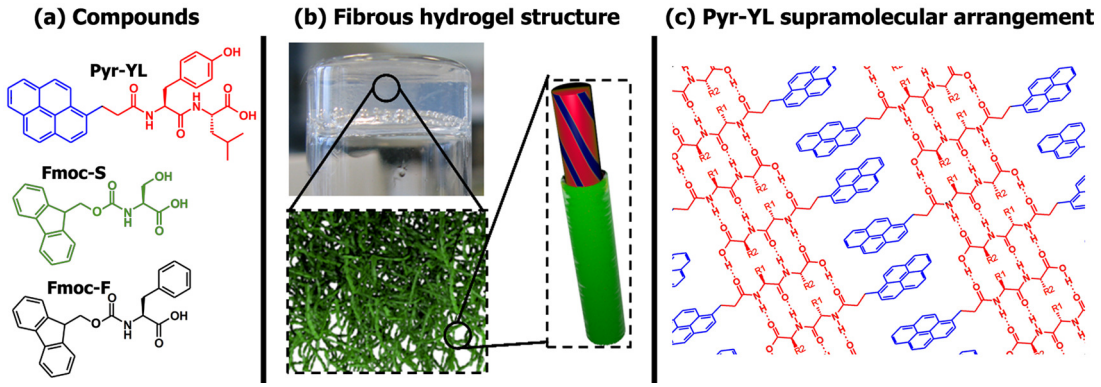

Figure 7.1 (a) Compounds utilised in coating study; (b) Nanoscale hydrogel structure and orthogonal summary, where green represents the Fmoc-S coating over the; (c) Pyr-YL interlocked antiparallel supramolecular fibrous structure.

7.3.1 Coating optimisation

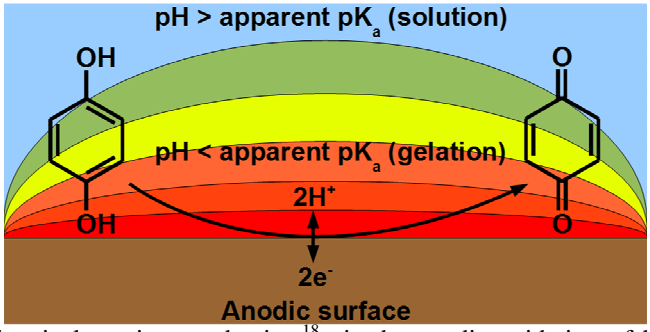

Figure 7.2 Electrochemical coating mechanism[18] via the anodic oxidation of hydroquinone, which produces a local pH drop and gelation at the electrode surface.

Due to the influence of pH upon the assembly of aromatic peptide amphiphiles,[28–32] the self-assembly and gelation of these materials can be coupled to any chemical process that releases protons. For example, self-assembly can be achieved *via* an electrochemically induced change in the local pH; effecting gelation of Fmoc-LG at pH values less than 4.[18] Here, the local pH change was brought about *via* the anodic two-electron oxidation of hydroquinone to 1,4-benzoquinone, thus releasing two protons at the surface of the gold electrode (Fig. 7.2). Although a pH drop could also be induced in the absence of hydroquinone, this inevitably requires a greater potential difference and results in potential degradation of the electrode surface. This electro-deposition process produces a thin layer of the desired hydrogel, which can only form within the local low pH region. The membrane thickness can be controlled to some extent by altering the time and magnitude of the applied

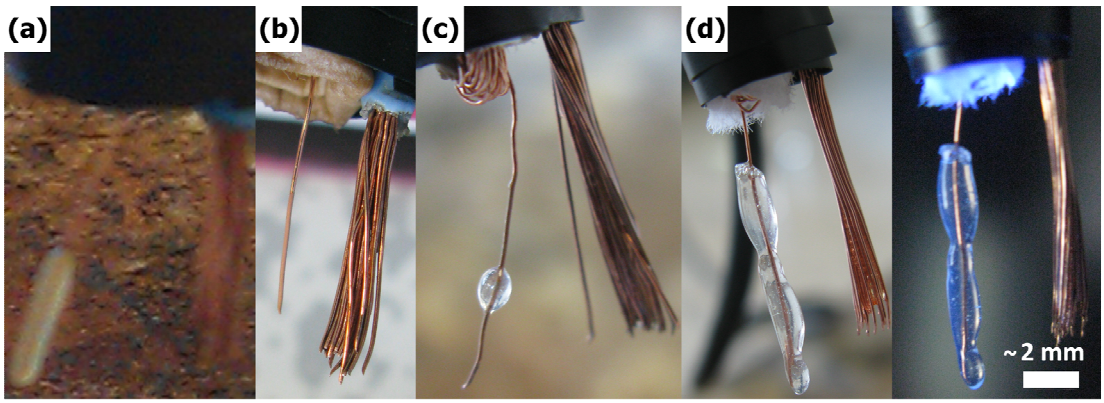

Figure 7.3 Bulk coating photographs corresponding to conditions summarised in Table. 1

Table 7.1: Coating conditions utilised

	(a)	(b)	(c)	(d)
Coating	**Yes**	**No**	**Partial**	**Yes**
Gelator	Fmoc-F	Pyr-YL	Pyr-YL	Pyr-YL
Solution pH	8.0	8.0	6.7	6.7
Current density	100 μA cm^{-2}	100 μA cm^{-2}	300 μA cm^{-2}	4500 μA cm^{-2}
NaCl concentration	100 mM	100 mM	N/A	N/A
***PO_4 concentration**	N/A	N/A	20 mM	10 mM

*Sodium phosphate buffer

current. In addition, this procedure can be reversed with dissolution of the hydrogel membrane when a reversed bias is applied. Similar results have also been reported for the electro-deposition of Fmoc-F,[17] indicating the generality of this process.

Hence, using Fmoc-F as a model system, bulk hydrogel coatings could be applied to copper wire using similar conditions to those reported previously.[17] However, when an identical methodology was applied to Pyr-YL, no coating was observed. Various gelator and ion concentrations, initial pH values, and current densities were then utilised in an attempt to rationalise this initial unexpected negative result (Fig. 7.3, Table 7.1). It was noted that the addition of sodium phosphate buffer ions proved vital to achieving a Pyr-YL coating, whereas in comparison NaCl was ineffective – thus electrostatic screening alone cannot account for this. This observation can be related to the Hofmeister anion sequence, where phosphate is classed as a kosmotrope and can encourage H-bonding with water. This effect has been previously found to improve the mechanical properties of aromatic peptide amphiphile hydrogels,[33,34] and hence is likely responsible for improved adhesion to the electrode surface. However, the addition of phosphate also buffers against the very pH change necessary for local hydrogelation. So in order to achieve a consistent coating, a compromise must be reached between a relatively low phosphate buffer concentration (10 mM), and a relatively high current density (4.5 mA cm^{-2}).

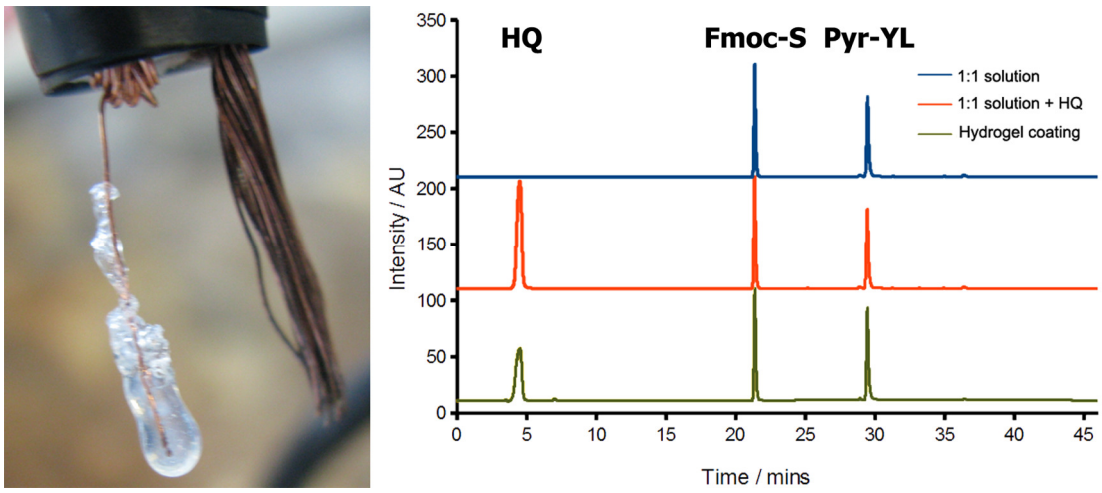

Figure 7.4 Pyr-YL/Fmoc-S coating and HPLC verification of compositional consistency throughout coating procedure.

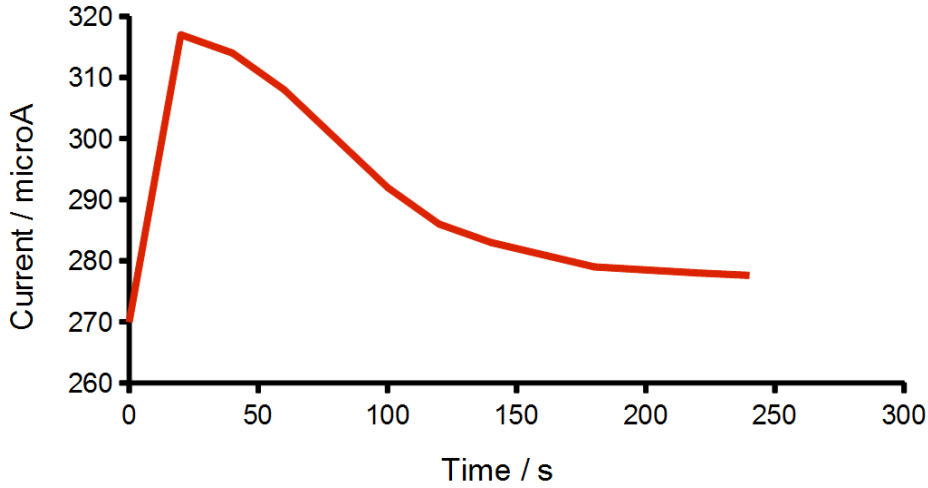

Figure 7.5 Current timecourse for Pyr-YL bulk coating procedure.

Identical conditions can also be applied to achieve a Pyr-YL/Fmoc-S coating. Here HPLC analysis (of a scraped off Pyr-YL/Fmoc-S coating) was used to confirm that the composition of the pregelation solution - or the ratio between Pyr-YL and Fmoc-S - is essentially retained in the final hydrogel coating (Fig. 7.4). In addition all deposited Pyr-YL based gels were found to be stable in PBS (pH 7.4) – indicating their suitability for use under physiological conditions.

The kinetics of the coating process were also assessed by monitoring the applied current over time (Fig. 7.5). After an initial rise in current thought to be related to multimeter response limitations, the current was observed to decrease over time before reaching a plateau, corresponding to an increase in the DC resistance as the hydrogel layer increased in depth before stabilising. This is believed to be a consequence of both the phosphate buffer limiting the influence of the local pH gradient, and the hydrogel coating inhibiting diffusion and conductivity, such that hydrogel growth ceases. It is believed that increasing the applied

current could overcome this effect, however given the preliminary nature of the bulk coating study, and the limited level of control offered by the experimental setup, this was not attempted.

7.3.2 MEA coating

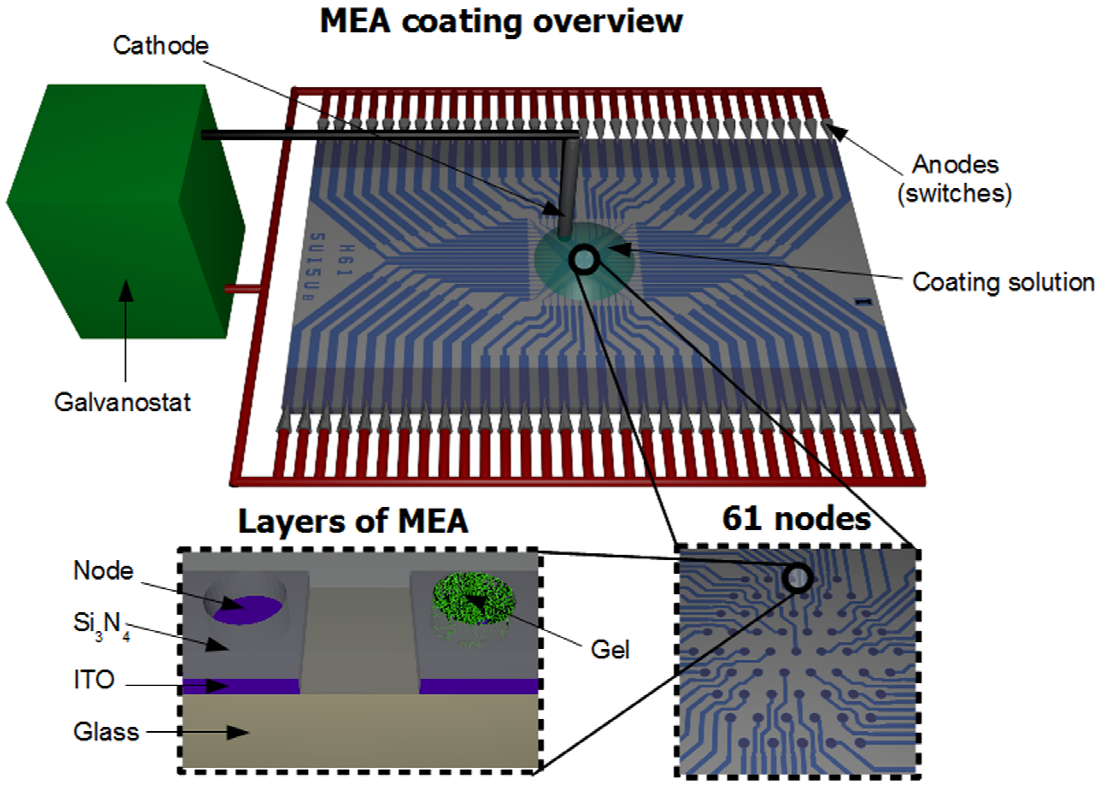

Figure 7.6 Overall schematic depicting MEA coating setup, hexagonal array of microelectrodes (each node is ~5 µm in diameter; ~1 µm in depth), and layered structure of the MEA device.

An identical Pyr-YL coating solution was also applied to the MEA device (Fig. 7.6), however, in this instance a 4.5 mA cm^{-2} current density for four minutes was ineffective. Keeping the coating time constant and varying the current density it was found that a significantly higher current density of approximately 40 mA cm^{-2} was required – equating to 8 nA per node. The reason for this difference is not well understood, but most likely relates to edge effects that limit the stability of the growing membrane at this scale, given that each node is only ~5 µm in diameter and ~1 µm in depth (Fig. 7.7). In any case, a similar kinetic profile associated with the coating process was observed, with the DC resistance seen to increase slightly before reaching a plateau at the end of the four minute cycle – though as might be anticipated, the plateau region of the resistance plot is relatively unstable (Fig. 7.8).

Using a printed circuit board (PCB) setup individual nodes could be selectively addressed (Fig. 7.9). In this way some nodes were electroplated with platinum, whilst the others were separately coated with hydrogel. Platinum black scatters light due to its microcrystalline

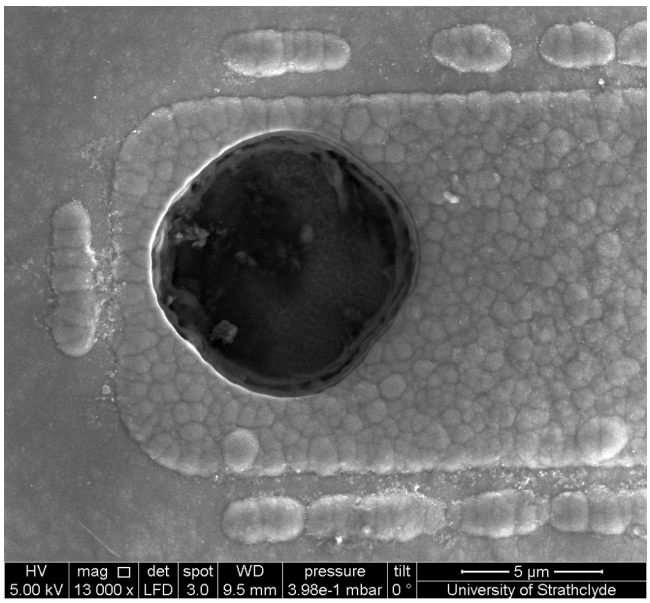

Figure 7.7 SEM image of a single MEA node. Note the conductivity associated with the ITO (dark) relative to the surrounding silicon nitride.

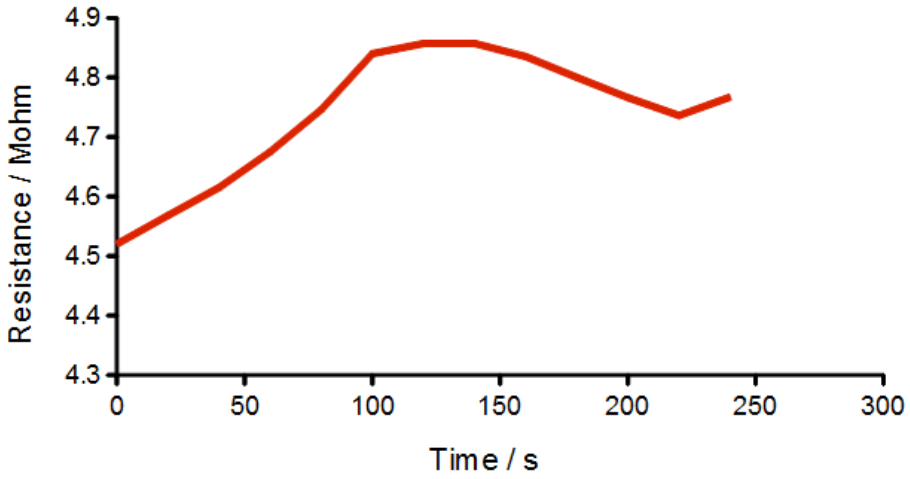

Figure 7.8 Resistance timecourse (galvanostatic control) for Pyr-YL MEA coating procedure.

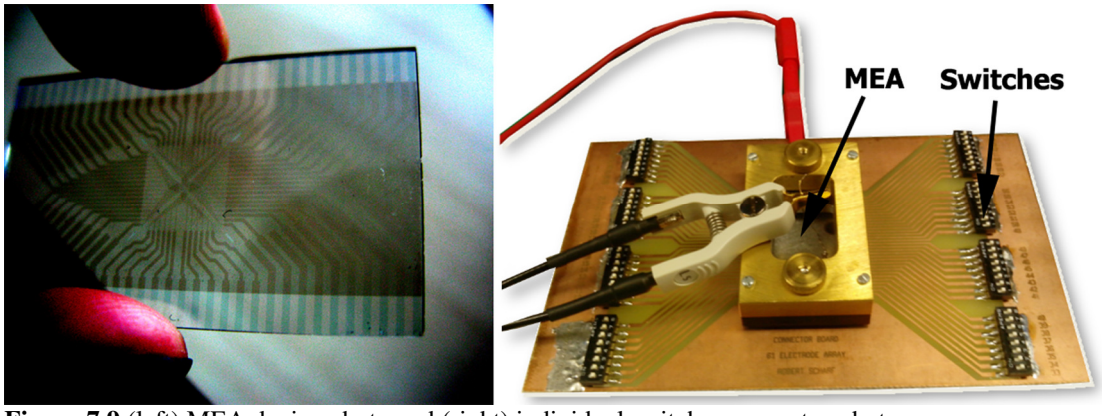

Figure 7.9 (left) MEA device photo and (right) individual switches apparatus photo.

structure and appears dark under brightfield microscopy (Fig. 7.10, nodes below black line), while the presence of the Pyr-YL based coatings could be easily inferred using fluorescence

microscopy (Fig. 7.10, nodes above black line).[14,35] Although some general inhomogeneity is observed, and the hydrogel coatings themselves were apparently only 61% effective based on a visual inspection (i.e. the percentage of the relevant nodes that appear fluorescent) of the MEA device, this is believed to be a terminal contact issue.

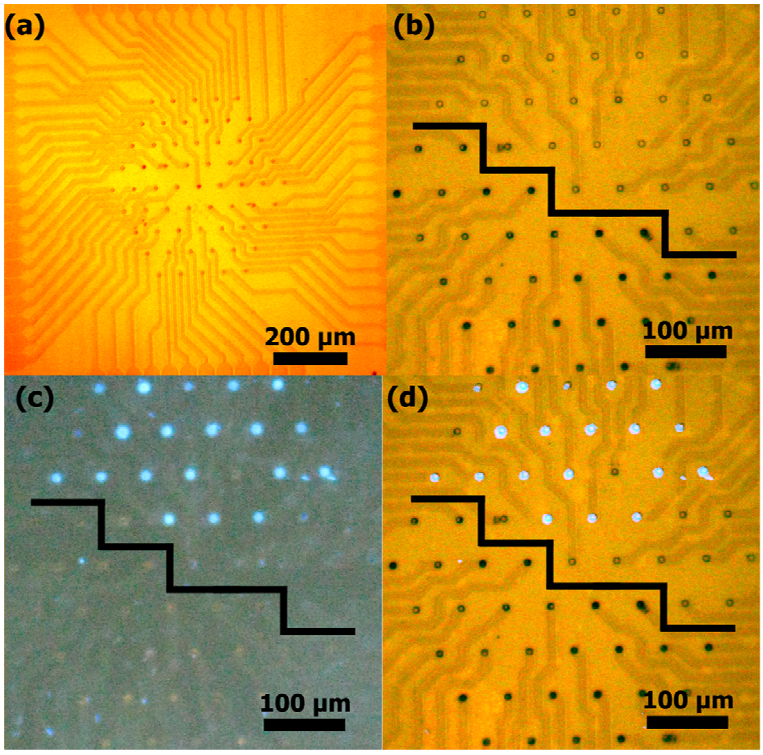

Figure 7.10 (a) Brightfield image of hexagonal MEA grid; (b) brightfield image with lower (darker) nodes electroplated with platinum black; (c) fluorescence image of upper Pyr-YL coated nodes; (d) overlay of brightfield and fluorescence images.

7.3.3 Impedance measurements

Impedance[36] equates to the resistance experienced by an AC current. When measuring the impedance associated with an electrochemical setup, this can be generalised to a simple circuit diagram (Fig. 7.11).[3] Where, R_s is the resistance associated with the solution, while the electrode-solution interface has two terms connected in parallel; $Z_{faradaic}$ and C_{dl}, corresponding with the resistive and capacitive terms, respectively. The resistive term relates to electrochemical redox processes, whilst the capacitive term results from the redistribution of charge. Hence, if a DC current is applied the capacitance will be quickly saturated and the system will have to resort to faradaic processes to maintain a current, so in this case the resistance is essentially $R_s + Z_{faradaic}$. However, if an AC current is applied, the capacitance is repeatedly charged and discharged, such that as the frequency of the applied current tends towards infinity the measured resistance tends towards R_s.

In the first instance the impedance of conventionally (not electrochemically) prepared Pyr-YL and Fmoc-YL (**F3YL**) hydrogels were compared; 20 mM gels were prepared both by the

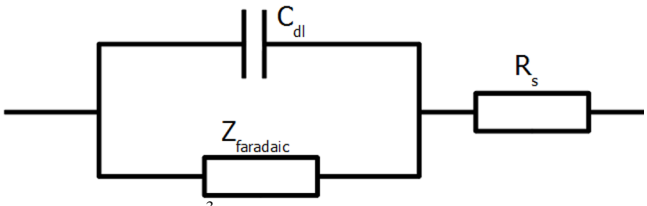

Figure 7.11 Generalised circuit diagram[3] to illustrate the principles of impedance measurements.

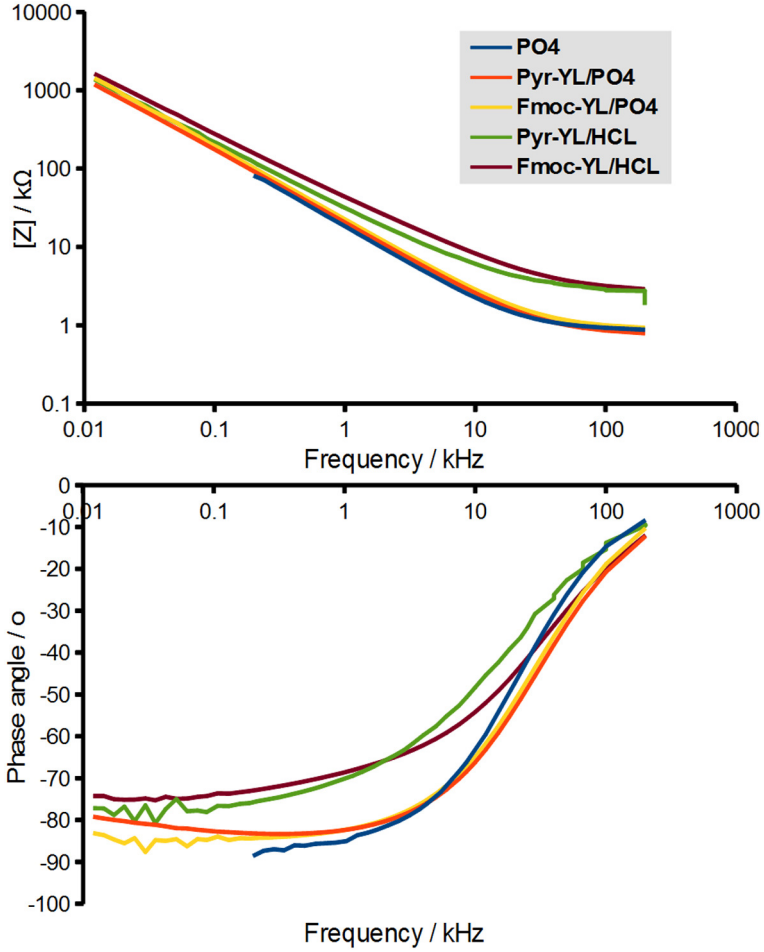

Figure 7.12 Bulk impedance graphs: [top] magnitude; [bottom] phase angle.

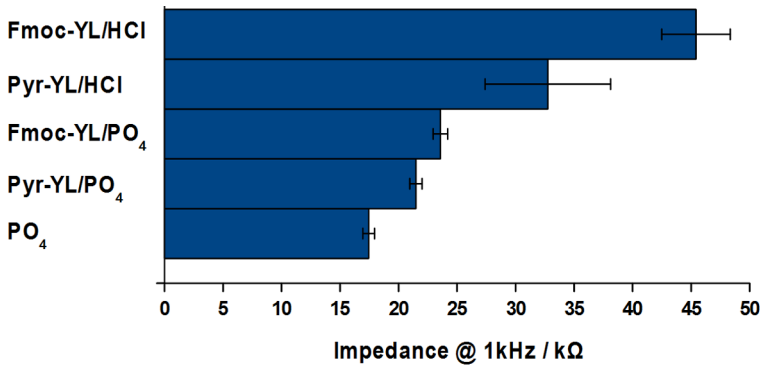

Figure 7.13 Bulk impedance summary at 1 kHz.

dropwise addition of HCl and in pH 7.3 100 mM phosphate buffer. Fmoc-YL was used as it provides a direct comparison with the Pyr-YL system of interest; addressing the impact of

aromaticity. As anticipated, the dominant factor is ionic conductivity, as evidenced by the lower impedances associated with the phosphate buffered hydrogels (Fig. 7.12 and 7.13). In addition, the impedance associated with phosphate buffer alone appears to be lower than that of either of the corresponding phosphate buffered gels; indicating that hydrogel formation may be restricting ion mobility. However, in each case the Pyr-YL gel possesses a significantly lower impedance than the equivalent Fmoc-YL system – indicating the effect of additional aromaticity upon the conductivity of the supramolecular constructs. The phase angle associated with the bulk impedance is approximately -80^{o} at low frequencies and then tends towards 0^{o} as the frequency is increased – hence the system increasingly behaves as an ideal resistor (i.e. R_s) as the frequency is increased.[37]

For the MEAs, the impedance of the platinised, Pyr-YL hydrogel coated, and naked ITO substrate were compared (Fig. 7.14 and 7.15). Notably, compared to the bulk impedance measurements, there is a larger error associated with the impedance of these low area electrodes, which is unsurprising since edge effects (i.e. note the depicted curvature in Fig. 7.2) are likely to significantly affect these measurements. In addition, during the coating process the local pH achieved at the edges of an electrode is likely to be higher than that at the centre, resulting in structural inhomogeneity associated with the gel coating. In any event, it is observed that the Pyr-YL coated nodes are comparable to the uncoated nodes, whilst those electroplated with platinum demonstrate an impedance approximately half that of the other nodes at the 1 kHz frequency of interest. In order to ensure a good signal to noise ratio for neuronal applications, ideally an impedance of < 1MΩ would be desirable. Hence, although these preliminary results are encouraging, optimisation of the MEA coating procedure is required. The phase angles associated with the impedance of the uncoated and hydrogel coated MEAs are approximately -90^{o} at low frequencies before reaching -75^{o} at higher frequencies - this observation combined with the linear impedance plots indicates that the $Z_{faradaic}$ term is still contributing (because of insufficient capacitance) even at high frequencies – this is likely a consequence of the much smaller surface area compared to that of the bulk impedance measurements. However, the phase angle associated with the platinised electrodes is consistently less negative (about -60^{o}) than that of the equivalent gel and ITO systems - which is thought to be a consequence of the high conductive surface area associated with platinised electrodes. There also appears to be some anomaly associated with the platinised resistance at high frequencies above ~20 kHz, where the platinised nodes exhibit a higher resistance than the equivalent gel and ITO systems – this is believed to be a consequence of the electroplating conditions not being optimal (i.e. see variability in the appearance of the platinised nodes in Fig. 7.10). Hence, in general terms, future work is to

focus on optimisation of the MEA coating/electroplating conditions, and a means of monitoring this process *in situ*.

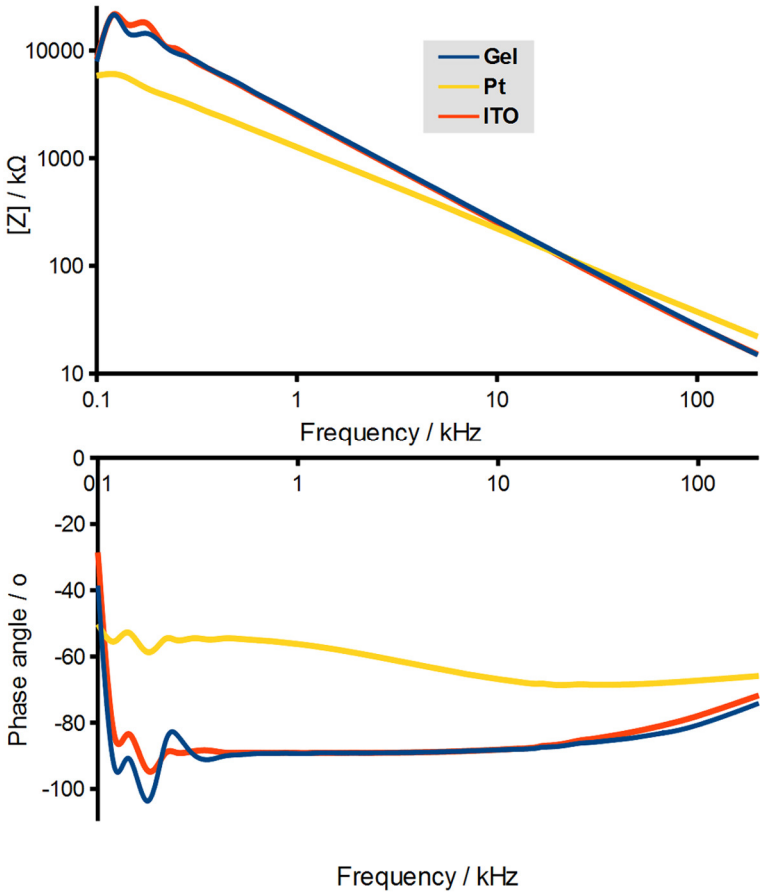

Figure 7.14 MEA impedance graphs: [top] magnitude; [bottom] phase angle.

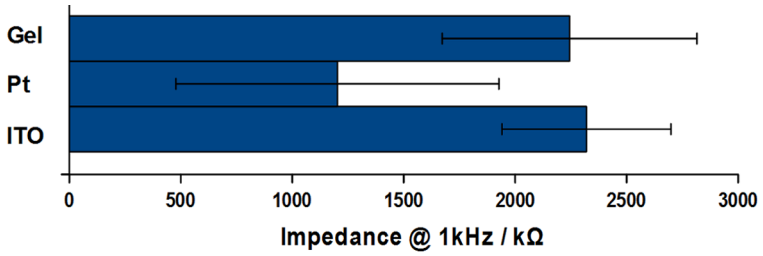

Figure 7.15 MEA impedance summary at 1 kHz.

7.4 Conclusions

In summary, the anodic oxidation of hydroquinone has been successfully utilised for the deposition of Pyr-YL based hydrogels upon MEA devices. The Hofmeister anion phosphate, is found to improve adhesion of gel to the electrode surface. Pyr-YL is a judicious choice of aromatic peptide amphiphile gelator, on account of its facile visualisation by fluorescence microscopy, and the extensive aromatic interactions that underpin its assembly and can (in future) potentially contribute to the conductivity of the coated arrays. Bulk impedance

measurements demonstrate the lower resistance associated with Pyr-YL gels compared to equivalent Fmoc-YL gels. MEA impedance is essentially unaffected by deposition of the Pyr-YL hydrogel, however this setup has a higher impedance than platinised MEAs, and in its current form is unsuitable for neuronal electro-characterisation. Additional optimisation of the MEA coating procedure with iodine doping (and potentially other additives) will likely be required in an attempt to lower the 1 kHz impedance to at least 1MΩ for neural applications. Furthermore, the orthogonal co-assembled Pyr-YL/Fmoc-S system will be applied to MEA devices in future, as the serine fibre coating should improve biocompatibility, neuron-device contact, and signal fidelity.

7.5 References

1. D. E. Gunning, J. M. Beggs, W. Dabrowski, P. Hottowy, C. J. Kenney, A. Sher, A. M. Litke, and K. Mathieson, *J. Neural Eng.*, 2013, **10**, 016007.
2. P. Hottowy, A. Skoczeń, D. E. Gunning, S. Kachiguine, K. Mathieson, A. Sher, P. Wiącek, A. M. Litke, and W. Dąbrowski, *J. Neural Eng.*, 2012, **9**, 066005.
3. D. R. Merrill, M. Bikson, and J. G. R. Jefferys, *J. Neurosci. Methods*, 2005, **141**, 171–198.
4. M. Meister, J. Pine, and D. A. Baylor, *J. Neurosci. Methods*, 1994, **51**, 95–106.
5. A. M. Litke, *Nucl. Instrum. Methods Phys. Res. Sect. Accel. Spectrometers Detect. Assoc. Equip.*, 1999, **435**, 242–249.
6. D. E. Discher, D. J. Mooney, and P. W. Zandstra, *Science*, 2009, **324**, 1673–1677.
7. M. Zhou, A. M. Smith, A. K. Das, N. W. Hodson, R. F. Collins, R. V. Ulijn, and J. E. Gough, *Biomaterials*, 2009, **30**, 2523–2530.
8. V. Jayawarna, S. M. Richardson, A. R. Hirst, N. W. Hodson, A. Saiani, J. E. Gough, and R. V. Ulijn, *Acta Biomater.*, 2009, **5**, 934–943.
9. H. X. Xu, A. K. Das, M. Horie, M. S. Shaik, A. M. Smith, Y. Luo, X. F. Lu, R. Collins, S. Y. Liem, A. M. Song, P. L. A. Popelier, M. L. Turner, P. Xiao, I. A. Kinloch, and R. V. Ulijn, *Nanoscale*, 2010, **2**, 960–966.
10. N. Amdursky, E. Gazit, and G. Rosenman, *Adv. Mater.*, 2010, **22**, 2311–2315.
11. S. Roy and A. Banerjee, *RSC Adv.*, 2012, **2**, 2105–2111.
12. H. Shao, T. Nguyen, N. C. Romano, D. A. Modarelli, and J. R. Parquette, *J. Am. Chem. Soc.*, 2009, **131**, 16374–16376.
13. H. Shao and J. R. Parquette, *Chem. Commun.*, 2010, **46**, 4285–4287.
14. J. R. Moffat and D. K. Smith, *Chem. Commun.*, 2011, **47**, 11864–11866.
15. M. Zelzer, D. J. Scurr, M. R. Alexander, and R. V. Ulijn, *ACS Appl. Mater. Interfaces*, 2012, **4**, 53–58.
16. M. Zelzer, L. E. McNamara, D. J. Scurr, M. R. Alexander, M. J. Dalby, and R. V. Ulijn, *J. Mater. Chem.*, 2012, **22**, 12229–12237.
17. Y. Liu, E. Kim, R. V. Ulijn, W. E. Bentley, and G. F. Payne, *Adv. Funct. Mater.*, 2011, **21**, 1575–1580.
18. E. K. Johnson, D. J. Adams, and P. J. Cameron, *J. Am. Chem. Soc.*, 2010, **132**, 5130–5136.
19. E. K. Johnson, L. Chen, P. S. Kubiak, S. F. McDonald, D. J. Adams, and P. J. Cameron, *Chem. Commun.*, 2013, **49**, 8698–8700.
20. J. E. Ferguson, C. Boldt, and A. D. Redish, *Sens. Actuators A Phys.*, 2009, **156**, 388–393.

21. C. K. Chiang, Y. W. Park, A. J. Heeger, H. Shirakawa, E. J. Louis, and A. G. MacDiarmid, *J. Chem. Phys.*, 1978, **69**, 5098–5104.
22. S. Aronson, A. Liss, and R. Hirsh, *J. Chem. Phys.*, 1977, **66**, 877–879.
23. J. Puigmartí-Luis, V. Laukhin, Á. Pérez del Pino, J. Vidal-Gancedo, C. Rovira, E. Laukhina, and D. B. Amabilino, *Angew. Chem., Int. Ed.*, 2007, **46**, 238–241.
24. D. Canevet, A. P. del Pino, D. B. Amabilino, and M. Sallé, *Nanoscale*, 2011, **3**, 2898–2902.
25. S. K. M. Nalluri and R. V. Ulijn, *Chem. Sci.*, 2013, **4**, 3699–3705.
26. S. K. M. Nalluri, C. Berdugo, N. Javid, P. W. J. M. Frederix, and R. V. Ulijn, *Angew. Chem. Int. Ed.*, 2014, n/a–n/a.
27. Y. M. Abul-Haija, S. Roy, P. W. J. M. Frederix, N. Javid, V. Jayawarna, and R. V. Ulijn, *Small*, 2013, Advance article.
28. C. Tang, A. M. Smith, R. F. Collins, R. V. Ulijn, and A. Saiani, *Langmuir*, 2009, **25**, 9447–9453.
29. C. Tang, R. V. Ulijn, and A. Saiani, *Langmuir*, 2011, **27**, 14438–14449.
30. C. Tang, R. V. Ulijn, and A. Saiani, *Eur. Phys. J. E*, 2013, **36**, 111–121.
31. D. J. Adams, M. F. Butler, W. J. Frith, M. Kirkland, L. Mullen, and P. Sanderson, *Soft Matter*, 2009, **5**, 1856–1862.
32. K. L. Morris, L. Chen, J. Raeburn, O. R. Sellick, P. Cotanda, A. Paul, P. C. Griffiths, S. M. King, R. K. O'Reilly, L. C. Serpell, and D. J. Adams, *Nat. Commun.*, 2013, **4**, 1480–1485.
33. S. Roy, N. Javid, J. Sefcik, P. J. Halling, and R. V. Ulijn, *Langmuir*, 2012, **28**, 16664–16670.
34. S. Roy, N. Javid, P. W. J. M. Frederix, D. A. Lamprou, A. J. Urquhart, N. T. Hunt, P. J. Halling, and R. V. Ulijn, *Chem.–Eur. J.*, 2012, **18**, 11723–11731.
35. D. J. Welsh, P. Posocco, S. Pricl, and D. K. Smith, *Org. Biomol. Chem.*, 2013, **11**, 3177–3186.
36. J. R. Macdonald and W. B. Johnson, in *Impedance Spectroscopy*, eds. E. Barsoukov and J. R. Macdonald, John Wiley & Sons, Inc., 2005.
37. M. Mahdavian and M. M. Attar, *Corros. Sci.*, 2006, **48**, 4152–4157.

– Chapter 8 –

Conclusions and future work

8.1 Overall conclusions

In summary, various self-assembled aromatic peptide amphiphile based hydrogels have been prepared, encompassing a variety of aromatic and corresponding linker functionality - beyond that of the ubiquitous Fmoc motif. In the first instance, experiments have highlighted that FTIR in itself cannot be used to infer an antiparallel β-sheet type H-bonding structure on the basis of the ~1685 cm^{-1} absorption. Instead, for both fluorenyl and pyrenyl based aromatic peptide amphiphiles, this peak is shown to be dependant upon the choice of linker, specifically the methoxycarbonyl moiety. Regardless, this does not preclude the existence of an antiparallel arrangement; which can still be inferred for these materials on the basis of a combination of characterisation techniques. Hence, the interlocked antiparallel conformation remains our working model for aromatic peptide amphiphile assembly – environmental factors excepted.

Although often an overlooked parameter, the choice of linker segment has proven to be vital to achieving the hydrogelation of aromatic peptide amphiphiles. Furthermore, the optimal linker has been found to vary depending upon the corresponding aromatic and dipeptide functionality present within the molecule. Broadly speaking, relatively rigid linkers such as carbonyl and methoxycarbonyl are found to facilitate the self-assembly and gelation of fluorenyl based systems. Here, the Fmoc moiety is believed to be a relatively rigid motif on account of a partial double bond resonance structure that acts to inhibit rotation around the carbamate. In contrast, the hydrogelation of the pyrenyl systems was shown benefit from a relatively flexible ethylcarbonyl linker. However, for pyrenyl systems in particular, the choice of dipeptide sequence also played a vital role in tailoring the hydrophobics of the molecule – with the YL sequence consistently providing a more effective balance for gelation compared to LL, which has been shown to cause precipitation or the formation of a metastable gel. Ultimately, the choice of linker is believed to influence the orientations available to both the aromatic moiety and dipeptide sequence of these materials. Hence, the choice of linker can augment self-assembly in both the aromatic and peptidic domains, as seen by significant changes in the inferred aromatic stacking and H-bonding interactions by fluorescence and FTIR - with sub-optimal linkers, either or both of these aromatic peptide amphiphile self-assembly processes can be impaired. In addition, particularly for fluorenyl YL hydrogels, supramolecular chirality by CD was found to be dependant upon the length of

the linker segment – with a reversal of handedness observed with the addition of each methylene unit. Hence, although in terms of self-assembly it is difficult to deconvolute the influence of the respective aromatic, linker, and peptide parts of these molecules, it is clear that the choice of linker has an important role in adjusting the properties of these aromatic peptide amphiphile hydrogel systems.

The co-assembly of aromatic peptide amphiphiles has also proven to be an effective means of tailoring the properties of the corresponding hydrogel materials in a modular fashion. Here, the adopted co-assembly arrangement has been found to depend upon the relative aromatic and peptide segments of the co-assembly constituents. The orthogonal co-assembly structure was inferred in instances where both the aromatic and peptide parts of the respective aromatic peptide amphiphiles are distinct; Pyr-YL/Fmoc-S and Fmoc-YL/Pyr-S. Here the YL based *gelators* form a fibrous core, with the hydrophilic serine *surfactants* adhering to the surface of the said fibres. This nanoscale phase separation of constituents was inferred from spectroscopic and rheological evidence, which broadly demonstrated that for orthogonal systems, the properties specific to the arrangement of the individual constituents were preserved in the co-assembled state. An exception to this rule being the loss of the distinct supramolecular chirality (CD) associated with the Pyr-S worm-like micelles in the co-assembled state; a result which was consistent with the fibre coating mechanism as opposed to an interpenetrating network of fibres and micelles. In contrast to the orthogonal coating mechanism, for cooperative (Pyr-YL/Fmoc-YL and Pyr-S/Fmoc-S) and disruptive (Pyr-YL/Pyr-S and Fmoc-YL/Fmoc-S) co-assembly systems, constituents share either the same peptide sequence or aromatic moiety, respectively. In these instances, extensive intercalation and mixing of the respective constituents was inferred. For cooperative systems, either a mixed fibrous or a mixed micellar structure was proposed for the gelators and surfactants, respectively. For example, a reduced fluorescence emission redshift associated with Pyr-YL in the Pyr-YL/Fmoc-YL system indicated extensive (random) intercalation of pyrene and fluorene moieties within the shared interlocked antiparallel structure. Similarly, in disruptive systems, extensive aromatic intercalation between constituents was inferred; resulting in disruption of the corresponding H-bonding arrangement by FTIR and CD. Furthermore, in contrast to the orthogonal case, cooperative and disruptive systems were seen to exhibit significant changes in material properties relative to their respective individual constituents. Hence, this work highlights some co-assembly design principles important for aromatic peptide amphiphiles and potentially further afield – mainly that the nanoscale phase separation of constituents requires dissimilar co-assembly partners.

An electrochemical hydrogel deposition process that operates *via* the anodic oxidation of

HQ has been demonstrated for both a bulk and MEA setup. Here, the local lowering of pH at the anode surface has been shown to promote the spatioselective gelation of the Pyr-YL (and Pyr-YL/Fmoc-S systems). In both of these systems, phosphate buffer is found to be necessary to facilitate gelation and adherence to the electrode surface. HPLC analysis of the co-assembly coating confirmed preservation of the 1:1 ratio of the Pyr-YL/Fmoc-S pregelation solution. Bulk impedance results on conventionally prepared Fmoc-YL and Pyr-YL gels showed that increased aromaticity improves conductivity. However, MEA impedance results indicated that although not detrimental to the conductivity of the native ITO electrodes, the hydrogel coated nodes proved inferior to their platinised counterparts.

8.2 Future work

Future work on the elucidation of aromatic peptide amphiphile assembly should firstly focus on unambiguously determining whether an antiparallel, parallel, or other conformation is adhered to – although it is anticipated that the same supramolecular representation will not be applicable to all systems under all conditions. In any case, novel approaches such as utilising experimental and computational evidence in parallel, and/or solid state NMR experiments are cited as a potential means of taking this research forward.

In terms of molecular design rules, the linker work presented here should be expanded considerably in order to increase understanding of this structural facet. For example, since the methoxycarbonyl linker has proven effective based upon the partial double bond resonance structure associated with the carbamate moiety, it is proposed that replacing the methoxy oxygen with an alternative heteroatom could be a means of tailoring the gel properties. For example, urea, thiocarbamate, and dithiocarbamate based linker derivatives are cited as some potential structural motifs to explore. Furthermore, the rigidity and conformation of the linker could instead be amended by the inclusion of a formal double bond – that could also be conjugated to the aromatic, carbonyl, or both. In essence, since the linker, like the aromatic, is an arbitrary synthetic segment, potentially unlimited variability can be accommodated here.

Future co-assembly investigations, could attempt to expand upon the orthogonal, cooperative, and disruptive supramolecular structures, by taking greater account of the influence of pH. As within the current co-assembly systems, in effect there are four components, if taking into account the ionised and neutral form of each constituent. In this respect, it is anticipated that the so-called gelators will behave increasingly as surfactants at higher pH values, with a micellar arrangement adopted in place of the interlocked antiparallel structure. In addition, if and how the different co-assembly regimes affect the

apparent pK_a of the gelator constituents has yet to be established. Furthermore, kinetic factors could be explored in detail within the co-assembly context – for example, potentially an interpenetrating Pyr-YL/Fmoc-YL co-assembly structure could be attained by utilising a slow change of pH. Elsewhere, since the orthogonal coating mechanism is thought to be a useful means of chemically functionalising existing fibrous systems, this approach could be extended to multiple amenable surfactants within the one system. In this regard, an unambiguous means of validating the surfactant coating mechanism is desirable. For instance, HR-TEM could possibly be used to observe contrast between fibre and coating if a substantial disparity in the atomic distribution were created – e.g. by using cysteine and gold nanoparticles.

The MEA work presented is evidently at a preliminary stage. However, future work should attempt to optimise the hydrogel coating conditions, both to improve consistency and in an attempt to tailor the electrode properties in a rational manner *via* altering the precise coating methodology utilised. This could begin by adjusting the solution composition/concentration, applied current density, and gel deposition time. To this end, a means of monitoring the hydrogel coating process in real time would be advantageous. Further to this, besides fluorescence microscopy, the MEA gel coatings have not been characterised – in order to assess the morphology and height of the deposited material, environmental SEM should be considered. However, the most important issue is that the current MEA Pyr-YL setup has demonstrated a resistance that is too high for eventual application with neurons. If future coating optimisation fails to address this issue, then there are several approaches that could be explored. For example, since a slight correlation between increased aromatic stacking interactions and conductivity has been inferred, augmenting the current system with for example a PDI derivative could potentially increase this effect through complementary stacking interactions between pyrene and PDI. Furthermore, given the generality of the electrochemical hydrogel deposition process, an entirely different aromatic peptide amphiphile system could be utilised instead. Ultimately, in any case doping of the aromatic peptide amphiphile system with iodine will likely be required to facilitate substantial electro-conductivity. Alternatively, the benefits of the high conductivity associated with platinised nodes could in principle be combined with the soft biocompatible gel coating by adopting the sequential electrodeposition of these features. Since the hydrogel coating required a lower current density than the corresponding platinisation process, it is thought that the reversed DC bias of the gel coating would not overly affect any existing Pt already deposited on the electrode surface.

Appendices

A.1 Intranet based repository

A.1.1 Background and motivation

Due to the wide range of aromatic peptide amphiphile hydrogelators studied in the literature it can be difficult to rationalise overall trends or patterns. In addition, even within the confines of the Uiljn group it can be challenging to keep track of unpublished results others have obtained for particular systems. If this wealth of information could be organised, this would potentially facilitate research activities by reducing the repetition of previous work. The old adage "a negative result is still a result" is particularly relevant here, as while it is tempting to disregard unsuccessful gelators and move on, recording this information could save someone else a lot of time later. Hence, a systematic means of keeping track of aromatic peptide amphiphile systems was sought.

A.1.2 Data structure

An intranet based repository would allow for the storing and retrieval of relevant research data; whereby information could be organised according to the molecular structure of the aromatic peptide amphiphiles. To achieve this, a MySQL database was utilised, which contained the following visible fields: Sequence, Synthesis/Structure, AFM, CD, DLS, F, HPLC, IR, Modelling, SEM, SLS, TEM, and Miscellaneous. Using these fields, entries can be organised in a table alphabetically, and information accessed on an individual technique, or alternatively the entire record pertaining to a particular molecule. Associated with each field or category is a title and a full description - with the option of also uploading a single jpg image.

In addition, because each record corresponds with a particular hydrogelator that may have been studied in one or more publications, it became necessary to allow multiple pdf files to be associated with a particular record. To achieve this, another MySQL table was implemented, whose sole purpose was to link records with uploaded pdf files. When a pdf file is uploaded a unique key is generated and stored in this database; so if the same pdf is uploaded again in future (for association with a different record) then this key is recognised and duplication of pdf files on the server is avoided.

Furthermore, a final MySQL table was used to store user login details - with the password field being hashed. In principle this login facility could have been used in conjunction with the other tables to allow (for example) users to have ownership privileges over certain

records. However, in practice such features were never implemented, and each registered user has equivalent permissions (full read/write access) when logged in. The overall data structure is summarised in Figure A.1.

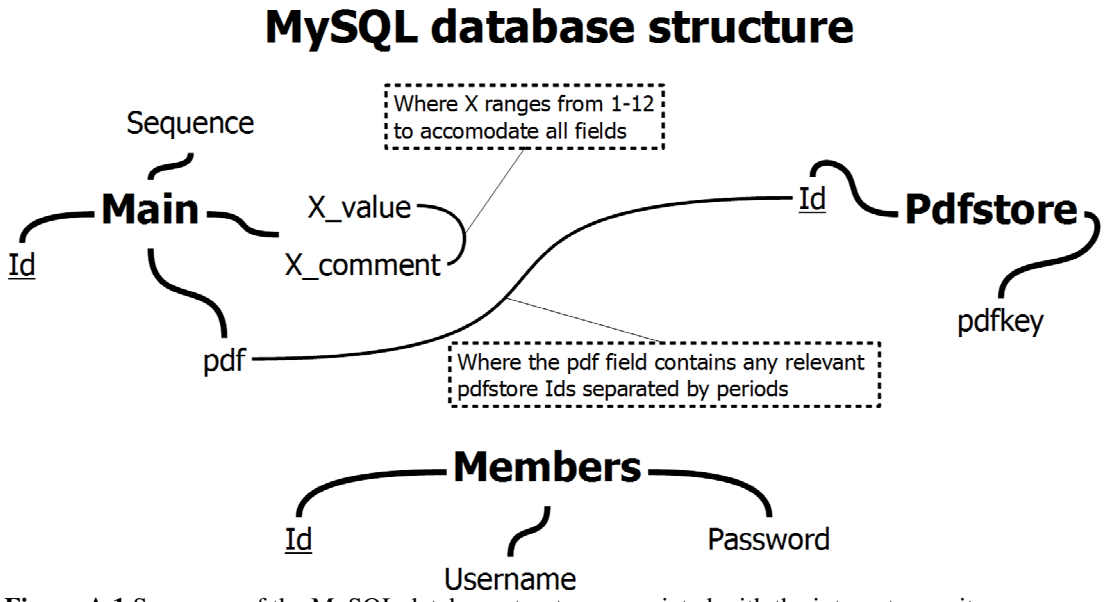

Figure A.1 Summary of the MySQL database structure associated with the intranet repository.

A.1.3 Description of each "webpage"

Note that the full source code of each file is available as supplementary information on the attached compact disc. This section is merely intended to be a brief guide as to the purpose or function of each of the listed files.

A.1.3.1 Design template files

Template files define certain design features common to all pages – potentially facilitates future amendments affecting the entire website. Note that the majority of the design is largely unaltered from a variant of the Microsoft Webmatrix starter site template. However, the underlying source code was altered extensively, which included a conversion from asp to php in order to work with the linux server available to us.

_Sitelayout.php

A.1.3.2 Login details template files

MySQL database access was required for all webpages; hence login details were retained within the following templates for easier editing if necessary (i.e. after a database password change).

ulijndb.php

membersdb.php

A.1.3.3 Main menu pages

These files define the pages accessible from the main menu. Note that the appearance of Database.php depends upon whether a user is logged in or not (Figure A.2).

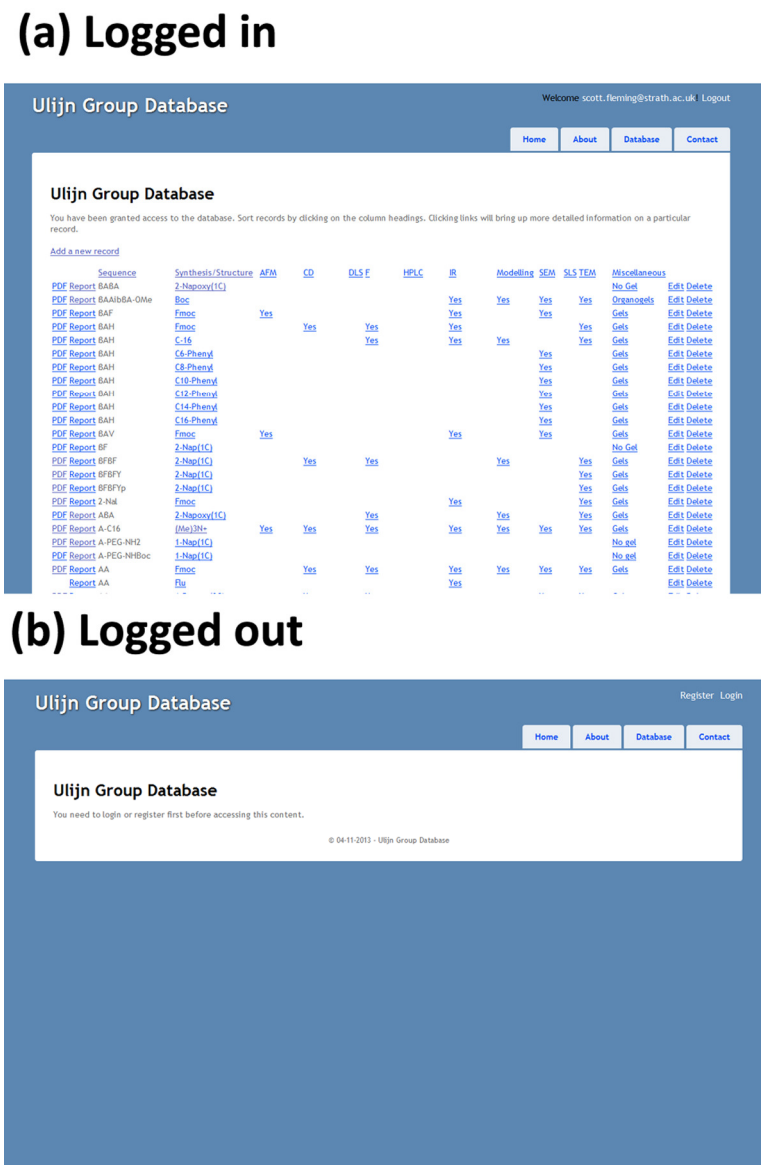

Figure A.2 Appearance of Database.php page when (a) logged in and (b) logged out.

index.php – Default homepage

About.php – Contains instructions for use

Contact.php – Contact form for emailing admin

Database.php – Access to aromatic peptide amphiphile database

A.1.3.4 Database access pages

These pages are generally accessed via Database.php and allow: the adding, deleting, editing, and viewing of records; and the association, disassociation, and viewing of relevant pdf files. As a consequence, the contents of these pages vary extensively and are only

accessible when logged in.

RecordInfo.php – Displays full or partial record information

NewRecord.php – Create a new record

EditRecord.php – Edit an existing record

DeleteRecord.php – Delete an existing record

Papers.php – View associated pdf files

A.1.3.5 Account pages

These pages are required for registering, logging in, logging out, and changing password.

Register.php

success.php

Login.php

Logout.php

ChangePassword.php

A.1.4 Processing of data for literature review analysis

The preparation of the dipeptide sequence figure (Chapter 2, Fig. 2.11) necessitated the processing of data largely contained within the intranet based repository. The starting point was the export of a text file from the MySQL database containing aromatic, sequence, C-termini, and basic (Boolean) gelation data. This text file was manually edited, removing records out with the narrow remit of aromatic dipeptide amphiphiles. This file was then processed using a C++ program (see source code below) that outputted the data necessary to prepare the figure. The general process can be summarised as follows: for each dipeptide sequence, aromatic, or C-terminus, "points" are assigned based on literature occurrences and the cited gelation ability in each case (gel +1, no gel -1, co-assembly gel + ½); for the dipeptide table, hexadecimal colour codes are computed such that the full range of "scores" are suitably represented by a colour gradient; results are then outputted in HTML format.

Source code:

```
// lit_rev_processing.cpp : Defines the entry point for the console application.
// modified to only consider Fmoc functionalised compounds as far as the dipeptide table is concerned...
// this necessitates differentiation using the number of papers as opposed to gel/no gel etc...
// fresh_start modifications:
// input, 4 variables Aromatic/linker, (di)peptide, C-termini, Y/N/C/O
//

#include "stdafx.h"

int loaddata(string arg[][4]) {
  int a;
  string f;
  char str[80]="fresh_start.txt";
  ifstream in(str);
```

```
  if(!in) {
        cout << "Cannot open file. \n";
        // ERROR
  }
  // can begin reading actual data
  a = -1;
  while (in) {
        a++;
        in >> f;
        if (in) { arg[a][0] = f; } // aromatic + linker
        in >> f;
        if (in) { arg[a][1] = f; } // peptide
        in >> f;
        if (in) { arg[a][2] = f; } // C-termini
        in >> f;
        if (in) { arg[a][3] = f; } // Y/N/C/O
  }
  in.close(); // close file
  a = a - 1;
  return a;
}

void twentytwenty(string arg[][4], int a) {

  double table[21][21][4];
  // first 0 not used, second is if single amino acid sequence
  char title[22] = { 'Z','A','V','I','L','M','F','W','Y','S','T','N','Q','R','H','K','D','E','C','G','P','\0' };
  // first entry bogus to keep things simple
  int i;
  int b;
  for (i=0; i<=20; i++) {
        for (b=0; b<=20; b++) {
              table[i][b][0] = 0;
              table[i][b][1] = 0;
              table[i][b][2] = 0;
              table[i][b][3] = 0;
        }
  }
  // double o=0;
  double result;
  int resultr;
  double x1, y1;
  string aa1, aa2;
  int x=0, y=0;
  for (i=0; i<=a; i++){
        // interpret dipeptide sequence and translate onto 20x20 array
        aa1 = arg[i][1];
        // consider only dipeptides and amino acids
        // ignore anything with d b or brackets (it'll be more than 2 long so don't need to worry
        if (aa1.length() <= 2 && aa1[0] != 'd' && aa1[0] != 'b') {
              // entry is valid
              if (aa1.length() == 1) {
                    // amino acid
                    aa2 = 'Z';
              } else {
                    // dipeptide
                    aa2 = aa1[1];
                    aa1 = aa1[0];
              }
        }
        else {
              // entry is invalid
              aa1 = 'Z';
              aa2 = 'Z';
```

```
		}
		// aa1 = aa1[0];
		for (b=0; b<=20; b++) {
			if (aa1[0] == title[b]) { x = b; }
			if (aa2[0] == title[b]) { y = b; }
		}

		// use for only Fmoc
		if (arg[i][0] != "Fmoc") { x = 0; }
		// ends here

		if (x > 0) { // ignore invalid entries
			// now have the appropriate x and y coordinates
			// determine gelation characteristics and enter into table
			if (arg[i][3] == "Y") { table[x][y][0] = table[x][y][0] + 1; } // it's a gel
			if (arg[i][3] == "N") { table[x][y][1] = table[x][y][1] + 1; } // not a gel
			if (arg[i][3] == "C") { table[x][y][2] = table[x][y][2] + 1; } // co-assembly gel
			if (arg[i][3] == "O") { table[x][y][3] = table[x][y][3] + 1; } // omit for some other reason
		}
		// ready for next entry
}
// table ready just need a nice visual way to interpret
// let hydrogel be worth 1 point
// no gel worth -1
// co-assembly be worth .5 points
// omit be worth 0 points
// total up points into 0 slot
x1 = -1000; // use to find max
y1 = 1000; // use to find min
// if we want to omit FF...
table[6][6][0] = 0;
table[6][6][1] = 0;
table[6][6][2] = 0;
table[6][6][3] = 0;
// resume here */
for (i=0; i<=20; i++) {
		for (b=0; b<=20; b++) {
			table[i][b][0] = table[i][b][0] - table[i][b][1] + 0.5 * table[i][b][2]; //MODIFIED
			if (x1 < table[i][b][0]) { x1 = table[i][b][0]; }
			if (y1 > table[i][b][0]) { y1 = table[i][b][0]; }
			// if (o < table[i][b][2]) { o = table[i][b][2]; }
		}
}
// now with max and min values we have range that we can correlate with hexadecimal values
// UPDATE ffffff background and gels from 000000 -> ff0000
// output to file
ofstream out("peptide_table.htm");
if(!out) {
		cout << "Cannot open file. \n";
		// ERROR
}

// can begin outputting actual data

out << "<html><head><title>Peptide table output</title></head>\n";
out << "<body>\n<table>\n";
out << "<tr>";

// titles
out << "<td></td>";
for (i=1; i<=20; i++) {
		out << "<td><b>" << title[i] << "</b></td>";
}
out << "</tr>\n";
```

```
  // main body
  for (b=0; b<=20; b++) {
            if (b>0) { out << "<tr><td><b>" << title[b] << "</b></td>"; } else { out << "<tr><td></td>"; }
            for (i=1; i<=20; i++) {
                        if (table[i][b][0] == 0 && table[i][b][1] == 0 && table[i][b][2] == 0 && table[i][b][3] == 0){
                                    // if no data is available
                                    out << "<td style='height:20px;width:20px' bgcolor='ffffff'>";
                        } else {
                                    out << "<td style='height:20px;width:20px' bgcolor='";
                                    result = 255 * ((table[i][b][0] - y1) / (x1 - y1));
                                    result = result + 0.5;
                                    resultr = (int)result;
                                    if (resultr < 16) { out << "0"; }
                                    out << hex << resultr;
                                    out << "0000'>";
                                    /*
                                    result = (255 - (((table[i][b][0] - y1) / (x1-y1)) * 255));
                                    result = result + 0.5;
                                    resultr = (int)result;
                                    if (resultr < 16) { out << "0"; }
                                    out << hex << resultr;
                                    if (resultr < 16) { out << "0"; }
                                    out << hex << resultr;
                                    out << "'>";
                                    */
                                    // out << dec << table[i][b][0];
                        }
                        out << "</td>";
            }
            out << "</tr>\n";
  }
  out << "</table></body>\n";
  out << "</html>";
  out.close(); // close file

}

void cter(string arg[][4], int a) {
  double table[51][4];
  // may need more later - okay for now
  // four stems from qualitative assessment of system reported as hydrogel, viscous, organogel, or no_gel
  string title[51]; // don't know what the titles are going to be initially

  int i;
  unsigned int b;

  //double o=0;
  double result;
  int resultr;
  double x1, y1;
  string aa1, aa2;
  int x=0, y=0;
  for (i=0; i<=50; i++) {
            title[i] = " ";
            table[i][0] = 0;
            table[i][1] = 0;
            table[i][2] = 0;
            table[i][3] = 0;
  }

  for (i=0; i<=a; i++){

            aa2 = arg[i][2]; // simpler than before!
```

```
		// now need to determine whether aa2 is novel or has been encountered previously
		x=0;
		for (b=0; b<=50; b++) {
			if (title[b] == " ") {
				title[b] = aa2; // assign title to blank entry
			}

			if (title[b] == aa2) {
				x=b; // Entry
				b=50; // escape loop
			}
		}

		// now have the appropriate x coordinates
		// determine gelation characteristics and enter into table

		if (arg[i][3] == "Y") { table[x][0] = table[x][0] + 1; }
		if (arg[i][3] == "N") { table[x][1] = table[x][1] + 1; }
		if (arg[i][3] == "C") { table[x][2] = table[x][2] + 1; }
		if (arg[i][3] == "O") { table[x][3] = table[x][3] + 1; }

		// ready for next entry

	}
	// table ready just need a nice visual way to interpret (plot values in excel later)
	// need to simplify interpretation to be consistent with dipeptide table
	// let hydrogel be worth 1 point
	// no gel worth -1
	// co-assembly worth 0.5 point
	// omit neutral
	// organogels separate table (actually can't really do this as some were both - leave for now) 1 point but separate
from above
	// total up points into 0 slot

	x1 = -1000; // use to find max
	y1 = 1000; // use to find min

	for (i=0; i<=50; i++) {
			table[i][0] = table[i][0] - table[i][1] + 0.5 * table[i][2];		//MODIFIED
			if (x1 < table[i][0]) { x1 = table[i][0]; }
			if (y1 > table[i][0]) { y1 = table[i][0]; }
			//if (o < table[i][2]) { o = table[i][2]; }
	}

	// don't need any of the hexadecimal stuff this time around....
	ofstream out("C_table.htm");
	if(!out) {
		cout << "Cannot open file. \n";
		// ERROR
	}

	// can begin outputting actual data - CONTINUE EDITING FROM THIS POINT FORWARD

	out << "<html><head><title>Peptide table output</title></head>\n";
	out << "<body>\n<table>\n";

	// main body
	for (i=0; i<=50; i++) {
		if (title[i] == " ") {
			i=50; // escape
		} else {
			out << "<tr><td><b>" << title[i] << "</b></td>";
			out << "<td>" << table[i][0] << "</td></tr>\n";
		}
```

```
  }

  out << "</table></body>\n";
  out << "</html>";
  out.close(); // close file

}

void nter(string arg[][4], int a) {
  double table[51][4];
  // may need more later - okay for now
  // four stems from qualitative assessment of system reported as hydrogel, viscous, organogel, or no_gel
  string title[51]; // don't know what the titles are going to be initially

  int i;
  unsigned int b;

  double o=0;
  double result;
  int resultr;
  double x1, y1;
  string aa1, aa2;
  int x=0, y=0;
  for (i=0; i<=50; i++) {
            title[i] = " ";
            table[i][0] = 0;
            table[i][1] = 0;
            table[i][2] = 0;
            table[i][3] = 0;
  }

  for (i=0; i<=a; i++){
            // interpret N-termini and record or confirm previous existence
            // N-termini modification defined in slot 0
            x=0;
            y=0;
            aa2 = arg[i][0];
            // now need to determine whether aa2 is novel or has been encountered previously
            x=0;
            for (b=0; b<=50; b++) {
                        if (title[b] == " ") {
                                    title[b] = aa2; // assign title to blank entry
                        }

                        if (title[b] == aa2) {
                                    x=b; // Entry
                                    b=50; // escape loop
                        }

            }

            // now have the appropriate x coordinates
            // determine gelation characteristics and enter into table

            if (arg[i][3] == "Y") { table[x][0] = table[x][0] + 1; }
            if (arg[i][3] == "N") { table[x][1] = table[x][1] + 1; }
            if (arg[i][3] == "C") { table[x][2] = table[x][2] + 1; }
            if (arg[i][3] == "O") { table[x][3] = table[x][3] + 1; }
            // ready for next entry

  }
  // table ready just need a nice visual way to interpret (plot values in excel later)
  // need to simplify interpretation to be consistent with dipeptide table
  // let hydrogel be worth 1 point
```

```
  // no gel worth -1
  // coassembly worth 0.5
  // omit neutral
  // organogels separate table (actually can't really do this as some were both - leave for now) 1 point but separate
from above
  // total up points into 0 and 2 slots respectively

  x1 = -1000; // use to find max
  y1 = 1000; // use to find min

  for (i=0; i<=50; i++) {
                        table[i][0] = table[i][0] - table[i][1] + 0.5 * table[i][2];        //MODIFIED
                        if (x1 < table[i][0]) { x1 = table[i][0]; }
                        if (y1 > table[i][0]) { y1 = table[i][0]; }
                        //if (o < table[i][2]) { o = table[i][2]; }

  }

  // don't need any of the hexadecimal stuff this time around....
  ofstream out("N_table.htm");
  if(!out) {
            cout << "Cannot open file. \n";
            // ERROR
  }

  // can begin outputting actual data - CONTINUE EDITING FROM THIS POINT FORWARD

  out << "<html><head><title>Peptide table output</title></head>\n";
  out << "<body>\n<table>\n";

  // main body
  for (i=0; i<=50; i++) {
            if (title[i] == " ") {
                        i=50; // escape
            } else {
                        out << "<tr><td><b>" << title[i] << "</b></td>";
                        out << "<td>" << table[i][0] << "</td></tr>\n";
            }
  }

  out << "</table></body>\n";
  out << "</html>";
  out.close(); // close file

}

int _tmain(int argc, _TCHAR* argv[])
{
  string structures[1000][4]; //data
  int number; // number of entries
  // input from file => dipeptide [at least initially], aromatic (and only aromatics), gel/no gel/organogel
  number = loaddata(structures); // remember 0 entries
  // now free to process data as you desire based on:
  // dipeptide sequence
  // aromatic
  // linker
  // gelation ability

  // so in first instance how about successful gels based on dipeptide sequence... (20x20 table)
  twentytwenty(structures, number);

  // count C-termini modifications in similar manner to above - obviously simpler; values can simply be
outputting and utilised in a bar graph
  cter(structures, number);
```

```
  // count N-termini modifications in similar manner to above - obviously simpler; values can simply be outputted
and utilised in a bar graph
  nter(structures, number);

  return 0;
}
```

A.2 Rheological data for linker hydrogels

Representative examples of strain and frequency sweep plots for each successful gelator that features in Chapter 5.

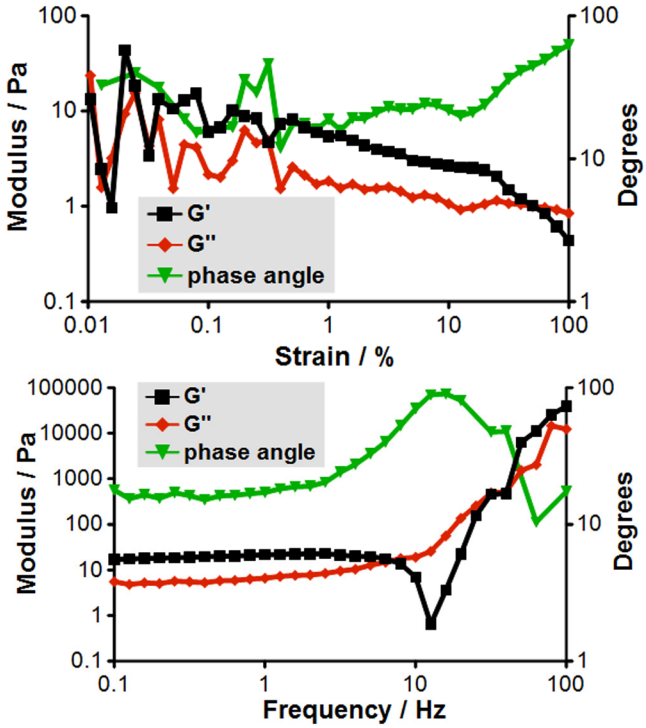

Figure A.3 System **F1YL** elastic (G') and viscous (G'') moduli; (top) strain and (bottom) frequency sweep (~1%) examples.

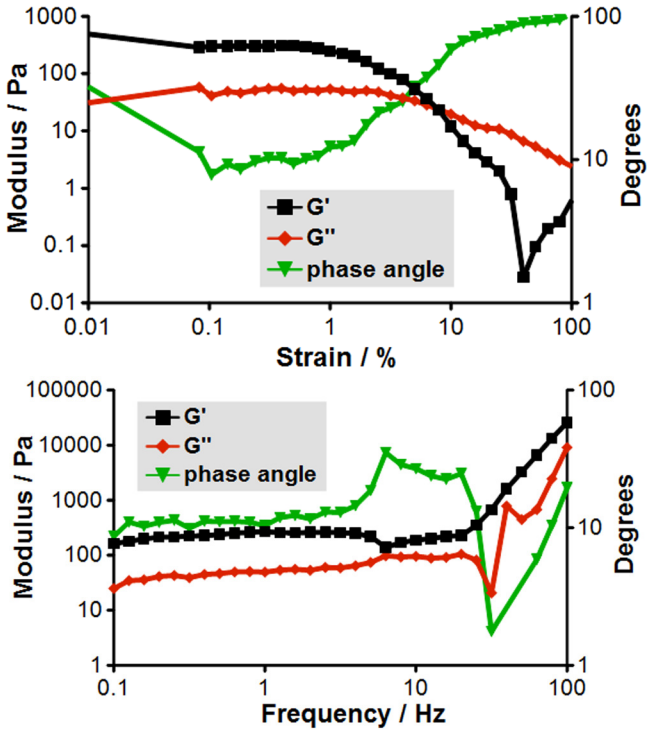

Figure A.4 System **F2YL** elastic (G') and viscous (G'') moduli; (top) strain and (bottom) frequency sweep (~0.2%) examples.

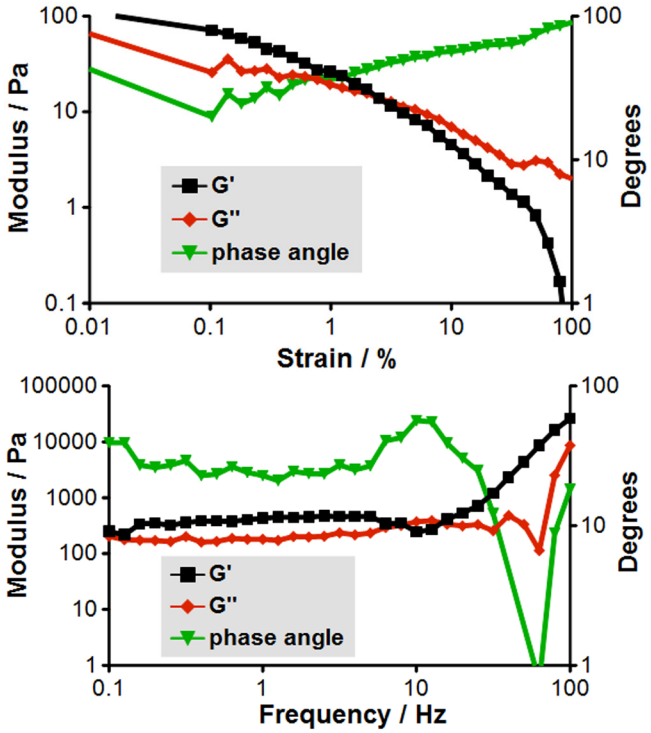

Figure A.5 System **F3YL** elastic (G') and viscous (G'') moduli; (top) strain and (bottom) frequency sweep (~0.2%) examples.

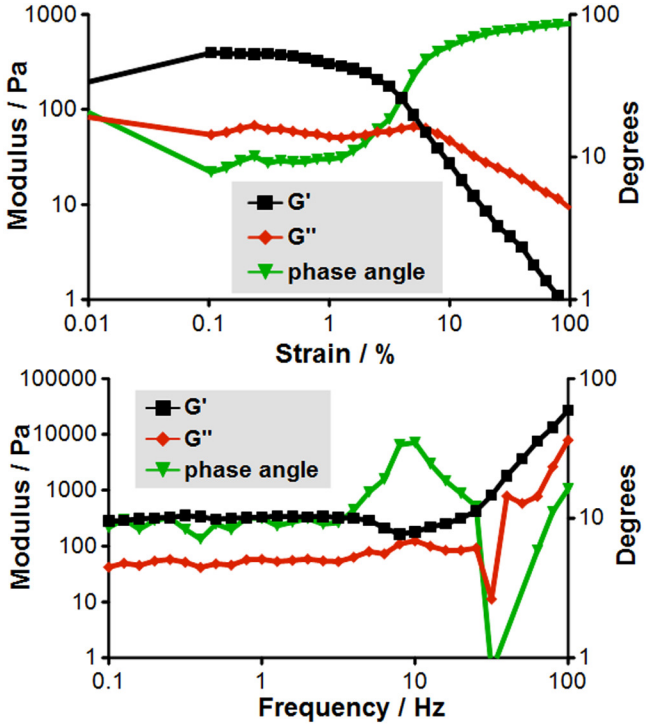

Figure A.6 System **F4YL** elastic (G') and viscous (G'') moduli; (top) strain and (bottom) frequency sweep (~0.2%) examples.

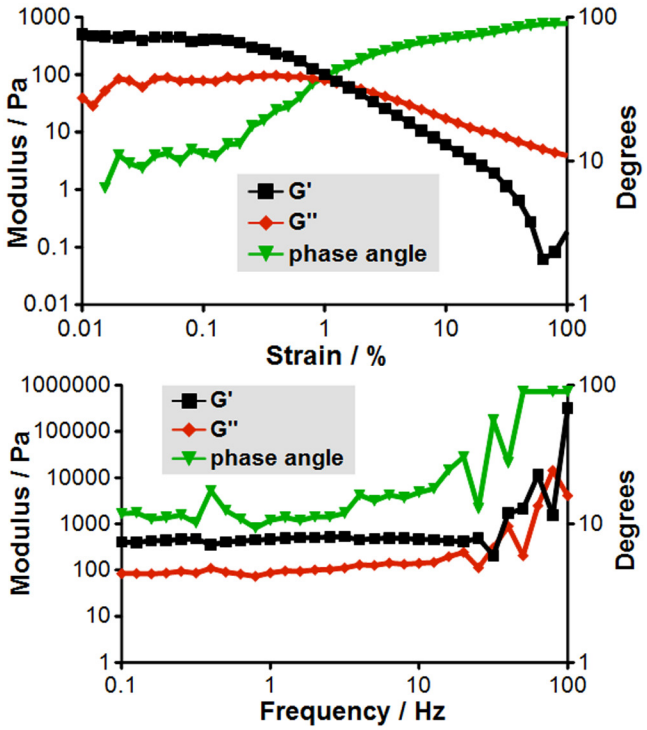

Figure A.7 System **F1LL** elastic (G') and viscous (G'') moduli; (top) strain and (bottom) frequency sweep (~0.2%) examples.

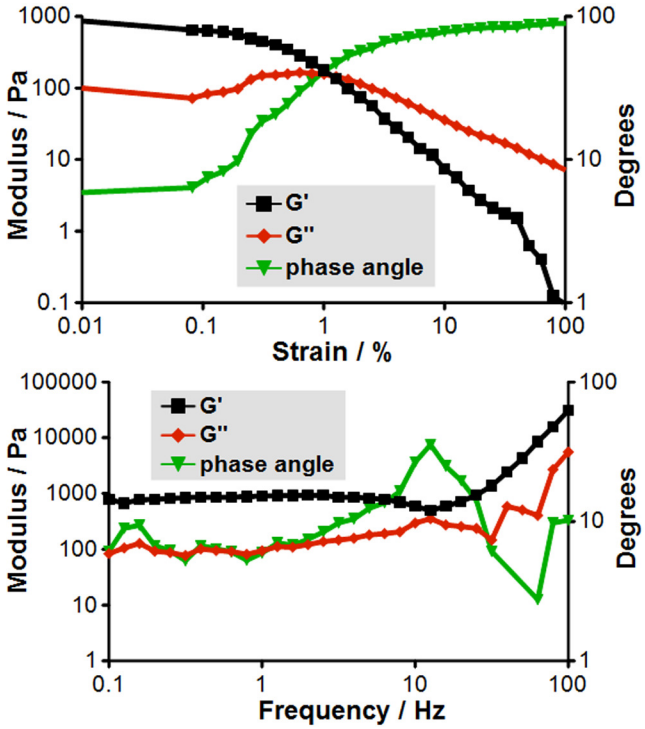

Figure A.8 System **F2LL** elastic (G') and viscous (G'') moduli; (top) strain and (bottom) frequency sweep (~0.2%) examples.

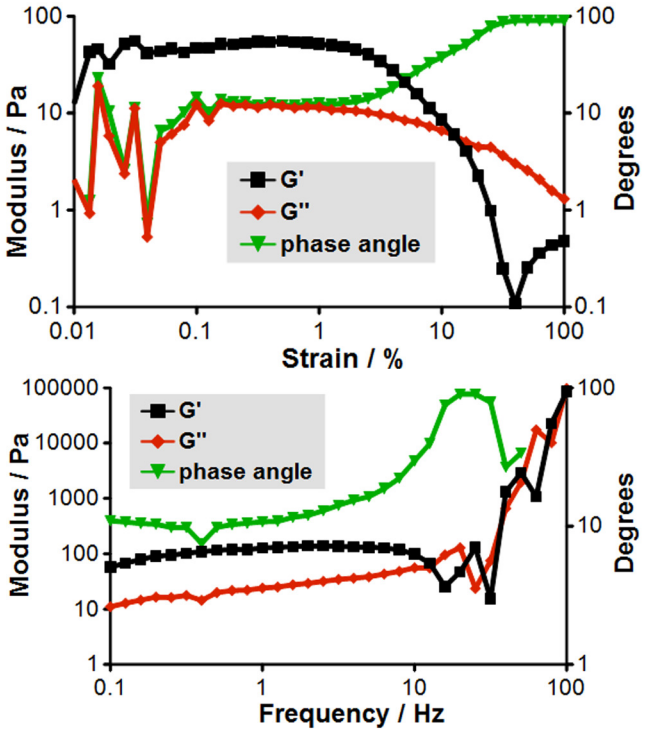

Figure A.9 System **F3LL** elastic (G') and viscous (G'') moduli; (top) strain and (bottom) frequency sweep (~0.2%) examples.

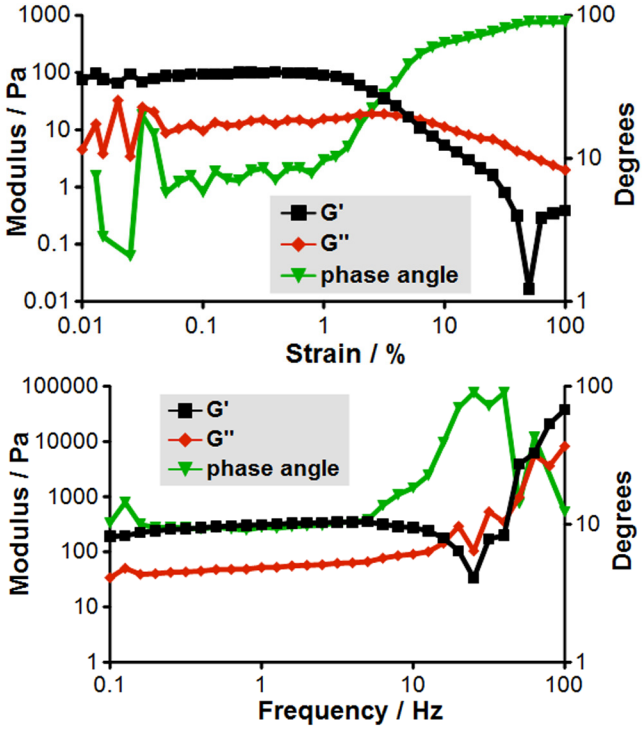

Figure A.10 System **P1YL** elastic (G') and viscous (G'') moduli; (top) strain and (bottom) frequency sweep (~0.2%) examples.

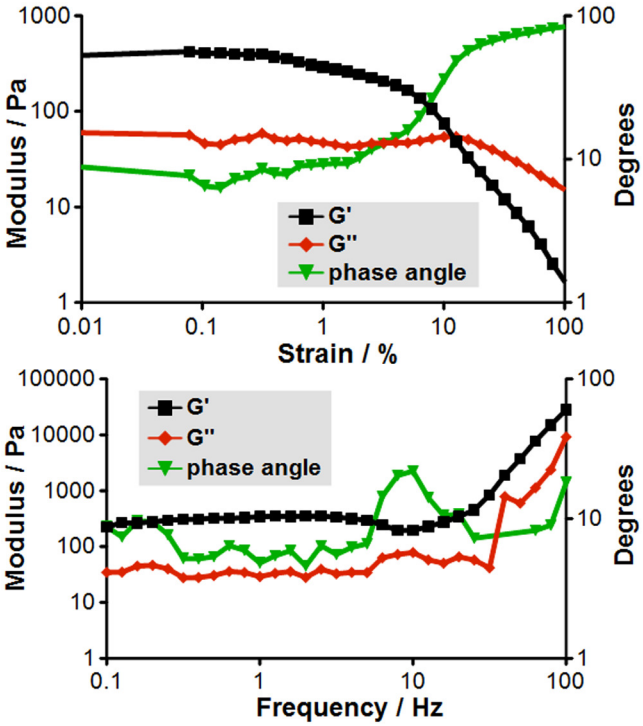

Figure A.11 System **P2YL** elastic (G') and viscous (G'') moduli; (top) strain and (bottom) frequency sweep (~0.2%) examples.

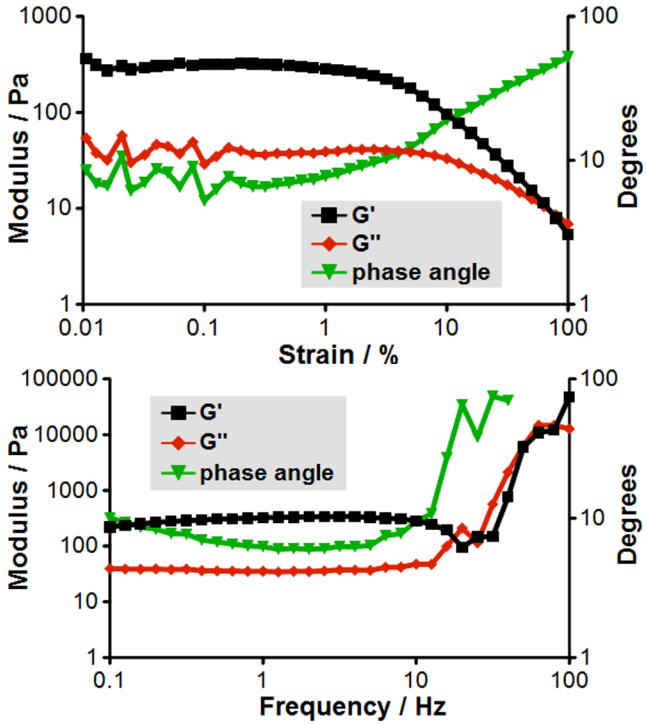

Figure A.12 System **P3YL** elastic (G') and viscous (G'') moduli; (top) strain and (bottom) frequency sweep (~0.2%) examples.

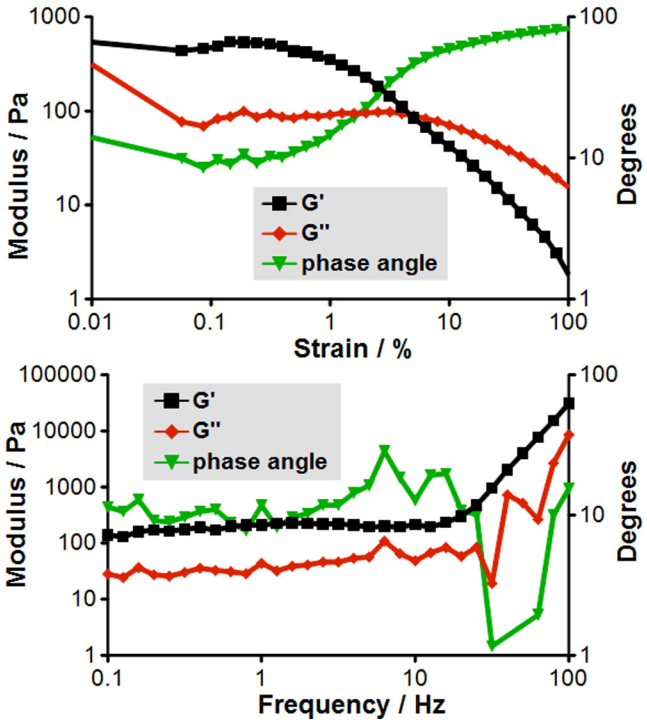

Figure A.13 System **P4YL** elastic (G') and viscous (G'') moduli; (top) strain and (bottom) frequency sweep (~0.2%) examples.

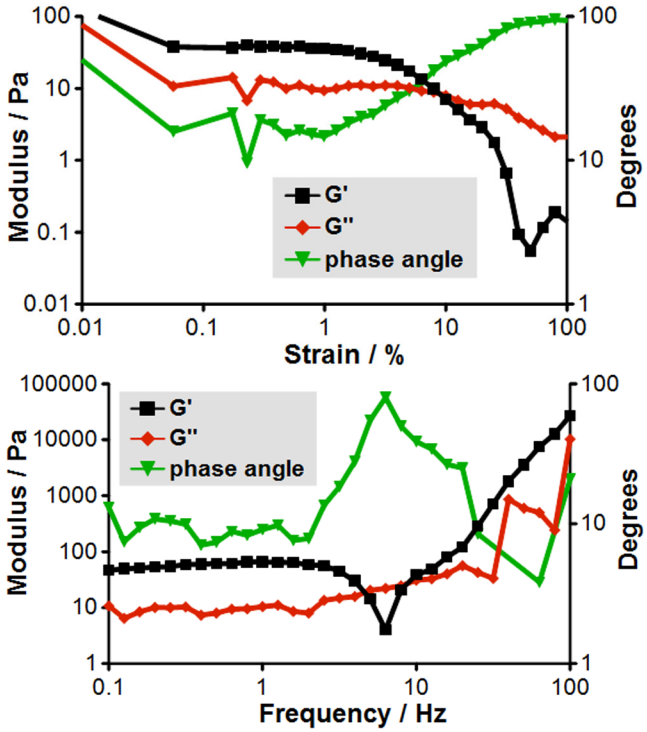

Figure A.14 System **P2LL** elastic (G') and viscous (G'') moduli; (top) strain and (bottom) frequency sweep (~0.4%) examples.

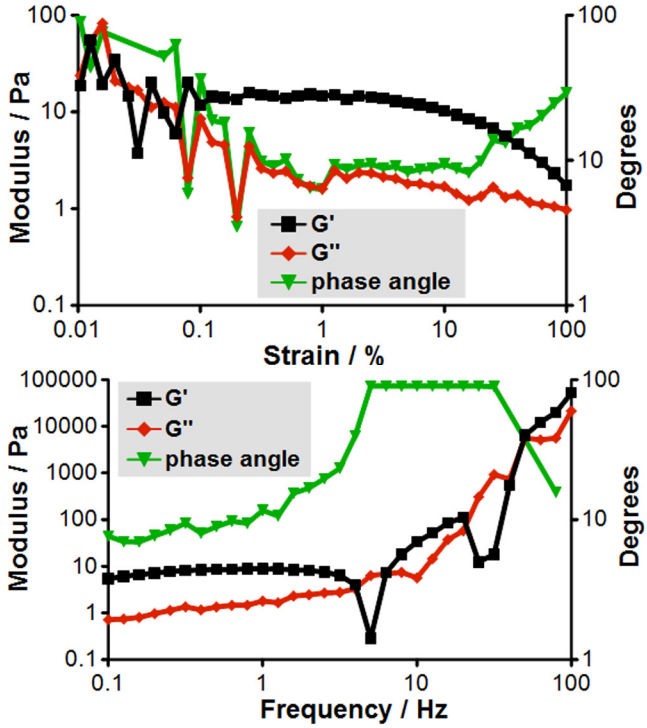

Figure A.15 System **P3LL** elastic (G') and viscous (G'') moduli; (top) strain and (bottom) frequency sweep (~1%) examples.

A.3 Additional co-assembly results

A.3.1 FTIR

Linear combinations (Fig. A.16) of the single component FTIR spectra are provided to compare with the co-assembly FTIR spectra in the main text.

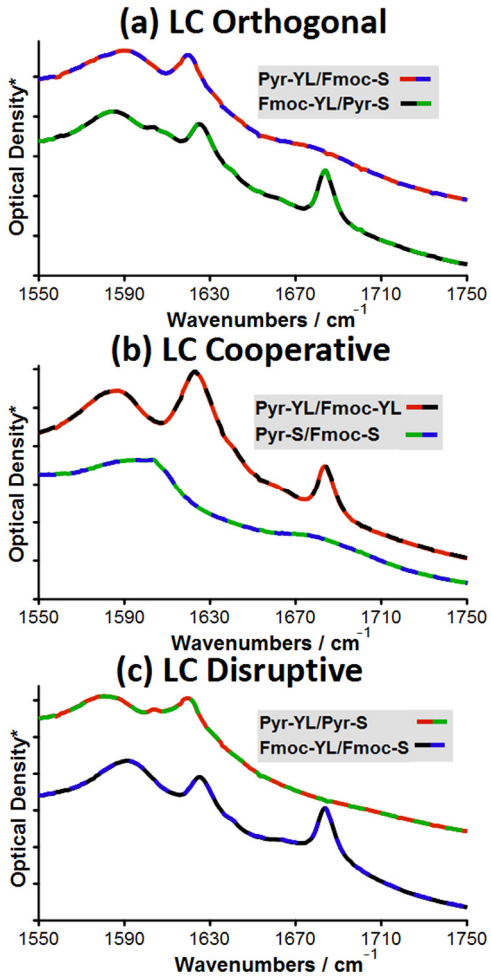

Figure A.16 Linear combinations of single component systems: (a) Orthogonal Pyr-YL/Fmoc-S and Fmoc-YL/Pyr-S; (b) Cooperative Pyr-YL/Fmoc-YL and Pyr-S/Fmoc-S; and (c) Disruptive Pyr-YL/Pyr-S and Fmoc-YL/Fmoc-S. *Spectra have been vertically offset for clarity; each division corresponds to 0.1 units. Note that a phosphate buffer spectrum (without peptides) has been subtracted from the linear combinations to achieve a similar background optical density.

A.3.2 Fluorescence emission

In the dilute solution (< 2 mM) spectra of mixed Fmoc/pyrene systems (Chapter 6, Fig. 6.5(c,d)), a fluorene quenching mechanism is found to disproportionately reduce the intensity of the ~315 nm fluorene aggregate peak. Where we can clearly see the contribution at ~306 nm become dominant, with the suppressed 315 nm fluorene aggregates (dimers etc) only appearing as a shoulder. The 306 nm contribution is believed to be most evident in these dilute Fmoc/pyrene systems as the formation of mixed Fmoc/pyrene aggregates

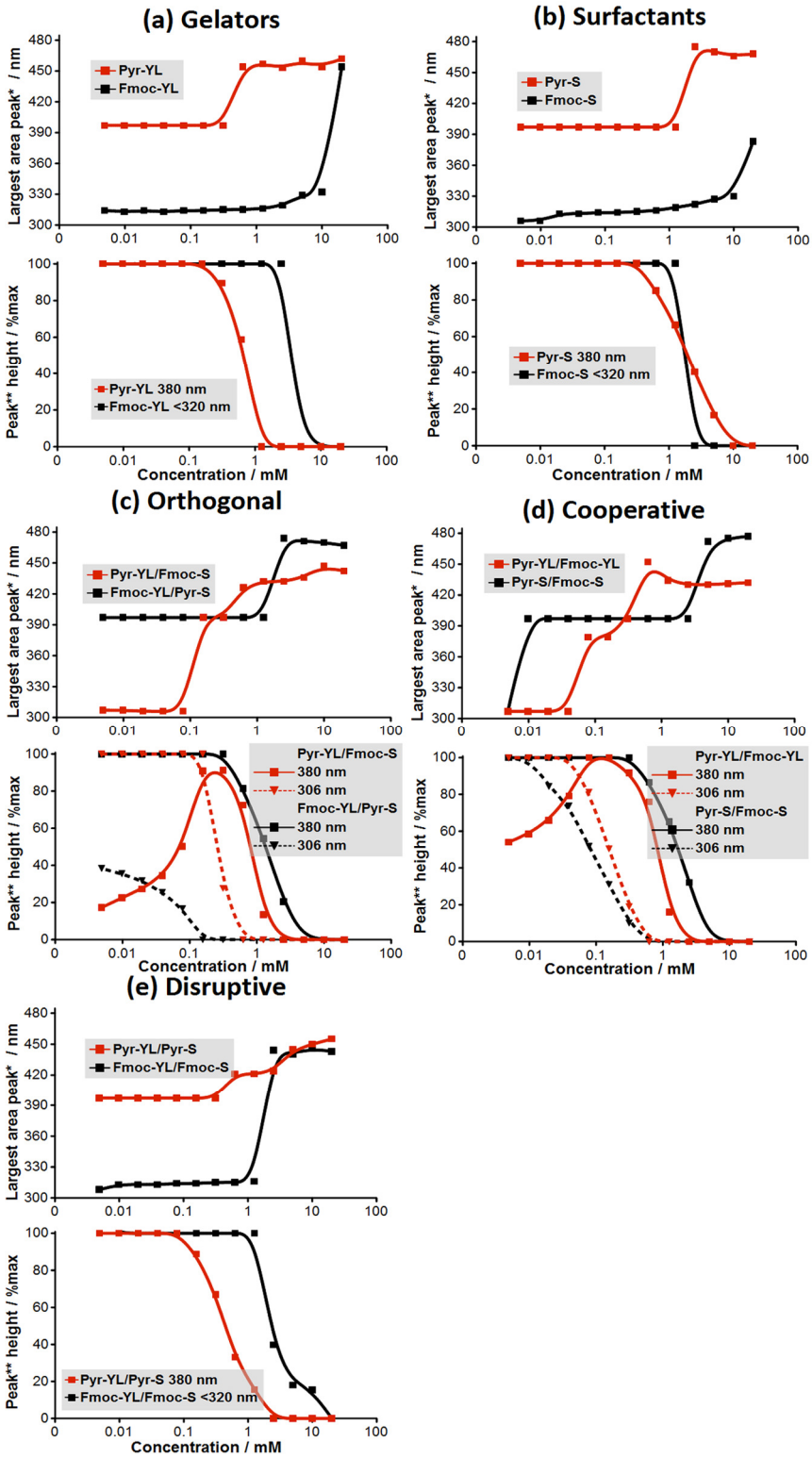

Figure A.17 Most intense fluorescence emission peaks (top panels) and monomer emission peak heights (bottom panels) as a function of concentration. (a) The gelators Pyr-YL and Fmoc-YL; (b) The surfactants Fmoc-S and Pyr-S; (c) Orthogonal Pyr-YL/Fmoc-S and Fmoc-YL/Pyr-S; (d) Cooperative Pyr-YL/Fmoc-YL and Pyr-S/Fmoc-S; and (e) Disruptive Pyr-YL/Pyr-S and Fmoc-YL/Fmoc-S. Note that in the co-assembly systems the concentration refers to that of each constituent e.g. 20:20 mM. *Peak data originates from extracted Gaussians (see below for more information). **Due to the concentration-dependent redshift associated with aggregate (dimers etc) fluorene emissions, the monomer/unassembled peaks are arbitrarily defined as those <320 nm.

(dimers etc) results in efficient energy transfer to pyrene and the consequent quenching of the 315 nm peak, while the monomer emission (which by definition is not in contact with pyrene) is not quenched. These observations mean that in the mixed Fmoc/pyrene systems the 306 nm fluorene monomer fluorescence can be monitored directly against concentration (Fig. A.17(c,d) and Chapter 6, Fig. 6.6(c,d)). In contrast, for Fmoc only systems, interference from the fluorene aggregate peaks at ~315 nm necessitates that the unassembled fluorene "monomer" be arbitrarily defined as those <320 nm in Fig. A.17(a,b,e) and Chapter 6 Fig. 6.6(a,b,e) in the main text.

A.3.2.1 Peak extraction procedure

1. Spectra normalised and maxima selected
2. Gaussian modelled so as not to exceed leeway parameter (4), otherwise noise in the spectrum results in unnaturally sharp peaks. Only whole number stddev considered as otherwise gaussians are consistently too broad due to the influence of leeway parameter. Current values selected simply by trial and error.
3. Gaussian subtracted from spectra and process repeated.
4. Program terminates when maxima < 10% (essentially noise at this stage)
5. Peaks summarised in output file
6. Individual gaussian xy values also outputted, though for processing batches a prepared excel sheet which utilises the summary file is more efficient.

Source code (C++) follows:

```
// deconvolute.cpp : Defines the entry point for the console application.
//

#include "stdafx.h"
/*
Organised all functions and the majority of variables within
class decon to improve readability of main procedure and to
minimize the repeated passing of parameters.
*/
class decon {
  int i, a, mean; // i (for loops), a (number of xy values)
  float f, stddev, area, spectra[1000][4], summary[100][5]; // f (scaling factor)
  /*
  Spectra and summary array sizes are more than enough for my purposes.
  It's not worth the effort of dynamically assigning memory since there's
  no straightforward way of knowing in advance how many peaks there will
  be to summarise!
  */
public:
  int peaks;
  float max;
  void readxy(int);
  void findmax(void);
  void normarea(void);
  void outputsummary(int);
  void outputgauss(int);
  void updatesummary(void);
```

```
  void gausscalc(float);
} ;

int _tmain(int argc, _TCHAR* argv[])
{
  int b=0, number;
  float leeway;
  decon process;

  // prompt for vital details
  cout << "Files to be processed must be numbered from 1 onwards.\n";
  cout << "Please enter number of files : ";
  cin >> number;
  cout << "\nPlease enter the leeway (4 is a sensible starting point) : ";
  cin >> leeway;

  // loop starts here
  for (b=1; b<=number; b++) {
            // establishes filename to open and populates and normalises spectra array:-
            process.readxy(b);

            // the next section should loop around until remaining signal is under threshold value
            process.peaks = 0;
            while (process.max > 10) {

                        // Calculate the gaussian for most notable peak
                        process.gausscalc(leeway);

                        // output each peak gaussian to a separate file (for method validation purposes mostly)
                        process.outputgauss(b);

                        // Update peak info to array (and to the screen)
                        process.updatesummary();

                        // find max value for NEXT run
                        process.findmax();

            }
            // work out the normal area
            process.normarea();
            // time to output the summary
            process.outputsummary(b);
  }

  cin >> number; // pauses the program
  return 0;
}

// various class decon functions
void decon::readxy(int b) {
  float min;
  char str[80];
  sprintf(str, "%d", b);
  strcat(str, ".txt");
  ifstream in(str);
  if(!in) {
            cout << "Cannot open file. \n";
            // ERROR
  }

  // read from the file
  do {
            in >> str;
  } while (strcmp(str,"XYDATA"));
```

```
  // can begin reading actual data
  a = 0;
  while (in) {
            a++;
            in >> f;
            if (in) { spectra[a][1] = f; }
            in >> f;
            if (in) { spectra[a][2] = f; }
  }
  in.close(); // close file
  a = a - 1;

  // find max and min values
  for (i=1; i<=a; i++) {
            if (i==1) {
                        max = spectra[i][2];
                        min = spectra[i][2];
            } else {
                        if (spectra[i][2] > max) { max = spectra[i][2]; }
                        if (spectra[i][2] < min) { min = spectra[i][2]; }
            }
  }
  // normalise
  for (i=1; i<=a; i++) {
            if (max == spectra[i][2]) { mean = i; } // records location of max in array
            spectra[i][2] = 100 * (spectra[i][2] - min) / (max-min);
  }
  max = 100;
}
void decon::gausscalc(float leeway) {
  bool conlp = true; // initially use to know when to exit the loop
  float inten;
  stddev = 0;
  mean = mean + (spectra[1][1] - 1); // converts mean into a more physically meaningful variable
  // best fit being defined as the one before we start getting negative intensity values!!!
  do {
            stddev++;
            f = max; // scaling factor
            for (i=1; i<=a; i++) {
                        inten = f * exp(-0.5 * ((spectra[i][1] - mean) / stddev) * ((spectra[i][1] - mean) / stddev)); //
where inten is intensity of gaussian at this wavelength
                        spectra[i][3] = spectra[i][2] - (inten); // gaussian intensity temporarily subtracted from spectra

                        if ((spectra[i][2] >= 0 && spectra[i][3] < - leeway) || (spectra[i][2] < 0 && (inten) > leeway))
{ // allow some leeway - 10 seems to give fairly sensible results

                                    // stddev too large!!!
                                    conlp = false;
                                    stddev = stddev - 1;
                                    if (stddev == 0) { cout << "Error:- stddev is zero!"; }
                                    i = a; // escape loop
                        }
            }
  } while (conlp);
  f = max;
}
void decon::outputgauss(int b) {
  // output gaussian (not strictly necessary), also convenient to calculate area
  float inten;
  char str[80];
  char str2[80];
  area = 0;
  peaks++;
```

```
  sprintf(str, "%d", b);
  sprintf(str2, "%d", peaks);
  strcat(str, "-");
  strcat(str, str2);
  strcat(str, ".txt");
  // open gaussian file for output
  ofstream out(str);
  if (!out) { cout << "Cannot open " << str << " for output."; }
  // subtract and calculate area under gaussian curve...
  for (i=1; i<=a; i++) {
            inten = f * exp(-0.5 * ((spectra[i][1] - mean) / stddev) * ((spectra[i][1] - mean) / stddev)); // where inten
is intensity of gaussian at this wavelength
            spectra[i][2] = spectra[i][2] - inten; // gaussian intensity PERMANENTLY subtracted from spectra
            area = area + inten;
            out << spectra[i][1] << "," << inten << "\n";
  }
  out.close();
}
void decon::updatesummary(void) {
  cout << "Peak" << peaks << "\n" << "Lambda max @ " << mean << "nm, Intensity = " << max << "\n";
  cout << "Standard Deviation = " << stddev << ", Gaussian area = " << area << "\n\n";
  summary[peaks][0] = mean;
  summary[peaks][1] = max;
  summary[peaks][2] = stddev;
  summary[peaks][3] = area;
  // can't do the normal area yet!
}
void decon::findmax(void) {
  for (i=1; i<=a; i++) {
            if (i==1) {
                      max = spectra[i][2];
                      mean = i;
            } else {
                      if (spectra[i][2] > max) { max = spectra[i][2]; mean = i; }
            }
  }
}
void decon::normarea(void) {
  for (i=1; i<=peaks; i++) {
            if (i == 1) {
                      max = summary[i][3];
            } else {
                      if (summary[i][3] > max) { max = summary[i][3]; }
            }
  }
  for (i=1; i<=peaks; i++) {
            summary[i][4] = 100 * summary[i][3] / max;
  }
}
void decon::outputsummary(int b) {
  // order peaks by wavelength
  int short_wl = 1; // location of shortest wavelength
  char str[80];
  // open peaklist file for output
  sprintf(str, "%d", b);
  strcat(str, "-peaklist.txt");
  ofstream out(str);
  if (!out) { cout << "Cannot open " << str << " for output."; }

  for (i=1; i<=peaks; i++) {
            if (summary[i][0] != 0 && (summary[i][0] < summary[short_wl][0] || summary[short_wl][0] == 0)) {
                      short_wl = i;
            }
            if (i == peaks && summary[short_wl][0] != 0) { // if we've reached the end of the loop and still have
```

```
valid entries left
                    out << summary[short_wl][0] << "," << summary[short_wl][1] << "," <<
summary[short_wl][2] << "," << summary[short_wl][3] << "," << summary[short_wl][4] << "\n";
                    summary[short_wl][0] = 0; // avoid duplication
                    i = 0; // return to the start of the loop
            }
  }

  out.close();
}
```

A.3.2.2 Example Output

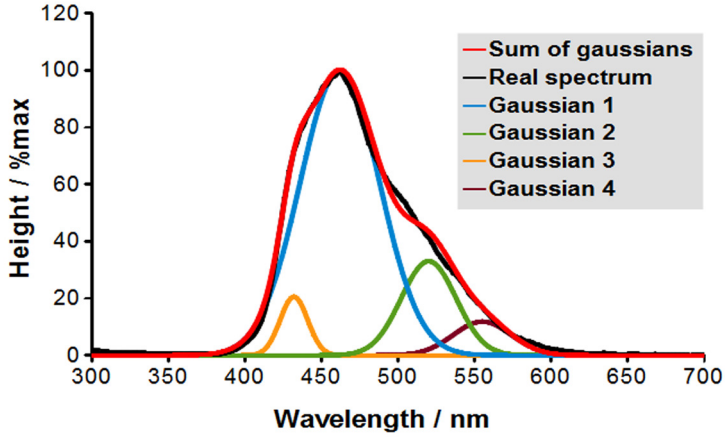

Figure A.18 An example of Gaussians extracted from a typical spectrum; Pyr-YL @ 20 mM

Table A.1 Example of data output; Pyr-YL @ 20 mM

Wavelength / nm	Height / %max	Line width / nm	Area / AU	Area / %max
432	20.58	9	464.23	7.12
462	100	26	6517.23	100
520	33.03	18	1490.45	22.87
555	11.86	19	565.02	8.67

A.3.3 Rheological data

Representative examples of strain and frequency sweep plots for each successful gelator system that features in Chapter 6 – for Pyr-YL and Fmoc-YL see **P4YL** (Fig. A.13) and **F3YL** (Fig. A.5) above.

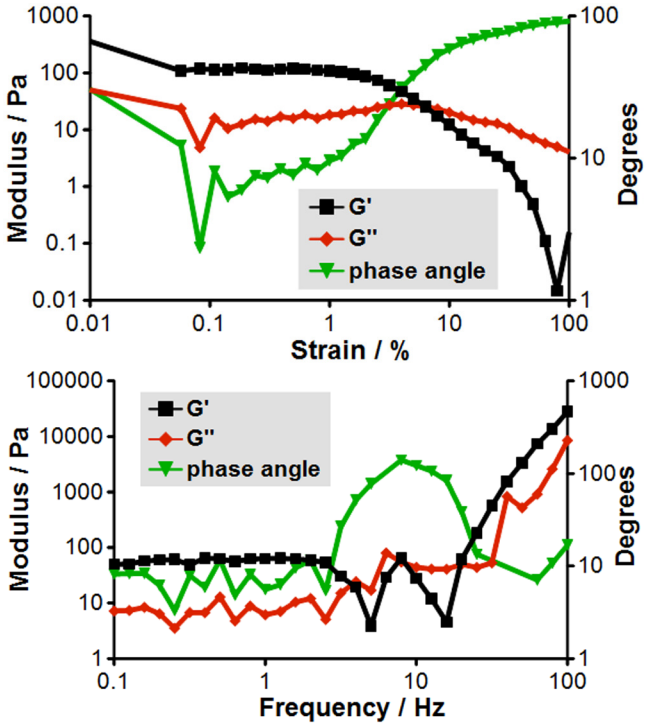

Figure A.19 System Pyr-S elastic (G') and viscous (G'') moduli; (top) strain and (bottom) frequency sweep (~0.2%) examples.

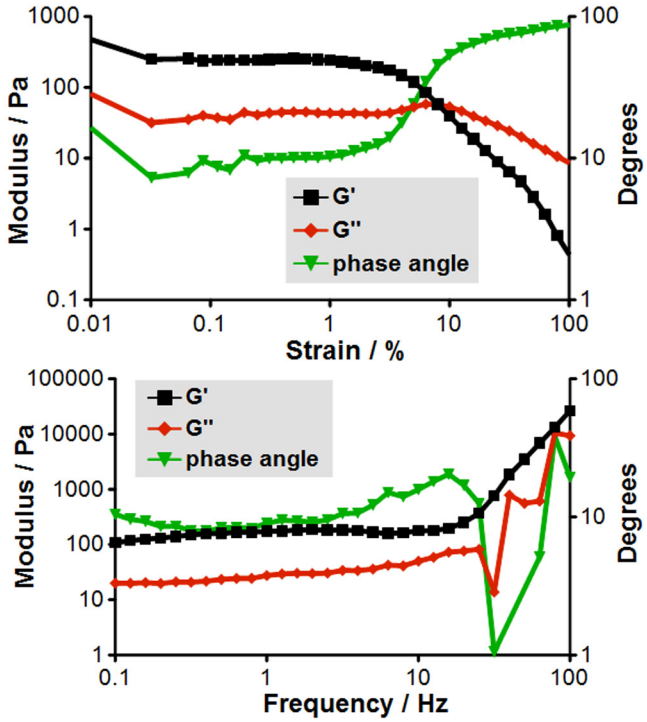

Figure A.20 System Pyr-YL/Fmoc-S elastic (G') and viscous (G'') moduli; (top) strain and (bottom) frequency sweep (~0.2%) examples.

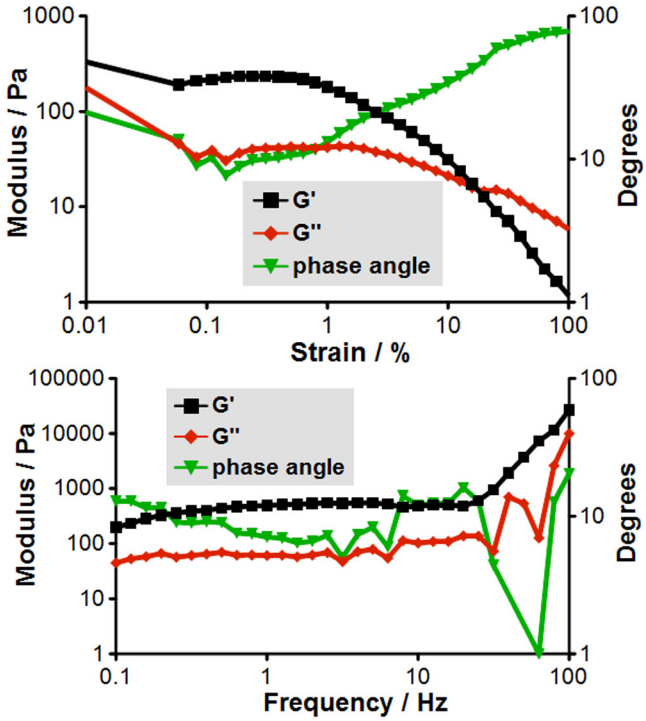

Figure A.21 System Fmoc-YL/Pyr-S elastic (G') and viscous (G'') moduli; (top) strain and (bottom) frequency sweep (~0.2%) examples.

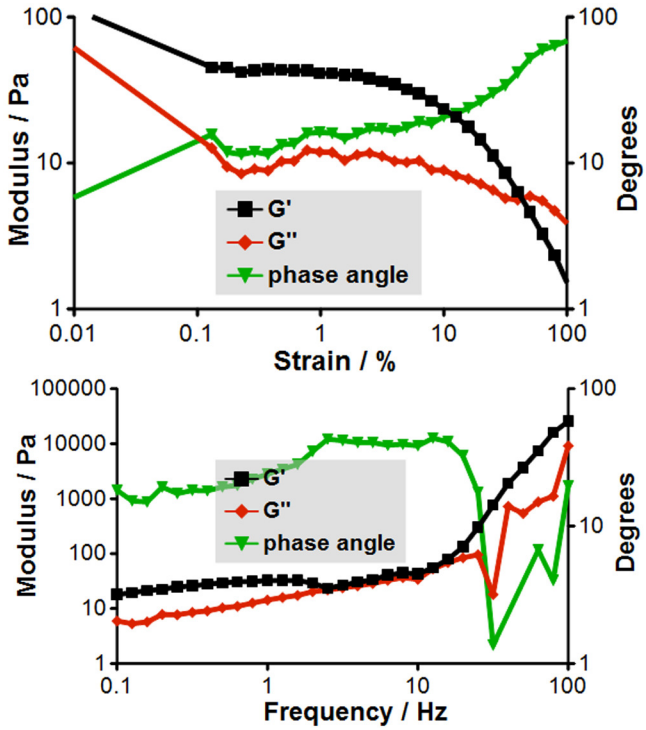

Figure A.22 System Pyr-YL/Fmoc-YL elastic (G') and viscous (G'') moduli; (top) strain and (bottom) frequency sweep (~0.2%) examples.

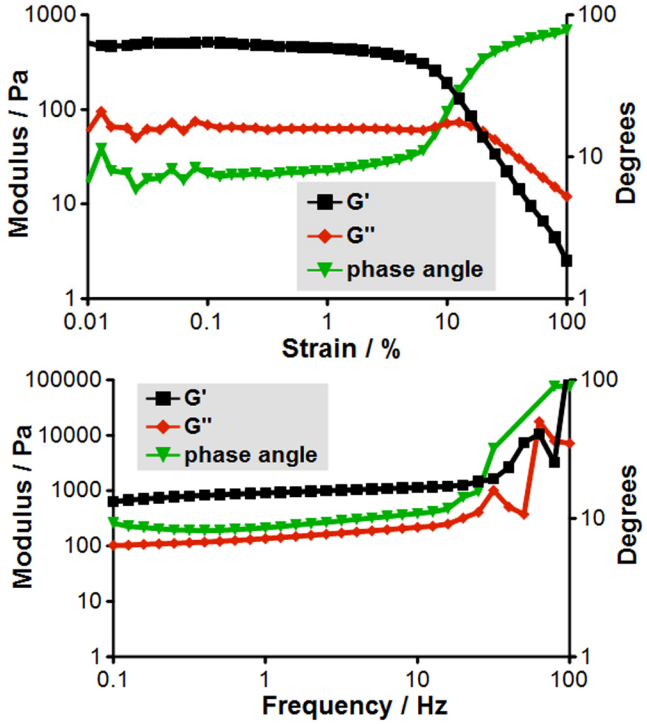

Figure A.23 System Pyr-S/Fmoc-S elastic (G') and viscous (G'') moduli; (top) strain and (bottom) frequency sweep (~0.2%) examples.

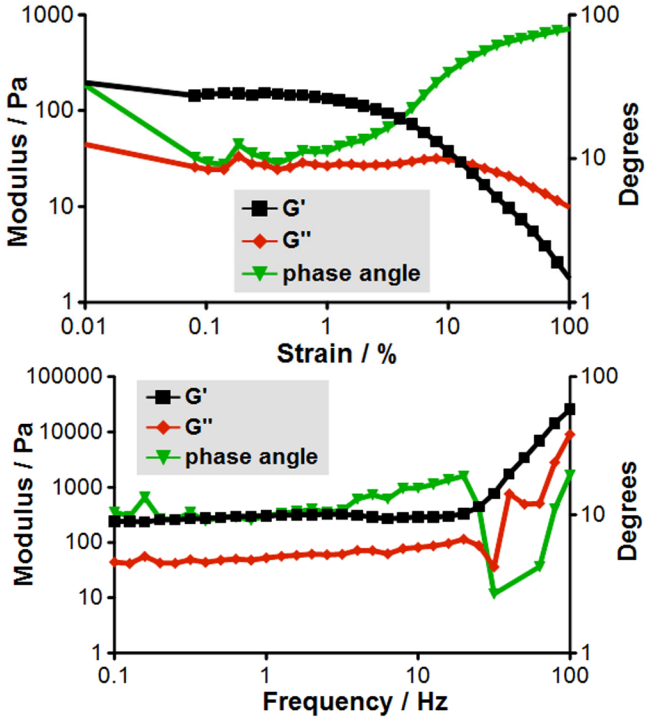

Figure A.24 System Pyr-YL/Pyr-S elastic (G') and viscous (G'') moduli; (top) strain and (bottom) frequency sweep (~0.2%) examples.

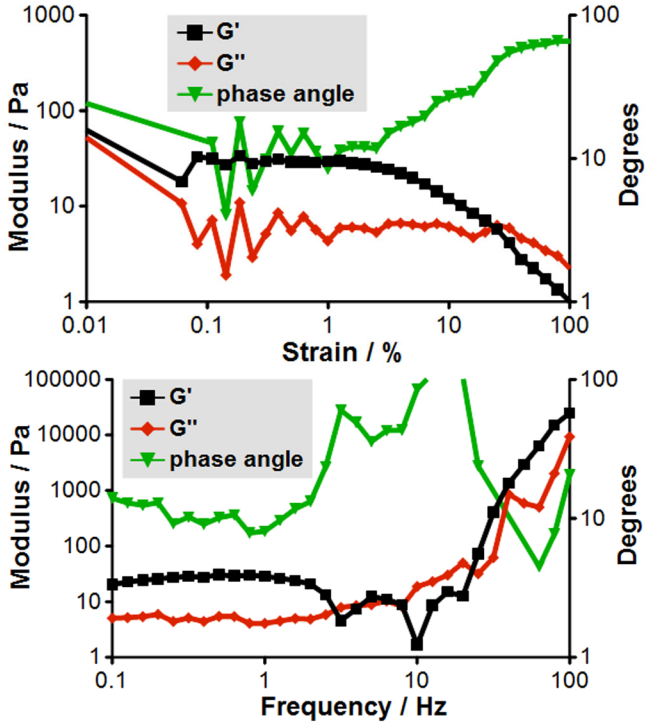

Figure A.25 System Fmoc-YL/Fmoc-S elastic (G') and viscous (G'') moduli; (top) strain and (bottom) frequency sweep (~0.2%) examples.